The role of the tail of fungal kinesin-3 in binding to early endosomes and their role in plant pathogenicity.

Submitted by Ewa Bielska

to the University of Exeter as a thesis for the degree of Doctor of Philosophy in Biological Sciences

February 2013

I certify that all material in this thesis which is not my own work has been identified and that no material has previously been submitted and approved for the award of a degree by this or any other University.

Ewa Bielska

Abstract

The dimorphic fungus *Ustilago maydis* is a pathogen of maize and it was used for decades to understand the molecular basis of plant pathogenicity aspects. Recently, much effort went into understanding the cell biology that underlies the virulence of *U. maydis*. It was shown previously that early endosomes (EEs) move bidirectionally within fungal hyphal cells. Although it was shown that the motility of EEs facilitates growth of the infectious hypha and mutants defective for kinesin-3 (Kin3), the major EE transporter, exhibit impaired polarized growth, the importance of EEs and their motility in plant colonization is not known. The first part of this thesis is focused on the role of EE motility during plant infection. In collaboration with Natalie Steinberg, who performed the plant infection assays, I used a synthetic molecular anchor, K1rPX, to block the motility of EEs at early and late stages during the host plant infection and I found that EE motility is essential during the first two days of pathogenic development, when infectious hyphae exhibit most prominent elongation, whereas blockage of EE motility after 3 days post infection does not inhibit plant colonization. Moreover, I documented that the blockage of EE motility during early stages of the infection causes high plant defence response, which means that the pathogen becomes recognized by the host plant defence system. These results indicate that EE motility is crucial during initial stages of the plant host infection and enables colonization by *U. maydis* and additionally suggests involvement of EEs in some defence response machinery. The second part of the thesis addresses the relationship between Kin3, the major motor for EE motility, and the microtubule (MT) array. I demonstrate here that Kin3 uses all MT tracks available in the cell, which is in contrast to published results in other systems. In the third part I focused on the interaction between Kin3 and the EEs. I found that the pleckstrin homology (PH) domain localized at the distal part of the Kin3 tail is of minor importance for EE association. This conclusion is supported by *in vivo* experiments, showing that truncated Kin3ΔPH, which lacks the PH domain, was still able to bind to the organelles. By systematic truncation of parts of the Kin3 tail I found two adjacent regions, a DUF3694 domain and a "linker" region, that are important for binding of Kin3 to EEs. By using a synthetic anchor

composed of Kin1 rigor domain and selected Kin3 domains I proved that both domains anchor the EEs to MTs and inhibit EE motility. I also showed that the PH domain is not able to block EE motility. In collaboration with Dr. Nicholas Harmer, who performed structural modelling of selected PH domains, I demonstrated that the PH domain is likely to interact with the motor domain of Kin3. This result was confirmed by using a yeast-two hybrid approach and a protein affinity assay. This indicates a globular organization of the Kin3 motor, which was confirmed by a split-YFP assay in living cells. Deletion of the PH domain and most probably lack of intramolecular interaction between the tail and motor domain reduces Kin3 motility parameters like velocity, frequency and run length indicating that the interaction of the PH domain with the motor domain has a role in the control of Kin3 motility.

Table of Contents

List of Tables

List of Figures

List of accompanying material

The attached CD contains:

Supplementary movies Chapter 3

3.1 Movie S1. Motility of EEs in *U. maydis* cells inside *planta*.

3.2 Movie S2. Block of dynein motility in the presence of a kinesin-1 rigor protein.

3.3 Movie S3. Motility of EEs in cells containing $K1^{r}PX$.

3.4 Movie S4. Motility of Kin3 in cells containing $K1^{r}PX$.

3.5 Movie S5. Motility of EEs in infectious hyphae in the presence and absence of $K1^{r}PX$.

Supplementary movies Chapter 4

4.1 Movie 1. Bidirectional motility of Kin3-GFP on fluorescently labelled MTs in *U. maydis* hyphal cells.

Supplementary movies Chapter 5

5.1 Movie S1. Motility of mCherry-Rab5a labelled EEs in a *kin3* null mutant, a *kin3* null mutant complemented with Kin3-GFP and a *kin3* null mutant complemented with Kin3ΔPH-GFP.

5.2 Movie S2. Structural model of the PH domain of Kin3 from *Ustilago maydis*.

5.3 Movie S3. Motility of YFP^{N}-Kin3-YFP^{C}.

The movies can be watched using QuickTime Player program.

Author’s declaration

This work was undertaken with the help of co-workers.

Chapter 3

Ms Natalie Steinberg established plant infection method, performed research and analysed data.

Dr. Martin Schuster performed FRAP experiments.

Dr. George Litlejohn performed confocal microscopy.

Ms Laura Yeves-Gonzalez did plant infections and performed staining of plant infected tissues.

Prof. Gero Steinberg designed research, conceived the project, analysed data and wrote the manuscript.

Chapter 4

Prof. Gero Steinberg provided overall project management, read and corrected the manuscript.

Chapter 5

Dr. Nicholas Harmer developed PH domains modelling.

Dr. Martin Schuster performed FRAP experiments and analysed Kin3 number on EEs.

Prof. Gero Steinberg analysed data, provided overall project management and supervision and wrote the final version of the manuscript.

I would like to thank all co-author for their support and help.

Abbreviations

a, *b*	mating type loci
aa	amino acid
Aba	aureobasidin A; antifungal antibiotic
AD	activation domain (Y2H); activates transcription of the reporter genes
Amp	ampicillin
ap	acid phosphatase
ATP	adenosine triphosphate
BAR	Bin–Amphiphysin–Rvs
BD	binding domain (Y2H); binds to Gal4 promoter
BIFC	bimolecular fluorescence complementation
ble^R	phleomycin resistance
bp	base pair
°C	degree Celcius
cAMP	cyclic adenosine monophosphate
CAP_Gly	cytoskeleton-associated protein Glycine-rich
cbx^R	carboxin resistance
CC	coiled coil
CM	complete medium
cm	centimeter
cMTOC	cytoplasmic MTOC
crg; r	conditional arabinose-induced promoter
CSD	cell separation defect
C-terminus	carboxy terminus
D2	conserved fragment within "linker" region of Kin3
DAB	diaminobenzidine
DCVs	large dense-core vesicles
DENN	differentially expressed in normal and neoplastic cells
dH_2O	distilled water
DIC	differential interference contrast
DL	DUF3694-"linker" region of Kin3
DLP	DUF3694-"linker"-PH region of Kin3
DNA	deoxyribonucleic acid
dNTP	deoxyribonucleotide
dpi	day post infection
DUF3694, D	domain of unknown function 3694
dyn2	dynein heavy chain
E1, W2	genes of the *b* mating-type locus
EB1	end-binding protein 1
ECL	enhanced chemiluminescence
EE	early endosome
EEA1	early endosome antigen 1
EGFP	enhanced green fluorescent protein
EGTA	ethylene glycol-bis(beta-aminoethyl ether)-N,N,N',N'-tetra acetic acid
EM	electron microscopy
f	forward primer
FHA	forkhead associated domain
FM4-64	amphiphilic styryl dye
FRAP	fluorescence recovery after photobleaching
FYVE	zinc finger domain
g	acceleration due to gravity, equal to 9.81 m s^{-2}

G2 stage	final subphase during interphase within the cell cycle
Gal4	encodes the yeast transcription activator protein Gal4
*g*DNA	genomic DNA
GEF	guanine nucleotide exchange factor
GFP	green fluorescent protein with excitation peak at 395 nm and emission peak at 509 nm
GTP	guanosine triphosphate
h	hour
Hepes	4-(2-hydroxyethyl)-1-piperazineethanesulfonic acid
Hisx6	hexahistidine
hpi	hour post infection
HRP	horseradish peroxidase
hyg^R	hygromycin resistance
IgG	immunoglobulin G
IPTG	isopropyl-β-D-thiogalactoside
$K1^rPX$	synthetic endosomal anchor
Kb	kilo base
kD	kilo Dalton
Khc73	kinesin-3 homologue (*Drosophila melanogaster*) containing CAP-Gly domain
KIF16B	kinesin-3 containing PX domain (human, mice)
KIF1A	kinesin-3 containing PH domain (human, mice)
Kin1	kinesin-1
Kin3	kinesin-3
L	"linker" region of Kin3
LIC	ligation independent cloning
LN_2	liquid nitrogen
M	molar
mA	milliampere
MADD	MAP kinase activating death domain
MAP	mitogen activated protein
MAPK	mitogen activated protein kinase
MAPKK	mitogen activated protein kinase kinase
mCherry	monomeric Cherry fluorescent protein with excitation peak at 587 nm and emission peak at 610 nm
MDCK	Madin–Darby canine kidney
mfa2	gene of the Mfa2 pheromone
mg	milligram
mig1	maize-inducible promoter
min	minute
min/kb	time in minutes required for amplification of 1 kb of DNA
ml	milliliter
mm	millimeter
mM	millimolar
mRNPs	ribonucleoprotein complexes
ms	millisecond
MT	microtubule
MTOC	microtubule organizing centres
mW	milliwatt
µg	microgram
µl	microliter
µm	micrometer
µM	micromolar
n	sample size
nar	conditional nitrate reductase promoter

nat^R	nourseothricin resistance
Ni-NTA	nickel-nitrilotriacetic acid
NM	nitrate medium
nm	nanometer
N-terminus	amino terminus
OD	optical density
ori	origin of replication
otef	constitutive *otef* promoter
P	probability
P	promoter
p75	neurotrophin receptor
PBS	phosphate buffered saline
PCR	polymerase-chain reaction
PEG	polyethylene glycol
pGADT7	contains the GAL4 DNA-AD and the LEU2 marker
pGBKT7	contains the GAL4 DNA-BD and the TRP1 marker
PH	pleckstrin homology domain
PI(3)P	phosphatidylinositol 3-phosphate
PI(4,5)P2	phosphatidylinositol 4,5-bisphosphate
PKA	cAMP-dependent protein kinase
PM	plasma membrane
Pra1	pheromone receptor
PTM	post-translational modification
PX	Phox domain
r	reverse primer
Rab	Ras-associated binding protein
Rab5a	small endosomal Rab5-like GTPase
Ras	small GTPase (Rat sarcoma); contains Rho, Rab, Arf, Ran proteins
RFP	red fluorescent protein
Rho	small GTPase belonging to Ras superfamily proteins
RNA	ribonucleic acid
rpm	rotation per minute
RT	room temperature
s	second
Sc-Ura	*S. cerevisiae* medium depleted of uracil
SD	synthetically defined medium for culturing *S. cerevisiae* (Clontech)
SDO	SD medium lacking of Trp
SD/-DDO	SD double dropout (SD/-Trp/-Leu); low stringency
SD/-TDO	SD triple dropout medium lacking of Trp, Leu and His; medium stringency
SD/-QDO	SD quadruple dropout medium lacking of Trp, Leu, His and Ade; high stringency
SDS	sodium dodecyl sulfate
SEM	standard error of the mean
s/kb	time in seconds required for amplification of 1 kb of DNA
SPB	spindle pole body
STVs	small transport vesicles
SV2	synaptic vesicle protein 2
SYD-2	synapse defective; *C. elegans* homologue of human Liprin-a
TBS	Tris buffered saline
Tm	melting temperature
ts	temperature-sensitive allele
t-SNARE	target soluble *N*-ethylmaleimide attachment protein receptor
Tub1	a-tubulin of *U. maydis*
Unc-104	kinesin-3 homologue of KIF1A (*C. elegans*, *D. discoideum*, *D. melanogaster*)

UncA	kinesin-3 homologue of KIF1A from *A. nidulans*
URA3	*S. cerevisiae* gene involved in the novo synthesis of uracil
UTR	untranslated region
v/v	volume per volume
w/v	weight per volume
WGA-AF488	wheat germ agglutinin-Alexa Fluor®488; lectin which binds to sialic acid and *N*-acetylglucosaminyl residues
WT	wildtype
X-a-Gal	5-Bromo-4-Chloro-3- indolyl-a-D-galactopyranoside; substrate for yeast galactosidase (MEL1); used for detecting GAL4-based Y2H interactions
Y2H	yeast two-hybrid system
YFP	yellow fluorescent protein with excitation peak at 514 nm and emission peak at 527 nm
YFP^C	C-terminal half of YFP
YFP^N	N-terminal half of YFP
YPDA	yeast peptone dextrose adenine
Yup1	early endosomal t-SNARE 1 of *U. maydis*
Δ	deletion

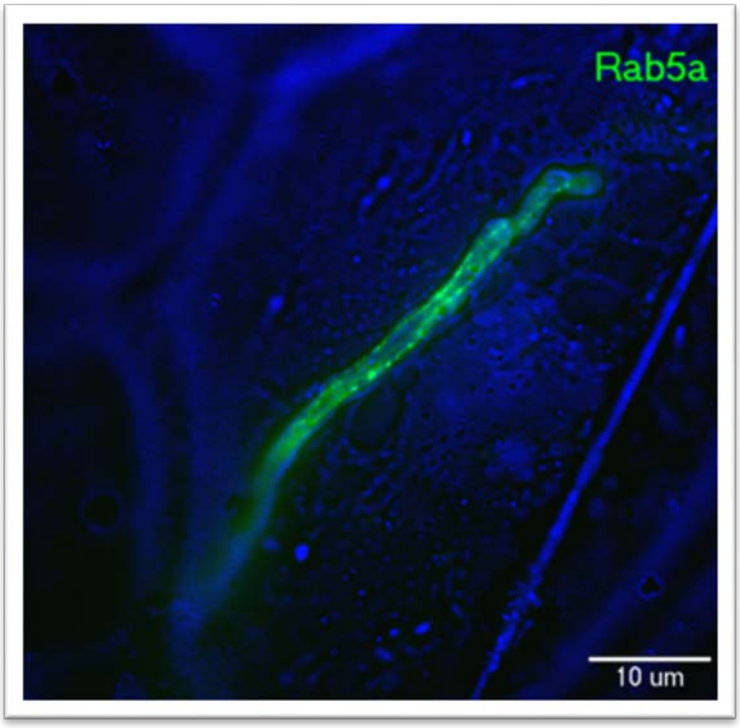

***Ustilago maydis* during infection of its host plant *Zea mays*.**
Elongated fungal hypha penetrates the host leaf tissue (blue). Early endosomes within the fungal hyphal cell are labelled with GFP-Rab5a (green) and their bidirectional motility is synthetically blocked (green dotted lines). Bar is given.

Chapter 1

Introduction

1.1 The model fungus *Ustilago maydis*

Basidiomycete, the smut fungus of corn (*Zea mays*) and teosinte (*Zea mays ssp. parviglumis*), *Ustilago maydis* belongs to top ten plant pathogens (Dean *et al.*, 2012; Fisher *et al.*, 2012). This biotrophic fungus proliferates in the living plant (Kämper *et al.*, 2006) and forms plant galls (called tumors) on the leaves, stems and the corncob of the plant, which decrease the maize crop yield (Christensen, 1963; Banuett and Herskowitz, 1996; Martinez-Espinoza *et al.*, 2002; Fisher *et al.*, 2012). This can lead to loss of nearly $1.0 billion annually (Smith, 2011). Interestingly, infected corncobs have been used in Mexico as a special tasty delicacy known as 'Huitlacoche' or Mexican 'truffle' since Aztecs' time (Valverde *et al.*, 1995; Juarez-Montiel *et al.*, 2011). A recent study on biomass degradation revealed that *U. maydis* has the best-performing secretome (complex mixture of enzymes that are secreted) in comparison to other filamentous fungi and can be used in the industry (Couturier *et al.*, 2012).

U. maydis serves as a model organism which allows studying *in vivo* cellular processes that are not found in the standard fungal model *Saccharomyces cerevisiae* (Münsterkötter and Steinberg, 2007; Steinberg and Perez-Martin, 2008). This fungal model organism has been extensively studied for more than sixty years and that allowed the discovery of DNA recombination via Holliday junctions (reviewed in Holliday, 2004) and many cellular processes underlying fungal pathogenic development (reviewed in Basse and Steinberg, 2004; Brefort *et al.*, 2009; Vollmeister *et al.*, 2011). Its sequenced genome (Kämper *et al.*, 2006) shares with humans genes encoding most components of the endocytic and long distance transport machinery (Fuchs and Steinberg, 2005b), and, in the last decade, *U. maydis* became a model for the long-distance motility of early endosomes driven by kinesin-3 and dynein (Wedlich-Söldner *et al.*, 2000; Wedlich-Söldner *et al.*, 2002; Lenz *et al.*, 2006; Steinberg, 2007c; Schuster *et al.*, 2011c). The fungus is easy to cultivate under laboratory conditions and molecular tools have been established (Steinberg and Perez-Martin, 2008), therefore *U. maydis* is a perfect model organism for *in vivo* studies of the cell biological processes underlying the long-distance transport machinery (Dean *et al.*, 2012).

U. maydis dimorphic life cycle (reviewed in Vollmeister *et al.*, 2011; Fig. 1 and 2) is composed of two stages: a saprotrophic, non-pathogenic stage (haploid yeast-like cells also known as sporidia; Fig. 1A and 2) and an invasive, host-associated pathogenic stage (dikaryotic filamentous hyphal cells; Fig. 2).

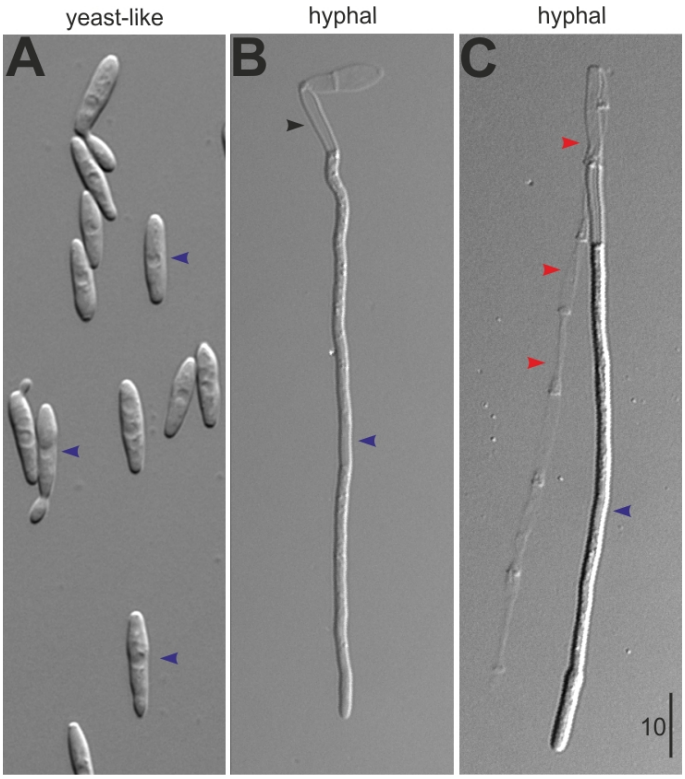

Figure 1. Morphological stages of the dimorphic fungus *U. maydis*.
(**A**) Yeast-like cells have a cigar shape and they multiply by budding. Note the localization of the nucleus in the middle of the mother cell (blue arrows). (**B**)* Hyphal cell contains basal vacuole (black arrow). Note the localization of the nucleus in the middle of hypha (blue arrow). (**C**)* Hyphal cell elongates and leaves behind basal vacuole followed by empty regions (red arrows) separated by retraction septa. Note the localization of the nucleus still in the middle of hypha (blue arrow). Bar is given in micrometers. *Note that the haploid AB33 strain (Brachmann *et al.*, 2001) is shown. This strain expresses both halves of the heterodimeric *b*-transcription factor (*bE* and *bW*; explained in Chapter 1.1.1) under the control of inducible *nar1* promoter which allows formation of *b*-dependent filaments in a liquid medium containing nitrate as nitrogen source under laboratory conditions.

Haploid yeast-like cells multiply vegetatively by budding (Fig. 1A and 2). Induction of the host disease is dependent on the transition from the non-pathogenic haploid budding yeast-like cells to hyphae obtained after mating (fusion/sexual development) of compatible haploid cells with different *a* and *b* loci (Bölker *et al.*, 1992; Fig. 2). Invasion starts with an appressorium formation that penetrates the plant cuticle by invading the host plasma membrane,

although penetration through the stomata has also been observed (Mills and Kotzé, 1981; Banuett and Herskowitz, 1996). The invading hypha exocytoses enzymes involved in cell wall synthesis (e.g. chitin synthases; chitin synthases exochitinases, chitin deacetylases, and exo- and endoglucanases; Doehlemann *et al.*, 2008a; Heimel *et al.*, 2010a) and virulence effectors (Doehlemann *et al.*, 2009; Doehlemann *et al.*, 2011) and remains 'invisible' for the host plant defence system. This allows cell proliferation in meristematic host tissue and tumor formation composed of round, diploid teliospores (Banuett, 1995; Banuett and Herskowitz, 1996). Meiosis of the spores during germination and production of the haploid yeast-like cells finishes the life cycle (see Fig. 2).

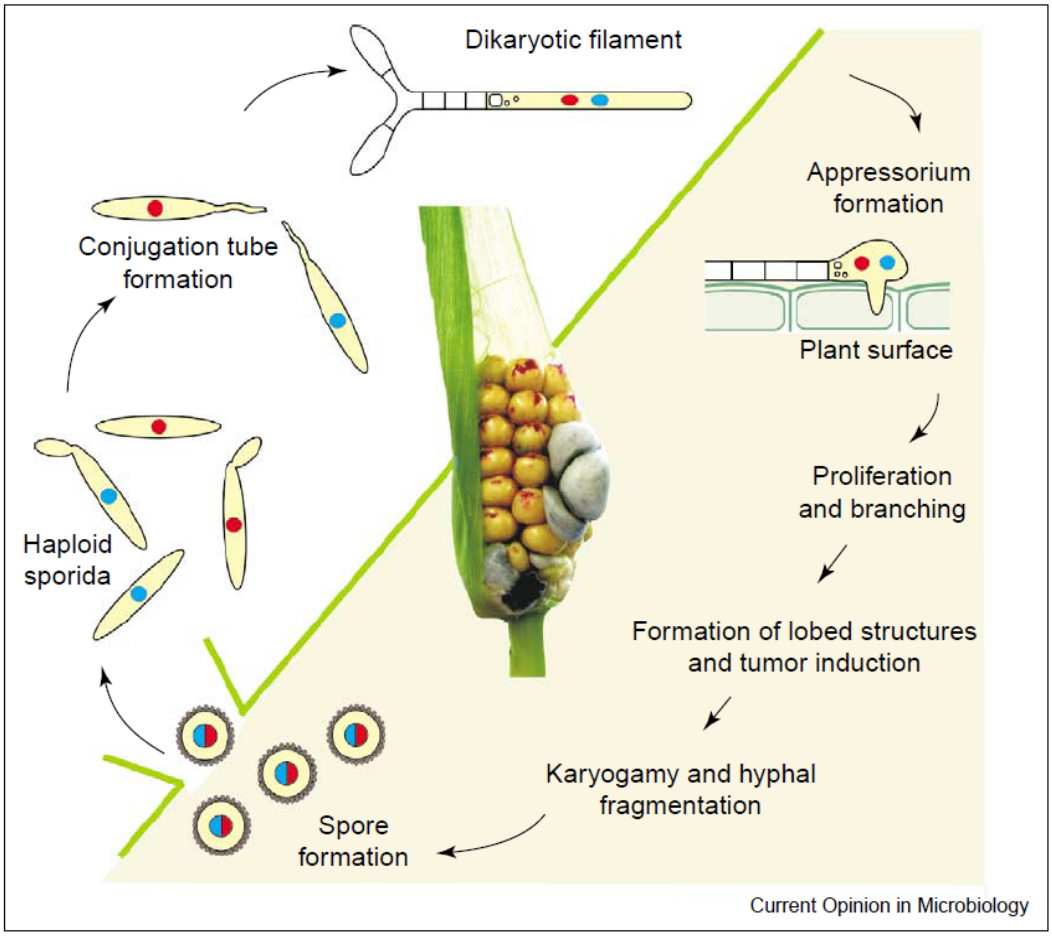

Figure 2. Life cycle of *Ustilago maydis*.
In the presence of the surface of a plant, compatible haploid sporidia (presented with red and blue nuclei) exchange their pheromones what leads to formation of conjugation tubes and fusion. This results in formation of a dikaryotic hypha which forms an appressorium and starts to colonize the host. After spreading within the plant, the fungus proliferates and induces the tumor, a typical disease symptom presented in the centre of the figure. After nuclear fusion, diploid spores are formed (represented as circles with bi-colour nuclei and a black region in the lower part of the tumor). Meiosis of the spores is followed by formation of haploid sporidia. The figure is taken from Feldbrügge *et al.*, 2004.

1.1.1 Molecular basis of the transition from yeast-like to filamentous growth

Pathogenic development of *U. maydis* is initiated with the transition from sporidia to hypha through the mating process. Regulation of the mating between two compatible haploid yeast-like cells is based on two independent mating type loci, *a* and *b*.

The *a* locus has two alleles, *a1* and *a2*, and both of them are idiomorphs (with no similarity to each other; Froeliger and Leong, 1991). The biallelic *a* locus encodes a pheromone-based cell recognition system: a lipopeptide pheromone precursor (mating factor; *mfa1* or *mfa2*) and a transmembrane pheromone receptor (*pra1* or *pra2*) which controls cell fusion by recognition of the pheromones of the opposite mating type (Bölker *et al.*, 1992; Spellig *et al.*, 1994a). In other words an *a1* cell may only mate with an *a2* cell and this triggers conjugation tube formation and a fusion process at the tips of the tubes (Banuett and Herskowitz, 1994; Spellig *et al.*, 1994a; Spellig *et al.*, 1994b; Snetselaar *et al.*, 1996).

The multiallelic *b* locus, which has at least 25 alleles (Rowell, 1955; Holliday, 1961; Day *et al.*, 1971; Kronstad and Leong, 1990; Froeliger and Leong, 1991), contains two separate genes: *bE* – encodes a homeodomain protein, DNA-binding protein (Kronstad and Leong, 1989, 1990; Schulz *et al.*, 1990), and *bW* – encodes regulatory polypeptide (Gillissen *et al.*, 1992). In other words, a *b1* allele contains *bW1 bE1, b2* contains *bW2 bE2,* etc. Both *b* genes, *bE* and *bW*, from different alleles/different strains, form heterodimers (e.g. *bE1-bW2*) through their N-terminal variable domains (Kämper *et al.*, 1995; Romeis *et al.*, 1997; Schlesinger *et al.*, 1997). If pairwise combination of *bW* and *bE* polypeptides is derived from different alleles of the *b* locus (Gillissen *et al.*, 1992) then active heterodimer is formed (Kämper *et al.*, 1995) which acts as a transcriptional factor specific for pathogenicity genes involved in cell cycle regulation, cell wall remodelling and secretion of effector candidates (Gillissen *et al.*, 1992; Spellig *et al.*, 1994b; Romeis *et al.*, 1997; Brachmann *et al.*, 2001; Heimel *et al.*, 2010a) triggering initiation of filamentous growth (Rowell, 1955; Puhalla, 1968) and pathogenic development (Banuett and Herskowitz, 1989;

Gillissen *et al.*, 1992; Spellig *et al.*, 1994a; Kämper *et al.*, 1995; Brachmann *et al.*, 2003). Temperature sensitive allele of *bE*, bE^{ts}, is not able to proliferate *in planta* and contains multiple nuclei indicating the *bE* involvement in cell cycle and cell division (Wahl *et al.*, 2009). The majority of the *b*-dependently expressed genes are regulated via Rbf1 (regulator of *b*-filament), a transcription factor and a master regulator of the *b*-dependent transcriptional cascade (Heimel *et al.*, 2010a). Heterozygosity at the *b* loci also prevents further mating (Laity *et al.*, 1995).

After binding of a pheromone with its transmembrane receptor, the signalling pathway is initiated. Pheromone receptors are coupled to heterotrimeric G proteins, where one of their alpha subunits, Gpa3 (Regenfelder *et al.*, 1997) controls the cAMP signalling pathway (Krüger *et al.*, 1998) through cAMP-dependent protein kinase (PKA) activity independent of the *b* locus (Gold *et al.*, 1994). Decrease of intracellular cAMP levels is associated with the yeast-like to filamentous morphological transition (Gold *et al.*, 1994). Disruption of *adr1*, one of the catalytic subunits of PKA, results in a constitutive filamentous growth (Durrenberger *et al.*, 1998); budding can be restored by exogenously added cAMP (Gold *et al.*, 1994). In addition, the pheromone recognition-based filamentous growth is activated by mitogen-activated protein kinase (MAPK) Kpp2 signalling (Müller *et al.*, 1999) via phosphorylation of Prf1 protein (pheromone response factor; Hartmann *et al.*, 1996). This transcription factor, additionally phosphorylated by PKA Adr1 (Kaffarnik *et al.*, 2003), activates transcription of all genes in the *a* and *b* loci (Hartmann *et al.*, 1996; Urban *et al.*, 1996) by binding to special pheromone response elements located in the regulatory regions of these genes (Kaffarnik *et al.*, 2003). Expression of *prf1* gene is additionally regulated post-translationally by internal cAMP levels (Krüger *et al.*, 1998; Hartmann *et al.*, 1999). This leads to an amplification of the pheromone signal and to an increase of *b* gene expression before cell fusion (Kaffarnik *et al.*, 2003). Disruption of the genes encoding members of MAP, MAPK and MAPKK kinase cascade, required for filamentous growth, pheromone response and virulence (Banuett and Herskowitz, 1994; Gold *et al.*, 1994; Gold *et al.*, 1997; Mayorga and Gold, 1999; Andrews *et al.*, 2000; Mayorga and Gold, 2001; Lee and Kronstad, 2002; Garrido and Perez-Martin, 2003; Müller *et al.*, 2003), brought the evidence for the importance of signal transduction pathways of cAMP and MAP kinase in the control of

morphogenesis and pathogenicity in *U. maydis*. The pheromone recognition cascade also leads to the arrest of the cell cycle in a postreplicative G2 stage (Garcia-Muse *et al.*, 2003) which is additionally induced by formation of the active *bE/bW* heterodimer (Mielnichuk *et al.*, 2009; Heimel *et al.*, 2010a). The cell cycle arrest is released by interaction between Clp1 and *bW* only after penetration of the host plant (Heimel *et al.*, 2010b).

1.1.2 *Zea mays* - *U. maydis* relation

One of the forms of invasion by fungi is invading by elongated hyphae (reviewed in Gow *et al.*, 2002) and this is correlated in time with the expression of virulence factors (Talbot, 2012). Recognition of the pathogen by its host is an early process and requires fast reaction to prevent it – defence related maize genes are upregulated by the pathogen's presence in very early stages of the *U. maydis* biotrophic stage, when the fungal cells develop filaments and appressoria on the plant surface (12 and 16 hours post infection, respectively; Doehlemann *et al.*, 2008b; Mendoza-Mendoza *et al.*, 2009). Interestingly, maize tissues differ in response to fungus infection (Skibbe *et al.*, 2010).

Although *U. maydis* genome sequencing revealed 12 gene clusters encoding mainly uncharacterized, predicted secreted proteins expressed *in planta* and many secreted proteins have been described already (Kämper *et al.*, 2006; Mueller *et al.*, 2008; Müller *et al.*, 2008; Doehlemann *et al.*, 2009; Wahl *et al.*, 2009; Heimel *et al.*, 2010a; Djamei *et al.*, 2011; Doehlemann *et al.*, 2011; Robledo-Briones and Ruiz-Herrera, 2012), it is still not exactly clear how the fungus recognizes its host and which effector proteins must be secreted in order to survive maize defence system. There is evidence from *in vitro* studies that corn oil, hydroxy-fatty acids (especially 12-hydroxystearic acid and 16-hydroxyhexadecanoic acid; most abundant plant cutin monomers) and a hydrophobic surface promote a filamentous growth and appressorium formation through activation of *Kpp2* of the cAMP/MAPK pathway (Klose *et al.*, 2004; Mendoza-Mendoza *et al.*, 2009).

Depending on the infected maize organ, *U. maydis* exhibits specific expression patterns (Skibbe *et al.*, 2010; Walbot and Skibbe, 2010). Microarray experiment

revealed that 206 genes were induced and 139 were repressed in response to *b*-induction (Heimel *et al.*, 2010a). Among those genes, 20 genes encoding cell wall proteins (chitin synthases exochitinases, chitin deacetylases, and exo- and endoglucanases) were induced 3 hours after *b*-induction (Heimel *et al.*, 2010a). The transcription factor Rbf1 was upregulated already 1 hour after *b*-induction (Heimel *et al.*, 2010a). Deletion of Rbf1 led to filamentous growth inhibition and inability to form the appressoria; cells were also not arrested in G2 stage (Heimel *et al.*, 2010a).

Pathogen attack induces a rapid plant defence reaction, the oxidative burst, which is mainly based on the production of reactive oxygen species (e.g. H_2O_2; Apostol *et al.*, 1989; Wojtaszek, 1997). *U. maydis* encodes Yap1, an ortholog of AP-1-like from *S. cerevisiae*, which functions as a redox sensor. Yap1 is localized in the nucleus up to 2 to 3 days post infection (dpi) and regulates a large set of genes like peroxidases (Molina and Kahmann, 2007). Recently, Pep1 (protein essential during penetration-1), has been indicated as a secreted effector which inhibits the plant peroxidase POX12 driven oxidative burst. Indeed, the *pep1* null mutants induce strong early defence of the host plant (Hemetsberger *et al.*, 2012) although they are still able to form normal penetration structures (Doehlemann *et al.*, 2009). Additionally, it is though that *U. maydis* manipulates the host cells through metabolic priming via secretion of a virulence factor, chorismate mutase Cmu1 into the biotrophic interface. Cmu1 is highly upregulated during biotrophic growth (10,000 fold in filamentous cells 20 h after infection and after 5 dpi – more than 100,000 fold) and is taken up by the plant where it spreads to the surrounding cells and suppresses plant production of salicylic acid (Djamei *et al.*, 2011).

1.2 The basic requirements for fast growing hypha

The need for fast growing hypha is to explore and to penetrate the environment, and more specifically, in case of pathogenic filamentous fungi, to colonize the host organism. In case of human fungal pathogens (*Candida* and *Aspergillus*) and the majority of plant fungal pathogens which undergo dimorphic transition, avirulence is usually correlated with an inability of hyphae formation (Lo *et al.*,

1997; Sanchez-Martinez and Perez-Martin, 2001; Nadal *et al.*, 2008; Brand, 2012; Wang and Lin, 2012). Hyphal cells are expanded by polar tip growth. In order to elongate the cell into polarized filaments the cell has to possess (reviewed in Harris, 2006; Steinberg, 2007b):

1. the long-distance transport between the subapical part and the apex of the tip cell;
2. microtubules (MTs) and F-actin array (reviewed in Steinberg, 2007d; Berepiki *et al.*, 2011);
3. molecular motors like kinesins, dynein and myosins (reviewed in Steinberg, 2007a);
4. organelles to transport fungal cell wall material precursors and enzymes (polarized exocytosis) and to recycle membranes (endocytosis) at the hyphal tip (reviewed in Steinberg, 1998b);
5. vacuole formation in older segments of hyphae, cytoplasm streaming to build up turgor pressure on the cell wall (Steinberg *et al.*, 1998a; Heath and Steinberg, 1999; Plamann, 2009) and septation (Boyce *et al.*, 2005; Freitag *et al.*, 2011) which enables high-speed movement of infectious filament and allows covering long distances;
6. a Spitzenkörper (apical body) which is an accumulation of vesicles within the hyphal apex that serves for local cell wall synthesis and that is thought to direct hyphal growth (Howard, 1981; Harris, 2009b; reviewed in Harris *et al.*, 2005; Steinberg, 2007b);
7. post-transcriptional control through MT-dependent transport of mRNAs encoding polarity factors and secreted proteins (Feldbrügge *et al.*, 2008; König *et al.*, 2009; Vollmeister and Feldbrügge, 2010; Koepke *et al.*, 2011).

1.2.1 Role of microtubules in tip growth of fungi

Fungal hyphal cells, similarly to neurons (Heidemann *et al.*, 1981; Baas *et al.*, 1988), are highly polarized and require precise transport machinery in order to survive (Steinberg and Perez-Martin, 2008). Cellular trafficking in fungi and other eukaryotes is based on actin and MTs (reviewed in Lichius *et al.*, 2011).

MTs are dynamic, long filaments built of alpha and beta tubulin heterodimers that polymerise at their plus ends (Desai and Mitchison, 1997). In the elongated hyphal cells of *U. maydis*, MTs form long, often bended and bundled tracks (Steinberg *et al.*, 2001). Their orientation in the cell has been precisely described by the usage of fluorescently tagged EB1-homologue Peb1 (Straube *et al.*, 2003) that binds only to the growing MT plus-ends (Straube *et al.*, 2003; Lenz *et al.*, 2006; Schuster *et al.*, 2011c): unipolar plus-ends of MTs are localized in the distal parts of the hyphal cell (growing apex and the basal septum) and antipolar bundles containing plus- and minus-ends are localized in the middle region of the cell (Schuchardt *et al.*, 2005; Lenz *et al.*, 2006; Schuster *et al.*, 2011c).

Nucleation of MTs requires microtubule organizing centres (MTOC) containing e.g. gamma tubulin (Wiese and Zheng, 2006) acting as a scaffold for dimers of alpha and beta tubulins for initiation of polymerization and serves as a cap protecting MT minus ends. In fungi, the spindle pole body (SPB) act as MTOC localized in the cell, although not exclusively e.g. *U. maydis*, in addition to SPB, uses cytoplasmic MTOCs to rearrange MTs during the cell cycle (during G2 stage) in sporidia (Straube *et al.*, 2003). As hyphal cells are arrested in G2 stage (Garcia-Muse *et al.*, 2003), only cytoplasmic MTOCs are used during early stages of pathogenic development. Additionally cytoplasmic MTOCs have not been found within the 10–15 µm behind the hyphal tip and the septum what makes these regions ‘filled’ with uniformly oriented MTs (Schuster *et al.*, 2011c).

MTs in *U. maydis* are involved in determining and supporting the cell polarity (Steinberg *et al.*, 2001), however, not in all filamentous fungi (Heath *et al.*, 2000). MT polarity and orientation allows differentiation of transport direction by molecular motors and delivering appropriate content to its destination (Vale, 2003), therefore MTs are involved in long-range transport of vesicles to the hyphal tip region (reviewed in Egan *et al.*, 2012b). Although involvement of MTs in initial pathogenic development is not required (in the case of *U. maydis* – during the formation of conjugative hyphae; Fuchs *et al.*, 2005a), lack of MTs during extended hyphal growth impairs polarized growth, directionality of the tip growth and reduces the rate of hypha elongation in many fungi (Horio and Oakley, 2005; Sampson and Heath, 2005; Fuchs *et al.*, 2005a; Horio, 2007; Taheri-Talesh *et al.*, 2008).

1.2.2 Molecular motors and tip growth

Filamentous fungi encode a large spectrum of molecular motors involved in delivery of various components to the hyphal tip (Yamashita and May, 1998a; Steinberg, 1998b, 2000; Schoch *et al.*, 2003; Steinberg, 2007c). Dynein (retrograde motor) and kinesins (anterograde motors) move along MTs, while most of the myosins use actin filaments to deliver the cargo into the fast growing hyphal tip. The energy necessary for such transport comes from ATP hydrolysis (Vale *et al.*, 1985; Vale and Milligan, 2000). The same group of motors is involved in transport of various cargoes in neurons and some of them are critically involved in neuronal disease pathogenesis (Hirokawa *et al.*, 2010).

Kinesins

Among ten kinesins encoded by the *U. maydis* genome (Table 1; Schuchardt *et al.*, 2005) only two of them, conventional kinesin (Kin1) and KIF1A/Unc-104 homologue (Kin3) have been found to be involved in fast growing hypha (Lehmler *et al.*, 1997; Schuchardt *et al.*, 2005) where their expression is upregulated (~4-5 fold; Schuchardt *et al.*, 2005). Interestingly, these two kinesins were initially discovered in neurons as synaptic vesicle transporters (reviewed in Hirokawa *et al.*, 2010), but none of these kinesins is present in the small yeast *S. cerevisiae*. Although Kin7 in *U. maydis* is not involved in polarized growth (Schuchardt *et al.*, 2005), the role in such a process has been found in *Aspergillus nidulans* (KipA; Konzack *et al.*, 2005). Involvement of the conventional kinesin in hyphal growth has been also reported in other filamentous fungi like *Nectria haematococca* (Wu *et al.*, 1998), *A. nidulans* (Requena *et al.*, 2001) and *Neurospora crassa* (Seiler *et al.*, 1997).

Table 1. Kinesins encoded by the *U. maydis* genome.

No.	Entry	Gene	Description
1	um00896	Kin7a	Kinesin-7a motor protein
2	um01560		related to kinesin
3	um04218	Kin1	Kinesin-1 motor protein
4	um04524		related to Kinesin
5	um04727		related to Kinesin-like protein KIF23
6	um06251	Kin3	Kinesin-3 motor protein
7	um06427		related to Kinesin-like protein KIF2C
8	um10383		related to KIP1 - kinesin-related protein
9	um10678		related to KIP1 - kinesin-related protein
10	um11986	Kin4	c-terminal kinesin

Source: MIPS *Ustilago maydis* http://mips.helmholtz-muenchen.de/genre/proj/ustilago/

Myosins

For hyphal morphogenesis, cell polarity and endocytosis additionally filamentous fungi use myosins. This enables the switch between MT-based long distance transport of vesicles and organelles to short, F-actin dependent transport localized within the hyphal apex (Langford, 1995; reviewed in Steinberg, 2000 and in Akhmanova and Hammer, 2010). Among four classes of myosins encoded by filamentous fungi (classes I, II, V and XVII - a myosin–chitin synthase; Weber *et al.*, 2006; Banuett *et al.*, 2008), two classes of myosins (classes I and V) are mainly involved in establishing the filamentous morphology and tip growth: class I myosins [*A. nidulans* myoA (McGoldrick *et al.*, 1995; Osherov *et al.*, 1998; Yamashita and May, 1998b) and *Candida albicans* myo5 (Oberholzer *et al.*, 2002)] and class V myosins (*A. nidulans* myoV; Zhang *et al.*, 2011; *C. albicans* myo2; Woo *et al.*, 2003). In *U. maydis* class V myosin, myo5 (Weber *et al.*, 2003), is involved in establishing the filamentous morphology and tip growth (Schuchardt *et al.*, 2005; Schuster *et al.*, 2011d).

Dynein

The involvement of two oligomers, dynein and its effector, dynactin, in the morphology and cytology of hyphae was reported in *N. crassa* (Plamann *et al.*, 1994; Riquelme *et al.*, 2000), where mutants deficient in each of the proteins were manifesting frequent loss of growth directionality, slow growth and disturbance in Spitzenkörper formation and positioning. In *U. maydis* conditional mutants of dynein heavy chain, dyn2 (contains MT-binding site; Straube *et al.*, 2001), showed defects in hyphal growth, where hyphae were ~50% shorter in comparison to the wildtype (Fuchs *et al.*, 2005a). This defect in hyphal morphology has been linked to dynein role in nuclear migration (Straube *et al.*, 2001; Fuchs *et al.*, 2005a). Dynein accumulation found in the hyphal apex of *U. maydis* ('dynein loading zone'; Lenz *et al.*, 2006; Steinberg, 2012) and of *A. nidulans* (Xiang *et al.*, 1995; Han *et al.*, 2001; Abenza *et al.*, 2009) is though as a component of endocytic recycling machinery also necessary for hyphal growth (Abenza *et al.*, 2009).

1.2.3 Endocytosis and tip growth

Fast and polarized fungal tip growth not only requires synthesis and extension of cell wall, delivery of secretory vesicles containing components of the cell wall like glucans and chitin (Bartnicki-Garcia, 1968; Ruiz-Herrera *et al.*, 1996; Ruiz-Herrera *et al.*, 2008), but also needs the recycling of membrane proteins and lipids which is triggered by endocytosis (Wedlich-Söldner *et al.*, 2000; Fuchs *et al.*, 2006; Shaw *et al.*, 2011). Although endocytosis has been found in yeast *S. cerevisiae* (Makarow, 1985) and endocytic machinery has been discovered in budding yeast (Geli and Riezman, 1998), the existence of internalization during hyphal growth was unclear (Read and Kalkman, 2003). Interestingly, an endocytosis-like process has been recently found in a budding bacterium *Gemmata obscuriglobus* where internalized proteins were associated with vesicles (Jermy, 2010; Lonhienne *et al.*, 2010).

First indirect evidence for endocytosis during polar fungal growth was delivered by experiments with the amphiphilic styryl dye FM4-64, a membrane-selective marker of endocytosis, which was rapidly internalized by growing hyphal tip and

delivered to the fungal vacuole via the endocytic pathway (Hoffmann and Mendgen, 1998; Steinberg *et al.*, 1998a; Fischer-Parton *et al.*, 2000; Wedlich-Söldner *et al.*, 2000). In *U. maydis*, which genome encodes most components of the endocytic machinery (Fuchs and Steinberg, 2005b), first outstanding evidence for occurrence of the endocytosis process during pathogenic development was delivered by Fuchs *et al.*, 2006, who found that pheromone receptor Pra1, necessary for recognition of mating, is constitutively endocytosed from plasma membrane to vacuoles via EEs. Disruption of an endosomal putative target soluble *N*-ethylmaleimide-sensitive fusion protein attachment protein receptor (t-SNARE), Yup1 (Wedlich-Söldner *et al.*, 2000), which controls the fusion of endocytic vesicles with EEs, led to defects in endocytosis, conjugation hyphae formation, polarized growth and in cell-cell recognition (Fuchs *et al.*, 2006). Additional evidence for endocytosis occurrence in filamentous fungi was found in *A. nidulans* (Penalva, 2005), *Aspergillus oryzae* (Higuchi *et al.*, 2006), *Fusarium graminearum* (Kim *et al.*, 2009) and was reviewed in Penalva, 2010 and in Shaw *et al.*, 2011. Polarized tip growth mediates also growth and motility of neurites in higher eukaryotes (Cosker *et al.*, 2008; Tang, 2008; Shieh *et al.*, 2011) and pollen and root hairs in plants (Voigt *et al.*, 2005; Campanoni and Blatt, 2007; Du and Chong, 2011; Richter *et al.*, 2011). Interestingly, polarized tip growth has been linked to endocytosis recently in fast-growing pollen and root hairs in plants, where polar endosomal recycling was shown to facilitate polar tip growth in *Arabidopsis thaliana* (Richter *et al.*, 2011). This is in agreement with the previous study in *U. maydis* (Wedlich-Söldner *et al.*, 2000) and in agreement with the Apical Recycling Model proposed by Shaw *et al.*, 2011, where balance between endocytosis and exocytosis at the hyphal tip controls growth and cell shape of growing tip. This also raises more questions whether bidirectional motility of EEs might support the pathogenic development of *U. maydis* and other filamentous fungi.

1.3 Early endosomes

EEs are small, irregularly shaped, intracellular membrane-bound compartments usually located in the periphery of the animal cell (Parton *et al.*, 1992; Wilson *et al.*, 2000); they also cluster at growth sites in plants (Voigt *et al.*, 2005). EEs are compartments of the endocytic pathway. They receive transport vesicles from the plasma membrane and either send them back to the plasma membrane (recycling) or to recycling endosomes, or via late endosomes to the lysosomes for degradation. Thus, EEs are involved in sorting of endocytosed material. In addition, EEs are involved in signalling between the plasma membrane and the nucleus by transporting of effector proteins mediating signal transduction (reviewed in Platta and Stenmark, 2011), which was reported in plants (Geldner *et al.*, 2007; Raikhel and Hicks, 2007; Viotti *et al.*, 2010) and in animals (Hayes *et al.*, 2002; Miaczynska *et al.*, 2004). So far, there is no direct evidence for such a role of EEs in fungi, although blockage of fusion of endocytic vesicles carrying pheromone receptor with EEs (by disrupting t-SNARE Yup1) provided first indirect evidence for a signalling role of EEs in filamentous fungi (Fuchs *et al.*, 2006). It is though that bidirectional motility of EEs in *U. maydis* serves for communication purposes with the distantly localized nucleus (Steinberg, 2007c).

1.3.1 Long-distance and bidirectional transport of EEs

EEs transport endocytosed material over long distances. Their ATP-dependent bidirectional motility along MTs has been reconstituted *in vitro* (Pollock *et al.*, 1998; Bananis *et al.*, 2000; Murray *et al.*, 2000) and reported *in vivo* in animals (Clarke *et al.*, 2002; Hoepfner *et al.*, 2005; Driskell *et al.*, 2007; Loubery *et al.*, 2008; Soppina *et al.*, 2009; Huckaba *et al.*, 2011) and in hyphae of filamentous fungi (Wedlich-Söldner *et al.*, 2000; Higuchi *et al.*, 2006; Abenza *et al.*, 2009; Zekert and Fischer, 2009; Penalva, 2010; Egan *et al.*, 2012a). Fast motility of EEs has been also observed in plants during root hair formation in *Medicago truncatula* and in *A. thaliana*, although this motility was actin-based (Voigt *et al.*, 2005).

In *U. maydis*, rapid, bidirectional motility of EEs was first observed by using Yup1 (Wedlich-Söldner *et al.*, 2000). Organelles labelled with Yup1-GFP were colocalized with the endocytic dye FM4-64 and their motility was abolished by using a MT inhibitor (benomyl), but not an actin inhibitor (cytochalasin D). The involvement of Yup1 in endosome movement and in mediating of fusion of incoming endocytic vesicles with EEs (endocytic membrane fusion) was discovered by using of *yup1*^{ts} (Wedlich-Söldner *et al.*, 2000). Disruption of EE motility by using *yup1*^{ts} under restrictive conditions led to a cell separation defect and impairment of polar growth as a result of a defect in secretion of cell wall components (Wedlich-Söldner *et al.*, 2000). Subsequently, the endosomal identity of the Yup1-binding membranes was confirmed by localising Rab5a to the moving organelles (Fuchs *et al.*, 2006). Their bidirectional motility has been studied in great detail in *U. maydis* and revealed that this mechanism is a stochastic process (Schuster *et al.*, 2011a), based on transient binding and dissociation of the retrograde motor, dynein, to EEs (Schuster *et al.*, 2011b).

1.3.2 EE specific markers

PI(3)P

EE membranes are enriched in phosphatidylinositol 3-phosphate (PI(3)P; Gillooly *et al.*, 2000) and it is suggested that the exclusive presence of this phosphoinositide on EEs, but not on endocytic vesicles, serves the directionality of the fusion reaction and to recruit the endosomal sorting machinery (Roth, 2004). The evidence that *U. maydis* EE membranes are indeed enriched in PI(3)P was delivered by a lipid overlay assay where the FYVE domain of Don1, an endosomal protein, was used (Schink and Bölker, 2009). Many proteins found on EEs are bound through the recognition of EE specific lipid PI(3)P. Among domains being able to specific recognition of this phosphoinositide are the FYVE (Kutateladze *et al.*, 1999; Misra and Hurley, 1999; Driscoll, 2001; Gillooly *et al.*, 2001) and the PX domains (Bravo *et al.*, 2001; Xu *et al.*, 2001; Seet and Hong, 2006), reviewed in Lemmon, 2008.

EEA1

EEA1 (an early endosomal antigen; Mu *et al.*, 1995) is a ubiquitous marker of EEs found in higher eukaryotes but not in filamentous fungi, although Pep7 is considered as EEA1 homologue in the yeast *S. cerevisiae*. EEA1 decorates a subset of EEs (Wilson *et al.*, 2000) through direct binding with PI(3)P (Stenmark *et al.*, 1996) and Rab5 (Lawe *et al.*, 2000) via its FYVE domain.

Yup1

The other EE marker is Yup1, a t-SNARE-like protein (homologue of *S. cerevisiae* Vam7p) found in *U. maydis*, which uses its N-terminal PX domain for direct interaction with EE lipids (Wedlich-Söldner *et al.*, 2000).

Rab4 and Rab5

The conserved group of Ras-associated binding (Rab) proteins, small GTPases can be found in the entire tree of life. Among the large group of Rab proteins (Rojas *et al.*, 2012), Rab4 and Rab5 are the main EE markers (van der Sluijs *et al.*, 1991; Bucci *et al.*, 1992; Bananis *et al.*, 2003); Rab homologues have been found in plants (Ara7/Rha1; Ueda *et al.*, 2004) and surprisingly even in bacteria (Yutin *et al.*, 2009). Rab5 proteins have been also found in *U. maydis* (Fuchs and Steinberg, 2005b) where the role of Rab5a as EE marker was confirmed *in vivo* (Fuchs *et al.*, 2006). In *A. nidulans* EEs have two Rab5 markers: RabA and RabB (Abenza *et al.*, 2009) and deletion of RabB prevents EE movement (Abenza *et al.*, 2010). Rab5 proteins, despite a marker role, are the master regulators of the endocytic machinery: they control fusion between EEs (Gorvel *et al.*, 1991) and are involved in EE docking (Christoforidis *et al.*, 1999) and targeting motor protein recruitment (Hoepfner *et al.*, 2005; Jordens *et al.*, 2005; Ueno *et al.*, 2011). By stimulating local production of endosomal lipid PI(3)P, Rab5 regulates motility of EEs on MTs (Nielsen *et al.*, 1999). Additionally, Rab5 proteins are essential for the biogenesis of the endolysosomal system (Zeigerer *et al.*, 2012), can be involved in mitosis (Lanzetti, 2012) and can promote the switch between MT-based long distance transport of vesicles and organelles to short, F-actin dependent transport (Caviston and Holzbaur, 2006). In neurons, Rab5a proteins were detected in axons and dendrites and were colocalized with

EEs and with a subpopulation of synaptic vesicles containing synaptophysin, which indicates, that the axonal endosomes participate in the biogenesis of synaptic vesicles or that synaptic vesicles are able to fuse with the endosomal compartment (de Hoop *et al.*, 1994); additionally they are essential for efficient signal transmission across synapses through preventing homotypic fusion between synaptic vesicles (Shimizu *et al.*, 2003). Unfortunately none of the above roles of Rab5 other than marker function has been studied in *U. maydis*.

1.3.3 EE involvement in cellular processes – universal platforms

It is well known that EEs are the first endocytic station and serve to sort incoming signals and cargo from the outside of the cell for recycling or degradation. In addition, EEs are involved in other processes thanks to the attached proteins which make EEs kind of universal platforms involved in distinct cellular processes (summarized in Fig. 3).

1.3.3.1 EE involvement in cellular processes in sporidia

Mating – pheromone recycling – Pra1 and Yup1

As mentioned previously, pheromone receptor Pra1 (Fig. 3, red), necessary for the recognition process of two compatible haploid cells (mating), is constitutively endocytosed from the plasma membrane to vacuoles via EEs (Fuchs *et al.*, 2006) and after disruption of the endosomal t-SNARE Yup1 (Fig. 3, aquamarine; Wedlich-Söldner *et al.*, 2000) Pra1 does not reach the vacuoles (Fuchs *et al.*, 2006). In addition, *yup1*^{ts} deactivation leads to a defect in EE motility, cell separation and polar growth (Wedlich-Söldner *et al.*, 2000). This impairs the conjugation hyphae formation, polarized growth and cell-cell recognition (Fuchs *et al.*, 2006) resulting in defects of pathogenic development. It is tempting to speculate that bidirectional motility of EEs could additionally serve as a kind of sensor of the environment (Bahn *et al.*, 2007).

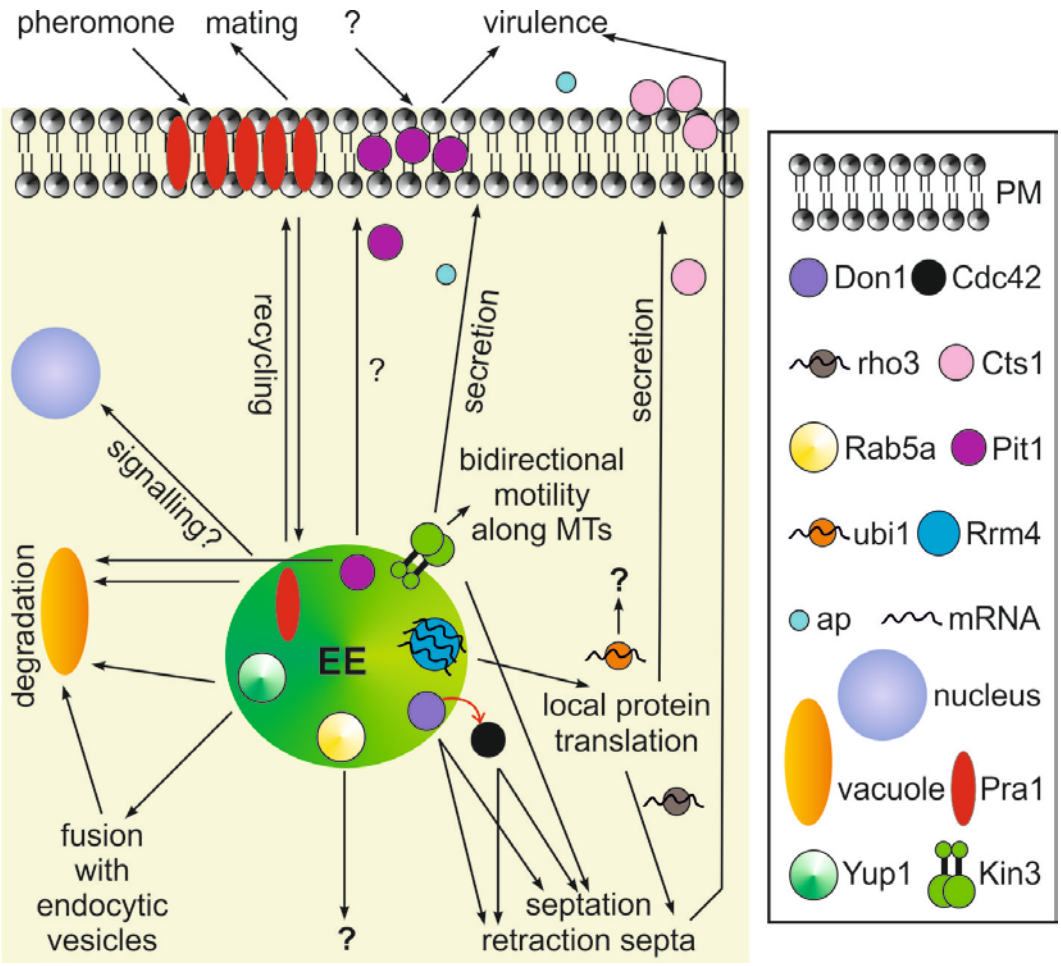

Figure 3. Scheme of EE involvement in cellular processes in *U. maydis* based on known EE-interacting proteins.
Description can be found in the text below. Abbreviations: PM, plasma membrane; Kin3, kinesin-3; ap, acid phosphatase. Red arrow indicates activation of Cdc42 by its GEF specific protein, Don1. For the simplicity the cell wall is not shown and the proportions in the size of organelles are not kept.

EEs support septum formation – the role of Kin3, Don1, Cdc42

The last step of cytokinesis in *U. maydis*, separation between yeast-like sporidia, mother and daughter cells, requires the formation of two distinct septa delimiting a vacuolar fragmentation zone, where breakdown of the cell wall occurs thus allowing dissociation of mother and daughter cells (Weinzierl *et al.*, 2002). The failure in physical separation between relative haploid cells results in a cell separation defect (CSD) where tree-like aggregates are formed in liquid culture and *U. maydis* colonies form typical 'donut' structures on a solid medium. This defect in morphology phenotype was found among others in *kin3* (Fig. 3, green; Wedlich-Söldner *et al.*, 2002), *don1* (Fig. 3, navy; a GEF specific for Cdc42; Weinzierl *et al.*, 2002; Hlubek *et al.*, 2008), *cdc42* (Fig. 3, black;

small GTP-binding protein of the Rho family; Mahlert *et al.*, 2006) and *drf1* mutants (Freitag *et al.*, 2011). In the case of the *kin3* mutant two septa are formed between mother and daughter cells (Wedlich-Söldner *et al.*, 2002), but in cells defective for either *don1*, *cdc42* on *drf1* only a single septum is formed suggesting that these proteins are necessary in secondary septum formation required for proper cell separation (Weinzierl *et al.*, 2002; Mahlert *et al.*, 2006; Freitag *et al.*, 2011). Interestingly, among the proteins necessary for secondary septum formation only Cdc42 is essential for pathogenic development (Mahlert *et al.*, 2006). Although a null *don1* mutant showed reduced virulence (Freitag *et al.*, 2011), Don1 is not required for mating, filamentous growth of the dikaryon, spore production or pathogenic development *in planta* (Weinzierl *et al.*, 2002).

Accumulation of EEs labelled with Yup1-GFP or Don1-GFP in the fragmentation zone between mother and daughter cell and between primary and secondary septum suggests involvement of these organelles in septum formation and cytokinesis (Schink and Bölker, 2009; Fig. 4). Don1 protein interacts with EEs via its lipid binding domain, FYVE, and specifically recognizes PI(3)P lipids on EEs (Schink and Bölker, 2009). The FYVE domain is critical for efficient targeting of the GEF Don1 to the site of septation (Schink and Bölker, 2009), but the presence of Don1 is not required for correct septation (Mahlert *et al.*, 2006). Don1 triggers cell separation by activating the small GTPase Cdc42; a constitutive active variant $Cdc42^{Q61L}$ is able to suppress the CSD in *don1* null cells (Mahlert *et al.*, 2006). Overexpression of Don1 lacking a functional FYVE domain rescues CSD which suggests that the presence of Don1 is not required for Don1 GEF activity (Schink and Bölker, 2009), therefore it is now not clear how important is motility of the EEs for the septum formation. During cytokinesis EEs accumulate at both sides of the septum when the primary septum is formed (Fig. 4E). After closure of the primary septum, EEs accumulate only at the daughter side of the septum (Fig. 4F) where Don1 initiates secondary septum formation and formation of the vacuolated fragmentation zone between mother and daughter cell. Finally, when the secondary septum is formed (Fig. 4G), EEs are enclosed within the developing fragmentation zone between the two septa (Schink and Bölker, 2009).

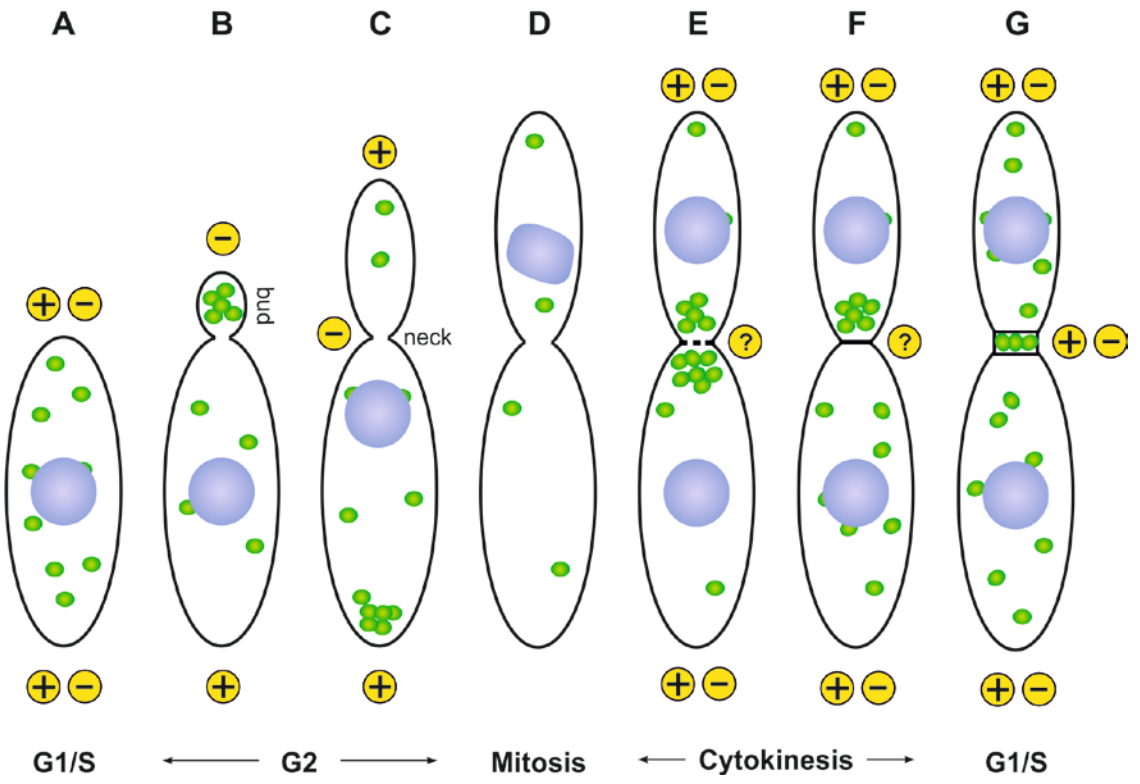

Figure 4. Distribution of EEs during the cell cycle in yeast-like cells of *U. maydis*. The figure was adopted from (Wedlich-Söldner *et al.*, 2002) and updated by data published in: Steinberg *et al.*, 2001; Banuett and Herskowitz, 2002; Straube *et al.*, 2003; Theisen *et al.*, 2008; Schink and Bölker, 2009. (**A**) In unbudded cells EEs (green spheres) are localized unicellularly and they show bidirectional movement along MTs (orientation of MTs indicated by '+' and '–'; for simplicity MTs are not shown); nucleus is localized centrally in the cell. (**B**) Polar budding is accompanied by the formation of an EE cluster at the minus-end of the MTs which are localized only in a small bud; EE motility is significantly enhanced towards the bud; nucleus is localized centrally in the cell. (**C**) In a medium-budded cell EE clusters are localized at their rear cell pole; the nucleus is shifted towards the neck. (**D**) Mitosis starts when the proper bud size is reached; prior to mitosis the nucleus migrates into the bud (metaphase stage is shown); EEs are dispersed and they do not move as cytoplasmic MTs (but not astral MTs) are depolymerised. (**E**) During formation of the primary septum between mother and daughter cell EEs accumulate at both sides of the septum; EE motility occurs in both direction within mother and daughter cells and nuclei are localized centrally in the cells. (**F**) After closure of the primary septum, accumulation of EEs occurs solely at the daughter side of the septum; EE motility occurs in both direction within mother and daughter cells and nuclei are localized centrally in the cells. (**G**) During formation of the secondary septum, EEs are enclosed within the developing fragmentation zone between the two septa; EE motility occurs in both directions within mother and daughter cells and nuclei are localized centrally in the cells.

A recent study on the establishment of filamentous growth in *U. maydis* revealed an additional gene, Rrm75, which encodes an RNA binding protein and is involved in dimorphism and virulence, and is upregulated during hyphal

development (Rodriguez-Kessler *et al.*, 2012). Interestingly, mutants deleted for Rrm75 showed a donut-like morphology on solid medium which suggests the presence of a cell separation defect observed previously in *don1* (Weinzierl *et al.*, 2002) and *kin3* mutants (Wedlich-Söldner *et al.*, 2002), therefore the evidence of impairment of EE traffic in *rrm75* mutants should be only a matter of time.

1.3.3.2 EE involvement in cellular processes in hyphae

If the pheromone recognition and mating are successful, filamentous growth is induced (Spellig *et al.*, 1994a) and the cell cycle of the dikaryon filament is arrested in pre-mitotic G2 stage (Garcia-Muse *et al.*, 2003). In addition to the role in the septum formation in sporidia, EEs are involved in processes necessary for hyphal extension, where EEs are needed to overcome long distance to deliver proteins described below:

Pit1 – protein of unknown function

Pit1 (Fig. 3, purple), a transmembrane protein belonging to a newly discovered gene cluster, ‘protein important for tumor’, is upregulated during biotrophic development and specifically expressed in filaments that form appressoria, where Pit1 accumulates. In addition, Pit1 colocalizes with EEs, vacuoles and plasma membrane and mutants depleted of *pit1*, although still able to proliferate inside the plant, are completely avirulent (Doehlemann *et al.*, 2011). Interestingly, Pit1 is thought to act in the pathway of receptor mediated endocytosis to trigger the uptake of an unknown apoplastic ligand or to have a function which requires continuous replacement of the protein (Doehlemann *et al.*, 2011).

Post-transcriptional control – the role of Rrm4

Fast growing hypha might require locally translated proteins, therefore the role of the RNA-binding proteins, e.g. Rrm4 (Fig. 3, blue), in filamentous growth and pathogenicity of *U. maydis* (Becht *et al.*, 2005; Becht *et al.*, 2006) through

localized translation of proteins involved in maintaining polarity is not a surprise. RNA-binding proteins associated with accessory factors recognise their target mRNA and deliver mRNA to their designated localization within the cell in the form of ribonucleoprotein complexes (mRNPs; reviewed in Zarnack and Feldbrügge, 2010). Local translation of proteins involved in local cellular processes is more efficient, additionally controlled and contributes to the establishment of polarity, asymmetric division and migration during development (reviewed in Zarnack and Feldbrügge, 2010; Jung *et al.*, 2012). As binding of Rrm4 proteins with poly(A)-binding protein Pab1 to a distinct set of CA-rich mRNAs encoding, e.g. polarity factors (small G protein Rho3 and the septin Cdc3; König *et al.*, 2009), translation factors and mitochondrial proteins (König *et al.*, 2009; Vollmeister and Feldbrügge, 2010) was not surprising, their bidirectional shuttling via EEs (Baumann *et al.*, 2012) is a phenomenon. The binding between Rrm4 and RNA and recruitment of Rrm4 into particles is increased during filamentation (Becht *et al.*, 2006). Rrm4 does not need its RNA-binding domain to be transported by EEs, therefore Rrm4 is considered as an integral component of the transport machinery (König *et al.*, 2009). Mutants depleted of *rrm4* are affected in filamentous growth and pathogenicity (Becht *et al.*, 2005). Deletion of *rrm4* or its RNA-binding domain disturbs polar growth of the filaments (Becht *et al.*, 2006) similarly to *kin1*Δ mutants, where short, bipolar hyphae depleted of vacuolated hyphal parts were observed (Schuchardt *et al.*, 2005).

One of the transcripts upregulated during filamentous growth and transported by EE-Rrm4 (in mRNP complex) is mRNA encoding a ribosomal protein Ubi1 (Fig. 3, orange; a natural fusion protein of ubiquitin and Rpl40, the large ribosomal subunit; König *et al.*, 2009) which contains a CA-rich 3' untranslated region (UTR) recognized by Rrm4. It is assumed that it serves as a zipcode during Rrm4-dependent mRNA transport (König *et al.*, 2009). The function of Ubi1 is unknown.

The role of Rrm4 in secretion of endochitinase Cts1

Recently, Rrm4 has been linked to the polarized secretion of a cell wall remodelling enzyme, an endochitinase Cts1 (Fig. 3, pink; Koepke *et al.*, 2011). mRNA encoding Cts1 is transported with Rrm4-EE complex to the growth cone

where it is secreted and associated most likely with the cell wall of hypha; secretion of Cts1 is drastically impaired in filaments lacking Rrm4, but is dispensable for the regulation of morphology and pathogenicity (Koepke *et al.*, 2011).

The role of Kin3 in secretion of acid phosphatase

Kin3 (Fig. 3, green) is almost always associated with EEs (Schuster *et al.*, 2011b; Schuster *et al.*, 2011c) and can be considered as one of EE cargoes. Deletion of *kin3*, despite impairing long distance transport of EEs and extended hyphal growth, leads to a reduction in secretion of acid phosphatase by 50% (Fig. 3, light blue; Schuchardt *et al.*, 2005), which implies that EEs might be involved in secretion.

Formation of the retraction septa - the role of Don1, Cdc42 and Rho3

The distal end of the hypha contains vacuolated compartments devoid of cytoplasm which are thought to be crucial for the formation of the empty sections necessary for supporting cytoplasmic migration during the growth of dikaryotic hyphae (Steinberg *et al.*, 1998a). Empty compartments that are left behind are divided and isolated from the rest of the hypha by retraction septa what enables high-speed growth of infectious filament and allows covering long distances. Formation of distal retraction septa depends on actomyosin ring formation by formin Drf1, an effector of Cdc42 GTPase, Don1 (Fig. 3, navy) and Don3 implying EE-bound Don1 in such process (Freitag *et al.*, 2011). Deletion of *drf1* or *don1* genes abolishes formation of retraction septa, long filament formation and leads to reduced virulence (Freitag *et al.*, 2011).

In addition, accumulation of the polarity factor, Rho3 in retraction septa is dependent on EE-Rrm4 transport of *rho3* mRNA transcript (Fig. 3, grey; König *et al.*, 2009). Formation of distal retraction septa is also critical for appressorium formation and virulence in *U. maydis* (Freitag *et al.*, 2011).

1.3.4 Molecular motors involved in EE transport

Motility of EEs, well documented in *U. maydis* and *A. nidulans*, involves kinesin-3 and dynein (Wedlich-Söldner *et al.*, 2002; Lenz *et al.*, 2006; Zekert and Fischer, 2009; Zhang *et al.*, 2010; Yao *et al.*, 2011; Egan *et al.*, 2012a). The same pair of molecular motors (dynein and DdUnc-104) is involved in EE bidirectional movement in *Dictyostelium discoideum* (Pollock *et al.*, 1999; Soppina *et al.*, 2009). In higher organisms human kinesin-3 homologue KIF16B (Hoepfner *et al.*, 2005), *Drosophila melanogaster* kinesin-3 homologue Khc73 (Huckaba *et al.*, 2011) and kinesin-1 from rat and mouse liver (Bananis *et al.*, 2000; Nath *et al.*, 2007) and from human (Nielsen *et al.*, 1999; Loubery *et al.*, 2008) have been shown as involved in plus-end directed motility of EEs, whereas minus end-directed motility of EEs is mediated by a retrograde kinesin-14B family member KIFC2 in rat liver (Bananis *et al.*, 2003), KIFC1 in mouse liver (Nath *et al.*, 2007) or in most cases by dynein (Driskell *et al.*, 2007; Loubery *et al.*, 2008). In neurons kinesin-1 and dynein trigger bidirectional EE motility (Satoh *et al.*, 2008; Lloyd *et al.*, 2012).

In *U. maydis* each EE contains one dynein and three to five Kin3 on its membrane (Schuster *et al.*, 2011b), whereas transport of endosomes from *D. discoideum* utilizes 1-2 kinesins-3 (DdUnc-104) and 4-8 dyneins (Soppina *et al.*, 2009). Although dynein is a retrograde motor, the retrograde motility of EEs in *U. maydis* is dynein-dependent only in the first 10-20 µm from the tip and later Kin3 takes the control (Schuster *et al.*, 2011c). Comet-like accumulation of ~55 dynein motors at MT plus-ends serve as a capturing and loading station for incoming EEs thus preventing their ‘falling off’ from MTs and ensuring continuation of their bidirectional motility (Lenz *et al.*, 2006; Abenza *et al.*, 2009; Schuster *et al.*, 2011a; Schuster *et al.*, 2011b). Dynein, which can leave the plus end of MTs without EEs (Schuster *et al.*, 2011a), must be actively transported back by conventional kinesin (Zhang *et al.*, 2003; Lenz *et al.*, 2006), therefore Kin1 is indirectly involved in EE transport in fungi but promotes their retrograde motility (Lenz *et al.*, 2006). Recent work revealed that dynein and kinesin-3 motors cooperate in EE retrograde motility which allows long-distance transport of EEs (Schuster *et al.*, 2011c). Inactivation of Kin3 by using a fast reacting temperature sensitive allele stops all long-range EE motility (Schuster

et al., 2011c), therefore Kin3 can be named the main transporter of EEs. Although the importance of kinesin-3 motors in membrane trafficking is well documented, the interaction of the motor with its cargo is not well understood.

1.4 Kinesin-3 is a major membrane transporter

In squid axons, movement of membranous organelles was visualised by video-enhanced differential interference contrast microscopy (Allen *et al.*, 1982). Electron-microscopy studies showed 10-20 nm long cross-bridges between MTs and membranous organelles, which suggests that proteins are involved in the motility of organelles (Hirokawa, 1982). Shortly after, a mechano-enzyme was identified which was able to move beads and vesicles along MTs and was therefore named ‘kinesin’ (Miller and Lasek, 1985; Vale *et al.*, 1985). Since MT orientation in axons and in dendrites was described (Heidemann *et al.*, 1981; Baas *et al.*, 1988) and anterograde directed motility on MTs was shown as ATP-dependent (Vale *et al.*, 1985; Vale and Milligan, 2000), huge progress in the kinesin field has been made. The first kinesin-3 family member, CeUnc-104, was discovered by a genetic screen of the nematode *Caenorhabditis elegans* mutants, which were not able to move in a fast and coordinated way (Otsuka *et al.*, 1991). Moreover, the observed number of synaptic vesicles and synapses was reduced in axons, which suggested that CeUnc-104 is a neuron-specific motor used for anterograde transport (Hall and Hedgecock, 1991; Nonet, 1999). The homologue of Unc-104, KIF1A, which is expressed almost exclusively in brain, was discovered a year later by screening of murine brain cDNA by PCR amplification (Aizawa *et al.*, 1992). Most mice deficient in KIF1A died within a day after birth showing motor and sensory disturbances as a result of neuronal degeneration of axons due to the decreased transport of synaptic vesicle precursors, decreased density of synaptic vesicles in nerve terminals and accumulation of clustered vesicles in neuronal cell bodies (Yonekawa *et al.*, 1998). The low angle rotary-shadowing electron micrography pictures have demonstrated that KIF1A adopts a globular shape with no clearly discernible tail observed (Okada *et al.*, 1995; Hirokawa, 1998). Biochemical and biophysical analyses revealed that KIF1A is the fastest (1.2 – 1.5 µm/s *in vitro*) neuronal

anterograde motor which transports various synaptic vesicle proteins (Okada *et al.*, 1995; Nonet *et al.*, 1998; Liu *et al.*, 2012). Confirmation of the role of CeUnc-104 and rat KIF1A in vesicle transport *in vivo* was derived by expression of fusion proteins tagged by GFP (Zhou *et al.*, 2001; Lee *et al.*, 2003). CeUnc-104-GFP fusion proteins were able to rescue the *unc-104* mutant phenotype and were visualized as fluorescent puncta moving bidirectionally along axons and dendrites *in vivo* (Zhou *et al.*, 2001). Bidirectional motility of KIF1A-GFP was also observed in living cultured hippocampal neurons where most motors were moving anterogradely along the neurites with an average velocity of 1.0 µm/s and 17% of KIF1A-GFP motors exhibited retrograde movements of 0.72 µm/s (Lee *et al.*, 2003). Similar results were obtained for a fusion protein of *D. melanogaster*, DmUnc-104, where bidirectional motility of the tagged protein with a mean anterograde velocity of 1.05±0.08 µm/s was observed (Barkus *et al.*, 2008).

Immunofluorescence staining and EM confirmed the localization of KIF1A in both dendrites and axons, suggesting that KIF1A plays a role in both dendritic and axonal transport in neurons (Shin *et al.*, 2003) which was recently confirmed by others (Huang and Banker, 2012; Jenkins *et al.*, 2012). This supports the notion that KIF1A (and KIF1B) are not selective motors and are found in both axons and dendrites termini. Although kinesin-3 is a plus-end directed motor, the anterograde movement of KIF1A does not lead to a detectable accumulation of the kinesin-3 motors in the periphery of neurons which was explained by a potential degradation process that KIF1A must undergo after reaching the synapse (Okada *et al.*, 1995; Lee *et al.*, 2003) or an inactivation process suggested by others (Goldstein and Yang, 2000; Lee *et al.*, 2003). Indeed, as shown recently (Kumar *et al.*, 2010), CeUnc-104 does not go back after reaching the synapse and is degraded most probably through the ubiquitin pathway.

1.4.1 Kinesin-3 in *U. maydis*

U. maydis kinesin-3 (Kin3; 1676 aa) is a homologue of KIF1A/Unc-104 and was discovered by PCR amplification using primers designed against the motor

domain of KIF1A/Unc-104 kinesins (Wedlich-Söldner *et al.*, 2002). Kin3 moves along MTs and is responsible for anterograde motility of EEs (Wedlich-Söldner *et al.*, 2002; Lenz *et al.*, 2006). Deletion of the N-terminal part of Kin3 (aa 12-885) leads to a reduction of EE motility (to ~33%; Wedlich-Söldner *et al.*, 2002), EE clustering, defects of polar growth (mono-polar budding pattern) and cell separation (tree-like cell aggregates). In yeast-like cells residual EE motility is dynein-dependent (Wedlich-Söldner *et al.*, 2002) whereas the inactivation of a temperature sensitive kin3^{ts} allele stopped all long-range EE motility in hyphal cells (Schuster *et al.*, 2011c). During filamentous growth *kin3* is upregulated and deletion of *kin3* (aa 12-885) leads to bipolar and short hyphae formation (Schuchardt *et al.*, 2005) and clustering of EEs around the nucleus (Lenz *et al.*, 2006). On the other hand, depletion of dynein by using *dyn2*^{ts} 'strengthens' anterograde motility of EEs which leads to EE accumulation at MT plus ends (Lenz *et al.*, 2006) which is consistent with an anterograde role of Kin3 in organelle transport. Kin3 colocalizes with all moving EEs in both directions (Lenz *et al.*, 2006; Schuster *et al.*, 2011b). During bidirectional movement of EEs, >95% of all Kin3-GFP signals are located on these organelles (Schuster *et al.*, 2011b; Schuster *et al.*, 2011c) which suggests that the phenotype of kinesin-3 deletion mutants is associated with a defect in EE transport. The number of Kin3 bound to a single EE during anterograde motility equals three to five Kin3 dimers (Schuster *et al.*, 2011b). In addition, Kin3 participates in secretion which was shown in *kin3* null mutant where 50% reduction in secretion of acid phosphatase was found (Schuchardt *et al.*, 2005). This raises the possibility that Kin3 has additional roles in the secretion pathway, which would correspond to the role of its close human homologue KIF1A.

1.4.2 Kinesin-3 organization and regulation

U. maydis Kin3 is a molecular motor belonging to the Kinesin superfamily (KIFs) which is divided into 15 families (termed kinesin 1 to kinesin 14B) depending on the homology within a ~350 amino acids motor domain containing an ATP- and a MT-binding site and on multiple sequence comparisons of the nonmotor domain (Hirokawa, 1998; Miki *et al.*, 2001; Lawrence *et al.*, 2004; Hirokawa *et*

al., 2009). Thus, based on the overall structure in domain organization (shown in Fig. 5), Kin3 belongs to the Kinesin-3 family (Wedlich-Söldner *et al.*, 2002). Members of this family possess a highly conserved motor domain localized at the N-terminus (Fig. 5; motor), which allows them to drive MT plus end-directed transport (Hirokawa, 1998). The tail region is composed of the forkhead associated domain (FHA; Westerholm-Parvinen *et al.*, 2000), coiled-coil regions (Fig. 5; CC), DUF3694 (domain of unknown function; based on Pfam protein prediction; http://pfam.sanger.ac.uk/family/duf3694; Fig. 5; DUF3694) and the PH, PX or Cap-Gly domain (Fig. 5). In most cases the distal part of the tail region has been found to be involved in cargo binding and the proximal part of the tail as an autoregulation region responsible also for dimerization (see below).

1.4.2.1 The distal part of the kinesin-3 tail is responsible for cargo binding.

Despite having such a high similarity in the domain organization (Fig. 5), proteins of the Kinesin-3 family transport different cargoes. Mammalian KIF1A and *C. elegans* CeUnc-104 bind to vesicle precursors and presynaptic vesicles. KIF1Bβ, another Kinesin-3 family protein, obtained by alternative splicing of KIF1B (Matsushita *et al.*, 2009) requires its tail region (aa 885–1770) for association with presynaptic vesicles (Zhao *et al.*, 2001). *D. melanogaster* DmUnc-104 transports small transport vesicles (STVs) and large dense-core vesicles (DCVs; Barkus *et al.*, 2008), while HsKIF1Bα (Nangaku *et al.*, 1994) and *N. crassa* NcKin2 (Fuchs and Westermann, 2005) have been found to be involved in transport of mitochondria. Recently, the involvement of the rat KIF1A in bidirectional transport of DCVs (with KIF1A attached to the cargo during retrograde transport) in mammalian neurons has also been shown (Lo *et al.*, 2011).

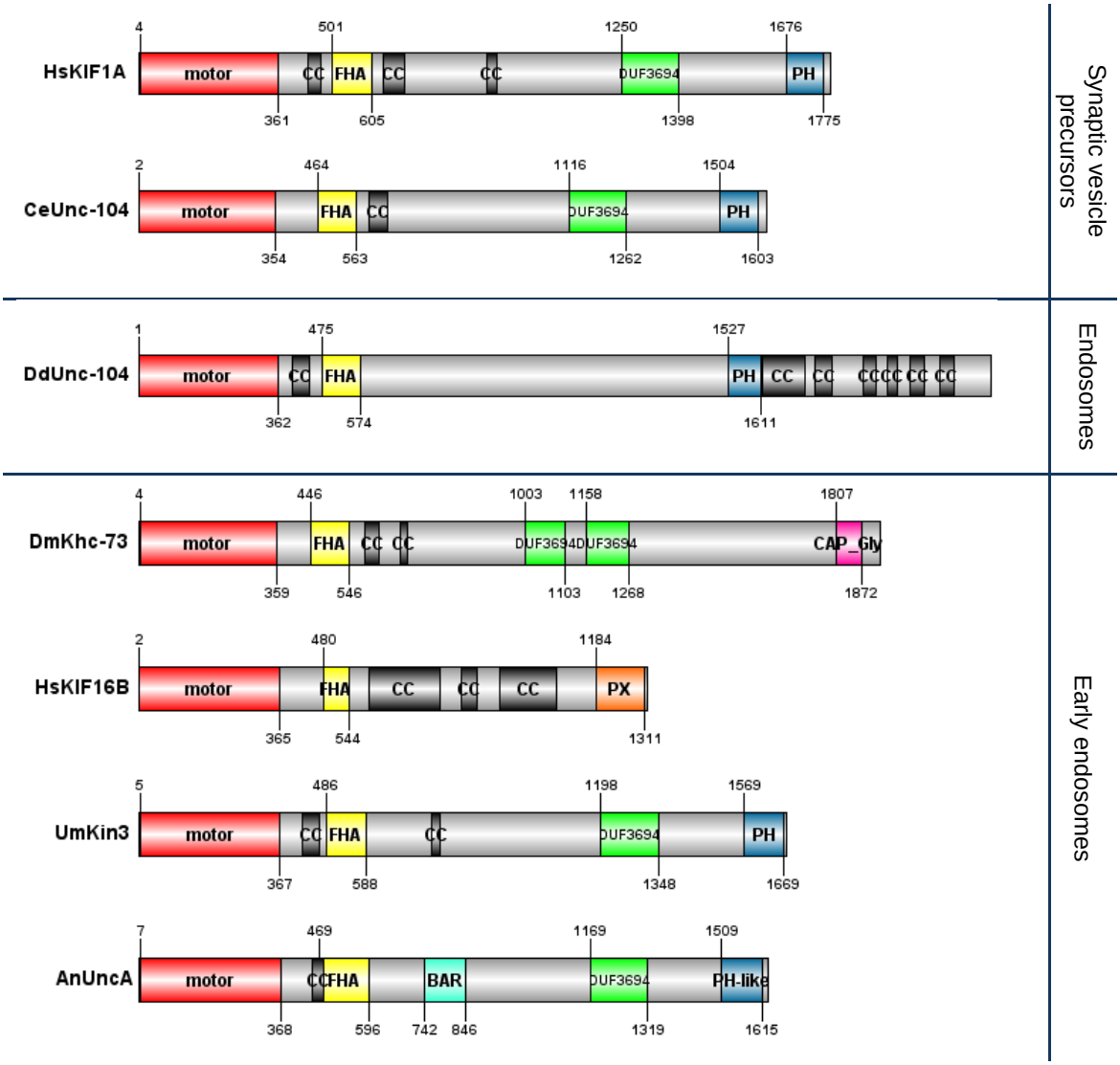

Figure 5. Domain architecture of selected kinesin-3 family proteins.
All kinesins-3 family members presented in this figure contain a motor domain (red) which is localized N-terminally, forkhead associated domain (FHA; yellow) and coiled-coil domains (CC; black). Additionally most of them comprise DUF3694 (Domain of Unknown Function based on Pfam prediction; green) and the pleckstrin homology domain (PH; blue). There are also gene specific domains: Phox domain of human KIF16B (PX; orange), CAP_Gly of *D. melanogaster* Khc-73 (Gly-rich domain; pink) and BAR domain of *A. nidulans* UncA (BAR; cyan). Numbers above and below the domains represent amino acid positions. Accession numbers: human HsKIF1A (NP_001230937), worm *C. elegans* CeUnc-104 (NP_001022041), slime mold *D. discoideum* DdUnc-104 (XP_635456), fly *D. melanogaster* DmKhc-73 (NP_609201), human HsKIF16B (NP_078980), fungi *U. maydis* UmKin3 (XP_762398) and *A. nidulans* AnUncA (XP_680816). The BAR domain of *A. nidulans* UncA covers coiled-coil region. Figure was made using Dog 2.0 software (Ren *et al.*, 2009).

The largest differences in the C-terminal part of the tail region are found in the Kinesin-3 family proteins involved in EE transport. Human KIF16B contains a PX domain instead of the PH domain or DUF3694 (Hoepfner *et al.*, 2005; Blatner *et al.*, 2007) and a long coiled-coil region required for the oligomerization in order of the PI(3)P-targeting (Lemmon, 2003). Indeed, KIF16B uses the PX domain for direct association with endosomal PI(3)P lipids (Hoepfner *et al.*, 2005). *D. melanogaster* Khc-73 contains a CAP-Gly domain (cytoskeleton-associated protein Glycine-rich; Li *et al.*, 1997; Huckaba *et al.*, 2011) and two DUF3694 domains localized in the middle of the tail; by using its C-terminal part of the tail Khc-73 interacts with Rab5-containing endosomes in interphase. *D. discoideum* Unc-104 comprises of a lipid binding PH domain (Klopfenstein *et al.*, 2002) which is localized in front of an extended coiled-coil region required for dimerization (Pollock *et al.*, 1999). Fungal kinesin-3 homologues contain the PH domain (*U. maydis* Kin3; Wedlich-Söldner *et al.*, 2002) and the PH-like domain (*A. nidulans* UncA; Zekert and Fischer, 2009), which, according to NCBI (http://www.ncbi.nlm.nih.gov/), has a PH fold, but lacks a significant sequence similarity. Unfortunately, the role of fungal PH and PH-like domains in lipid binding has not been verified. Additionally, UncA contains the BAR domain which can be involved in membrane binding and membrane shaping (reviewed in Frost *et al.*, 2009).

The presence of different C-terminally localized domains within the proteins involved in the transport of the same cargo (although in different organisms), like KIF16B, Khc-73 and fungal Kin3 and UncA, raises a challenge in defining common cargo binding domains within a class of so differently organized kinesin-3 proteins.

PH domain

PH domains (~120 amino acids) share low sequence similarity (maximum of ~20%; Lemmon, 1999), although their core structure is highly conserved and is composed of a core made of a seven-stranded β-barrel sandwich, an α-helix at the carboxyl terminus and loops between the β-sheets (Lemmon, 1999). The loops and positively charged surface of the domain allows binding to lipids, especially to phosphoinositides (Lemmon, 1999). Such binding to

phosphoinositides by DdUnc-104 and CeUnc-104 PH domains *in vitro* is well documented (Klopfenstein *et al.*, 2002; Klopfenstein and Vale, 2004), however, binding of these motors to the native vesicles is reduced by 40% by protease treatment. This suggests the presence of unknown adaptor proteins that are involved in cargo binding (Pollock *et al.*, 1999; Klopfenstein *et al.*, 2002). The PH domain of KIF1A/KIF1Bβ has been also shown as a binding domain of p75 neurotrophin receptor vesicles in post-Golgi trafficking in non-polarized MDCK cells *in vitro*. However, the overexpression of these PH domains did not inhibit strongly the exit of p75 from the Golgi *in vivo* suggesting that additional regions of the kinesin tails are important for vesicle binding (Xue *et al.*, 2010). Alternatively, the PH domain of CeUnc-104 was suggested to be an ubiquitin binding domain, as truncated CeUnc-104 motors that lack the PH domain are highly expressed and do not undergo ubiquitination (Klopfenstein and Vale, 2004; Kumar *et al.*, 2010). Moreover, studies in *S. cerevisiae* (Lemmon, 2004; Yu *et al.*, 2004) revealed that only a small fraction of known PH domains is able to specific binding to phosphoinositides suggesting that the role of the PH domain in lipid binding might be overestimated or not relevant *in vivo*.

Stalk region

Available evidence on kinesin-3 homologues indicates that the tail is involved in cargo binding. Study on mouse KIF1A and KIF1Bβ showed that the carboxyl terminal part of their tails binds to DENN/MADD protein which next binds to Rab3-GTP localized on the Rab3-carrying vesicles (Niwa *et al.*, 2008). One of the Rab3-GTP interactors is also Liprin-α (SYD-2 homologue), a homomultimer (Taru and Jin, 2011), which has been shown to be a KIF1A (Shin *et al.*, 2003) and CeUnc-104 (Hsu *et al.*, 2011) binding protein necessary during local binding of vesicles in the active zone (Dai *et al.*, 2006) and along the axons (Wyszynski *et al.*, 2002). In addition, the kinesin-3 tail is implied in dimerization and autoinhibition.

1.4.2.2. The proximal part of the kinesin-3 tail is an autoregulation region.

Dimerization and autoinhibition of kinesin-3 proteins are controlled by the proximal part of the tail with the exception of DdUnc-104. Dimerization allows fast processive movement along MTs and autoinhibition blocks the motility in the absence of cargo.

Dimerization

For years, it was debated whether kinesin-3 is a monomer or a dimer. Growing evidence suggests that kinesin-3 exists as a dimer *in vivo* even in the absence of cargo (Hammond *et al.*, 2009). The neck region, localized between the motor domain and first coiled-coil (CC1), is able to perform self-folding in CeUnc-104 *in vitro* and may regulate the monomer to dimer transition required for activation of fast processive motility (Al-Bassam *et al.*, 2003). Similarly, native KIF1A can exist as an inactive monomer and an active homodimer which is formed partially through its neck coiled-coil domain (Rashid *et al.*, 2005). In addition to the neck-CC1 region, direct interaction between CC1 and FHA of KIF1A (aa 430–607) triggers dimerization (Huo *et al.*, 2012) and may prevent additional inhibition mediated by interaction between the CC1 and neck coil (Hammond *et al.*, 2009).

Autoinhibition

KIF1A is able to form a dimer *in vivo* even in the absence of cargo but this requires relieving the autoinhibition occurring between FHA and the second coiled-coil domain (CC2; Lee *et al.*, 2004; Hammond *et al.*, 2009) and between the CC1 and the neck coil (Hammond *et al.*, 2009). The exact mechanism of relieving from the autoinhibition upon binding to the cargo is currently not known. It is also a matter of debate if the cargo binding mechanism is the only switch from the inhibited to activated form (Verhey and Hammond, 2009).

Taken together, it appears that the tail of kinesin-3 motors is involved in regulation of the motor activity, binding to cargo and dimerization of the motor

protein. KIF1A-like kinesin-3 motors contain a PH domain that was shown to bind to lipids typical for secretory vesicles, suggesting that cargo binding of KIF1A-like kinesins is mediated by this domain. However, recent studies in animal systems have suggested that additional regions of the tail are involved in cargo interaction. The importance of the PH domain in lipid binding is further challenged by the fact that fungal KIF1A-like kinesin-3 shares ~40% identity within its PH domain with human KIF1A but binds to early endosomes that contain different phosphoinositides. Thus, cargo interaction and the role of the PH domain are unresolved questions which will be addressed in this thesis.

1.5 Aims and objectives

This thesis focuses on the motility of early endosomes during pathogenic development of *U. maydis*. It further investigates the mechanism of long distance transport via uniform microtubule arrays that is supported by the fungal cells. The molecular motor, kinesin-3, which is responsible for the long distance transport of EEs, is also the focus of this thesis.

Quite recently, the motility of EEs has become a 'hot' scientific field of study, however not much is known about their function in pathogenic fungi. The bidirectional motility of EEs has also been described in neurons (reviewed in Yap and Winckler, 2012), but their characteristics (motors, cargo etc.) are still not well understood (Lasiecka *et al.*, 2010). Previous studies in *U. maydis* found that EEs move in a bidirectional fashion in yeast-like and hyphal cells (Wedlich-Söldner *et al.*, 2002; Lenz *et al.*, 2006) and their long distance transport is mainly dependent on Kin3 activity, the anterograde motor protein. Kin3 has been shown to be almost always associated with the EEs (Schuster *et al.*, 2011c). EEs play a major role in receptor recycling (Pra1; Fuchs *et al.*, 2006), however they are additionally indirectly implied in many other processes through different receptor proteins that they carry. To summarize, EEs might participate in processes like septation (Don1, Cdc42, Rho3 via Rrm4, Drf1), secretion (Kin3 and acid phosphatase, Cts1), recycling (Pra1 and probably Pit1) and post-transcriptional control (Rrm4). Although single proteins from the above 'EE-attached protein collection' have been studied to date, so far there is neither data about the role of EE motility during pathogenic development, nor on the importance of their motility during different stages of host infection. In order to test the importance of EE motility during pathogenic development and if their motility can support colonization of the host plant, the solo-pathogenic haploid strain SG200 (*a1 mfa2 bW2 bE1;* Bölker *et al.*, 1995) was used. The results are presented in **Chapter 3**.

Continuous bidirectional motility of EEs, which is observed in yeast-like and hyphal cells, is based on MT tracks. An analysis of the MT usage and selection of MT tracks by Kin3 are presented in **Chapter 4**, as to date the information on Kin3 selectivity in regard to MT subpopulations has been missing.

It is not known how Kin3 binds to the EEs and how the activity of Kin3 is regulated during continuous attachment to EEs. Based on homology in structure with known kinesin-3 proteins from other organisms, for a cargo binding domain the tail region appears to be the most promising candidate. To study how the tail of Kin3 binds to the EEs, several truncated alleles of Kin3 were designed. It has been shown before that the PH domain can serve as a lipid binding domain in many proteins, especially in proteins belonging to the kinesin-3 family. Deletion of the PH domain from Unc-104 resulted in inhibition of the transport of synaptic vesicle precursors (Klopfenstein *et al.*, 2002; Klopfenstein and Vale, 2004). There is high homology between the PH domains sequences of Kin3 and human kinesin-3 KIF1A and *C. elegans* Unc-104 (aa similarity: 53.3% and 49%, respectively). Based on that, the PH domain was selected as a potential lipid binding domain. The answers for the two main questions I asked 'How important is the Kin3 tail for cargo binding?' and 'How important is the Kin3 tail for motor protein motility?' are presented in **Chapter 5**.

Chapter 2

General methods

Standard molecular biology methods and protocols described in Sambrook *et al.*, 1989 were followed. Methods described here were routinely used and most of the *U. maydis* strains presented in this thesis were obtained in three steps (summarized in Fig. 6):

1. Plasmid generation using yeast-*E. coli* shuttle vector by *in vivo* recombination in *Saccharomyces cerevisiae* (Raymond *et al.*, 1999; Fig. 6A-F);
2. *Escherichia coli* transformation (Hanahan, 1985; Fig. 6G) and plasmid DNA miniprep purification followed by digestions (Fig. 6H-J);
3. *U. maydis* transformation (Schulz *et al.*, 1990) and antibiotic selection of appropriate transformants (Fig. 6K-L).

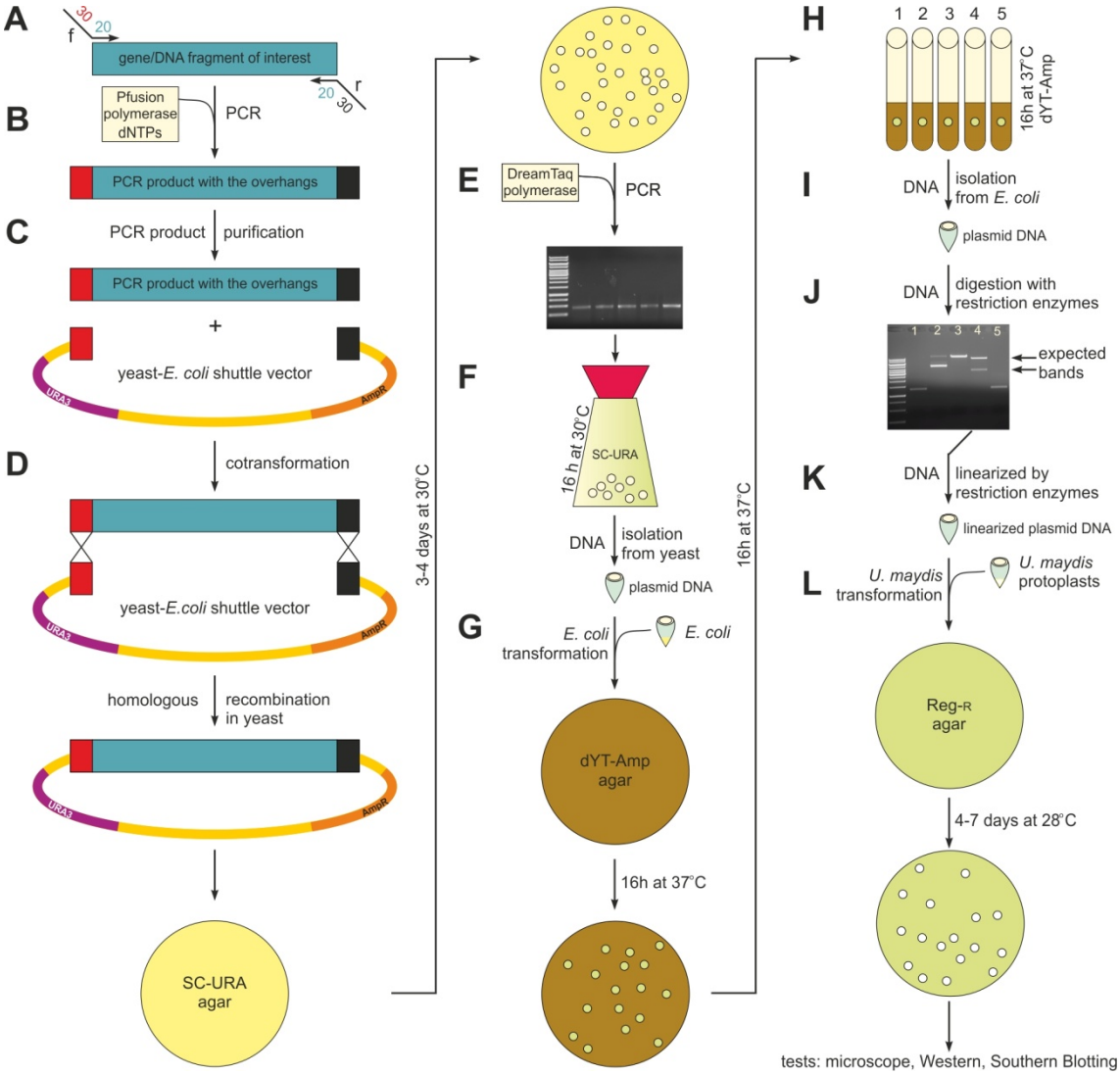

Figure 6. Scheme of methods used in order to obtain *U. maydis* transformants. Abbreviations: URA3 (see below), *S. cerevisiae* selectable marker; AmpR, *E. coli* ampicillin resistance; Reg-R agar, regeneration agar containing *U. maydis* selectable antibiotic. Detailed description of each method can be found in text below.

Yeast-*E. coli* shuttle vector (Fig. 7) contains the yeast *URA3* selectable marker which encodes orotidine-5'phosphate decarboxylase, an enzyme which is required for *de novo* synthesis of pyrimidine ribonucleotides such as uracil. Moreover, the vector contains yeast *2µ ori* (origin of replication) amplified from plasmid pEYA2 (Invitrogen, Paisley, UK), the ampicillin resistance cassette (amp^R), an *E. coli* origin of replication (oriC), and *U. maydis* resistance cassette, carboxin (cbx^R), which, if necessary, can be replaced with other resistance cassettes like hygromycin (hyg^R) or nourseothricin (nat^R).

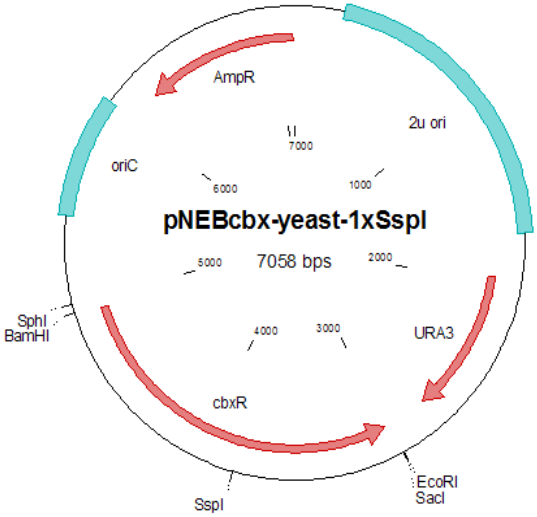

Figure 7. Yeast-*E. coli* shuttle vector pNEBcbx-yeast-1xSspI.
This plasmid contains three selectable markers for: yeast (*URA3*), *E. coli* (Amp^R) and *U. maydis* (cbx^R). Single restriction site for *SspI* within cbx^R allows targeting of the plasmid into the *succinate dehydrogenase* locus of *U. maydis*. Unique restriction sites for *EcoRI* and *SacI* or *BamHI* and *SphI* allows cloning of the gene of interest using *in vivo* recombination in *S. cerevisiae* (Raymond *et al.*, 1999). Graphic map was generated in Clone Manager 9 Professional Edition (Scientific & Educational Software).

2.1 Plasmid generation

2.1.1 PCR

In order to obtain plasmids by *in vivo* recombination in *S. cerevisiae* (Raymond *et al.*, 1999) firstly DNA fragments were amplified by the Phusion® High-Fidelity DNA Polymerase (New England Biolabs #M0530L) in a PCR reaction (using 35 cycles) as fragments with 30 bp overhangs with a homology to the appropriate regions within the yeast - *E. coli* shuttle vector (Fig. 6A-B). The components of

the PCR reaction mixture and PCR steps are shown below (where *f* means forward and *r* – reverse):

COMPONENT	25 µl reaction
template DNA	0.5 µl
Phusion polymerase	0.5 µl
10 µM f primer	1 µl
10 µM r primer	1 µl
10 mM dNTPs	2.5 µl
5x Phusion HF or GC buffer	5 µl
dH_2O	14.5 µl

STEP	TEMP	TIME
Initial denaturation	98°C	30 s
35 cycles	98°C	10 s
	Tm-4°C	20 s
	72°C	15 s/1 kb
Final extension	72°C	10 min
Hold	10°C	

2.1.2 Purification of PCR products

In order to purify DNA products obtained through PCR reactions (Fig. 6C), the purification was performed according to Boyle and Lew, 1995. Briefly, PCR products were ran on an agarose gel (usually 0.8%) and cut out, which was followed by incubation in ~1 ml of 6 M sodium iodide at 55^{o}C in order to allow agarose to dissolve. The solution was then mixed with 50 µl of 10% silica glass beads (Sigma #S-5631; in 3 M sodium iodide) and incubated at 55°C for 5 min what allowed binding of DNA to the beads. The mixture was spun down for 1 min in a bench microcentrifuge at maximum speed (13300 rpm; Thermo Scientific Sorvall Legend Micro 17) to precipitate the silica glass beads-bound DNA. After following three steps of washes in 500 µl of DNA wash buffer, DNA was eluted from the beads by adding 10-20 µl of distilled H_2O (dH_2O) and incubating at 55°C for 5 min. The supernatant fraction obtained after 1 min of spinning in a bench microcentrifuge at 13300 rpm was later used as purified DNA fragment for homologous recombination in yeast.

2.1.3 *S. cerevisiae* transformation

Yeast *S. cerevisiae* cells DS94 (MATα, *ura3-52*, *trp1-1*, *leu2-3*, *his3-111*, and *lys2-801*; Raymond *et al.*, 1999) were grown in 3 ml of liquid YPD medium at 30°C overnight with 200 rpm shaking. 2 ml of overnight culture served for the inoculation of 50 ml of YPD medium (flask volume: 250 ml) and was grown at 28-30°C with 200-230 rpm shaking. After 5 h cells were harvested by spinning down at 2200 rpm (centrifuge Heraeus Biofuge Stratos, using rotor Heraeus #3047 5600 rpm) for 5 min at RT. The cell pellet was resuspended in 10 ml of dH_2O and spun down again at 2200 rpm for 5 min at RT. Cell pellet was

resuspended in 300 µl of dH_2O. 50 µl of yeast cells were combined with 50 µl of denatured solution of 2 µg/µl salmon sperm DNA (w/v in dH_2O; SIGMA, Cat No: D1626), usually 2 µl of linearized shuttle vector backbone and 2-4 µl purified PCR fragments (Fig. 6D). To the transformation mixture 32 µl of 1 M lithium acetate (in dH_2O; SIGMA) and 240 µl 50% PEG 4000 (w/v in dH_2O; Prolabo) was added and mixed by pippeting. After that, the transformation mixture was incubated at 30°C for 30 min and it was further incubated at 45°C in a water bath for 15 min in order to generate heat shock. Cells were later spun down in a bench microcentrifuge at 2000 rpm for 2 min at RT and resuspended in 200 µl dH_2O. The obtained mixture was spread onto two Sc-Ura plates in a 1:1 dilution and a 1:10 dilution and incubated at 30°C for usually 3 days.

2.1.4 *S. cerevisiae* PCR colony screening

Screening of yeast colonies in order to find positive transformants (Fig. 6E) was done using DreamTaq Green PCR Master Mix polymerase (Fermentas #K1081) and appropriate primers which bind within the gene/fragment of interest and within the shuttle vector. The components of the PCR reaction mixture and PCR steps are shown below:

COMPONENT	20 µl reaction
yeast colony	-
2x DreamTaq Green PCR Master Mix	10 µl
10 µM f primer	1 µl
10 µM r primer	1 µl
dH_2O	8 µl

STEP	TEMP	TIME
Initial denaturation	95°C	3 min
35 cycles	95°C	30 s
	Tm-4°C	30 s
	72°C	1 min/1 kb
Final extension	72°C	10 min
Hold	10°C	

2.1.5 Plasmid DNA isolation from *S. cerevisiae*

A positive colony of selected yeast strain was grown overnight in 15 ml of Sc-Ura medium at 30°C with 200 rpm shaking (Fig. 7F). Next day cells were harvested by spinning down at 1500 rpm (centrifuge Heraeus Biofuge Stratos, using rotor Heraeus #3047 5600 rpm) for 5 min at RT and the cell pellet was resuspended in 0.5 ml sterile dH_2O. Cells were transferred into 1.5 ml eppendorf tube and spun down for 5 s in a bench microcentrifuge at 13300 rpm. After discarding of the supernatant, the cell pellet was vortexed in the residual water and 200 µl of yeast lysis buffer and 200 µl

phenol:chloroform:isoamylalcohol (25:24:1) was added. The cells were disrupted by adding 0.3 g of acid washed glass beads (size 425 – 600 µm), followed by 10 min vibration on a IKA Vibrax VXR (IKA-Werke, Staufen, Germany). After adding 200 µl of TE buffer (pH 8.0) cell debris and organelles were removed by centrifugation for 5 min at RT in a bench microcentrifuge at 13300 rpm. The aqueous phase was then transferred to a new tube and separated from the lower organic phase containing proteins, polysaccharides and lipids. To the aqueous phase containing nucleic acids 1/10th volume of 3M sodium acetate (pH 5.5) and 1 ml of 96% ethanol was added and obtained mixture was incubated at -20°C for 15 min. After that the mixture was spun down in a bench microcentrifuge at 13300 rpm for 20 min. The supernatant was discarded and the pellet was resuspended in 400 µl of TE buffer (pH 8.0) and 4 µl of RNase A (10mg/ml). The incubation at 37^{o}C allowed the pellet to get dissolved. To the resuspended pellet 10 µl of 4 M ammonium acetate and 1 ml of 96% ethanol was added followed by 2 min spinning in a bench microcentrifuge at 13300 rpm. After discarding of the supernatant, the pellet was washed twice with 500 µl of 70% ethanol. Finally, the air dried pellet was resuspended in 20 µl dH_2O.

2.2 *E. coli* transformation

For all cloning and plasmid construction *E. coli* strain DH5α (Hanahan, 1985) was used. Briefly, 6 to 8 µl of isolated yeast DNA was used for chemically competent *E. coli* cell transformation (Fig. 6G). Heat shock was performed at 42ºC for 45-60 s followed by 5 min on ice and 1 h incubation in 200 µl of dYT at 37ºC in a Thermomixer (Eppendorf; Fisher Scientific) with shaking at 1000 rpm. Cells were plated onto dYT agar plates containing 100 µg/ml ampicillin and were grown overnight at 37ºC.

2.2.1 Plasmid DNA isolation from *E. coli* by alkaline lysis

In order to find positive transformants, screening of *E. coli* colonies (Fig. 6H) was done using DreamTaq Green PCR Master Mix polymerase (Fermentas

#K1081) or by isolation of DNA from *E. coli* using an alkaline lysis method (Birnboim and Doly, 1979; Birnboim, 1983; Fig. 6I) and performing digestion using restriction enzymes. In order to isolate DNA from *E. coli* 3-4 ml dYT-Amp cultures inoculated with a single colony were grown overnight at 37ºC with shaking at 200 rpm. Next day cells were spun down in the eppendorf tubes and after removing supernatant, they were resuspended in 150 µl of TE (pH 8.0) containing 5 µl of RNase A (10mg/ml). After adding 150 µl of alkaline lysis solution (see buffers and media recipes below) and inverting, the mixture was kept for 5 min at -20°C. This step allowed denaturing of bacterial proteins by SDS whereas chromosomal and plasmid DNA were denatured by NaOH treatment. Addition of 500 µl of neutralization solution (containing sodium acetate and NaCl; see buffers and media recipes below), invertion of tubes and incubation at -20°C for 10 min, followed by 10 min spinning down in a bench microcentrifuge at 13300 rpm, allowed precipitating most of the chromosomal DNA and bacterial proteins. After transferring of the supernatant to a new eppendorf tube, 750 µl of isopropanol (Fisher Scientific) was added, vortexed and centrifuged for 5 min in a bench microcentrifuge at 13300 rpm. The supernatant was removed and the pellet was washed with 500 µl of 70% (v/v) ethanol, vortexed and centrifuged for 5 min at 13300 rpm. The pellet was air dried and resuspended in 15-25 µl of dH_2O.

2.2.2 Plamid DNA digestion

Restriction enzymes were obtained from New England Biolabs (NEB) and were used as recommended. In order to test obtained plasmids (Fig. 6J) digestions were usually performed at 37ºC for 30 min; the components of the digestion reaction mixture are shown below:

COMPONENT	**10 µl reaction**
plasmid DNA	0.5 µl
restriction enzyme	0.3 µl
NEB buffer	1 µl
dH_2O	8.2 µl

When proper restriction pattern was obtained on agarose gels, plasmid DNA was linearized using appropriate restriction enzyme or a combination of enzymes (Fig. 6K), purified (as described in 2.1.2) and used for *U. maydis* transformation. Verified *E. coli* strain holding plasmid DNA was stored at -80°C in dYT- glycerol at 1:1 ratio.

2.3 *U. maydis* transformation

The transformation procedure follows the protocol described by Schulz *et al.*, 1990. 50 µl of *U. maydis* protoplasts (Fig. 6L; see also Protoplast generation below) were incubated for 30 min on ice with 4 µl of linearized plasmid DNA (1-5 µg) in the presence of 1 µl of heparin (1 mg/ml). After that 0.5 ml of PEG (40% w/v in STC; filter sterilized) was added on top of the protoplasts and carefully mixed by pipetting and left on ice for 15 min. The transformation mixture was spread onto two Reg-agar plates containing two layers (bottom layer contained selective antibiotic and top layer – without antibiotic) in volumes of 80% and 20% of transformation reaction. Plates were incubated for usually 4–7 days at 28ºC. Obtained transformants were singled-out and grown on CM-agar plates containing the appropriate antibiotic. After testing by microscope observations and/or Western and/or Southern blotting, strains were stocked at -80°C in NSY-glycerol at 1:1 ratio.

2.3.1 Protoplast generation

The protoplast generation procedure follows the protocol described by Schulz *et al.*, 1990. Briefly, an appropriate *U. maydis* strain was grown overnight in 50 ml of YEPS medium at 28ºC shaking at 200 rpm. When OD600 was in range 0.4–0.8 cells, the culture was spun down for 10 min at 3000 rpm (centrifuge Heraeus Biofuge Stratos, using rotor Heraeus #3047 5600 rpm). The obtained cell pellet was resuspended in 25 ml of SCS and centrifuged again for 10 min at 3000 rpm. In order to digest the cell wall material, the pellet was resuspended in 2 ml of SCS containing 7 mg/ml of lysing enzymes from *Trichoderma harzianum* (contains β-glucanase, cellulase, protease, and chitinase activities; Sigma #l1412) and left at RT for 10–15 min in order to digest the cell wall material. When 30–40% of the cells became rounded (protoplast formation was monitored microscopically), 10 ml of cold SCS was added, followed by centrifugation at 2400 rpm for 10 min at 4ºC. After discarding of the supernatant, previous step was repeated twice. Finally, the pellet was resuspended in 10 ml of cold STC and centrifuged as above. The obtained

pellet was resuspended in 500 µl of cold STC and 50 µl aliquots were ready for the transformation or stored at -80ºC.

2.4 Buffers and media

All chemicals used in this study were obtained from Fluka, Sigma, Prolabo, Fischer Scientific, Merck, Molecular Probes (Invitrogen), Roth and Duchefa Biochemie. The materials are given in alphabetical order and concentrations represent final concentrations.

Buffers/Media	**Final concentrations**
Alkaline lysis solution	1% (w/v) SDS, 0.2 M NaOH
CM (complete) medium, pH 7.0	0.25% (w/v) casaminoacids, 0.1% (w/v) yeast extract, 1% (v/v) vitamin solution (Holliday, 1974), 6.25% (v/v) salt solution (Holliday, 1974), 0.05% (w/v) DNA from herring sperm, 0.15% (w/v) NH_4NO_3
DNA wash buffer	50 mM NaCl, 10 mM Tris-HCl pH 7.5, 2.5 mM EDTA, 50% (v/v) ethanol
dYT-glycerol	1.6% (w/v) tryptone, 1% (w/v) yeast extract, 0.5% (w/v) NaCl, 69.6% (v/v) glycerol
dYT medium	1.6% (w/v) tryptone, 1% (w/v) yeast extract, 0.5% (w/v) NaCl
Neutralization solution	0.9 M sodium acetate pH 4.8, 0.5 M NaCl
NM (nitrate minimal) medium, pH 7.0	0.3% (w/v) KNO_3, 6.25% (v/v) salt solution (Holliday, 1974)
NSY-glycerol	0.8% (w/v) nutrient broth, 0.1% (w/v) yeast extract, 0.5% (w/v) sucrose, 69.6% (v/v) glycerol
PBS buffer	137 mM NaCl, 2.7 mM KCl, 4.3 mM $Na_2HPO_4*7H_2O$, 1.4 mM KH_2PO_4
Reg (regeneration) agar	1% (w/v) yeast extract, 2% (w/v) peptone, 2% (w/v) sucrose, 18.22% (w/v) sorbitol, 1.5% (w/v) agar

Salt solution (Holliday, 1974)	16% (w/v) KH_2PO_4, 4% (w/v) Na_2SO_4, 8% (w/v) KCl, 4.08% (w/v) $MgSO_4*7H_2O$, 1.32% (w/v) $CaCl_2*2H_2O$, 8% (v/v) Trace elements
SCS buffer	20 mM Na-citrate pH 5.8, 1 M sorbitol
Sc-Ura medium	0.17% (w/v) yeast nitrogen base without amino acids, 0.5% (w/v) ammonium sulphate, 0.5% (w/v) casein hydrolysate, 0.002% (w/v) adenine, 2% (w/v) glucose
STC buffer	10 mM Tris-HCl pH 7.5, 100 mM $CaCl_2$, 1 M sorbitol
TE buffer pH 8.0	10 mM Tris, 1 mM EDTA
Trace elements (Holliday, 1974)	0.06% (w/v) H_3BO_3, 0.14% (w/v) $MnCl*4H_2O$, 0.4% (w/v) $ZnCl_2$, 0.4% (w/v) $Na_2MoO_4*2H_2O$, 0.1% (w/v) $FeCl_3*6H_2O$, 0.04% (w/v) $CuSO_4*5H_2O$
Vitamin solution (Holliday, 1974)	0.1% (w/v) thiamine HCl, 0.05% (w/v) riboflavin, 0.05% (w/v) pyridoxine HCl, 0.2% (w/v) D-pantothenic acid hemicalcium salt, 0.05% (w/v) 4-aminobenzoic acid, 0.2% (w/v) nicotinic acid, 0.2% (w/v) choline chloride, 1% (w/v) myo-Inositol
Yeast lysis buffer	2% (v/v) Trition X-100, 1% (w/v) SDS, 100 mM NaCl, 1 mM EDTA, 10 mM Tris
$YEPS_{light}$ medium	1% (w/v) yeast extract, 0.4% (w/v) peptone, 0.4% (w/v) sucrose
YPD medium	1% (w/v) yeast extract, 2% (w/v) peptone, 2% (w/v) D-glucose

Agar media were obtained by adding 2% (final concentration; CM, Sc-Ura) or 1.3% (final concentration; dYT) of agar.

In addition to above methods, each result chapter (Chapters 3-5) contains a section with the Methods part used in the study.

Chapter 3

Early endosome motility is essential for colonizing of corn plants by the smut fungus *Ustilago maydis*.

Evidence that early endosomes (EEs) are involved in the initiation of pathogenic development of the corn smut *Ustilago maydis*, cell–cell fusion, spore formation and germination was previously shown by Fuchs *et al*, 2006, who found that endocytosed pheromone receptor Pra1 is recycled back to the plasma membrane via EEs. What is the role of rapid bidirectional motility of EEs during pathogenic development and how important is their motility during different stages of host infection? To answer this question I used the solo-pathogenic strain SG200 (Bölker *et al.*, 1995) which enables formation of an infectious haploid hypha without a mating partner and I constructed a synthetic anchor specific for EEs which was able to block their motility at early and later stages of maize infection. Blockage of the EE motility in the first two days after infection almost completely abolished pathogenic development, but did not alter fungal colonization when EE motility was blocked 3-4 days after infection. These observations were supported by analysis of the hyphal growth which rate was almost twofold decreased after blockage of the EE motility and accompanied with impaired polarity of growing hyphae.

This work was built on previous work and was undertaken with the help of co-workers. Ms Natalie Steinberg established the plant infection method, did plant infections, analysed disease symptoms and performed staining and microscopy of infected plant tissues. Ms Laura Yeves-Gonzalez did plant infections and performed staining of plant infected tissues. Dr. Martin Schuster performed FRAP experiments. Dr. George Littlejohn performed confocal microscopy experiments. Prof. Gero Steinberg provided overall project management and supervision, analysed data and wrote the manuscript.

Early endosome motility is essential for colonizing of corn plants by the smut fungus *Ustilago maydis*.

Ewa Bielska[1], Natalie Steinberg[1], Martin Schuster[1], George Littlejohn[1] & Gero Steinberg[1,2]

[1]Department of Biosciences, College of Life and Environmental Sciences, University of Exeter, Exeter EX4 4PE, UK

[2]To whom correspondence should be addressed: G.Steinberg@exeter.ac.uk; phone: ++44-1392-263476; fax: ++44-1392-263434;

Key words: Early endosomes, membrane trafficking, plant pathogenicity, hyphal growth

Author contributions: E.B. generated strains, performed research, analysed data and wrote the manuscript; N.S. established methods, performed research and analysed data; M.S. performed research; G.L. performed research; G.S. designed research, conceived the project, analysed data and wrote the manuscript.

Abstract

In the corn smut *Ustilago maydis*, morphogenesis and cell-cell recognition at early stages of plant pathogenicity depend on recycling processes that involve early endosomes (EEs). These organelles rapidly move by the activity of the motors kinesin-3 and dynein, which is thought to support cell separation and polarized growth of the invasive hyphal cell. The importance of EEs and their motility in plant colonization and later pathogenic development is not known. Here we establish a synthetic linker protein (K1^{r}PX), consisting of a tightly binding kinesin-1^{rigor} head and an endosome binding PX domain. K1^{r}PX specifically immobilizes the EEs along microtubules, and live cell imaging shows that this did not affect motility of free kinesin-3, suggesting that EE-independent functions of the motor are still operating. Indeed, the synthetic immobilization of EEs in yeast-like cells caused significantly less cell separation defect then deletion of kinesin-3, suggesting that cytokinesis occurs largely independent of motile EEs. In contrast, anchoring the EEs severely impaired hyphal growth, suggesting that EEs are a crucial cargo of kinesin-3 during the invasive stage. Blockage of EE motility during the first 2 days of invasion almost abolished the ability of the fungus to cause plant disease. However, blockage of EEs at later stages by expressing K1^{r}PX from a plant-stage specific *mig1* promoter had almost no effect on virulence of the fungus. The importance of EE motility during the first 2 days correlates with hyphal growth of the intruding fungus, whereas the cells are much less polar during later stages of infection. These data suggest that EE motility is crucial during early invasion, probably by allowing rapid hyphal growth to escape recognition and defence by the plant.

Introduction

The basidiomycete *Ustilago maydis* is a pathogen on corn (*Zea mays*). It causes significant yield loss and is considered to be an important threat to food security (Fisher *et al.*, 2012). Outside of the plant, the hemi-biotrophic fungus grows as a saprotrophic yeast that is thought to populate soil (Christensen, 1963). Pathogenic development is initiated by a morphogenic switch from a

yeast-like stage to a hyphal cell (Snetselaar and Mims, 1993). This elongated hyphal cell is the infectious form of the fungus, which expands by apical tip growth to invade the plant tissue. During the early biotrophic phase of infection, the fungus continues hyphal growth and secrets effectors that prevent the intruder from being recognised by the plant defence system (Kämper *et al.*, 2006; Molina and Kahmann, 2007; Mueller *et al.*, 2008; Müller *et al.*, 2008; Doehlemann *et al.*, 2009; Wahl *et al.*, 2009; Heimel *et al.*, 2010a; Djamei *et al.*, 2011; Doehlemann *et al.*, 2011; Hemetsberger *et al.*, 2012). After spreading within the plant, the cells round up and cause tumors on the leaves, stems and the corncob of the plant (Christensen, 1963; Banuett and Herskowitz, 1996). Intensive studies on the role of the cytoskeleton in hyphal growth and pathogenicity revealed that motor proteins are of crucial importance for pathogenicity of *U. maydis*. The class V myosin Myo5 and the class XVII myosin Mcs1 were shown to control filamentous growth inside the plant host (Weber *et al.*, 2003; Weber *et al.*, 2006; Treitschke *et al.*, 2010), suggesting that polar secretion is required for plant infection. In addition, microtubule and kinesin motors are required for extended hyphal growth in *U. maydis* (Schuchardt *et al.*, 2005; Fuchs *et al.*, 2005a), and it is tempting to speculate that their ability to deliver secretory cargo to the hyphal tip underlies the importance of MTs in pathogenic development of *U. maydis*. Indeed, Myo5, kinesin-1 and kinesin-3 cooperate in secretion, with kinesin-1 and Myo5 delivering chitin-synthase containing vesicles (Schuster *et al.*, 2011d), and kinesin-3 participating in acid phosphatase secretion (Schuchardt *et al.*, 2005). However, the main role of kinesin-3 appears to be in trafficking of early endosomes (EEs; Wedlich-Söldner *et al.*, 2002; Lenz *et al.*, 2006; Schuster *et al.*, 2011b). These organelles are rapidly moving within the hyphal cell (Wedlich-Söldner *et al.*, 2000) and are involved in recycling of the pheromone receptor at the hyphal tip, a process essential for the initiation of the pathogenic development (Fuchs *et al.*, 2006). Consistent with an important role of the EEs in hyphal growth, deletion of kinesin-3 or immobilising the motor by introduction of a point-mutation in the motor domain abolishes rapid tip growth (Lenz *et al.*, 2006). Thus, reduced virulence of kinesin-3 null mutants could be linked to impaired hyphal growth, as a consequence of impaired EE motility and endocytic recycling. Alternatively, the deletion of kinesin-3 could cause defects in secretion, which in turn might affect the biotrophic growth phase and alerts

the plant defence system. Here we set out to distinguish between both possibilities. We specifically inhibit the motility of EEs by a synthetic anchor of EEs that freezes the organelles to the microtubule track, but does not impair the motility of free kinesin-3. Using this tool, we show that EE motility is of minor importance for cell separation, but is essential for hyphal growth outside of the plant. Inhibition of EE motility during early steps of plant infection drastically reduced virulence, whereas EE motility was dispensable at later stages of maize infection. This correlates with a change in cell shape during infection, with elongate cells colonizing the plant during early stages, and rounded cells at later infection stages. These results demonstrate that EE motility is crucial for hyphal morphogenesis, which is of particular importance during early infection of maize tissue.

Results

Early endosomes show prominent motility with invading fungal hypha.

As a first step towards an understanding of the role of early endosomes (EEs) in pathogenicity of *U. maydis*, we visualized the fungus within the host plant. In agreement to previous reports (Snetselaar and Mims, 1994; Banuett and Herskowitz, 1996) we found that the fungus forms long hyphal cells when growing within the host plant cell (Fig. 1A; 2 dpi). With time the fungal cells grew shorter and increased branching (Fig. 1A, 4 dpi, 6 dpi; Fig.1B). We next infected plants with an *U. maydis* strain that expressed the EE-specific small GTPase Rab5a (Fuchs *et al.*, 2006) fused to the green fluorescent protein (GFP). We observed EEs at all stages of infection (Fig. 1C, 2 dpi; 1D, 8 dpi), which were moving in cells of all stages of infection (Fig. 1E; a contrast-inverted kymograph is shown that documents motility as diagonal lines, while stationary signals are indicated by vertical lines; see also Supplementary Movie S1). Motility of these organelles is mediated by the motor proteins dynein and kinesin-3 (Wedlich-Söldner *et al.*, 2002; Lenz *et al.*, 2006). These mechano-enzymes utilize ATP, and the presence of long-range bidirectional EE motility indicates that this process serves an important purpose during the plant invasion.

The synthetic molecular anchor K1^{r}PX blocks EE motility.

Most EE motility is mediated by Kinesin-3 (Kin3; Schuster *et al.*, 2011c) and it was suggested that the phenotype of *kin3* deletion mutants reflects the importance of EE motility (Lenz *et al.*, 2006). However, Kin3 was also implied in the motility of secretory vesicles (Schuchardt *et al.*, 2005). To test more specifically for the importance of EE motility, we generated a molecular anchor for EEs. This synthetic motor consisted of a kinesin-1^{rigor} motor head, containing a point mutation that confers tight binding to the MT track (Straube *et al.*, 2006), and a coiled coil region that was followed by a EE-membrane binding PX domain from the endosomal t-SNARE Yup1 (Wedlich-Söldner *et al.*, 2000). In *U. maydis*, dynein is a cargo of kinesin-1 (Lenz *et al.*, 2006). To test if the kinesin-1^{rigor} motor head was able to suppress motility, we expressed full-length kinesin-1^{rigor} protein in cells that contained wildtype kinesin-1 and GFP-labelled dynein (strain AB33G$_3$Dyn2_Kin1^{rigor}; for genotype of all strains see Supplementary Table S1, for strain usage see Supplementary Table S2). Indeed, the presence of Kin1^{rigor} immobilized the fluorescent dynein (Fig. 2B; Supplementary Movie S2), demonstrating that the Kin1^{rigor} motor head firmly binds to MTs and is able to block endogenous motility. On the other hand, a fusion protein of the GFP and PX^{Yup1} domain bound to mCherry-Rab5a labelled EEs (Fig. 2C), demonstrating that the PX domain was sufficient to target K1^{r}PX to the EEs. Having done these controls, we next expressed K1^{r}PX under the arabinose-inducible *crg* promoter in *U. maydis* cells that contained GFP-Rab5a labelled EEs. In the presence of glucose the promoter is switched off (Bottin *et al.*, 1996) and EEs are moving in a bidirectional fashion (Fig. 2D; OFF). After shift to arabinose-containing medium for 16h, K1^{r}PX was expressed (Fig. 2E; Western blot shows expression of a K1^{r}-GFP-PX fusion protein). The presence of the synthetic anchor almost completely abolished the motility of EEs in hyphal cells and yeast-like cells (Fig. 2F, ON; Fig. 2G, compare to motility in a kinesin-3 null mutant, ΔKin3; Supplementary Movie S3). This treatment did not result in a global "roadblock" of MT-dependent transport, as GFP-labelled kinesin-3 was still motile after immobilization of EEs by K1^{r}PX (Fig. 2H; Supplementary Movie S4). Instead, the motility of Kin3-GFP signals significantly increased (Fig. 2G), suggesting that some kinesin-3 was released from EEs. Taken together, these results suggested that K1^{r}PX is a useful tool to specifically block EE motility.

EE motility is crucial for hyphal growth but of minor importance for cell separation.

Yeast-like cells of *U. maydis* are cigar-shaped and grow by budding. It was previously shown that deletion of *kin3* results in a cell separation defect (Wedlich-Söldner *et al.*, 2002; Fig. 3A, 3B). A similar phenotype was found when a kinesin-3^{rigor} mutant allele was expressed (Wedlich-Söldner *et al.*, 2002; Fig. 3A, 3B; Kin3^{r}), and it was suggested that EEs participate in cell separation in *U. maydis* (Schink and Bölker, 2009). To test more specifically for an involvement of EEs, we expressed the anchor K1^{r}PX. Surprisingly, we found that most cells did not exhibit a cell separation defect (Fig. 3A, 3B; K1^{r}PX) and no large tree-like cell aggregates were found (Fig. 3A, compare Kin3^{r} and K1^{r}PX). This suggests that EE motility is of minor importance for cell separation. Instead, defects in an EE-independent role of kinesin-3 in secretion of wall-degrading enzymes, such as chitinase, might account for the severe cell separation defect in kinesin-3 null mutants.

Kin3 null mutants are impaired in hyphal growth and form short and often bipolar hyphae (Fig. 3C; Lenz *et al.*, 2006). In addition, the hyphal extension rate is reduced to half (Fig. 3D), which corresponds well with previous growth defects in the absence of MTs (Fuchs *et al.*, 2005a). Expression of K1^{r}PX in wildtype hyphal cells resulted in short and bipolar hyphae and reduced growth rates, too (Fig. 3C, 3D). This demonstrated that EE motility is of crucial importance for hyphal growth and that EE motility is a major function of kinesin-3 in these cells.

EE motility is crucial for early plant infection but dispensable for late pathogenic development.

We previously reported that EEs are involved in recycling of the pheromone receptor, which was found to be an essential step for initiation of the pathogenic development (Fuchs *et al.*, 2006). To assess the importance of EE motility during subsequent plant infection stages, we expressed K1^{r}PX under the strong *crg* promoter and the *mig1* promoter, which is expressed at ~3-4 days after infecting the plant (Basse *et al.*, 2000). We confirmed this behaviour by expressing cytoplasmic GFP under both promoters. In hyphae grown in

arabinose containing medium, the *crg* promoter is active and induces GFP formation (Fig. S1A). Expression remains switched on during early infection (Fig. S1B, *crg*GFP, 1 dpi; Fig. S1C), but GFP fluorescence disappears after 36 hours after infection, suggesting that the promoter is repressed (Fig. S1D). In contrast, no GFP expression was detected from the *mig1* promoter in hyphae *ex planta* (Fig. S1A) and during early infection (Fig. S1B, *mig*GFP, 1 dpi). However, expression starts at 3 dpi (Fig. S1B, S1C; *mig*GFP), confirming that the promoter controls plant-specific genes in the fungus (Basse *et al.*, 2000).

We next set out to inhibit EE motility during early and late stages of plant infection by expressing K1^{r}PX under the control of the *crg* and the *mig1* promoters. In control cells EEs were motile at all-time points prior to spore formation (Fig. 4A, Control, 2 dpi and 6 dpi; Fig. 4B; see also Fig. 1E and Supplementary Movie S1). In contrast, no motility was seen in kinesin-3 deletion mutants (Fig. 4A, Fig. 4B; ΔKin3). In cells that express the K1^{r}PX anchor under the *crg* promoter, motility was abolished at 2 dpi, but restored at 3 dpi and the following days (Fig. 4A, 4B; crgK1^{r}PX; Supplementary Movie S5). In contrast, when K1^{r}PX was put under the control of the *mig1* promoter, EEs were motile at 2 dpi (Fig. 4A, 4B, 2 dpi; migK1^{r}PX), but motility was blocked at ~4-5 dpi and was almost abolished at later time points (Fig. 4A, 6 dpi; 4B; K1^{r}PX; Supplementary Movie S5). When plants were infected with control strains, large tumors on leaves and stems appeared, and plants often remained very small (Fig. 4C, 4D, 4E; Control). In contrast, deletion of kinesin-3 led to very few symptoms and plants grew to full height (Fig. 4C, 4D, 4E; ΔKin3), suggesting that kinesin-3 is essential for fungal virulence. A similar phenotype was obtained when motility of EEs was blocked by expressing of K1^{r}PX under the *crg* promoter, suggesting that motility of EEs is essential for early infection (Fig. 4C, 4D, 4E; crgK1^{r}PX). Surprisingly, inhibition of EE motility at 3-4 dpi by expressing K1^{r}PX from the *mig1* promoter had almost no effect on virulence of the fungus. Plants showed large tumors and reduced growth, suggesting that the fungus was fully virulent (Fig. 4C, 4D, 4E; migK1^{r}PX).

Inhibition of EE motility during early infection triggers plant defence.

The biotrophic phase of *U. maydis* requires the secretion of effectors that actively suppress the plant defence and allow the colonization of the host tissue (Kämper *et al.*, 2006; Brefort *et al.*, 2009). In addition, it was suggested that rapid hyphal growth allows the fungus to escape plant recognition (Gow *et al.*, 2002; Steinberg, 2007c; Brand, 2012). The inability of the K1^{r}PX expressing cells to colonize the plant suggested that the intruding fungus became recognized by the plant. Such recognition is accompanied by an oxidative burst that can be visualized using diaminobenzidine (DAB; Thordal-Christensen *et al.*, 1997; Liu *et al.*, 2007). We applied this method to control cells, Δ*kin3* mutants and K1^{r}PX expressing strains. Consistent with previous results (Treitschke *et al.*, 2010), we only rarely found the dark precipitate derived from a reaction of diaminobenzidine and H_2O_2 (Fig. 5A, 5B; Control). However, both Δkin3 mutants and cells expressing K1^{r}PX under the *crg* promoter showed prominent staining, suggesting that they were recognized by the plant defence system (Fig. 5A, 5B; ΔKin3, crgK1^{r}PX). In contrast, cells that expressed K1^{r}PX under the *mig1* promoter showed only weak staining (Fig. 5A, 5B; migK1^{r}PX). These results suggest that motility of EEs is necessary for the fungus to escape the recognition by the plant defence system.

Discussion

In eukaryotes bidirectional motility of EEs was reported *in vivo* in plants during root hair formation in *Medicago truncatula* and in *Arabidopsis thaliana* (Voigt *et al.*, 2005) and in animals (Clarke *et al.*, 2002; Hoepfner *et al.*, 2005; Driskell *et al.*, 2007; Loubery *et al.*, 2008; Soppina *et al.*, 2009; Huckaba *et al.*, 2011). EEs are small and usually irregularly shaped intracellular membrane-bound compartments mostly found in the periphery of the animal cell (Parton *et al.*, 1992; Wilson *et al.*, 2000), they also cluster at growth sites in plants (Voigt *et al.*, 2005). This localization results from the main role of EEs which is endocytic membrane transport pathway from the plasma membrane to the plasma membrane (recycling) or via late endosomes to the lysosomes/vacuoles (sorting/degrading). Additionally in higher eukaryotes EEs can be directed from

the plasma membrane to the nucleus where their transported effector proteins mediate signal transduction (Miaczynska *et al.*, 2004; Platta and Stenmark, 2011). In filamentous fungi EEs move bidirectionally over long distances (Wedlich-Söldner *et al.*, 2000; Higuchi *et al.*, 2006; Abenza *et al.*, 2009; Zekert and Fischer, 2009; Penalva, 2010) and their movement is kinesin-3 and dynein dependent (Wedlich-Söldner *et al.*, 2002; Lenz *et al.*, 2006; Zekert and Fischer, 2009; Zhang *et al.*, 2010; Yao *et al.*, 2011; Egan *et al.*, 2012a). Bidirectionality of EE motility has been studied in great detail in *U. maydis* and revealed that this mechanism is a stochastic process (Schuster *et al.*, 2011a) based on transient binding of dynein to EEs (Schuster *et al.*, 2011b). Although much effort has been put recently on understanding how EEs can move over long distances (Schuster *et al.*, 2011c), the role of this motility is not known. It was speculated that EEs could serve in hypha for signalling purposes with the nucleus (Steinberg, 2007c) or for communication between cell ends that could synchronize septum formation and tip advancement (Schuster *et al.*, 2011c), but the experimental evidence is missing. We previously reported that EEs participate in early steps of transition from yeast-like to hyphal cells via pheromone receptor Pra1 recycling necessary during mating of two compatible haploid cells (Fuchs *et al.*, 2006). In addition, a defect in EE motility, caused by using of *yup1*^{ts} under restrictive conditions, led to a cell separation defect (CSD) and an impairment of polar growth as a result of a defect in secretion of cell wall components (Wedlich-Söldner *et al.*, 2000). In this study we were therefore focused on the complex role of EE motility during the entire cell cycle of *U. maydis*.

EE motility is of minor importance for septum formation in yeast-like cells.

Previously we have shown that EE motility in yeast-like cells is dependent on the cell cycle (Wedlich-Söldner *et al.*, 2002), which reorganizes the MT array via cell-cycle dependent nucleation sites (Straube *et al.*, 2003). Indeed, EE motility is observed during all cell cycle stages except for mitosis when cytoplasmic MTs disappear and nonmotile EEs are dispersed in the cell (Wedlich-Söldner *et al.*, 2002). In the last step of cytokinesis in *U. maydis*, when separation occurs between yeast-like sporidia, mother and daughter cells, EEs accumulate at both

sides of the septum (Wedlich-Söldner *et al.*, 2002). Further study revealed that this happens only during formation of the primary septum; after its closure accumulation of EEs occurs solely at the daughter side of the septum where Don1, a GEF of the small GTPase Cdc42 (Mahlert *et al.*, 2006), initiates a secondary septum and formation of the vacuolated fragmentation zone between mother and daughter cell (Schink and Bölker, 2009). When the secondary septum is formed, EEs are enclosed between the two septa within the developing vacuolar fragmentation zone (Schink and Bölker, 2009), where breakdown of the cell wall occurs (Weinzierl *et al.*, 2002). Accumulation of EEs labelled with Yup1-GFP or Don1-GFP in the fragmentation zone between mother and daughter cell and between primary and secondary septum suggested involvement of these organelles in septum formation and cytokinesis through the activity of Don1 protein attached to the endosomal membrane via its FYVE domain (Schink and Bölker, 2009). The failure in physical separation between relative haploid cells results in a cell separation defect (CSD) where tree-like aggregates are formed in liquid culture and *U. maydis* colonies form typical 'donut' structures on a solid medium. This defect in morphology phenotype was found among others in *kin3* (Wedlich-Söldner *et al.*, 2002), *don1* (a GEF specific for Cdc42; Weinzierl *et al.*, 2002; Hlubek *et al.*, 2008), *cdc42* (small GTP-binding protein of the Rho family; Mahlert *et al.*, 2006) and *drf1* mutants (Freitag *et al.*, 2011). In this study we confirm that EE motility is involved in septum formation, as blockage of EE motility leads to changes in yeast-like cell morphological phenotypes and increases CSD in liquid cultures expressing K1^{r}PX. However, this effect is less prominent in comparison to cells depleted of *kin3* or expressing kinesin-3 rigor, both exhibited more than 90% of CSD. This result rather suggests kinesin-3 involvement in septum formation than motile EEs. It is supported by previously shown evidence that the presence of Don1 is not required for correct septation (Mahlert *et al.*, 2006) and was supported by a study where overexpression of Don1 lacking a functional FYVE domain, necessary for binding to endosomal membrane lipids, rescues CSD and suggests that the presence of Don1 is not required for its GEF activity (Schink and Bölker, 2009). We hypothesise that kinesin-3 might be involved in delivery of lytic enzymes necessary for lysis of the septal cell wall components like polysaccharides (e.g. chitin and glucan) and polypeptides (Ruiz-Herrera *et al.*, 1996). In the case of the *kin3* mutant two septa are formed between mother

and daughter cells (Wedlich-Söldner *et al.*, 2002), but in cells defective for either *don1*, *cdc42* or *drf1* only a single septum is formed suggesting that these proteins are necessary in secondary septum formation required for proper cell separation (Weinzierl *et al.*, 2002; Mahlert *et al.*, 2006; Freitag *et al.*, 2011). Interestingly, among the proteins necessary for secondary septum formation only Cdc42 is essential for pathogenic development (Mahlert *et al.*, 2006). Although a null *don1* mutants showed reduced virulence (Freitag *et al.*, 2011), Don1 is not required for mating, filamentous growth of the dikaryon, spore production or pathogenic development *in planta* (Weinzierl *et al.*, 2002).

EE motility is required for hyphal growth.

During filamentous growth of *U. maydis* the cell cycle is arrested in a postreplicative G2 phase (Garcia-Muse *et al.*, 2003) and MT array span the entire length of the hypha thanks to the presence of cytoplasmic MT-organizing centres (Schuster *et al.*, 2011c). Antipolar oriented MTs form bundles in the centre of the cell, whereas distal parts of the hypha contain unipolarly oriented MTs (Schuster *et al.*, 2011c) thus providing long tracks for vesicular transport. This allows long range bidirectional motility of EEs mainly mediated by kinesin-3 activity (Schuster *et al.*, 2011c). We have shown previously that kinesin-1 and kinesin-3 cooperate in hyphal growth and mutants depleted of each of the kinesins exhibit bipolar morphology and twofold reduction in hyphal growth rates (Schuchardt *et al.*, 2005). In this study we show that blockage of EE motility by overexpression of K1^{r}PX also leads to changes in the hyphal phenotype where bipolar hyphae grow twofold slower in comparison to the wildtype. Similar bipolar hyphae which exhibit slow growth rates were observed in a null *kin3* mutant presented previously (Schuchardt *et al.*, 2005) and in this study. This result indicates disturbed cell polarity, probably as an effect of blocked EE motility.

EE motility occurs during all pathogenic stages.

Endocytosis has been shown to be essential during initial steps of pathogenic development (Fuchs *et al.*, 2006) and that EEs link exo- and endocytosis (Wedlich-Söldner *et al.*, 2000). In addition to the endocytic pathway, EEs are

involved in Rrm4 mediated local protein translation (Baumann *et al.*, 2012), although not many transcripts have been described to date. In order to test the importance of EE motility at different stages of pathogenic development we infected maize plants with strains expressing K1^{r}PX under the control of *crg* and maize inducible *mig1* promoters (Basse *et al.*, 2000). As shown in control strains, the *crg* promoter is active for the first 30 hours while *mig1* is activated on the third day after infection. Moreover, we tested the motility of EEs *in planta* and we found that in strain expressing K1^{r}PX under the control of *crg* promoter EEs did not move for the first 2-3 dpi, whereas in strain expressing K1^{r}PX under the control of *mig1* promoter motility of EEs was blocked after 3-4 dpi. Infection by the strain expressing K1^{r}PX under the control of *crg* promoter led to very small disease symptoms, comparable to the symptoms developed after infection with SG200 strain depleted of *kin3*. It suggests that kinesin-3 serves mainly as an EE transporter and some role in secretion previously reported (Schuchardt *et al.*, 2005) is of minor importance in virulence. Interestingly, the strain expressing K1^{r}PX under the control of *mig1* promoter was fully infectious and all disease symptoms were observed similarly to those observed after infecting maize plants with the control strain.

The results presented here demonstrate that motility of EEs is crucial for early pathogenic development, whereas blocking of EE motility at later stages does not affect the virulence of the fungus. During the first two days after infection, according to previous studies (Snetselaar and Mims, 1994; Doehlemann *et al.*, 2008b; Mendoza-Mendoza *et al.*, 2009), *U. maydis* cells undergo a morphological transition from non-pathogenic yeast-like cells to invasive elongated hyphae. 12 hours post infection fungal cells develop filaments and soon after (up to 16 hpi) – appressoria. The invasion starts with an appressorium formation that penetrates the plant cuticle by breaching the host cell wall and by invading the host plasma membrane, although penetration through the stomata has also been observed (Mills and Kotzé, 1981; Banuett and Herskowitz, 1996). After 24-48 hpi most fungal cells are inside the host tissue. In the first 2-3 days of infection, epidermal cells of infected leaves contain unbranched hyphae growing intracellularly (Snetselaar and Mims, 1994). Three days after infection, hyphae start to scatter and start to grow intercelullarly. In other words, elongation of the infectious hyphae occurs mainly during the first two days of the pathogenic development. We confirmed these

observations by measuring the ratio between length and width of hypha. Indeed, from the second day post infection hyphae undergo shortening which is in agreement with previous observations (Snetselaar and Mims, 1994). This suggests that only the elongated shape of the fungal cell allows intracellular growth and can be supported by previous observations that sporulation occurs mainly between the host cells (Snetselaar and Mims, 1994).

Hyphal growth and escape from the host defence.

Hyphal cells are expanded by polar tip growth. The need for fast growing hypha is to explore and to penetrate the environment, and more specifically in case of pathogenic filamentous fungi – to colonize the host organism. In the case of human fungal pathogens (*Candida* and *Aspergillus*) and the majority of plant fungal pathogens, which undergo dimorphic transition, avirulence is usually correlated with an inability of hyphae formation (Lo *et al.*, 1997; Sanchez-Martinez and Perez-Martin, 2001; Nadal *et al.*, 2008; Brand, 2012; Wang and Lin, 2012). As observed previously, infection performed by individual *U. maydis* haploid strains leads to neither mating, nor pathogenic development and most of the cells have a budding morphology (Snetselaar and Mims, 1993). Based on phylogenetic analyses hyphae represent the ancestral growth form before yeast (Hibbett *et al.*, 2007; Harris, 2011). Yeast fungi like *S. cerevisiae* have lost a number of genes implicated with filamentous growth (Harris *et al.*, 2009a) like some motor proteins (kinesin-1 and kinesin-3), which have been shown as necessary for hyphae formation in the filamentous fungi *U. maydis*, *N. crassa*, *Nectria haematococca*, *A. nidulans* (Lehmler *et al.*, 1997; Seiler *et al.*, 1997; Wu *et al.*, 1998; Requena *et al.*, 2001; Schuchardt *et al.*, 2005; Zekert and Fischer, 2009). Together with losing some genes involved in morphologic transition, the yeast *S. cerevisiae* has also lost some components of defence (Takemoto *et al.*, 2007; Harris *et al.*, 2009a; Harris, 2011). Among mutants affecting both filamentous growth and virulence of *U. maydis* are motor proteins involved in vesicle transport (Lehmler *et al.*, 1997; Weber *et al.*, 2003; Schuchardt *et al.*, 2005) and proteins associated with the EEs (Wedlich-Söldner *et al.*, 2000; Becht *et al.*, 2006; Fuchs *et al.*, 2006; Doehlemann *et al.*, 2011; Freitag *et al.*, 2011; Baumann *et al.*, 2012). Among these proteins is a RNA-binding protein, Rrm4 (Baumann *et al.*, 2012), which is implicated in pathogenic development of

U. maydis (Becht *et al.*, 2005) and is considered as an integral component of the transport machinery (König *et al.*, 2009). Recruitment of Rrm4 into particles is increased during filamentation (Becht *et al.*, 2006) and deletion of *rrm4* leads to impairment of filamentous growth and pathogenicity (Becht *et al.*, 2005) and disturbs polar growth of the filaments (Becht *et al.*, 2006), similarly to *kin1*Δ mutants, where short, bipolar hyphae depleted of vacuolated hyphal parts were observed (Schuchardt *et al.*, 2005). Early blockage of EEs by expression of the synthetic anchor under *crg* promoter would also block delivery of the translation machinery to the hyphal tip thus preventing local translation of the secreted proteins although there is lack of evidence for such proteins to date. Recent finding of a gene cluster of 'proteins important for tumor' (Doehlemann *et al.*, 2011) possibly links the EEs and virulence. The secreted effector protein Pit2, an essential virulence factor, requires a transmembrane protein, Pit1 to induce tumor formation. The linkage between the virulence and EEs would be Pit1, as it is most probably recycled from the plasma membrane via EEs to vacuoles and back like Pra1 pheromone receptor (Fuchs *et al.*, 2006). It is also suggested that Pit1, which is upregulated during biotrophic development and specifically expressed in filaments that form appressoria where it accumulates, could act in the pathway of receptor mediated endocytosis to trigger the uptake of unknown apoplastic ligands or has a function which requires continuous replacement of the protein (Doehlemann *et al.*, 2011).

Our work provides clear evidence that EE motility is crucial during early stages of pathogenic development which is correlated with yeast to hypha formation. Furthermore, we prove that EE motility is necessary for filamentous cell formation. This dimorphic switch is correlated in time with suppressing of the host defence – oxidative burst, which is mainly based on the production of reactive oxygen species (e.g. H_2O_2; Apostol *et al.*, 1989; Wojtaszek, 1997). We showed that by using DAB staining (Doehlemann *et al.*, 2009), accumulation of H_2O_2 around fungal cells was found in the majority of plant tissues infected by a strain depleted of *kin3* or a strain expressing $K1^rPX$ under the control of *crg* promoter. Almost no DAB staining was found in maize leaves infected by a control strain or a strain expressing $K1^rPX$ under the control of *mig1* promoter.

Although later stages of infection, apparently, do not depend of EE motility as was presented by expression of the synthetic anchor under *mig1* promoter, their

motility occurs during all infection stages as was shown *in planta*. The function of EE motility in later stages is unknown and requires further investigation.

Methods

Strains and plasmids

U. maydis strains used in this study have the genetic background of AB33 (*a2 PnarbW2 PnarbE1, ble*^{R}; Brachmann *et al.*, 2001) or SG200 (*a1 mfa2 bW2 bE1, ble*^{R}*;* Bölker *et al.*, 1995) and are summarized in Supplementary Table 1. For introducing recombinant DNA sequences into *U. maydis*, the homologous recombination technique was used (Brachmann *et al.*, 2004). In conditional strains, the respective genes were expressed under the conditional *crg* promoter (Bottin *et al.*, 1996). Further details can be found in the Supplementary Online Methods.

Growth conditions

All cultures of *U. maydis* were grown overnight at 28°C in complete medium (CM; Holliday, 1974) containing 1% (w/v) glucose, shaken at 200 rpm. Hyphal growth in the AB33_po^{N}GRab5a, AB33ΔKin3_po^{H}mChRab5a_Kin3G, AB33_po^{N}GRab5a and AB33ΔKin3_po^{C}GRab5a strains was induced by shifting to NM liquid medium supplemented with 1% (w/v) glucose (Brachmann *et al.*, 2001). To induce expression of proteins under *crg* promoter cells were grown overnight in CM containing 1% (w/v) arabinose. Hyphal growth in the AB33G$_3$Dyn2_Kin1^{rigor}, AB33_po^{N}GRab5a_r^{H}K1^{r}PX, AB33_po^{N}GRab5a_r^{H}K1^{r}PX, AB33Kin3G_po$_{m}$ChRab5a_rK1^{r}PX, AB33Kin3G_po$_{m}$ChRab5a_rK1^{r}PX, AB33_po^{N}GRab5a_r^{H}K1^{r}PX strains was induced by shifting to NM liquid medium supplemented with 1% arabinose for 5 h, unless stated otherwise (Brachmann *et al.*, 2001).

Protein extraction and immunodetection by Western Blotting

To analyse the expression level of a synthetic molecular anchor by Western Blotting, cell extracts of the AB33_mChRab5a_rK1rG-PX strain and a control strain AB33ΔKin3_po^{H}mChRab5a were derived from 200 ml overnight cultures and were obtained by disruption of LN_2-frozen Ustilago cells grown to OD600 0.9-1.2 in a mixer mill MM200 (Retsch) at frequency 30/s for 2 x 2.5 min. Thawed cell extracts were resuspended in 0.1-0.5 ml of 50 mM Hepes, 50 mM KCl, 1 mM EGTA, 1 mM $MgCl_2$, pH 7.0 complemented with protease inhibitor (Roche Complete Mini #11836153001) and centrifuged at 50,000 g for 30 minutes at 4°C. Concentrations of soluble fractions were analysed according to Bradford (Bradford, 1976). 30 ug of each sample was loaded on 8% SDS-polyacrylamide gels and transferred onto nitrocellulose membrane (GE Healthcare, United Kingdom) for 55 min at 190 mA in a semi-dry blot chamber (Fastblot, Analytik Jena, Germany). Each blot was blocked for an hour with 5% non-fat milk in TBS-1% Tween-20 and incubated with anti-GFP mouse IgG monoclonal antibodies in a 1:5000 dilution (Roche, #11814460001) overnight at 4°C followed by incubation with HRP-conjugated anti-mouse IgG in a 1:4000 dilution (Promega #W402B). Confirmation of the equivalent protein loading was done by stripping the membranes and re-probing them with mouse anti-α tubulin antibodies in a 1:4000 dilution (Oncogene Science, Cambridge, MA) followed by HRP-conjugated anti-mouse IgG in a 1:4000 dilution. All blots were developed using ECL Plus Western Blotting Detection system, following the manufacturer's instructions (GE Healthcare #RPN2132). Quantitative western analysis was performed using digital images and MetaMorph (Molecular Devices).

Laser-based epifluorescence microscopy

Microscopy was done essentially as previously described (Schuster *et al.*, 2011a; Schuster *et al.*, 2011b) using 488 and 561 nm solid-state lasers (488 nm/75 mW and 561 nm/75 mW; Visitron Systems, Munich, Germany) for excitation of fluorescent proteins. In brief, cells from logarithmically growing cultures (28°C, 200 rpm, overnight) were placed on a thin 2% agarose-layer and immediately observed using an IX81 microscope (Olympus, Hamburg, Germany) and a VS-LMS4 Laser-Merge-System (Visitron, Visitron Systems,

Munich, Germany). The photobleaching experiments were performed using a 2D-VisiFRAP system (Visitron Systems) consisting of a 405 nm/60 mW diode laser which was dimmed by a neutral density 0.6 filter, resulting in 15 mW output power. A Dual-View Microimager (Photometrics) and appropriate filters were used for colocalization studies. Images were captured using a Photometrics CoolSNAP HQ2 camera (Roper Scientific, Germany). All parts of the system were controlled by MetaMorph (Molecular Devices, Downingtown). Image processing was performed using MetaMorph.

Quantitative assessment of cell morphology and EE motility

To analyse the ratio of cell length to cell width of *U. maydis* cells during plant infection, DIC pictures were taken and the length of each cell was measured in the region from the tip to the first retraction septum. In the middle of each region measurement of the cell width was performed.

The number of motile EEs in the absence and in the presence of a synthetic molecular anchor was measured within the entire yeast-like cells (in liquid culture) and after plant infection using 488 nm observation laser at 50% output power. Signals that did not move during 75-frame movie (equivalent of 10 s) were considered as nonmotile EEs. Further details can be found in the Supplementary Online Methods.

Kin3 motility independent from EEs in the absence and in the presence of a synthetic molecular anchor was measured within the photobleached bud region in the middle-sized budded yeast-like cells and within the first 15 µm of the hyphal tip using kymographs obtained from 75-frame dual movies. The number of anterograde lines corresponding to Kin3-GFP motilities which were not colocalized with mCherry labelled Rab5a was divided by the number of anterograde lines derived from all Kin3-GFP signals. Further details can be found in the Supplementary Online Methods.

The cell separation defect [%] was calculated as a ratio of the number of cells with the cell separation defect (a cell composed of more than two cells) to the total number of cells including cells without that defect (composed of maximum of two cells).

To analyse the hyphal elongation rate, overnight grown cultures of the AB33_po^{N}GRab5a, AB33ΔKin3_po^{C}GRab5a and AB33_po^{N}GRab5a_r^{H}K1^{r}PX strains were shifted to NM media containing 1% (w/v) glucose or arabinose (Brachmann *et al.*, 2001). Brightfield images were taken for each strain immediately (time point: 0 h) and then after each hour for a period of 8 hours. Further details can be found in the Supplementary Online Methods.

Statistical analyses of data were performed using GraphPad Prism 5.03. Unless stated otherwise, all values are given as mean±standard error of the mean (SEM).

Microscopy of infected plant tissue

Unless stated otherwise, microscopy of infected plant tissue was performed as previously described (Doehlemann *et al.*, 2009). Maize leaves were harvested at 2, 4, 6 and 8 d post infection and sections of leaf 1-3 cm below infection sites were excised for microscopy.

To test *crg* and *mig1* promoter activities in *planta*, maize plants were infected with 0.5 ml of the SG200_crgGFP or SG200_mig1GFP strain cultures which were grown prior to infection in CM media containing 1% (w/v) arabinose or 1% (w/v) glucose, respectively. Maize tissue samples were collected at different time points and the maximum intensity of the region within the *U. maydis* cell was measured. Further details can be found in the Supplementary Online Methods.

H_2O_2 accumulation in infected plant tissues was detected using DAB (Sigma-Aldrich) as described (Molina and Kahmann, 2007) with few modifications (Bindschedler *et al.*, 2006; Daudi *et al.*, 2012). Further details can be found in the Supplementary Online Methods.

Infected plant leaves were stained with propidium iodide / WGA-AF488 as described (Doehlemann *et al.*, 2009; Treitschke *et al.*, 2010). Further details can be found in the Supplementary Online Methods.

Quantitative assessment of fungal virulence

Pathogenicity assays were performed as previously described (Kämper *et al.*, 2006). In brief, liquid cultures of the *U. maydis* strains were grown overnight at 28°C in complete medium (CM, Holliday, 1974) containing 1% (w/v) glucose or 1% (w/v) arabinose, shaken at 200 rpm to an OD600 of 0.4 to 1.0, centrifuged, resuspended in 10 ml of water and syringe injected into twenty of 8-9 days-old and 14-25 cm high maize (Zea mays) plants (variety Early Golden Bantam; 'Organic Gardening'). Disease symptoms were scored 8 days after infection as follows: 'no tumors' (no tumor, chlorosis, antocyan formation), 'small tumors' (tumors up to 3 mm) and 'large tumors' (tumors over 3 mm).

Acknowledgement

We thank Ms Laura Yeves-Gonzalez for technical assistance. We are grateful for receiving plasmids and strains from Dr. Sreedhar Kilaru (strain AB33ΔKin3_po^{C}GRab5a), Dr. Uta Fuchs (plasmid pSl-Yup-RFP-Hyg) and Dr. Isabel Schuchardt, Göttingen, Germany (plasmid po^{C}GRab5a). This work was supported by a grant from the Biotechnology and Biological Sciences Research Council (BB/F022956/1).

References

Abenza, J.F., Pantazopoulou, A., Rodriguez, J.M., Galindo, A., and Penalva, M.A. (2009). Long-distance movement of *Aspergillus nidulans* early endosomes on microtubule tracks. Traffic *10*, 57-75.

Apostol, I., Heinstein, P.F., and Low, P.S. (1989). Rapid Stimulation of an Oxidative Burst during Elicitation of Cultured Plant Cells: Role in Defense and Signal Transduction. Plant Physiol *90*, 109-116.

Banuett, F., and Herskowitz, I. (1996). Discrete developmental stages during teliospore formation in the corn smut fungus, *Ustilago maydis*. Development *122*, 2965-2976.

Basse, C.W., Stumpferl, S., and Kahmann, R. (2000). Characterization of a *Ustilago maydis* gene specifically induced during the biotrophic phase: evidence for negative as well as positive regulation. Mol Cell Biol *20*, 329-339.

Baumann, S., Pohlmann, T., Jungbluth, M., Brachmann, A., and Feldbrügge, M. (2012). Kinesin-3 and dynein mediate microtubule-dependent co-transport of mRNPs and endosomes. J Cell Sci *125*, 2740-2752.

Becht, P., Konig, J., and Feldbrügge, M. (2006). The RNA-binding protein Rrm4 is essential for polarity in *Ustilago maydis* and shuttles along microtubules. J Cell Sci *119*, 4964-4973.

Becht, P., Vollmeister, E., and Feldbrügge, M. (2005). Role for RNA-binding proteins implicated in pathogenic development of *Ustilago maydis*. Eukaryot Cell *4*, 121-133.

Bindschedler, L.V., Dewdney, J., Blee, K.A., Stone, J.M., Asai, T., Plotnikov, J., Denoux, C., Hayes, T., Gerrish, C., Davies, D.R., Ausubel, F.M., and Bolwell, G.P. (2006). Peroxidase-dependent apoplastic oxidative burst in *Arabidopsis* required for pathogen resistance. Plant J *47*, 851-863.

Bölker, M., Genin, S., Lehmler, C., and Kahmann, R. (1995). Genetic regulation of mating and dimorphism in *Ustilago maydis*. Canadian Journal of Botany *73*, 320-325.

Bottin, A., Kamper, J., and Kahmann, R. (1996). Isolation of a carbon source-regulated gene from *Ustilago maydis*. Mol Gen Genet *253*, 342-352.

Brachmann, A., König, J., Julius, C., and Feldbrügge, M. (2004). A reverse genetic approach for generating gene replacement mutants in *Ustilago maydis*. Mol Genet Genomics *272*, 216-226.

Brachmann, A., Weinzierl, G., Kämper, J., and Kahmann, R. (2001). Identification of genes in the *bW/bE* regulatory cascade in *Ustilago maydis*. Mol Microbiol *42*, 1047-1063.

Brand, A. (2012). Hyphal growth in human fungal pathogens and its role in virulence. Int J Microbiol *2012*, 517529.

Brefort, T., Doehlemann, G., Mendoza-Mendoza, A., Reissmann, S., Djamei, A., and Kahmann, R. (2009). *Ustilago maydis* as a Pathogen. Annu Rev Phytopathol *47*, 423-445.

Christensen, J.J. (1963). Corn smut caused by *Ustilago maydis.* In American Phytopathology Society Monograph *No. 2*, 1-41.

Clarke, M., Kohler, J., Heuser, J., and Gerisch, G. (2002). Endosome fusion and microtubule-based dynamics in the early endocytic pathway of *Dictyostelium*. Traffic *3*, 791-800.

Daudi, A., Cheng, Z., O'Brien, J.A., Mammarella, N., Khan, S., Ausubel, F.M., and Bolwell, G.P. (2012). The apoplastic oxidative burst peroxidase in *Arabidopsis* is a major component of pattern-triggered immunity. Plant Cell *24*, 275-287.

Djamei, A., Schipper, K., Rabe, F., Ghosh, A., Vincon, V., Kahnt, J., Osorio, S., Tohge, T., Fernie, A.R., Feussner, I., Feussner, K., Meinicke, P., Stierhof, Y.D., Schwarz, H., Macek, B., Mann, M., and Kahmann, R. (2011). Metabolic priming by a secreted fungal effector. Nature *478*, 395-398.

Doehlemann, G., Reissmann, S., Assmann, D., Fleckenstein, M., and Kahmann, R. (2011). Two linked genes encoding a secreted effector and a membrane protein are essential for *Ustilago maydis*-induced tumour formation. Mol Microbiol *81*, 751-766.

Doehlemann, G., van der Linde, K., Assmann, D., Schwammbach, D., Hof, A., Mohanty, A., Jackson, D., and Kahmann, R. (2009). Pep1, a secreted effector protein of *Ustilago maydis*, is required for successful invasion of plant cells. PLoS Pathog *5*, e1000290.

Doehlemann, G., Wahl, R., Horst, R.J., Voll, L.M., Usadel, B., Poree, F., Stitt, M., Pons-Kuhnemann, J., Sonnewald, U., Kahmann, R., and Kämper, J. (2008b). Reprogramming a

maize plant: transcriptional and metabolic changes induced by the fungal biotroph *Ustilago maydis*. Plant J *56*, 181-195.

Driskell, O.J., Mironov, A., Allan, V.J., and Woodman, P.G. (2007). Dynein is required for receptor sorting and the morphogenesis of early endosomes. Nat Cell Biol *9*, 113-120.

Egan, M.J., Tan, K., and Reck-Peterson, S.L. (2012a). Lis1 is an initiation factor for dynein-driven organelle transport. J Cell Biol *197*, 971-982.

Fisher, M.C., Henk, D.A., Briggs, C.J., Brownstein, J.S., Madoff, L.C., McCraw, S.L., and Gurr, S.J. (2012). Emerging fungal threats to animal, plant and ecosystem health. Nature *484*, 186-194.

Freitag, J., Lanver, D., Bohmer, C., Schink, K.O., Bölker, M., and Sandrock, B. (2011). Septation of infectious hyphae is critical for appressoria formation and virulence in the smut fungus *Ustilago maydis*. PLoS Pathog *7*, e1002044.

Fuchs, U., Hause, G., Schuchardt, I., and Steinberg, G. (2006). Endocytosis is essential for pathogenic development in the corn smut fungus *Ustilago maydis*. Plant Cell *18*, 2066-2081.

Fuchs, U., Manns, I., and Steinberg, G. (2005a). Microtubules are dispensable for the initial pathogenic development but required for long-distance hyphal growth in the corn smut fungus *Ustilago maydis*. Mol Biol Cell *16*, 2746-2758.

Garcia-Muse, T., Steinberg, G., and Perez-Martin, J. (2003). Pheromone-induced G2 arrest in the phytopathogenic fungus *Ustilago maydis*. Eukaryot Cell *2*, 494-500.

Gow, N.A., Brown, A.J., and Odds, F.C. (2002). Fungal morphogenesis and host invasion. Curr Opin Microbiol *5*, 366-371.

Harris, S.D. (2011). Hyphal morphogenesis: an evolutionary perspective. Fungal Biol *115*, 475-484.

Harris, S.D., Turner, G., Meyer, V., Espeso, E.A., Specht, T., Takeshita, N., and Helmstedt, K. (2009a). Morphology and development in *Aspergillus nidulans*: a complex puzzle. Fungal Genet Biol *46 Suppl 1*, S82-S92.

Heimel, K., Scherer, M., Vranes, M., Wahl, R., Pothiratana, C., Schuler, D., Vincon, V., Finkernagel, F., Flor-Parra, I., and Kämper, J. (2010a). The transcription factor Rbf1 is the master regulator for *b*-mating type controlled pathogenic development in *Ustilago maydis*. PLoS Pathog *6*, e1001035.

Hemetsberger, C., Herrberger, C., Zechmann, B., Hillmer, M., and Doehlemann, G. (2012). The *Ustilago maydis* effector Pep1 suppresses plant immunity by inhibition of host peroxidase activity. PLoS Pathog *8*, e1002684.

Hibbett, D.S., Binder, M., Bischoff, J.F., Blackwell, M., Cannon, P.F., Eriksson, O.E., Huhndorf, S., James, T., Kirk, P.M., Lucking, R., Thorsten Lumbsch, H., Lutzoni, F., Matheny, P.B., McLaughlin, D.J., Powell, M.J., Redhead, S., Schoch, C.L., Spatafora, J.W., Stalpers, J.A., Vilgalys, R., Aime, M.C., Aptroot, A., Bauer, R., Begerow, D., Benny, G.L., Castlebury, L.A., Crous, P.W., Dai, Y.C., Gams, W., Geiser, D.M., Griffith, G.W., Gueidan, C., Hawksworth, D.L., Hestmark, G., Hosaka, K., Humber, R.A., Hyde, K.D., Ironside, J.E., Koljalg, U., Kurtzman, C.P., Larsson, K.H., Lichtwardt, R., Longcore, J., Miadlikowska, J., Miller, A., Moncalvo, J.M., Mozley-Standridge, S., Oberwinkler, F., Parmasto, E., Reeb, V., Rogers, J.D., Roux, C., Ryvarden, L., Sampaio, J.P., Schussler, A., Sugiyama, J., Thorn, R.G., Tibell, L., Untereiner, W.A., Walker,

C., Wang, Z., Weir, A., Weiss, M., White, M.M., Winka, K., Yao, Y.J., and Zhang, N. (2007). A higher-level phylogenetic classification of the Fungi. Mycol Res *111*, 509-547.

Higuchi, Y., Nakahama, T., Shoji, J.Y., Arioka, M., and Kitamoto, K. (2006). Visualization of the endocytic pathway in the filamentous fungus *Aspergillus oryzae* using an EGFP-fused plasma membrane protein. Biochem Biophys Res Commun *340*, 784-791.

Hlubek, A., Schink, K.O., Mahlert, M., Sandrock, B., and Bölker, M. (2008). Selective activation by the guanine nucleotide exchange factor Don1 is a main determinant of Cdc42 signalling specificity in *Ustilago maydis*. Mol Microbiol *68*, 615-623.

Hoepfner, S., Severin, F., Cabezas, A., Habermann, B., Runge, A., Gillooly, D., Stenmark, H., and Zerial, M. (2005). Modulation of receptor recycling and degradation by the endosomal kinesin KIF16B. Cell *121*, 437-450.

Holliday, R. (1974). *Ustilago maydis.* In Handbook of Genetics, ed. RC King, New York. Plenum Press, 575-595.

Huckaba, T.M., Gennerich, A., Wilhelm, J.E., Chishti, A.H., and Vale, R.D. (2011). Kinesin-73 is a processive motor that localizes to Rab5-containing organelles. J Biol Chem *286*, 7457-7467.

Kämper, J., Kahmann, R., Bölker, M., Ma, L.J., Brefort, T., Saville, B.J., Banuett, F., Kronstad, J.W., Gold, S.E., Muller, O., Perlin, M.H., Wosten, H.A., de Vries, R., Ruiz-Herrera, J., Reynaga-Pena, C.G., Snetselaar, K., McCann, M., Perez-Martin, J., Feldbrügge, M., Basse, C.W., Steinberg, G., Ibeas, J.I., Holloman, W., Guzman, P., Farman, M., Stajich, J.E., Sentandreu, R., Gonzalez-Prieto, J.M., Kennell, J.C., Molina, L., Schirawski, J., Mendoza-Mendoza, A., Greilinger, D., Munch, K., Rossel, N., Scherer, M., Vranes, M., Ladendorf, O., Vincon, V., Fuchs, U., Sandrock, B., Meng, S., Ho, E.C., Cahill, M.J., Boyce, K.J., Klose, J., Klosterman, S.J., Deelstra, H.J., Ortiz-Castellanos, L., Li, W., Sanchez-Alonso, P., Schreier, P.H., Hauser-Hahn, I., Vaupel, M., Koopmann, E., Friedrich, G., Voss, H., Schluter, T., Margolis, J., Platt, D., Swimmer, C., Gnirke, A., Chen, F., Vysotskaia, V., Mannhaupt, G., Guldener, U., Munsterkotter, M., Haase, D., Oesterheld, M., Mewes, H.W., Mauceli, E.W., DeCaprio, D., Wade, C.M., Butler, J., Young, S., Jaffe, D.B., Calvo, S., Nusbaum, C., Galagan, J., and Birren, B.W. (2006). Insights from the genome of the biotrophic fungal plant pathogen *Ustilago maydis*. Nature *444*, 97-101.

König, J., Baumann, S., Koepke, J., Pohlmann, T., Zarnack, K., and Feldbrügge, M. (2009). The fungal RNA-binding protein Rrm4 mediates long-distance transport of ubi1 and rho3 mRNAs. EMBO J *28*, 1855-1866.

Lehmler, C., Steinberg, G., Snetselaar, K.M., Schliwa, M., Kahmann, R., and Bölker, M. (1997). Identification of a motor protein required for filamentous growth in *Ustilago maydis*. EMBO J *16*, 3464-3473.

Lenz, J.H., Schuchardt, I., Straube, A., and Steinberg, G. (2006). A dynein loading zone for retrograde endosome motility at microtubule plus-ends. EMBO J *25*, 2275-2286.

Liu, G., Greenshields, D.L., Sammynaiken, R., Hirji, R.N., Selvaraj, G., and Wei, Y. (2007). Targeted alterations in iron homeostasis underlie plant defense responses. J Cell Sci *120*, 596-605.

Lo, H.J., Kohler, J.R., DiDomenico, B., Loebenberg, D., Cacciapuoti, A., and Fink, G.R. (1997). Nonfilamentous *C. albicans* mutants are avirulent. Cell *90*, 939-949.

Loubery, S., Wilhelm, C., Hurbain, I., Neveu, S., Louvard, D., and Coudrier, E. (2008). Different microtubule motors move early and late endocytic compartments. Traffic *9*, 492-509.

Mahlert, M., Leveleki, L., Hlubek, A., Sandrock, B., and Bölker, M. (2006). Rac1 and Cdc42 regulate hyphal growth and cytokinesis in the dimorphic fungus *Ustilago maydis*. Mol Microbiol *59*, 567-578.

Mendoza-Mendoza, A., Berndt, P., Djamei, A., Weise, C., Linne, U., Marahiel, M., Vranes, M., Kämper, J., and Kahmann, R. (2009). Physical-chemical plant-derived signals induce differentiation in *Ustilago maydis*. Mol Microbiol *71*, 895-911.

Miaczynska, M., Christoforidis, S., Giner, A., Shevchenko, A., Uttenweiler-Joseph, S., Habermann, B., Wilm, M., Parton, R.G., and Zerial, M. (2004). APPL proteins link Rab5 to nuclear signal transduction via an endosomal compartment. Cell *116*, 445-456.

Mills, L.J., and Kotzé, J.M. (1981). Scanning Electron Microscopy of the Germination, Growth and Infection of *Ustilago maydis* on Maize. Journal of Phytopathology *102*, 21-27.

Molina, L., and Kahmann, R. (2007). An *Ustilago maydis* gene involved in H2O2 detoxification is required for virulence. Plant Cell *19*, 2293-2309.

Mueller, O., Kahmann, R., Aguilar, G., Trejo-Aguilar, B., Wu, A., and de Vries, R.P. (2008). The secretome of the maize pathogen *Ustilago maydis*. Fungal Genet Biol *45 Suppl 1*, S63-70.

Müller, O., Schreier, P.H., and Uhrig, J.F. (2008). Identification and characterization of secreted and pathogenesis-related proteins in *Ustilago maydis*. Mol Genet Genomics *279*, 27-39.

Nadal, M., Garcia-Pedrajas, M.D., and Gold, S.E. (2008). Dimorphism in fungal plant pathogens. FEMS Microbiol Lett *284*, 127-134.

Parton, R.G., Simons, K., and Dotti, C.G. (1992). Axonal and dendritic endocytic pathways in cultured neurons. J Cell Biol *119*, 123-137.

Penalva, M.A. (2010). Endocytosis in filamentous fungi: Cinderella gets her reward. Curr Opin Microbiol *13*, 684-692.

Platta, H.W., and Stenmark, H. (2011). Endocytosis and signaling. Curr Opin Cell Biol *23*, 393-403.

Requena, N., Alberti-Segui, C., Winzenburg, E., Horn, C., Schliwa, M., Philippsen, P., Liese, R., and Fischer, R. (2001). Genetic evidence for a microtubule-destabilizing effect of conventional kinesin and analysis of its consequences for the control of nuclear distribution in *Aspergillus nidulans*. Mol Microbiol *42*, 121-132.

Ruiz-Herrera, J., Leon, C.G., Carabez-Trejo, A., and Reyes-Salinas, E. (1996). Structure and chemical composition of the cell walls from the haploid yeast and mycelial forms of *Ustilago maydis*. Fungal Genet Biol *20*, 133-142.

Sanchez-Martinez, C., and Perez-Martin, J. (2001). Dimorphism in fungal pathogens: *Candida albicans* and *Ustilago maydis*--similar inputs, different outputs. Curr Opin Microbiol *4*, 214-221.

Schink, K.O., and Bölker, M. (2009). Coordination of cytokinesis and cell separation by endosomal targeting of a Cdc42-specific guanine nucleotide exchange factor in *Ustilago maydis*. Mol Biol Cell *20*, 1081-1088.

Schuchardt, I., Assmann, D., Thines, E., Schuberth, C., and Steinberg, G. (2005). Myosin-V, Kinesin-1, and Kinesin-3 cooperate in hyphal growth of the fungus *Ustilago maydis*. Mol Biol Cell *16*, 5191-5201.

Schuster, M., Kilaru, S., Ashwin, P., Lin, C., Severs, N.J., and Steinberg, G. (2011a). Controlled and stochastic retention concentrates dynein at microtubule ends to keep endosomes on track. EMBO J *30*, 652-664.

Schuster, M., Kilaru, S., Fink, G., Collemare, J., Roger, Y., and Steinberg, G. (2011c). Kinesin-3 and dynein cooperate in long-range retrograde endosome motility along a nonuniform microtubule array. Mol Biol Cell *22*, 3645-3657.

Schuster, M., Lipowsky, R., Assmann, M.A., Lenz, P., and Steinberg, G. (2011b). Transient binding of dynein controls bidirectional long-range motility of early endosomes. Proc Natl Acad Sci U S A *108*, 3618-3623.

Schuster, M., Treitschke, S., Kilaru, S., Molloy, J., Harmer, N.J., and Steinberg, G. (2011d). Myosin-5, kinesin-1 and myosin-17 cooperate in secretion of fungal chitin synthase. EMBO J *31*, 214-227.

Seiler, S., Nargang, F.E., Steinberg, G., and Schliwa, M. (1997). Kinesin is essential for cell morphogenesis and polarized secretion in *Neurospora crassa*. EMBO J *16*, 3025-3034.

Snetselaar, K.M., and Mims, C.W. (1993). Infection of Maize Stigmas by *Ustilago maydis*: Light and Electron Microscopy. Phytopathology *83*, 843-850.

Snetselaar, K.M., and Mims, C.W. (1994). Light and electron microscopy of *Ustilago maydis* hyphae in maize. Mycological Research *98*, 347-355.

Soppina, V., Rai, A.K., Ramaiya, A.J., Barak, P., and Mallik, R. (2009). Tug-of-war between dissimilar teams of microtubule motors regulates transport and fission of endosomes. Proc Natl Acad Sci U S A *106*, 19381-19386.

Steinberg, G. (2007c). On the move: endosomes in fungal growth and pathogenicity. Nat Rev Microbiol *5*, 309-316.

Straube, A., Brill, M., Oakley, B.R., Horio, T., and Steinberg, G. (2003). Microtubule organization requires cell cycle-dependent nucleation at dispersed cytoplasmic sites: polar and perinuclear microtubule organizing centers in the plant pathogen *Ustilago maydis*. Mol Biol Cell *14*, 642-657.

Straube, A., Hause, G., Fink, G., and Steinberg, G. (2006). Conventional kinesin mediates microtubule-microtubule interactions *in vivo*. Mol Biol Cell *17*, 907-916.

Takemoto, D., Tanaka, A., and Scott, B. (2007). NADPH oxidases in fungi: diverse roles of reactive oxygen species in fungal cellular differentiation. Fungal Genet Biol *44*, 1065-1076.

Thordal-Christensen, H., Zhang, Z., Wei, Y., and Collinge, D.B. (1997). Subcellular localization of H_2O_2 in plants. H_2O_2 accumulation in papillae and hypersensitive response during the barley-powdery mildew interaction. The Plant Journal *11*, 1187-1194.

Treitschke, S., Doehlemann, G., Schuster, M., and Steinberg, G. (2010). The myosin motor domain of fungal chitin synthase V is dispensable for vesicle motility but required for virulence of the maize pathogen *Ustilago maydis*. Plant Cell *22*, 2476-2494.

Voigt, B., Timmers, A.C., Samaj, J., Hlavacka, A., Ueda, T., Preuss, M., Nielsen, E., Mathur, J., Emans, N., Stenmark, H., Nakano, A., Baluska, F., and Menzel, D. (2005). Actin-based motility of endosomes is linked to the polar tip growth of root hairs. Eur J Cell Biol *84*, 609-621.

Wahl, R., Zahiri, A., and Kämper, J. (2009). The *Ustilago maydis b* mating type locus controls hyphal proliferation and expression of secreted virulence factors in planta. Mol Microbiol *75*, 208-220.

Wang, L., and Lin, X. (2012). Morphogenesis in fungal pathogenicity: shape, size, and surface. PLoS Pathog *8*, e1003027.

Weber, I., Assmann, D., Thines, E., and Steinberg, G. (2006). Polar localizing class V myosin chitin synthases are essential during early plant infection in the plant pathogenic fungus *Ustilago maydis*. Plant Cell *18*, 225-242.

Weber, I., Gruber, C., and Steinberg, G. (2003). A class-V myosin required for mating, hyphal growth, and pathogenicity in the dimorphic plant pathogen *Ustilago maydis*. Plant Cell *15*, 2826-2842.

Wedlich-Söldner, R., Bölker, M., Kahmann, R., and Steinberg, G. (2000). A putative endosomal t-SNARE links exo- and endocytosis in the phytopathogenic fungus *Ustilago maydis*. EMBO J *19*, 1974-1986.

Wedlich-Söldner, R., Straube, A., Friedrich, M.W., and Steinberg, G. (2002). A balance of KIF1A-like kinesin and dynein organizes early endosomes in the fungus *Ustilago maydis*. EMBO J *21*, 2946-2957.

Weinzierl, G., Leveleki, L., Hassel, A., Kost, G., Wanner, G., and Bölker, M. (2002). Regulation of cell separation in the dimorphic fungus *Ustilago maydis*. Mol Microbiol *45*, 219-231.

Wilson, J.M., de Hoop, M., Zorzi, N., Toh, B.H., Dotti, C.G., and Parton, R.G. (2000). EEA1, a tethering protein of the early sorting endosome, shows a polarized distribution in hippocampal neurons, epithelial cells, and fibroblasts. Mol Biol Cell *11*, 2657-2671.

Wojtaszek, P. (1997). Oxidative burst: an early plant response to pathogen infection. Biochem J *322 (Pt 3)*, 681-692.

Wu, Q., Sandrock, T.M., Turgeon, B.G., Yoder, O.C., Wirsel, S.G., and Aist, J.R. (1998). A fungal kinesin required for organelle motility, hyphal growth, and morphogenesis. Mol Biol Cell *9*, 89-101.

Yao, X., Zhang, J., Zhou, H., Wang, E., and Xiang, X. (2011). *In vivo* roles of the basic domain of dynactin p150 in microtubule plus-end tracking and dynein function. Traffic *13*, 375-387.

Zekert, N., and Fischer, R. (2009). The *Aspergillus nidulans* kinesin-3 UncA motor moves vesicles along a subpopulation of microtubules. Mol Biol Cell *20*, 673-684.

Zhang, J., Zhuang, L., Lee, Y., Abenza, J.F., Penalva, M.A., and Xiang, X. (2010). The microtubule plus-end localization of *Aspergillus* dynein is important for dynein-early-endosome interaction but not for dynein ATPase activation. J Cell Sci *123*, 3596-3604.

Figures legends

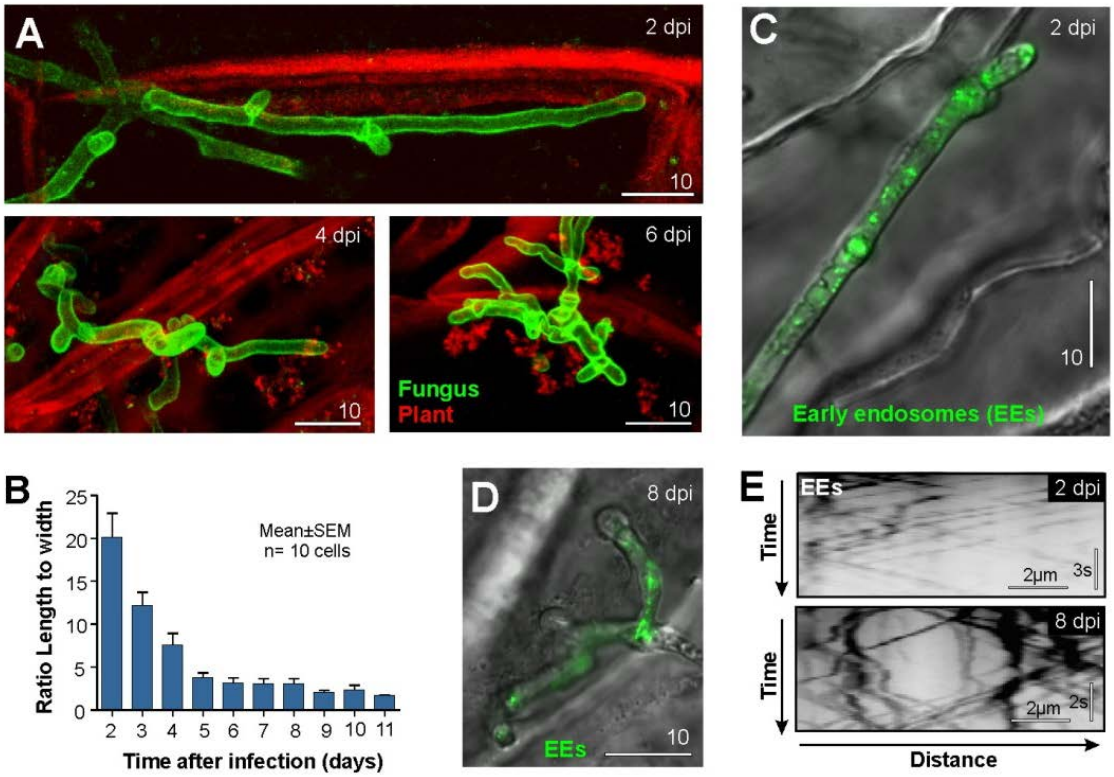

Figure 1. Visualization of *U. maydis* inside the host tissue.
(**A**) Hyphal cell of *Ustilago maydis* within plant leaf tissue at 2, 4 and 6 days after infection (2, 4, 6 dpi). The fungal cell wall (green) was stained using wheat germ agglutinin-AF488 and the plant cells were stained using propidium iodide (red) following published protocols (Doehlemann *et al.*, 2009). The bars represent 10 micrometers. (**B**) Bar chart showing the ratio of cell length to cell width of *U. maydis* cells at different times after infection. Bars are given as mean±SEM; the sample size is 10 cells. (**C**) Image overlay showing *U. maydis* within plant leaf tissue at 2 dpi. EEs are labelled with a fusion protein of GFP and the endosomal GTPase Rab5a (Fuchs *et al.*, 2006). The bar represents 10 micrometers. (**D**) Image overlay showing *U. maydis* within plant leaf tissue at 8 dpi. EEs are labelled with a fusion protein of GFP and the endosomal GTPase Rab5a (Fuchs *et al.*, 2006). The bar represents 10 micrometers. (**E**) Kymograph showing bidirectional motility of EEs, marked by GFP-Rab5a. Motility is indicated by diagonal lines, whereas stationary signals are shown as vertical lines. Note that most organelles are in motion. The bars represent seconds and micrometers. Contrast was inverted. See also Movie S1.

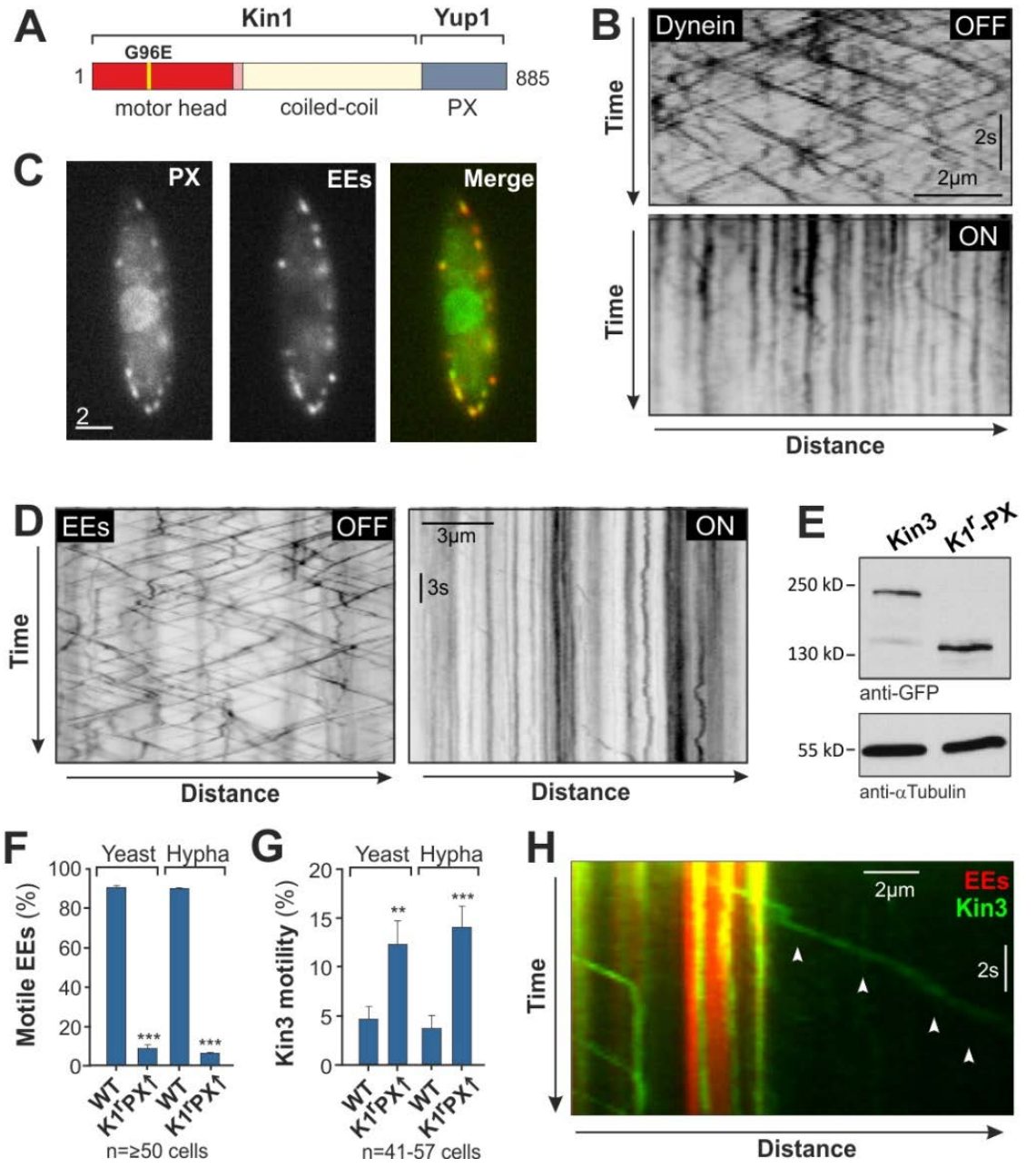

Figure 2. Establishment of a synthetic EE anchor.

(**A**) Diagram showing the organization of the EE anchor molecule K1^{r}PX. Large parts of an immobile kinesin-1^{rigor} protein (aa 1-739; (Straube *et al.*, 2006)) are fused to a lipid-binding PX domain of the putative t-SNARE Yup1 (Wedlich-Söldner *et al.*, 2000). (**B**) Kymographs showing the motility behaviour of GFP$_3$-labelled dynein (Lenz *et al.*, 2006) in the absence of kinesin-1^{rigor} protein (OFF, upper panel) and after expression due to induction of the *crg* promoter in the presence of arabinose (ON, lower panel). Note that kinesin-1^{rigor} protein was expressed in the presence of endogenous kinesin-1, indicating that the motor is able to overwrite the endogenous motor. The bars represent seconds and micrometers. Contrast was inverted. See also Supplementary Movie S2. (**C**) Colocalization of mCherry-Rab5a (EEs; red in merged image) and PX^{Yup1}-GFP (PX, green in merge). The PX^{Yup1} domain is sufficient to target GFP to the EEs. Bar represents micrometers. (**D**) Kymograph showing the motility behaviour of GFP-Rab5a labelled EEs in the absence of K1^{r}PX (OFF, upper panel) and after induced expression from the *crg* promoter (ON, lower panel). The synthetic anchor blocks all motility of the organelles. The bars represent seconds and micrometers. Contrast was inverted. See

also Supplementary Movie S3. (**E**) Western blot showing expression of K1^{r}-GFP-PX (K1^{r}-PX) and native kinesin-3-GFP (Kin3). (**F**) Bar chart showing the percentage of motile EEs in yeast-like (Yeast) and hyphal cells (Hypha) in control cells and after induction of K1^{r}PX, expressed under the *crg* promoter (5 h induction by arabinose). Triple asterisk indicates statistical significance at P<0.0001 (Mann Whitney test). All bars are given as mean±SEM, sample size *n* is indicated as total number of cells (758-3218 EEs) from two independent experiments. (**G**) Bar chart showing the percentage of motile kinesin-3-GFP that is not colocalizing with mCherry-Rab5a labelled EEs in control cells and after induction of K1^{r}PX, expressed under the *crg* promoter (5 h induction by arabinose). Double asterisk indicates statistical significance at P=0.0066 and triple asterisk indicates statistical significance at P=0.0004 (Mann Whitney test). All bars are given as mean±SEM, sample size *n* is indicated as total number of cells (198-400 EEs) from two independent experiments. (**H**) Kymograph showing motility of kinesin-3-GFP (green, arrowheads) that is not bound to the stationary EEs (red) in a hyphal cell that expressed the K1^{r}PX anchor for 5 h. The bars represent seconds and micrometers. See also Movie S4.

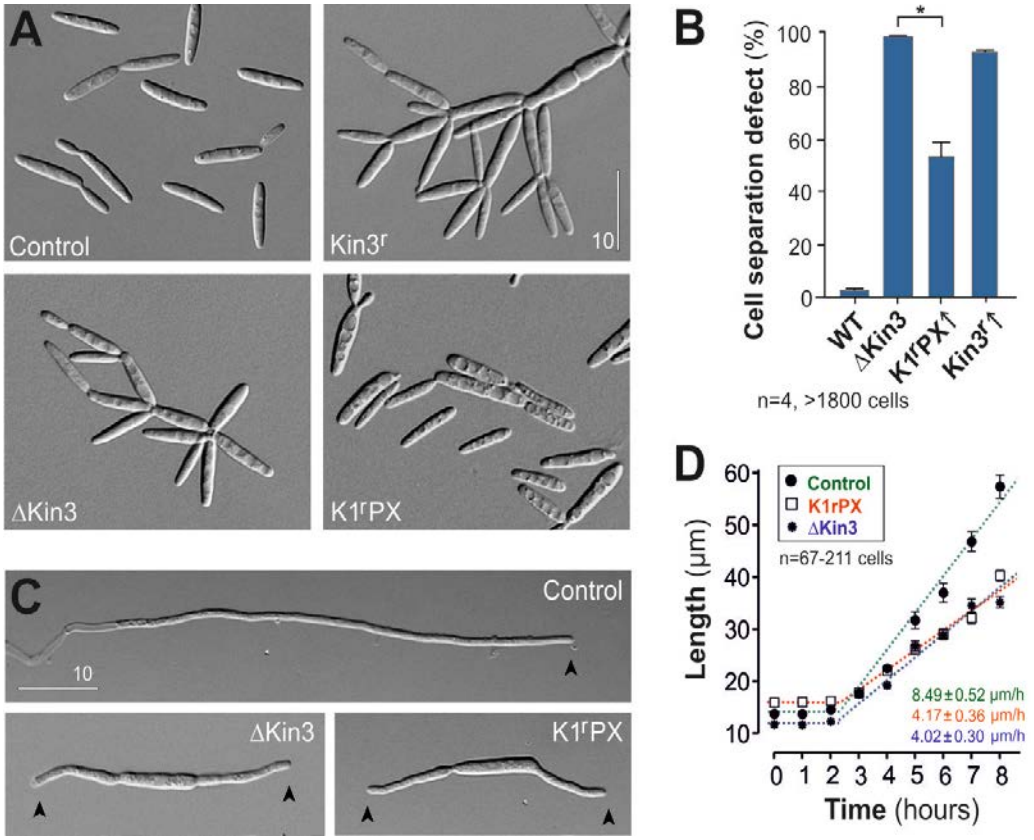

Figure 3. Morphological phenotypes associated with a block in EE motility.
(**A**) Images of yeast-like cells of a wildtype strain (Control), a kinesin-3 null mutant (ΔKin3), a mutant that expresses a kinesin-3^{rigor} protein under the *crg* promoter (Kin3^{r}, induction for 15 h in arabinose), and a mutant that expresses the EE anchor K1^{r}PX (K1^{r}PX; *crg* promoter was induced for 15 h in arabinose-containing media). Note that deletion of *kin3* and high expression of an immobile kinesin-3^{rigor} induces the formation of multi-cellular "tree-like" cell structures that fail to separate. This defect is reduced when EE motility is blocked by K1^{r}PX. Bar represents micrometers. (**B**) Bar chart showing the relative number of cells with a cell separation defect. Asterisk indicate significant difference to *kin3* null mutants (ΔKin3) at P=0.0286 (Mann Whitney test). All bars are given as mean±SEM, sample size is indicated as total number of cells from four independent experiments. (**C**) Images of hyphal cells of a wildtype strain (Control), the kinesin-3 null mutant (ΔKin3) and a mutant that expresses the EE anchor K1^{r}PX (K1^{r}PX; *crg* promoter was induced for 15 h in arabinose-containing media). Hyphal cells that lack Kin3 (ΔKin3) or that are blocked in EE motility due to the expression of K1^{r}PX (K1^{r}PX) form short hyphae and are often bipolar (growing cell pole is indicated by arrowheads). Bar indicates micrometers. (**D**) Graph showing the elongation of hyphal cells after induction of hyphal growth (given in hours after shift of yeast-like cells into inductive medium, see Material and Methods for details). Average elongation rates are given. Note that no statistical difference was found between the elongation rate of Δ*kin3* hyphae and hyphae expressing K1^{r}PX (Ancova-Prism test; P=0.7585). Sample size *n* is indicated as total number of cells per time point.

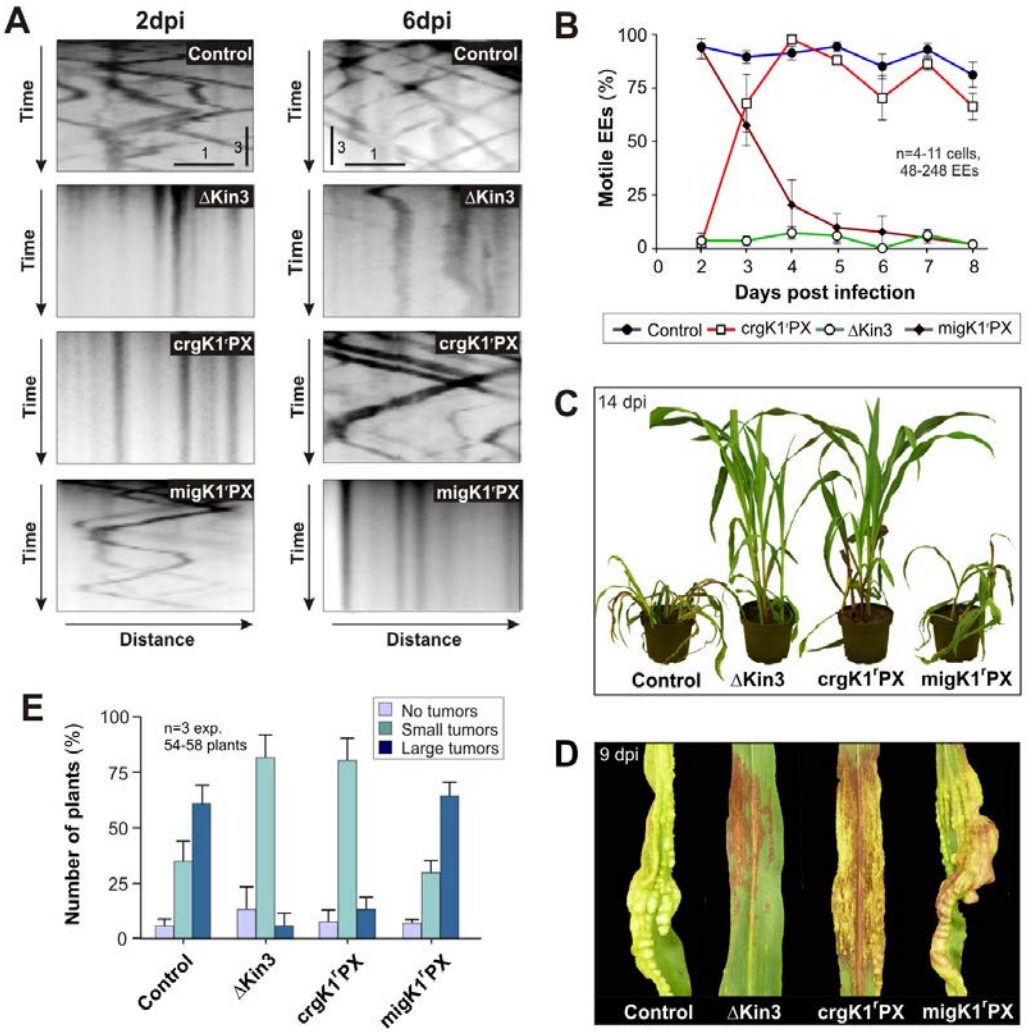

Figure 4. The importance of EE motility for pathogenicity of *U. maydis*.
(**A**) Kymographs showing motility behaviour of GFP-Rab5a labelled EEs in hyphae within the host tissue at 2 and 6 dpi. While EEs move bidirectionally in control cells, no directed motility was found in *kin3* null mutant (ΔKin3). When K1^{r}PX is expressed under the *crg* promoter, EE motility is initially blocked (2 dpi) but recovers at later time points (6 dpi). The opposite is found when the EE anchor is expressed under the plant-induced *mig1* promoter (migK1^{r}PX). The bars represent seconds and micrometers. Contrast was inverted. See also Movie S5. (**B**) Graph depicting the relative number of motile EEs in hyphal cells within the plant tissue at various days after infection and in various mutant strains. Most EEs are motile in control cells (Control, blue), whereas almost no motility was found in cells lacking kinesin-3 (ΔKin3, green). Motility recovers in cells expressing K1^{r}PX under the *crg* promoter (crgK1^{r}PX) at 3-4 dpi, whereas motility was inhibited at 4-5 dpi when K1^{r}PX was expressed under the *mig1* promoter. Values are given as mean±SEM in 4-11 cells per time point. (**C**) Plants 14 days after infection with control cells, *Δkin3* mutants and cells expressing the EE anchor K1^{r}PX under the *crg* promoter (crgK1^{r}PX) or the *mig1* promoter (migK1^{r}PX). (**D**) Leaf symptoms at 9 days after infection with control cells, *Δkin3* mutants and cells expressing the EE anchor K1^{r}PX under the *crg* promoter (crgK1^{r}PX) or the *mig1* promoter (migK1^{r}PX). (**E**) Bar chart showing the degree of symptoms at 8 dpi, caused by control cells, *Δkin3* mutants and cells expressing the EE anchor K1^{r}PX under the *crg* promoter (crgK1^{r}PX) or the *mig1* promoter (migK1^{r}PX). Bars are given as mean±SEM, *n*=3 experiments, in total 54-58 plants per bar.

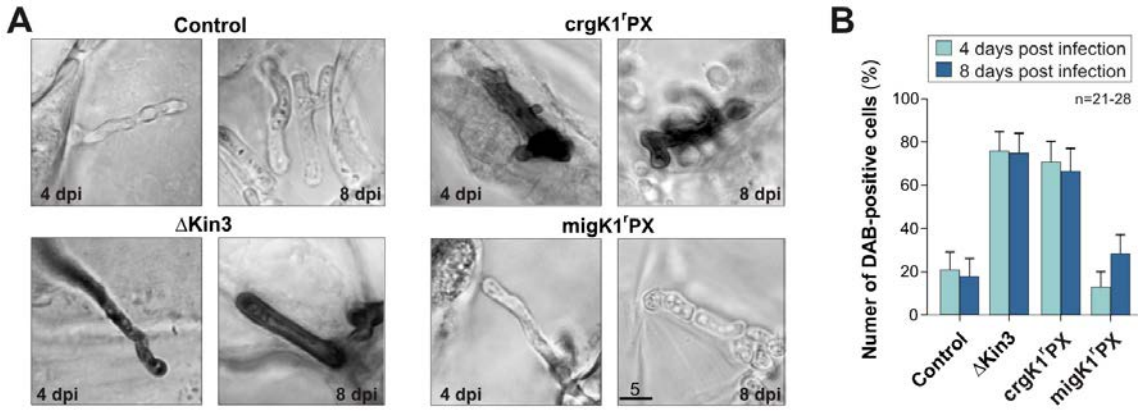

Figure 5. A blockage of EE motility at early stages of infection causes an oxidative burst in *U. maydis*.

(**A**) Images showing DAB-treated fungal cells within plant tissue at 4 and 8 dpi. No DAB-precipitate is seen in control cells and in cells that express K1^{r}PX under the *mig1* promoter. In contrast, DAB-precipitate concentrates around cells that express K1^{r}PX under the *crg* promoter, indicating that a blockage of EE motility at early stages of infection causes an oxidative burst. Bar represents micrometers. (**B**) Bar chart showing the relative number of cells that are associated with DAB precipitates. A minority of the cells show DAB-related staining in control strains and mutants that express K1^{r}PX under the *mig1* promoter. In contrast, deletion of *kin3* (ΔKin3) or early expression of K1^{r}PX (crgK1^{r}PX) results in strong DAB precipitation, indicating that an oxidative burst was induced. Bars are given as mean±SEM, *n*=1 experiment, in total 21-28 cells per bar.

Supplementary online material

Supplementary Figures

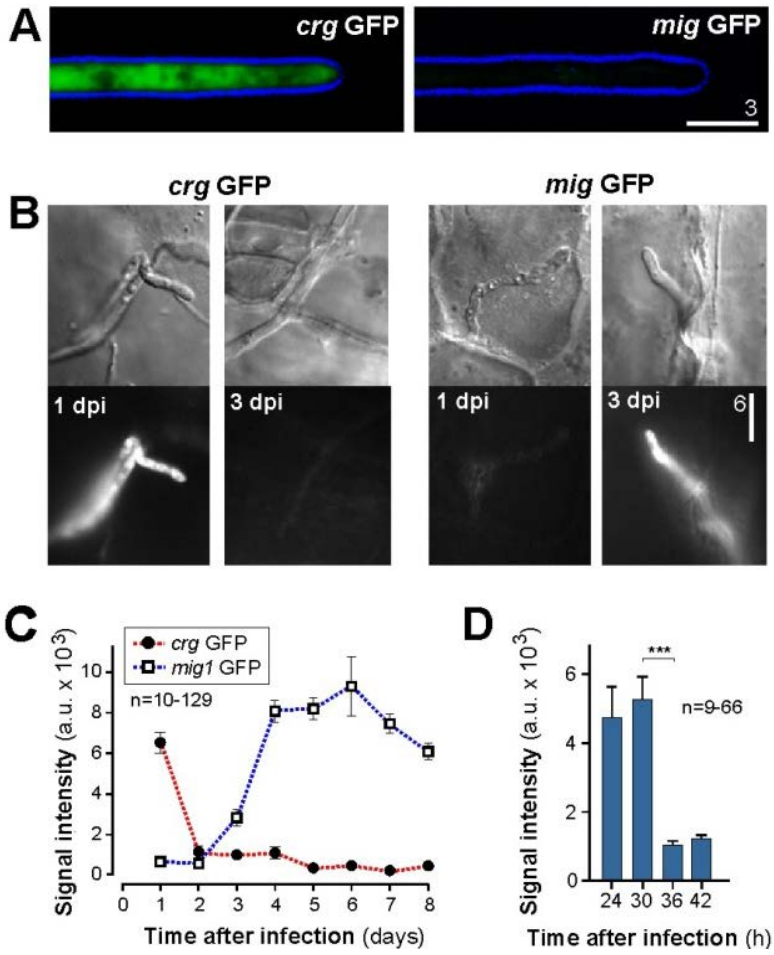

Figure S1. Expression of cytoplasmic GFP under the control of the *crg* and the *mig1* promoter.

(**A**) Hyphal cells containing cytoplasmic GFP (green) under the control of the *crg* promoter (*crg*GFP) and the *mig1* promoter (*mig*GFP) and grown in arabinose containing liquid medium. Strong GFP expression is driven by the *crg* promoter, whereas the plant-induced *mig1* promoter is not active. The cell edge is indicated in blue: the bar represents micrometers. (**B**) Hyphae containing cytoplasmic GFP (green) under the control of the *crg* promoter (*crg*GFP) and the *mig1* promoter (*mig*GFP) at 1 and 3 days after infection (1 and 3 dpi). In cells expressing GFP from the *crg* promoter, GFP is seen at early stages of infection (*crg*GFP, 1 dpi), whereas GFP signals vanish at later stages of infection (*crg*GFP, 3 dpi), when the promoter is turned off due to the presence of glucose. In contrast, the plant-induced *mig1* promoter is activated by unknown plant signals later during pathogenic development (*mig*GFP, 3 dpi). Bar represents micrometers. (**C**) Graph depicting the intensity of cytoplasmic GFP in hyphae expressing the protein under the *crg* and the *mig1* promoter. Data points given as mean±SEM, the sample size per data point is 10-129. (**D**) Bar chart showing the intensity of cytoplasmic GFP in hyphae expressing the protein under the *crg* promoter. Fluorescence is vanishing at 30-36h after infection. Bars are given as mean±SEM, the sample size per bar is 9-66. Triple asterisk indicates statistically significant difference at $P<0.0001$, Mann-Whitney test.

Supplementary Tables

Supplementary Table 1. Strains and plasmids used in this study.

Strain name	Genotype	Source
SG200	*a1 mfa2 bW2 bE1, ble^R*	(Bölker *et al.*, 1995)
AB33	*a2 Pnar-bW2 Pnar-bE1, ble^R*	(Brachmann *et al.*, 2001)
SG200_po^{N}GRab5a	*a1 mfa2 bW2 bE1, ble^R/ Potef-egfp-rab5a, nat^R*	This study
AB33G$_3$Dyn2_Kin1^{rigor}	*a2 Pnar-bW2 Pnar-bE1, ble^R, Pdyn2-3xegfp-dyn2, hyg^R/ Pcrg-kin1^{G96E}, cbx^R*	(Schuster *et al.*, 2011d)
AB33_mChRab5a	*a2 Pnar-bW2 Pnar-bE1, ble^R/ Potef-mcherry-rab5a, nat^R*	This study
AB33_mChRab5a_poPX-GFP	*a2 Pnar-bW2 Pnar-bE1, ble^R/ Potef-mcherry-rab5a, nat^R/ Potef- yup1$^{4-148}$-egfp, cbx^R*	This study
AB33_po^{N}GRab5a	*a2 Pnar-bW2 Pnar-bE1, ble^R/ Potef-egfp-rab5a, nat^R*	(Schuster *et al.*, 2011a)
AB33_po^{N}GRab5a_r^{H}K1rPX	*a2 Pnar-bW2 Pnar-bE1, ble^R/ Potef-egfp-rab5a, nat^R/ Pcrg-kin1$^{G96E,(1-739)}$-yup1$^{4-148}$, hyg^R*	This study
SG200_po^{N}GRab5a_r^{H}K1rPX	*a1 mfa2 bW2 bE1, ble^R/ Potef-egfp-rab5a, nat^R/ Pcrg-kin1$^{G96E,(1-739)}$-yup1$^{4-148}$, hyg^R*	This study
AB33_mChRab5a_rK1r-G-PX	*a2 Pnar-bW2 Pnar-bE1, ble^R/ Potef-mcherry-rab5a, nat^R/ Pcrg-kin1$^{G96E,(1-739)}$-egfp-^{BamHI}-yup1$^{4-148}$, cbx^R*	This study
AB33ΔKin3	*a2 Pnar-bW2 Pnar-bE1, ble^R Δkin3::nat^R*	This study
AB33ΔKin3_po^{H}mChRab5a	*a2 Pnar-bW2 Pnar-bE1, ble^R Δkin3::nat^R/ Potef-mcherry-rab5a, hyg^R*	This study
AB33ΔKin3_po^{H}mChRab5a_Kin3G	*a2 Pnar-bW2 Pnar-bE1, ble^R Δkin3::nat^R/ Potef-mcherry-rab5a, hyg^R / Pkin3-kin3-egfp, cbx^R*	This study
AB33Kin3G	*a2 Pnar-bW2 Pnar-bE1, ble^R, Pkin3-kin3-egfp, hyg^R*	(Schuster *et al.*, 2011c)
AB33Kin3G_po$_m$ChRab5a	*a2 Pnar-bW2 Pnar-bE1, ble^R, Pkin3-kin3-egfp, hyg^R/ Potef-mcherry-rab5a, nat^R*	This study
AB33Kin3G_po$_m$ChRab5a_rK1rPX	*a2 Pnar-bW2 Pnar-bE1, ble^R, Pkin3-kin3-egfp, hyg^R/ Potef-mcherry-rab5a, nat^R/ Pcrg-kin1$^{G96E,(1-739)}$-yup1$^{4-148}$, cbx^R*	This study
SG200ΔKin3	*a1 mfa2 bW2 bE1, ble^R Δkin3::nat^R*	This study
SG200ΔKin3_po^{C}GRab5a	*a1 mfa2 bW2 bE1, ble^R Δkin3::nat^R/ Potef-egfp-rab5a, cbx^R*	This study

SG200_po^{N}GRab5a_rKin3r	*a1 mfa2 bW2 bE1, ble^{R}/ Potef-egfp-rab5a, nat^{R}/ Pcrg-kin3^{G105E}, cbx^{R}*	This study
AB33ΔKin3_po^{C}GRab5a	*a2 Pnar-bW2 Pnar-bE1, ble^{R} Δkin3::nat^{R}/ Potef-egfp-rab5a, cbx^{R}*	This study
SG200_crgGFP	*a1 mfa2 bW2 bE1, ble^{R}/ Pcrg-egfp, cbx^{R}*	This study
SG200_mig1GFP	*a1 mfa2 bW2 bE1, ble^{R}/ Pmig1(-1019)-egfp, cbx^{R}*	This study
SG200_po^{N}GRab5a_m^{C}K1rPX	*a1 mfa2 bW2 bE1, ble^{R}/ Potef-egfp-rab5a, nat^{R}/ Pmig1(-1019)-kin1$^{G96E,(1-739)}$-yup1$^{4-148}$, cbx^{R}*	This study
po^{N}GRab5a	*Potef-egfp-rab5a, nat^{R}*	(Schuster *et al.*, 2011a)
po$_{m}$ChRab5a	*Potef-mcherry-rab5a, nat^{R}*	(Schuster *et al.*, 2011b)
poPX-GFP	*Potef- yup1$^{4-148}$-egfp, cbx^{R}*	This study
p^{C}crgKin1^{rigor}	*Pcrg-kin1^{G96E}, cbx^{R}*	(Schuster *et al.*, 2011d)
pcrg^{C}K1r-PX	*Pcrg-kin1$^{G96E,(1-739)}$-yup1$^{4-148}$, cbx^{R}*	This study
pcrg^{H}K1r-PX	*Pcrg-kin1$^{G96E,(1-739)}$-yup1$^{4-148}$, hyg^{R}*	This study
pcrg^{C}K1rG-PX	*Pcrg-kin1$^{G96E,(1-739)}$-egfp-^{BamHI}-yup1$^{4-148}$, cbx^{R}*	This study
ΔKin3	*Δkin3, nat^{R}*	(Schuster *et al.*, 2011b)
po$^{H}_{m}$ChRab5a	*Potef-mcherry-rab5a, hyg^{R}*	(Schuster *et al.*, 2011d)
pKin3G	*Pkin3-kin3-egfp, cbx^{R}*	(Wedlich-Söldner *et al.*, 2002)
po^{C}GRab5a	*Potef-egfp-rab5a, cbx^{R}*	This study
pcrgKin3^{G105E}	*Pcrg-kin3^{G105E}, cbx^{R}*	(Wedlich-Söldner *et al.*, 2002)
pcrgGFP	*Pcrg-egfp, cbx^{R}*	This study
pNEBcbx-yeast-1xSspI	*pNEBcbx-yeast-1xSspI, cbx^{R}*	This study
pmig1GFP	*Pmig1(-1019)-egfp, cbx^{R}*	This study
pmig1^{C}K1r-PX	*Pmig1(-1019)-kin1$^{G96E,(1-739)}$-yup1$^{4-148}$, cbx^{R}*	This study

a, *b*, mating type loci; *E1*, *W2*, genes of the b mating-type locus; *mfa2*, gene of the Mfa2 pheromone; *P*, promoter; -, fusion; *Δ*, deletion; */*, ectopically integrated; *hyg^{R}*, hygromycin resistance; *ble^{R}*, phleomycin resistance; *nat^{R}*, nourseothricin resistance; *cbx^{R}*, carboxin resistance; *crg*, conditional arabinose-induced promoter; *otef*, constitutive promoter; *nar*, conditional nitrate reductase promoter; *mig1*, maize-inducible promoter; *egfp*, enhanced green fluorescent protein; *mCherry*, monomeric Cherry; *kin1*, kinesin-1; *kin3*, kinesin-3; *PX*, Phox domain from Yup1; *rab5a*, small endosomal Rab5-like GTPase

Supplementary Table 2. Experimental usage of strains.

Strain name	Assay	Figure
SG200	Pathogenicity assay	Fig. 1A, 1B
SG200_po^{N}GRab5a	Motility of EEs; Cell separation defect; Pathogenicity assay	Fig. 1C, 1D, 1E, 2F, 3A, 3B, 4, 5; Movie S1
AB33G$_3$Dyn2_Kin1^{rigor}	Dynein motility in the presence of a kinesin-1 rigor protein	Fig. 2B; Movie S2
AB33_mChRab5a_poPX-GFP	Establishment of a synthetic EE anchor	Fig. 2C
AB33_po^{N}GRab5a_r^{H}K1rPX	EE motility in the presence of a K1rPX protein expressed under *crg* promoter; Hyphal growth	Fig. 2D, 2F, 3C, 3D
AB33ΔKin3_po^{H}mChRab5a_Kin3G	Expression level of Kin3G and independent from EE motility of Kin3G	Fig. 2E, 2G
AB33_mChRab5a_rK1rG-PX	Expression level of K1r-GFP-PX	Fig. 2E
SG200_po^{N}GRab5a_r^{H}K1rPX	EE motility in the presence of a K1rPX protein expressed under *crg* promoter; Cell separation defect	Fig. 2F, 3A, 3B, 4, 5; Movie S3, S5
AB33_po^{N}GRab5a	Motility of EEs; Hyphal growth	Fig. 2F, 3C, 3D
AB33Kin3G_po$_m$ChRab5a_rK1rPX	Independent from EE motility of Kin3G	Fig. 2G, 2H; Movie S4
SG200ΔKin3_po^{C}GRab5a	Cell separation defect; Pathogenicity assay	Fig. 3A, 3B, 4, 5
SG200_po^{N}GRab5a_rKin3r	Cell separation defect	Fig. 3A, 3B
AB33ΔKin3_po^{C}GRab5a	Hyphal growth	Fig. 3C, 3D
SG200_po^{N}GRab5a_m^{C}K1rPX	EE motility in the presence of a K1rPX protein expressed under *mig1* promoter; Pathogenicity assay	Fig. 4, 5; Movie S5
SG200_crgGFP	Expression of cytoplasmic GFP under the control of the *crg* promoter.	Fig. S1
SG200_mig1GFP	Expression of cytoplasmic GFP under the control of the *mig*1 promoter	Fig. S1

Supplementary Table 3. Primers used in this study.

Name	Sequence (5’ to 3’)
EB39	AATGTTGAATACTCATACTCTTCCTTTTTC GATGCCGGGAGCAGACAAGC
EB40	AAGCCCCAAAAACAGGAAGATTGTATAAGC AGTGTCACCTAAATCGTATG
EB170	GGTGAAACTCGATGAGGCCAAAAAAGATAC ATGTCCAACAACATCAAGGTC
EB171	AGTGGTGACGGCAAACGCGCG
EB172	GAGCTCAAGCGCGCGTTTGCCGTCACCACT ACACAGCCACTCCAAGGAATC
EB173	GAACGATCTGCAGCCGGGCGGCCGCTTTA CGGCCATTCGATAAACTGCTTG
EB192	CCATCAACGTGCTCGATGCGGCCGCGGCGC TACGTAGAGAGGCGTGATCTC
EB193	GAAAACGACAGACGACCTTGATGTTGTTGGACAT CTTGATCTGGAGGAAGAGAATG
EB195	GAGCTCAAGCGCGCGTTTGCCGTCACCACT ATGGTGAGCAAGGGCGAGGAG
EB197	GGATCC CTTGTACAGCTCGTCCATGCCG
EB277	GCAAGACCGGCAACAGGATTC
EB293	CAAAAAAGAAGAGAAAGGTCGAATTCCATATG ACACAGCCACTCCAAGGAATC
EB294	GGTGAACAGCTCCTCGCCCTTGCTCACCAT GGCTGCTGCTGC CGGCCATTCGATAAACTGCTTG
EB298	GCTTCCGGCTCGTATGTTGTG
EB306	GGTGAAACTCGATGAGGCCAAAAAAGATAC ATGGTGAGCAAGGGCGAGGAG
EB307	CTTAGTATTCCATTCTCTTCCTCCAGATCAAG ATGGTGAGCAAGGGCGAGGAG
EB308	CTTGATCTGGAGGAAGAGAATG

Supplementary Methods

Strains

To visualise and analyse EEs motility during plant infection the plasmid po^{N}GRab5a (Schuster *et al.*, 2011a) was linearized and integrated ectopically into the SG200 strain resulting in the SG200_po^{N}GRab5a strain. To obtain control strain AB33_mChRab5a, plasmid po$_{m}$ChRab5a (Schuster *et al.*, 2011b) was linearized and integrated ectopically into the AB33 strain. To confirm colocalization between the PX domain derived from the endosomal t-SNARE Yup1 (Wedlich-Söldner *et al.*, 2000) and EEs, plasmid potef-PX-GFP was linearized and ectopically integrated into the AB33_mChRab5a strain resulting in the AB33_mChRab5a_poPX-GFP strain. In order to block EE motility plasmid pcrg^{H}K1r-PX was linearized by *SspI* and *PsiI* and ectopically integrated into the AB33_GRab5a and SG200_po^{N}GRab5a strains resulting in the AB33_po^{N}GRab5a_r^{H}K1^{r}PX and SG200_po^{N}GRab5a_r^{H}K1^{r}PX strains, respectively. To analyse the expression level of a synthetic molecular anchor by Western Blotting plasmid pcrg^{C}K1rG-PX was linearized by *ScaI* and *BciVI* and was ectopically integrated into the strain AB33_mChRab5a resulting in the strain AB33_mChRab5a_rK1rG-PX. As a control for wildtype expression of Kinesin-3, the *kin3* gene was first deleted by homologous recombination using plasmid pΔKin3 (Schuster *et al.*, 2011b) which was digested with *PvuI* and homologously integrated into *kin3* locus of the *U. maydis* AB33 strain (Brachmann *et al.*, 2001) resulting in the AB33ΔKin3 strain. Deletion of the *kin3* gene was confirmed by Southern Blotting. Next the plasmid po$^{H}{}_{m}$ChRab5a (Schuster *et al.*, 2011d) was linearized and integrated ectopically into the AB33ΔKin3 strain resulting in the AB33ΔKin3_po^{H}mChRab5a strain. The plasmid pKin3G (Wedlich-Söldner *et al.*, 2002) was linearized within the carboxin resistance cassette (cut by *SspI*) and integrated into the *succinate dehydrogenase* locus of the AB33ΔKin3_mChRab5a strain, resulting in the AB33ΔKin3_po^{H}mChRab5a_Kin3G strain. To analyse the degree of Kinesin-3 independent motility from EEs in the presence of expressed synthetic molecular anchor, plasmid po$_{m}$ChRab5a (Schuster *et al.*, 2011b) was linearized and ectopically integrated into the AB33Kin3G strain (Schuster *et al.*, 2011c). Resulting AB33Kin3G_po$_{m}$ChRab5a strain was transformed with the linearized plasmid pcrg^{C}K1r-PX (cut by *ScaI* and *BciVI*) which was integrated ectopically

resulting in the AB33Kin3G_po$_m$ChRab5a_rK1^{r}PX strain. In order to analyse the morphology phenotype and involvement of EEs in cell separation after expression of the synthetic molecular anchor in yeast-like cells control strain SG200ΔKin3 was generated by homologous integration of digested (by *PvuI*) plasmid pΔKin3 (Schuster *et al.*, 2011b) into *kin3* locus. Deletion of *kin3* gene was confirmed by Southern Blotting. Next, plasmid po^{C}GRab5a was linearized and integrated ectopically into the SG200ΔKin3 strain resulting in the SG200ΔKin3_po^{C}GRab5a strain. To obtain SG200_GRab5a_rKin3r strain plasmid pcrgKin3^{G105E} (Wedlich-Söldner *et al.*, 2002) was linearized by *SspI* and integrated into the *succinate dehydrogenase* locus of the SG200_po^{N}GRab5a strain. In order to analyse morphology phenotype in hyphae and hyphal elongation rate after expression of synthetic molecular anchor, control AB33ΔKin3_po^{C}GRab5a strain was generated through ectopic integration of linearized plasmid po^{C}GRab5a into the AB33ΔKin3 strain. In order to block EE motility during the initial and later stages of plant infection two control strains were generated. Plasmid pcrgGFP was linearized by *AgeI* within the carboxin resistance cassette and integrated into the *succinate dehydrogenase* locus of the SG200 strain resulting in the SG200_crgGFP strain. Plasmid pmig1GFP was linearized by *SspI* within the carboxin resistance cassette and integrated into the *succinate dehydrogenase* locus of the SG200 strain resulting in the SG200_mig1GFP strain. The presence of the *eGFP* gene under *mig1* promoter was confirmed by PCR using SG200 *g*DNA as a negative control. In order to block EEs motility during the biotrophic phase, plasmid pmig1^{C}K1r-PX was linearized by *BsrGI* and ectopically integrated into the SG200_GRab5a resulting in the SG200_GRab5a_mig1^{C}K1^{r}PX strain. The presence of the chimera gene under *mig1* promoter was confirmed by PCR using SG200 *g*DNA as a negative control. The genotype of all strains is summarized in Supplementary Table 1; the experimental usage of all strains is summarized in Supplementary Table 2.

Plasmids

All plasmids were generated using standard techniques or *in vivo* recombination in *Saccharomyces cerevisiae* strain DS94 following published protocols (Raymond *et al.*, 1999).

potef-PX-GFP: This plasmid contains a PX encoding region from Yup1 (Wedlich-Söldner *et al.*, 2000) fused to eGFP. The construct is fused behind the constitutive *otef* promoter and contains a carboxin resistance cassette. The plasmid was generated using homologous recombination is the yeast *S. cerevisiae*. A 438-bp fragment encoding sequence of the PX domain (aa 4-148) from Yup1 (with overhangs designed for recombination with *otef* promoter and GFP) was amplified from the pSl-Yup-RFP-Hyg (provided by Dr Uta Fuchs) plasmid (using primers $_{f}$EB293 and $_{r}$EB294; Supplementary Table 3) and cloned into a yeast vector linearized between flanks composed of the *otef* promoter and sequence encoding eGFP.

pcrg^{C}K1r-PX: This plasmid contains a kin1 rigor (G96E) gene truncated in the third coiled-coil and the globular tail domain (Straube *et al.*, 2006) and fused to the PX domain from Yup1 (Wedlich-Söldner *et al.*, 2000). The construct is fused behind the *crg* promoter and the plasmid contains a carboxin resistance cassette. The construct was obtained by amplification of two fragments and cloning them into the yeast vector pcrgPeb1$^{211–268}$ (Schuster *et al.*, 2011a) by using *in vivo* recombination in the yeast *S. cerevisiae*. A fragment encoding a 30-bp overhang for the *crg* promoter and the sequence corresponding to the first 739 amino acids of Kin1^{G96E} was amplified from the plasmid p^{C}crgKin1^{rigor} (Schuster *et al.*, 2011d) using primers $_{f}$EB170 and $_{r}$EB171 (Supplementary Table 3). A 437-bp fragment encoding the PX domain (aa 4-148) from endosomal t-SNARE Yup1 (Wedlich-Söldner *et al.*, 2000) and overhang encoding 30-bp of Tnos terminator was amplified from the plasmid pSl-Yup-RFP-Hyg (provided by Dr Uta Fuchs) using primers $_{f}$EB172 and $_{r}$EB173 (Supplementary Table 3).

pcrg^{C}K1rG-PX: This plasmid contains a kin1 rigor (G96E) gene truncated in the third coiled-coil and the globular tail domain (Straube *et al.*, 2006), internal eGFP and fused to the PX domain from Yup1 (Wedlich-Söldner *et al.*, 2000). The construct is fused behind the *crg* promoter and the plasmid contains a carboxin resistance cassette. The construct was derived from the plasmid pcrg^{C}K1r-PX by internal introducing eGFP between the Kin1 rigor (aa 1-739) and the PX domain from Yup1 sequences using homologous recombination in the yeast *S. cerevisiae*. A fragment encoding sequence of the eGFP from the plasmid pKin3G (Wedlich-Söldner *et al.*, 2002) followed by added *BamHI* site

(by using primers $_{f}$EB195 and $_{r}$EB197; Supplementary Table 3) was cloned with two fragments described for pcrg^{C}K1r-PX into linearized yeast vector pcrgPeb1$^{211–268}$ (Schuster *et al.*, 2011a).

pcrg^{H}K1r-PX: This plasmid contains a kin1 rigor (G96E) gene truncated in the third coiled-coil and the globular tail domain (Straube *et al.*, 2006), internal eGFP and fused to the PX domain from Yup1 (Wedlich-Söldner *et al.*, 2000). The construct is fused behind the *crg* promoter and the plasmid contains a hygromycin resistance cassette. The plasmid was derived from the plasmid pcrg^{C}K1r-PX by replacement of the carboxin resistance cassette with a hygromycin resistance cassette.

pcrgGFP: This plasmid contains a eGFP encoding region fused behind the *crg* promoter and contains a carboxin resistance cassette. The plasmid was generated by amplification of a 827-bp region encoding the sequence of eGFP and a fragment of the Tnos terminator (using primers $_{f}$EB306 and $_{r}$EB277; Supplementary Table 3) into linearized (by *EcoNI* and *AflII*) pcrgPeb1$^{211–268}$ vector (Schuster *et al.*, 2011a).

pNEBcbx-yeast-1xSspI: This plasmid is a yeast-bacterial shuttle vector that was derived from the plasmid pNEBcbx-yeast (Schuster *et al.*, 2011a). The pNEBcbx-yeast plasmid was linearized by *ZraI* and modified by replacement of the fragment containing two *SspI* sites with the fragment containing one *NdeI* site amplified from the pKin3G plasmid (Wedlich-Söldner *et al.*, 2002) using primers $_{f}$EB39 and $_{r}$EB40 (Supplementary Table 3).

pmig1GFP: This plasmid contains a GFP encoding region fused behind the *mig1* promoter (Basse *et al.*, 2000) and contains a carboxin resistance cassette. The plasmid was generated by cloning two fragments into linearized (by *BamHI* and *SphI*) yeast vector pNEBcbx-yeast-1xSspI. A 1049-bp fragment encoding the sequence of the *mig1* promoter (-1019 bp; Basse *et al.*, 2000) and a 30-bp overhang was amplified from the plasmid pmig1^{C}K1r-PX using primers $_{f}$EB192 and $_{r}$EB308 (Supplementary Table 3). A 1135-bp sequence encoding eGFP and Tnos terminator was amplified from the pcrgGFP plasmid using $_{f}$EB307 and $_{r}$EB298 primers (Supplementary Table 3).

pmig1^{C}K1r-PX: This plasmid contains a kin1 rigor (G96E) gene truncated in the third coiled-coil and the globular tail domain (Straube *et al.*, 2006), internal

eGFP and fused to the PX domain from Yup1 (Wedlich-Söldner *et al.*, 2000). The construct is fused behind the *mig1* promoter (Basse *et al.*, 2000) and the plasmid contains a carboxin resistance cassette. The plasmid was derived from the plasmid pcrg^{C}K1r-PX in which the *crg* promoter was replaced by the *mig1* promoter amplified from *g*DNA of the SG200 strain using primers $_{f}$EB192 and $_{r}$EB193 (Supplementary Table 3).

Microscopy of infected plant tissue

To test *crg* promoter activity in *planta*, maize plants were infected with 0.5 ml of the SG200_crgGFP strain culture which was grown prior the infection in CM media containing 1% (w/v) arabinose. Maize tissue samples were collected after 24 h and then every 6 h and immediately observed using an IX81 microscope (Olympus) and a VS-LMS4 Laser-Merge-System (Visitron), the 488 nm observation laser at 100% output power at an exposure time of 150 ms and image binning 1. Maximum intensity of the region within the *U. maydis* cell was measured and was subtracted by the value obtained for the background. The same promoter activity test was done on the second day post infection and then on every following day for the *crg* and *mig1* promoters using the SG200_crgGFP and SG200_mig1GFP strains, respectively.

H_2O_2 accumulation in infected plant tissues was detected using DAB (Sigma-Aldrich) as described (Molina and Kahmann, 2007) with a few modifications (Bindschedler *et al.*, 2006; Daudi *et al.*, 2012). Freshly cut infected leaf sections were incubated in DAB staining solution (1 mg/ml DAB, 0.05% (v/v) Tween 20, 10 mM Na_2HPO_4) under vacuum for 60 minutes followed by 4 hours shaking (80 – 100 rpm). Next samples were decolorized by incubation for 15 minutes at 90˚C in ethanol:acetic acid:glycerol (3:1:1) destaining solution and stored at 4˚C in fresh destaining solution. Before acquiring the images samples were rehydrated in PBS pH7.4. Brightfield images were collected using an Olympus IX81 microscope equipped with a 100x/1.45 oil immersion lens and Visitron Visiview software. All incubations, storage and manipulations of samples after adding the staining solution was carried out with minimum exposure to light to avoid degradation of the DAB signal.

Propidium iodide / WGA-AF488 staining. Infected plant leaves were stained as described (Doehlemann *et al.*, 2009; Treitschke *et al.*, 2010) and the images were acquired using an LSM 510 confocal microscope (Zeiss) equipped with a Zeiss Plan-Apochromat 63x/1.40 oil immersion lens. The plant cell wall stained (for 30 min) with 20 ug/ml propidium iodide (Sigma-Aldrich)/0.02% Tween 20 was excited at 543 nm and detected at 615 nm using a long-pass filter. Fungal material labelled with 10 ug/ml wheat germ agglutinin-AF488 (Molecular Probes) was excited at 488 nm and detected between 505 and 570 nm. Maximum projections of Z-stacks were created using Zeiss LSM510 software.

Quantitative assessment of cell morphology and EE motility

The number of motile EEs in the absence and in the presence of a synthetic molecular anchor was measured within the entire yeast-like cells (in liquid culture) of the SG200_po^{N}GRab5a and SG200_po^{N}GRab5a_r^{H}K1^{r}PX strains and hyphal cells of the AB33_po^{N}GRab5a and AB33_po^{N}GRab5a_r^{H}K1^{r}PX strains (grown in NM media containing 1% (w/v) glucose for 15 h and shifted to NM media containing 1% (w/v) arabinose for 5 h; Brachmann *et al.*, 2001) using 488 nm observation laser at 50% output power. Signals that did not move during 75-frame movie (equivalent of 10 s) were considered as nonmotile EEs. The number of motile EEs after plant infection was measured as described above in the SG200_po^{N}GRab5a, SG200_po^{N}GRab5a_r^{H}K1^{r}PX, SG200ΔKin3_po^{C}GRab5a and SG200_po^{N}GRab5a_m^{C}K1^{r}PX strains.

Kin3 motility independent from EEs in the absence of a synthetic molecular anchor was measured within the photobleached bud region (using a 405 nm/60 mW diode laser which was dimmed by a neutral density 0.6 filter, resulting in 15 mW output power) in the middle-sized budded yeast-like cells and within the first 15 µm of the hyphal tip in the AB33ΔKin3_po^{H}mChRab5a_Kin3G strain using the Dual-View Microimager (Photometrics) and the 488 nm observation laser at 100% output power and the 561 nm observation laser at 80% output power at an exposure time of 150 ms and image binning 1. Kymographs obtained from 75-frame dual movies were merged and the number of anterograde lines corresponding to Kin3-GFP motilities which were not

colocalized with mCherry labelled Rab5a was divided by the number of anterograde lines derived from all Kin3-GFP signals.

Kin3 motility independent from EEs in the presence of a synthetic molecular anchor was measured within the photobleached bud region in the middle-sized budded yeast-like cells and within the first 15 µm of the hyphal tip in the AB33Kin3G_po$_m$ChRab5a_rK1^{r}PX strain using the Dual-View Microimager (Photometrics) and the 488 nm observation laser at 100% output power and the 561 nm observation laser at 3-10% output power at an exposure time of 150 ms and image binning 2. Analysis of the independent Kin3-GFP motilities was described above.

To analyse the hyphal elongation rate, overnight grown cultures of the AB33_po^{N}GRab5a, AB33ΔKin3_po^{C}GRab5a and AB33_po^{N}GRab5a_r^{H}K1^{r}PX strains were centrifuged and resuspended in 15 ml of NM media containing 1% (w/v) glucose or arabinose (to OD600<0.6; Brachmann *et al.*, 2001). Brightfield images were taken for 67-211 cells for each strain immediately (time point: 0 h) and then after each hour for a period of 8 hours. For hyphal length determination, the distance between the tip of the hypha and the mother cell (including the mother cell) was measured using MetaMorph (Molecular Devices); in case of the bipolar growing hyphae the length of the entire cell was determined. Average length of hyphae for each strain and for each time point was plotted on a graph as mean±SEM. To obtain hyphal growth rates, linear regression was used and the slopes were compared whether are significantly different using GraphPad Prism 5.03.

Supplementary Movie legends

Movie S1. Motility of EEs in *U. maydis* cells inside planta. The organelles were labelled with the endosomal small GTPase GFP-Rab5a. Time is given in seconds:milliseconds; the bar represents micrometers.

Movie S2. Block of dynein motility in the presence of a kinesin-1 mutant protein that contains a point mutation in the motor domain, conferring tight binding to the microtubule. Expressing this mutant protein in a wildtype hyphal cell anchors dynein (labelled by a triple GFP-tag fused to the dynein heavy chain protein Dyn2). Endogenous wildtype kinesin1 is also present but cannot overcome the blockage. Time is given in seconds:milliseconds; the bar represents micrometers.

Movie S3. Motility of EEs in cells that contain the synthetic motor K1^{r}PX under the control of the *crg* promoter. In the presence of glucose, the promoter is repressed and K1^{r}PX is not made (OFF, no K1^{r}PX) and EEs are moving. After shift to arabinose-containing medium for 5 hours, the synthetic protein is expressed and tightly anchors the EEs to the microtubules. Time is given in seconds:milliseconds; the bar represents micrometers.

Movie S4. Co-observation of EEs (marked by mCHerry-Rab5a; Rab5a, red in merged image) and GFP-labelled kinesin3 (Kin3; green in merged image). Most EEs are immobilized. An EE-independent Kin3 signal travels towards the hyphal apex (open arrowhead; apex indicated by closed arrowhead), Note that the apical part of the hyphal cell was photo-bleached to avoid interference with cytoplasmic background. Time is given in seconds:milliseconds; the bar represents micrometers.

Movie S5. Motility of EEs in infectious hyphae in the presence and absence of K1^{r}PX. Strong expression of the synthetic anchor under the *crg* promoter (crgK1rPX) blocked EE motility during early infection (crgK1rPX, 2 dpi). The presence of glucose, derived from invertase-dependent digestion of glucose provided by the plant, repressed the promoter and EE motility was restored at later stages of infection (crgK1rPX, 6 dpi). The reverse is found when K1rPX is expressed under the control of the plant-specific *mig1* promoter (migK1rPX). The promoter is repressed during early plant infection and EEs move normally (migK1rPX, 2 dpi). At later stages the promoter is induced and K1rPX is expressed. Consequently, EEs are anchored at microtubules and their motility is almost abolished. Time is given in seconds:milliseconds; the bar represents micrometers.

References for Supplementary online material

Basse CW, Stumpferl S, Kahmann R (2000) Characterization of a *Ustilago maydis* gene specifically induced during the biotrophic phase: evidence for negative as well as positive regulation. *Mol Cell Biol* **20**(1)**:** 329-339

Bindschedler LV, Dewdney J, Blee KA, Stone JM, Asai T, Plotnikov J, Denoux C, Hayes T, Gerrish C, Davies DR, Ausubel FM, Bolwell GP (2006) Peroxidase-dependent apoplastic oxidative burst in *Arabidopsis* required for pathogen resistance. *Plant J* **47**(6)**:** 851-863

Bölker M, Genin S, Lehmler C, Kahmann R (1995) Genetic regulation of mating and dimorphism in *Ustilago maydis*. *Canadian Journal of Botany* **73**(S1)**:** 320-325

Brachmann A, Weinzierl G, Kamper J, Kahmann R (2001) Identification of genes in the *bW/bE* regulatory cascade in *Ustilago maydis*. *Mol Microbiol* **42**(4)**:** 1047-1063

Bradford MM (1976) A rapid and sensitive method for the quantitation of microgram quantities of protein utilizing the principle of protein-dye binding. *Anal Biochem* **72:** 248-254

Daudi A, Cheng Z, O'Brien JA, Mammarella N, Khan S, Ausubel FM, Bolwell GP (2012) The apoplastic oxidative burst peroxidase in *Arabidopsis* is a major component of pattern-triggered immunity. *Plant Cell* **24**(1)**:** 275-287

Doehlemann G, van der Linde K, Assmann D, Schwammbach D, Hof A, Mohanty A, Jackson D, Kahmann R (2009) Pep1, a secreted effector protein of *Ustilago maydis*, is required for successful invasion of plant cells. *PLoS Pathog* **5**(2)**:** e1000290

Molina L, Kahmann R (2007) An *Ustilago maydis* gene involved in H2O2 detoxification is required for virulence. *Plant Cell* **19**(7)**:** 2293-2309

Raymond CK, Pownder TA, Sexson SL (1999) General method for plasmid construction using homologous recombination. *Biotechniques* **26**(1)**:** 134-138, 140-131

Schuster M, Kilaru S, Ashwin P, Lin C, Severs NJ, Steinberg G (2011a) Controlled and stochastic retention concentrates dynein at microtubule ends to keep endosomes on track. *EMBO J* **30**(4)**:** 652-664

Schuster M, Kilaru S, Fink G, Collemare J, Roger Y, Steinberg G (2011c) Kinesin-3 and dynein cooperate in long-range retrograde endosome motility along a nonuniform microtubule array. *Mol Biol Cell* **22**(19)**:** 3645-3657

Schuster M, Lipowsky R, Assmann MA, Lenz P, Steinberg G (2011b) Transient binding of dynein controls bidirectional long-range motility of early endosomes. *Proc Natl Acad Sci U S A* **108**(9)**:** 3618-3623

Schuster M, Treitschke S, Kilaru S, Molloy J, Harmer NJ, Steinberg G (2011d) Myosin-5, kinesin-1 and myosin-17 cooperate in secretion of fungal chitin synthase. *EMBO J* **31**(1)**:** 214-227

Straube A, Hause G, Fink G, Steinberg G (2006) Conventional kinesin mediates microtubule-microtubule interactions *in vivo*. *Mol Biol Cell* **17**(2)**:** 907-916

Treitschke S, Doehlemann G, Schuster M, Steinberg G (2010) The myosin motor domain of fungal chitin synthase V is dispensable for vesicle motility but required for virulence of the maize pathogen *Ustilago maydis*. *Plant Cell* **22**(7)**:** 2476-2494

Wedlich-Söldner R, Bölker M, Kahmann R, Steinberg G (2000) A putative endosomal t-SNARE links exo- and endocytosis in the phytopathogenic fungus *Ustilago maydis*. *EMBO J* **19**(9)**:** 1974-1986

Wedlich-Söldner R, Straube A, Friedrich MW, Steinberg G (2002) A balance of KIF1A-like kinesin and dynein organizes early endosomes in the fungus *Ustilago maydis*. *EMBO J* **21**(12)**:** 2946-2957

Chapter 4

Kinesin-3 from the fungus *Ustilago maydis* transports cargo along all interphase microtubule tracks.

Delivery of cellular cargoes is dependent not only on specialized molecular motors but also on their tracks. One of these tracks, microtubules (MTs), are long structures composed of α/β tubulin heterodimers that polymerise at their plus ends and trigger the direction of the transport. I analysed the number of MT tracks in hyphal *U. maydis* cells and I found that their amount can vary from 1 to 5 and the average is ~2 MT tracks per hypha. As EEs are transported exclusively along MT rails, I asked if all of the MT tracks are used by kinesin-3 motors or maybe Kin3 selects for a subpopulation of MTs like *Aspergillus nidulans* homologue of kinesin-3, UncA, which prefers less dynamic, detyrosinated MTs (Zekert and Fischer, 2009). For that reason I observed motility of full length Kin3 on labelled MTs in *U. maydis* hyphal cells *in vivo*. Interestingly, I found that Kin3 motors travel along all MT tracks available in the cell, suggesting that differently formed MT arrays in different fungi may induce changes in motor trafficking.

This work was built on previous work. Prof. Gero Steinberg provided overall project management, read and corrected the manuscript.

Kinesin-3 from the fungus *Ustilago maydis* transports cargo along all interphase microtubule tracks.

Ewa Bielska[1] and Gero Steinberg[1]

[1]Department of Biosciences, University of Exeter, Exeter EX4 4QD, UK

Author contributions: E.B. generated strains, performed research, analysed data and wrote the manuscript; G.S. conceived the project, read and corrected the manuscript.

Introduction

Kinesin-3 is a major molecular motor protein for membrane transport along microtubules in eukaryotic cells. In the filamentous fungi *Ustilago maydis* and *Aspergillus nidulans* kinesin-3 moves early endosomes (EEs; Wedlich-Söldner *et al.*, 2002; Lenz *et al.*, 2006; Zekert and Fischer, 2009; Egan *et al.*, 2012a). Mutants defective for kinesin-3 exhibit impaired polarized growth (Lenz *et al.*, 2006; Zekert and Fischer, 2009), which is thought to be due to a defect in long-distance transport of these organelles. To deliver EEs over long distance, fungal cells contain prominent MT arrays. In *U. maydis*, kinesin-3 mediates bidirectional EE motility along anti-polar MT bundles (plus-ends extend to both poles of the hyphal cell; Schuster *et al.*, 2011c). These are formed by cytoplasmic microtubule organizing centres (Schuster *et al.*, 2011c), whereas the spindle pole bodies at the nuclei are not involved in the formation of the MT array (Schuster *et al.*, 2011c). In *A. nidulans*, plus-ends of MTs are also directed towards both cell ends (Konzack *et al.*, 2005), but in contrast to *U. maydis* the cytoplasmic MTs are generated from the nucleus-localized spindle pole body (SPB) and from the septa (Konzack *et al.*, 2005; Veith *et al.*, 2005), although they also form antipolar bundles (Veith *et al.*, 2005). Interestingly, it was recently reported that the *A. nidulans* kinesin-3 (UncA) preferentially binds to a subset of stable and detyrosinated MTs (Zekert and Fischer, 2009). Here we report that kinesin-3 in *U. maydis* (Kin3) does not show such selectivity. Live

cell imaging reveals that fluorescent Kin3 utilizes all MT tracks to mediate bidirectional motility in hyphal cell. We speculate that this variation is due to difference in the organization of the MT array in both fungi.

Results

The MT array in elongated hyphal cells of *U. maydis* is composed of unipolar MT bundles near the cell poles and antipolar bundles in the middle region of the cell (Schuster *et al.*, 2011c). GFP-alpha tubulin labelled MT bundles form straight and sometimes slightly bent tracks throughout the entire hyphal cell (Fig. 1A). To determine if MT tracks are equally distributed within the hypha, we measured the number of MT tracks labelled with mCherry-αtubulin (see Table 1 for genotype of strains) at several distances from the hyphal tip by acquiring Z-axis stacks and merging images in maximum projections. In two independent experiments we found that the MT track number varied from one to five, which confirmed previous studies (Steinberg *et al.*, 2001). The lowest average number of the MT tracks was found near the hyphal tip (1.83±0.1; mean±SEM; n=48 cells) and at the septum (1.53±0.1; n=32 cells), while the highest number of MT bundles was found towards the middle of the cell, with 2.50±0.1 (mean±SEM; n=47 cells) at 25 µm behind the tip and 2.57±0.13 (mean±SEM, n=48 cells) at 50 µm behind the tip.

Next we set out to investigate if *U. maydis* kinesin-3 (Kin3) uses all of these MT tracks for bidirectional transport. We used a construct of Kin3 fused C-terminally to green fluorescent protein (eGFP; plasmid pKin3G; *pkin3-kin3-egfp, cbx*^{R}; Wedlich-Söldner *et al.*, 2002). The construct under control of the *kin3* promoter was described previously and was fully functional (Wedlich-Söldner *et al.*, 2002). The construct was integrated into the *succinate dehydrogenase* locus of the null *kin3* strain (AB33ΔKin3) resulting in the strain AB33ΔKin3_Kin3G (see Table 1). In addition, we ectopically integrated mCherry-α-tubulin into this strain and observed Kin3G motility on mChTub1 at various positions using laser-based epifluorescence. This was done in image series of 50-75 frames, taken at a rapid frame rate (exposure time 150 milliseconds). We found that Kin3G signals moved bidirectionally on 97.02±0.92% MT tracks (mean±SEM; n=39

cells; Fig. 2 and Movie 1). The remaining ~3% of MTs were short and not connected with other tracks.

Conclusions

Hyphal tip growth depends on delivery of compounds necessary for cell wall synthesis and cell expansion, but also requires the activity of molecular motors involved in EE transport (Lenz *et al.*, 2006; Penalva, 2010). Long-range motility of these organelles requires stable and consistent MT tracks, which in *A. nidulans* are provided by detyrosinated MTs (Zekert and Fischer, 2009). Selectivity of a long-distance kinesin-3 motor for these MT tracks seems to be an efficient way to avoid the more dynamic and less organized MTs emanating from the nuclear spindle pole bodies (Fig. 3). Furthermore, hyphal cells of *A. nidulans* undergo mitosis, which coincides with a major rearrangement of the MT cytoskeleton. However, the detyrosinated MT bundle persists during mitosis (Zekert and Fischer, 2009) and hyphal growth continues in these mitotic cells (Riquelme *et al.*, 2003). In contrast, *U. maydis* cells are arrested in G2 phase and do not enter into mitosis (Garcia-Muse *et al.*, 2003). Consequently, the MT array is constantly present. Furthermore, the MT tracks consist of anti-polar MTs that are dynamic, but bundled (Steinberg *et al.*, 2001; Schuster *et al.*, 2011c). This ensures that 2-3 MT tracks are always supporting long-distance motility of EEs. Thus, we propose that kinesin-3 in *U. maydis* has no need to be selective for more stable MT bundles. In this respect, Kin3 might represent kinesin-3 from mammalian cells, which was also shown to use all available MTs (Cai *et al.*, 2009). Interestingly, the putative MT-binding region in the tail of *A. nidulans* UncA (Seidel *et al.*, 2012) misses a short and highly conserved sequence stretch that is conserved between *U. maydis* Kin3 and human KIF1A (Fig. 1C), which might reflect a slightly different function of this region in *A. nidulans*. We conclude, that the differences in organisation and dynamic behaviour of the MT array in *A. nidulans* and *U. maydis* could explain the variation in MT selectivity of their kinesin-3 motors.

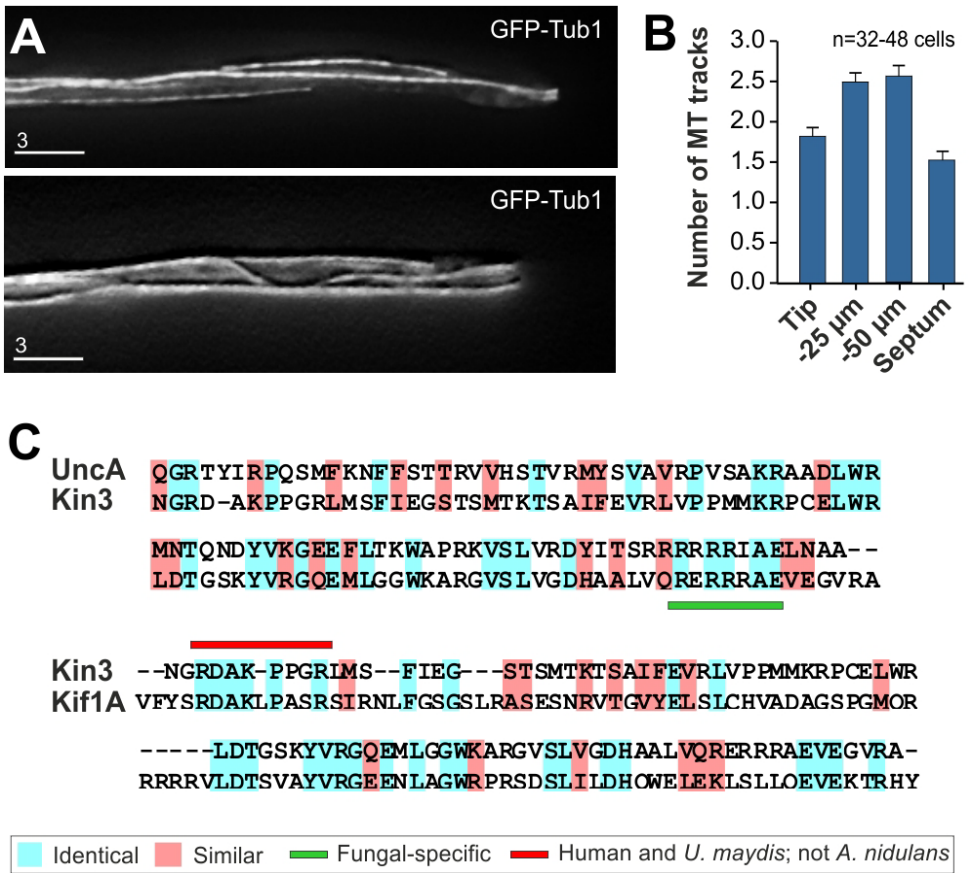

Figure 1. The microtubule array in the tip of hyphal cells of *U. maydis* and an alignment of a putative MT binding region in the tails of the kinesin-3 motors.
(**A**) Fluorescently labelled α-tubulin (eGFP-Tub1; Steinberg *et al.*, 2001) visualizes MT tracks which form straight and bended rods along whole hyphal cells. Bars represent micrometers. (**B**) Hypha contains 1-5 MT tracks per hyphal section. The lowest numbers of the MT tracks are at the tip (1.83±0.1; mean±SEM) and close to the septum 75 µm from the tip (2.17±0.16), the highest ones in the sections surrounding the nucleus (25 µm from the tip: 2.50±0.1 and 50 µm from the tip: 2.57±0.13). (**C**) Alignment between the putative MT binding domain in the tail of *A. nidulans* UncA (Seidel *et al.*, 2012), U. maydis Kin3 and human KIF1A. The alignment was done in ClustalW (http://www.ebi.ac.uk/Tools/msa/clustalw2/). Note that the tail of *U. maydis* Kin3 is more closely related to that of KIF1A from humans.

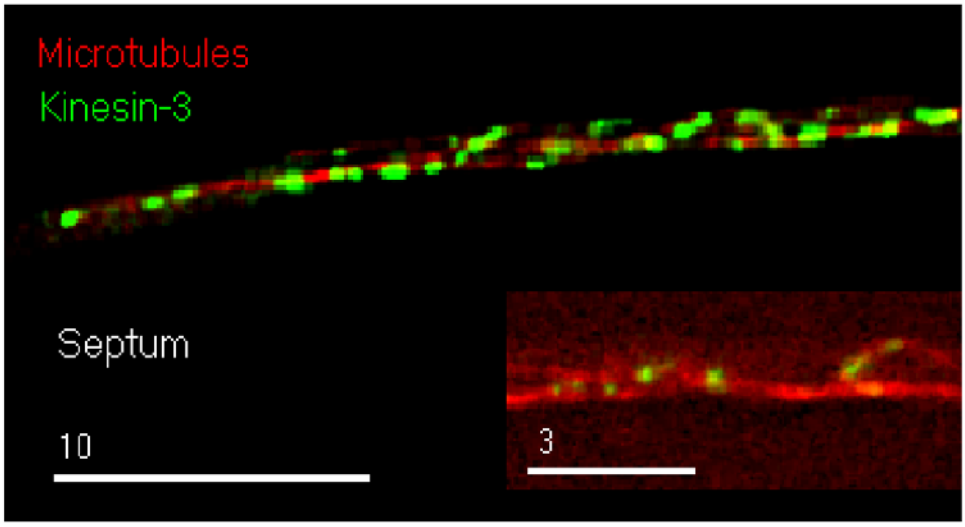

Figure 2. Kinesin-3 (Kin3-GFP, green) **colocalizes with all hyphal MT tracks** (mCherry-Tub1, red)**.** Bars represent micrometers.

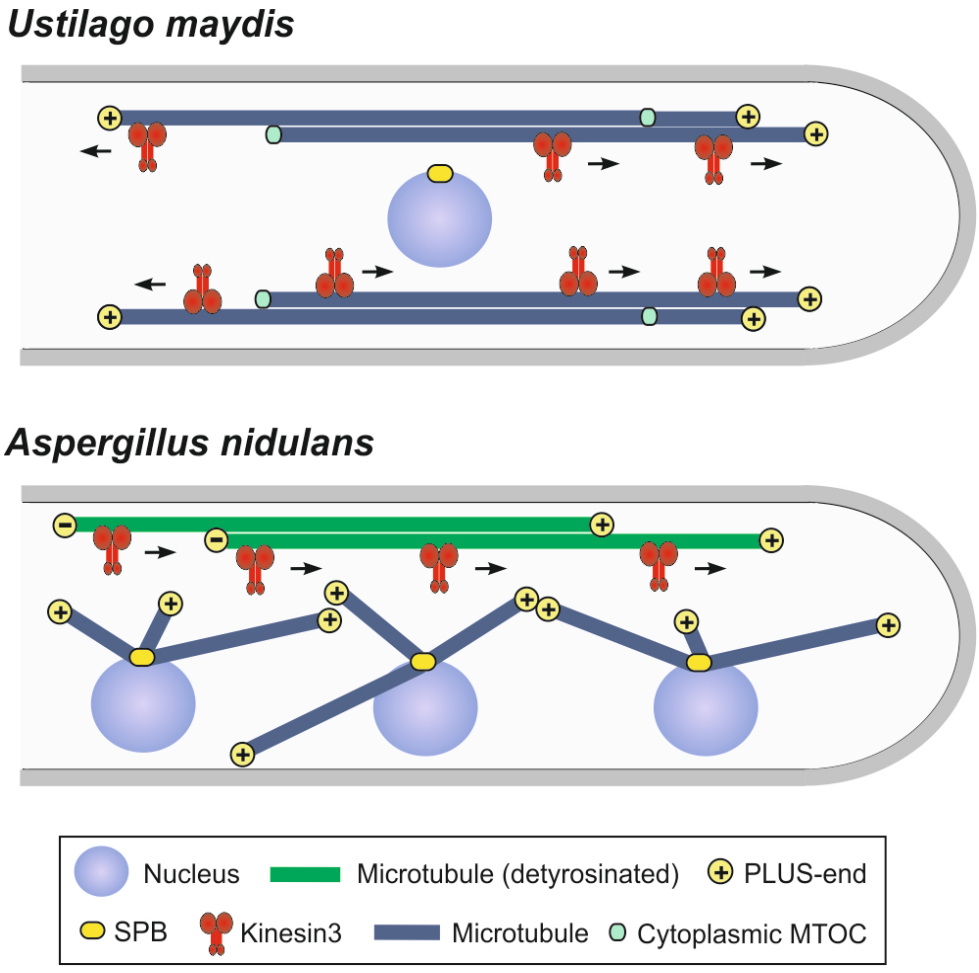

Figure 3. Selectivity of the kinesin-3 motors in hyphal cells during interphase. MT array in *U. maydis* hyphal cells allows kinesin-3 movement along all MT tracks (top; Schuster *et al.*, 2011c), while UncA in hyphal *A. nidulans* cells prefers detyrosinated MTs which are stable during mitosis (Zekert and Fischer, 2009).

Methods

Growth conditions

AB33ΔKin3_Kin3G_mCT strain was grown overnight at 28°C in complete medium (CM; Holliday, 1974) containing 1% (w/v) glucose, shaken at 200 rpm. Hyphal growth was induced by shifting to NM liquid medium supplemented with 1% (w/v) glucose for at least 6.5 hours (Brachmann *et al.*, 2001).

Table 1. Strains and plasmids used in this study.

Strain name	Genotype	Source
AB33GT	*a2 Pnar-bW2 Pnar-bE1, ble^R/ potefGFPTub1, cbx^R*	(Schuster *et al.*, 2011c)
AB33ΔKin3	*a2 Pnar-bW2 Pnar-bE1, ble^R Δkin3::nat^R*	Chapter 3
AB33ΔKin3_Kin3G	*a2 Pnar-bW2 Pnar-bE1, ble^R Δkin3::nat^R/ pkin3-kin3-egfp, cbx^R*	This study
AB33ΔKin3_Kin3G_mCT	*a2 Pnar-bW2 Pnar-bE1, ble^R Δkin3::nat^R/ pkin3-kin3-egfp, cbx^R/ Potef-mCherry-tub1, hyg^R*	This study
potefGFPTub1	*Potef-egfp-tub1, cbx^R*	(Steinberg *et al.*, 2001)
pHo$_m$ChTub1	*Potef-mCherry-tub1, hyg^R*	(Schuster *et al.*, 2011d)
pKin3G	*Pkin3-kin3-egfp, cbx^R*	(Wedlich-Söldner *et al.*, 2002)

a, *b*, mating type loci; *P*, promoter; -, fusion; /, ectopically integrated; *hyg^R*, hygromycin resistance; *ble^R*, phleomycin resistance; *nat^R*, nourseothricin resistance; *cbx^R*, carboxin resistance; *otef*, constitutive promoter; *nar*, conditional nitrate reductase promoter; *E1*, *W2*, genes of the b mating-type locus; *egfp*, enhanced green fluorescent protein; *mCherry*, monomeric Cherry; *tub1*, α-tubulin; *kin3*, kinesin-3

Laser-based epifluorescence microscopy and data analysis

Microscopy was done essentially as previously described (Schuster *et al.*, 2011a; Schuster *et al.*, 2011b). In brief, hyphal cells of the AB33ΔKin3_Kin3G_mCT strain were placed on 2% agar cushions and were observed using the 60x objective of an IX81 microscope (Olympus) and a VS-LMS4 Laser-Merge-System (Visitron). A Dual-View Microimager (Photometrics) and the 488 nm observation laser at 100% output power and the 561 nm

observation laser at 100% output power and image binning 1 were used for colocalization studies. Image sequences of 50 frames at an exposure time of 150 ms were taken using a Photometrics CoolSNAP HQ2 camera (Roper Scientific). All parts of the system were controlled by MetaMorph (Molecular Devices). Image processing was performed using MetaMorph (Molecular Devices). To analyse the degree of colocalization between Kin3 and MTs dual, 50-frame movies (2 sets) were used and the number of MTs colocalizing with the Kin3G signal was divided by the total number of MT tracks in the entire hypha. Analysis of the MT track number in each hypha section was done in the first frame of each movie (n=48 hyphal cells). All values are given as mean±SEM obtained by processing the data into the GraphPad Prism 5.03 software. The Movie 1, obtained as described above, was built from deconvolved image series using QuantX software (AutoQuant Imaging, Troy, NY).

Movie legends

Movie 1. Bidirectional motility of Kin3-GFP on fluorescently labelled MTs in *U. maydis* hyphal cells. Time is given in seconds:milliseconds. Bar represents 10 micrometers. Note that Kin3 motors use almost all of the MT tracks.

Acknowledgement

We thank Dr. Catherine Collins for providing strain AB33ΔKin3_Kin3G, which was used in order to generate AB33ΔKin3_Kin3G_mCT. This work was supported by the BBSRC (BB/F022956/1).

Further reading

Brachmann, A., Weinzierl, G., Kämper, J., and Kahmann, R. (2001). Identification of genes in the *bW/bE* regulatory cascade in *Ustilago maydis*. Mol Microbiol *42*, 1047-1063.

Cai, D., McEwen, D.P., Martens, J.R., Meyhofer, E., and Verhey, K.J. (2009). Single molecule imaging reveals differences in microtubule track selection between Kinesin motors. PLoS Biol *7*, e1000216.

Egan, M.J., Tan, K., and Reck-Peterson, S.L. (2012a). Lis1 is an initiation factor for dynein-driven organelle transport. J Cell Biol *197*, 971-982.

Garcia-Muse, T., Steinberg, G., and Perez-Martin, J. (2003). Pheromone-induced G2 arrest in the phytopathogenic fungus *Ustilago maydis*. Eukaryot Cell *2*, 494-500.

Holliday, R. (1974). *Ustilago maydis.* In Handbook of Genetics, ed. RC King, New York. Plenum Press, 575-595.

Konzack, S., Rischitor, P.E., Enke, C., and Fischer, R. (2005). The role of the kinesin motor KipA in microtubule organization and polarized growth of *Aspergillus nidulans*. Mol Biol Cell *16*, 497-506.

Lenz, J.H., Schuchardt, I., Straube, A., and Steinberg, G. (2006). A dynein loading zone for retrograde endosome motility at microtubule plus-ends. EMBO J *25*, 2275-2286.

Penalva, M.A. (2010). Endocytosis in filamentous fungi: Cinderella gets her reward. Curr Opin Microbiol *13*, 684-692.

Riquelme, M., Fischer, R., and Bartnicki-Garcia, S. (2003). Apical growth and mitosis are independent processes in *Aspergillus nidulans*. Protoplasma *222*, 211-215.

Schuster, M., Kilaru, S., Ashwin, P., Lin, C., Severs, N.J., and Steinberg, G. (2011a). Controlled and stochastic retention concentrates dynein at microtubule ends to keep endosomes on track. EMBO J *30*, 652-664.

Schuster, M., Kilaru, S., Fink, G., Collemare, J., Roger, Y., and Steinberg, G. (2011c). Kinesin-3 and dynein cooperate in long-range retrograde endosome motility along a nonuniform microtubule array. Mol Biol Cell *22*, 3645-3657.

Schuster, M., Lipowsky, R., Assmann, M.A., Lenz, P., and Steinberg, G. (2011b). Transient binding of dynein controls bidirectional long-range motility of early endosomes. Proc Natl Acad Sci U S A *108*, 3618-3623.

Schuster, M., Treitschke, S., Kilaru, S., Molloy, J., Harmer, N.J., and Steinberg, G. (2011d). Myosin-5, kinesin-1 and myosin-17 cooperate in secretion of fungal chitin synthase. EMBO J *31*, 214-227.

Seidel, C., Zekert, N., and Fischer, R. (2012). The *Aspergillus nidulans* kinesin-3 tail is necessary and sufficient to recognize modified microtubules. PLoS One *7*, e30976.

Steinberg, G., Wedlich-Söldner, R., Brill, M., and Schulz, I. (2001). Microtubules in the fungal pathogen *Ustilago maydis* are highly dynamic and determine cell polarity. J Cell Sci *114*, 609-622.

Veith, D., Scherr, N., Efimov, V.P., and Fischer, R. (2005). Role of the spindle-pole-body protein ApsB and the cortex protein ApsA in microtubule organization and nuclear migration in *Aspergillus nidulans*. J Cell Sci *118*, 3705-3716.

Wedlich-Söldner, R., Straube, A., Friedrich, M.W., and Steinberg, G. (2002). A balance of KIF1A-like kinesin and dynein organizes early endosomes in the fungus *Ustilago maydis*. EMBO J *21*, 2946-2957.

Zekert, N., and Fischer, R. (2009). The *Aspergillus nidulans* kinesin-3 UncA motor moves vesicles along a subpopulation of microtubules. Mol Biol Cell *20*, 673-684.

Chapter 5

The PH domain of kinesin-3 controls motor motility *in vivo*.

Ustilago maydis kinesin-3 (Kin3), a homologue of KIF1A and Unc-104 and member of the Kinesin-3 family, transports early endosomes (EEs) in a bidirectional manner (Wedlich-Söldner *et al.*, 2000; Wedlich-Söldner *et al.*, 2002) using its C-terminal part of the tail domain for cargo binding. By using a synthetic molecular trap I found two tail domains being involved in the binding of EEs. Surprisingly, deletion of the pleckstrin homology (PH) domain did not abolish binding to EEs. Kin3 lacking the PH domain was still able to transport EEs but at reduced motility parameters. By using the bimolecular fluorescence complementation (BIFC) method I showed that Kin3 has a globular organization. *In vitro* assays revealed that the PH domain directly interacts with the motor domain suggesting that this interaction may promote motor motility. Indeed, *in vivo* analysis confirmed that the PH domain controls the velocity and run length of Kin3.

This work was built on previous work and was undertaken with the help of co-workers. Dr. Nicholas Harmer (Biocatalysis Centre) performed modelling of the PH domains and discussed data. Dr. Martin Schuster performed FRAP experiments and analysed Kin3 number on EEs. Prof. Gero Steinberg provided overall project management and supervision, analysed data and wrote the final version of the manuscript.

The PH domain of kinesin-3 controls motor motility *in vivo*.

Ewa Bielska[1], Nicholas J. Harmer[1], Martin Schuster & Gero Steinberg[1,2]

[11]Biosciences, University of Exeter, Stocker Road, Exeter EX4 4QD, UK

[2]To whom correspondence should be addressed: G.Steinberg@exeter.ac.uk; phone: ++44-1392-263476; fax: ++44-1392-263434;

Key words: kinesin-3, membrane trafficking, early endosomes, pleckstrin homology domain

Author contributions: E.B. generated strains, designed research, performed research, analysed data and wrote the first draft of the manuscript; N.J.H. performed modelling of the PH domains and discussed data; M.S. performed research; G.S. designed research, conceived the project, analysed data and wrote the final version of the manuscript.

Abstract

Kinesin-3 motor proteins are ubiquitous membrane transporters in eukaryotes. Human KIF1A binds to secretory vesicles via a pleckstrin homology (PH) domain that interacts directly with the lipid phosphatidylinositol 4,5-bisphosphate (PI(4,5)P2). In contrast, the PH domains of a fungal kinesin-3 (Kin3) interacts with early endosomes (EEs) that are rich in phosphatidylinositol 3-phosphate (PI(3)P). Nevertheless, Kin3 and KIF1A share 40% identity in this domain, which raises the possibility that additional functions conserved the primary sequence of the PH domains. Here we set out to investigate this possibility using the fungal model system *Ustilago maydis*. We report that truncated Kin3ΔPH, lacking the PH domain, still binds to EEs and supports their motility. In contrast, deletion of adjacent highly conserved regions (DUF3694 and a "linker" region) abolishes binding and movement of EEs. A synthetic protein consisting of a nonmotile motor head fused to DUF3694 or the "linker" anchors the EEs to microtubules and inhibits EE motility, whereas the PH domain was not able to block EE motility. This suggests that the PH domain is of minor importance for membrane association of the motor. Structural modelling indicates that one surface of the PH domain faces away from the membrane. Interestingly, this region is conserved between KIF1A and Kin3, but not found in other PH domains, suggesting that the kinesin PH domain undergoes conserved intra- or inter-molecular protein-protein interaction. A split-YFP system demonstrates that the tail folds back to the motor domain while the motor travels along microtubules. Two hybrid and protein affinity assays suggest that the PH domain interacts with the motor domain and deletion of the PH domain reduces the motor velocity and run-length. Taken together, these results strongly indicate that the PH domain has a role in controlling the motor motility.

Introduction

Fungal hyphal cells, similarly to neurons, are highly polarized cells that rely on long-distance intracellular transport of membranous organelles for their function

and survival (Egan *et al.*, 2012b). This transport depends on the molecular motors kinesin and dynein, which move their cargo towards the plus- or the minus end of the microtubules (MTs; Vale, 2003). The model system *Ustilago maydis* shares unexpected similarities with human cells (Steinberg and Perez-Martin, 2008), which includes the need for long-distance transport of early endosomes (EEs; Wedlich-Söldner *et al.*, 2000), which is driven by kinesin-3 (Kin3) and cytoplasmic dynein (Wedlich-Söldner *et al.*, 2002; Lenz *et al.*, 2006). Quantitative life cell imaging demonstrated that ~3 Kin3 motors are constantly bound to the organelles (Schuster *et al.*, 2011b) and that almost all bidirectional long-range EE motility is driven by Kin3, which uses an antipolar MT array for long-range EE trafficking (Schuster *et al.*, 2011c). The biological function of this process is not known, but it was speculated that EEs serve long-distance retrograde signalling (Steinberg, 2007c) and delivery of mRNA for local protein translation (Baumann *et al.*, 2012).

Kinesin-3 motors are major membrane transporters in eukaryotes (Miki *et al.*, 2005). Their importance is reflected by the fact that 8 of the 45 kinesin motors encoded by the human genome are belonging to the kinesin-3 family (Hirokawa *et al.*, 2009). All members of this family share a highly conserved motor domain that contains the ATP- and MT-binding site (Hirokawa, 1998; Miki *et al.*, 2001; Lawrence *et al.*, 2004; Hirokawa *et al.*, 2009). This is followed by a forkhead associated domain, which is thought to be involved in phosphorylation regulated protein–protein interactions (Westerholm-Parvinen *et al.*, 2000). Beyond this region, the kinesin-3 motors exhibit much more variation, which in part reflects their association with a broad range of cargo. For example human KIF16B contains a C-terminal Phox-like domain that is thought to mediate interaction of the motor with endosomal phosphatidylinositol 3-phosphate lipids (PI(3)P; Fig. 1; Hoepfner *et al.*, 2005). In contrast, KIF1Bα binds to mitochondria (Nangaku *et al.*, 1994) and is lacking a lipid-binding domain in its tail, whereas a splice variant of the same gene (KIF1Bβ) contains a C-terminal DUF3694 (domain of unknown function 3694), followed by a PH domain (Fig. 1). This domain organization is characteristic of KIF1A-like kinesin-3 motors, including Unc104 from worms (Klopfenstein and Vale, 2004), and all members were shown to be involved in transport of synaptic vesicles in neurons (Hall and Hedgecock, 1991; Okada *et al.*, 1995; Nonet *et al.*, 1998; Yonekawa *et al.*, 1998; Zhao *et al.*, 2001;

Barkus *et al.*, 2008; Lo *et al.*, 2011; Liu *et al.*, 2012). *In vitro* experiments strongly suggested that the C-terminal PH domain of the KIF1A-like motors supports cargo binding and transport by a direct interaction with phosphatidylinositol 4,5-bisphosphate (PI(4,5)P2; Klopfenstein *et al.*, 2002; Klopfenstein and Vale, 2004). This lipid is mainly enriched in the plasma membrane (Vicinanza *et al.*, 2008; Mayinger, 2012), but also found in other compartments (Watt *et al.*, 2002), suggesting that the specificity of KIF1A-like kinesin-3 motors for synaptic vesicles is mediated by additional factors. Indeed, the stalk region of KIF1A and KIF1Bβ, which includes the DUF3694 but not the PH domain, mediates binding to synaptic vesicle precursors by interacting with the Rab3-effector DENN/MADD (Niwa *et al.*, 2008). In fact, lipid binding might not be essential for kinesin-3/cargo interaction, as *Drosophila* Khc-73 has no PH or PX domain, but binds to EEs via a region containing two DUF3694 regions. This argument gains further support by the finding that only 30% of the PH domains in *Saccharomyces cerevisiae* are involved in membrane targeting (Yu *et al.*, 2004).

The fungus *Ustilago maydis* contains a kinesin-3 motor, named Kin3, that shares 31.1% overall identity with human KIF1A and exhibits a very similar domain structure in its tail region (Wedlich-Söldner *et al.*, 2002). Interestingly, the PH domain of KIF1A and Kin3 share 40% amino acid identity. The sequence conservation between PH domains usually ranges between 7-24% (Lemmon, 1999). Considering that the PH domain of animal kinesin was implied in binding to the lipid PI(4,5)P2, the high amino acid identity suggests similarities in cargo interaction between both motors. However, fungal kinesin-3 is binding EEs (Wedlich-Söldner *et al.*, 2002), which are enriched in PI(3)P (Mayinger, 2012). This raises further doubt about an exclusive role of the kinesin-3 PH domain in cargo selection and binding. Here, we investigate the role of the PH domain of fungal Kin3 in cargo interaction. We show that that the PH domain is of minor importance for EE binding in living cells. Instead, it is required for the run-length and high velocity of Kin3, which is mediated by a direct interaction of the PH domain with the motor domain.

Results

The PH domain of Kin3 is of minor importance for cargo binding.

The PH domain of kinesin-3 was implicated in membrane lipid binding (Klopfenstein and Vale, 2004), suggesting that Kin3 associates with EEs via its C-terminal PH domain. To test whether the PH domain of Kin3 (PH^{Kin3}) is able to bind lipids, we expressed the region (aa 1566-1676) in bacteria. We purified the recombinant protein and tested for *in vitro* binding of the PH domain protein using a lipid overlay assay. However, we were unable to detect interaction of the recombinant protein with any lipid (Fig. S1A-C). We next expressed a PH^{Kin3}-GFP protein in living cells of *U. maydis* which co-expressed a red fluorescent EE marker. However, the protein was found in the cytoplasm and no specific localization was detected (Fig. S1D, S1E). We next tested for the ability of the entire Kin3 tail to bind to EEs. We fused red fluorescent mCherry to the C-terminus of the Kin3 tail region starting at the first coiled-coil region (amino acids 423-1676; K3T-mCherry) and analyzed colocalization with GFP-Rab5a labelled EEs *in vivo*. This was done in *kin3* null mutants to avoid interference with endogenous Kin3. Indeed, almost all EEs carried K3T-mCherry (Fig. 1B, 1C, K3T), confirming that the kinesin-3 tail confers association with the cargo. Next we expressed a truncated kinesin-3 tail that was fused to mCherry and was lacking the PH domain (Δ1566-1666; K3TΔPH). When co-expressed with GFP-Rab5a, the truncated kinesin-3 tail was still found on EEs (Fig. 1B, K3TΔPH), although the degree of colocalization was reduced by ~31% (Fig. 1C; from 95.56±1.87% to 66.27±5.26%; significantly different at $P<0.0001$, Mann-Whitney test). We confirmed this result by expressing full length Kin3 and $Kin3^{\Delta PH}$, both C-terminally fused to GFP, under the *kin3* promoter in a *kin3* null mutant background. Both proteins were detected in cell extracts (Fig. 1D), showing that deletion of the PH domain did not affect protein stability. Full length Kin3-GFP was found on most EEs labelled with mCherry-Rab5a and truncated Kin3ΔPH protein was still able to bind to EEs *in vivo*, albeit less EEs carried a Kin3ΔPH-GFP signal (Fig. 1E; Kin3: 87.67±1.92% of all EEs; Kin3ΔPH: 56.39±4.60% of all EEs; significant different at $P<0.0001$, Mann Whitney test). In addition, the amount of motor on the EEs was reduced, which was most obvious from the ratio of GFP fluorescence, derived from the bound

motors, to the red fluorescence signal from mCherryRab5a (Fig. 1F; Kin3-GFP to mCherry-Rab5a: 0.53±0.04, n=209; Kin3ΔPH-GFP to mCherry-Rab5a: 0.12±0.01, n=98). However, when expressed in *kin3* null mutants, the Kin3ΔPH protein was still able to mediate EE motility (Fig. 1G shows kymographs, vertical lines are stationary signals; +Kin3ΔPH; Movie S1). These results demonstrate that the PH domain is involved in cargo association. However, additional parts of the kinesin-3 tail seem to participate in membrane binding.

The DUF3694 and a highly conserved "linker" region are necessary for cargo binding.

We next set out to identify other regions in the Kin3 tail that participate in cargo binding. Previous work demonstrated that human KIF1A contains a liprin-binding domain that is located downstream of the FHA domain (Shin *et al.*, 2003) and that is involved in axonal transport (Miller *et al.*, 2005). However, sequence comparison of KIF1A and Kin3 from *U. maydis* suggested that Kin3 does not contain the liprin-binding region (Fig. S2), and no liprin homologue was found in the *U. maydis* genome. We therefore considered it most likely that the cargo-binding region of Kin3 was located towards the C-terminal end of the tail. This part of the molecule contains a DUF3694 domain that was shown to mediate binding of KIF1A and KIF1Bβ to a Rab3-effector and Rab3-positive vesicles (Niwa *et al.*, 2008). This was followed by a "linker" region that contained another highly conserved amino acid stretch of 42.3%/53.8% identity/similarity to KIF1A (amino acids 1388-1439; named D2). This region was found in all KIF1A/Unc104-like kinesin-3 motors (Fig. S3), suggesting that it is of crucial importance for these motors. To test for a role of both domains in association with EEs, we constructed various Kin3 proteins that were deleted in the entire C-terminal region (K3ΔDLP; amino acids 1198-1666 were truncated), the DUF3694 and the "linker" region (K3ΔDL; amino acids 1198-1565 were truncated), or only the DUF3694 or the "linker" region (K3ΔD [deleted in amino acid 1198-1348] and K3ΔL [deleted in amino acid 1349-1565], respectively (Fig. 2A). All proteins were expressed under the *kin3* promoter in a *kin3* null mutant that also contained mCherry-Rab5a labelled EEs. Western blotting confirmed that all proteins were stably expressed (Fig. S4). Deletion of either combinations

of the DUF3694 and the "linker" region, or truncation of either DUF3694 or the "linker" region resulted in a highly significant reduction in colocalization with EEs, indicated by a reduced number of mCherry-Rab5a signals that colocalize with GFP signals (Fig. 2C) and by the reduced ratio of Kin3-GFP to mCherry-Rab5a signals (Fig. 2D). These results demonstrate that the DUF3694 region and the conserved "linker" are crucial for association of Kin3 with the cargo membrane.

DUF3694 and highly conserved region D2 are involved in EEs binding.

We next set out to confirm a role of DUF3694 and the "linker" region in association of Kin3 to its cargo. Unfortunately, our attempts to prove direct binding of domains to purified EEs failed, as GFP-labelled domains were very poorly expressed or when produced in bacteria remained insoluble. We therefore designed a synthetic motor construct that consisted of various parts of the Kin3 tail, fused to the N-terminal half of an immobile kinesin-1 (amino acid 1-739), which carried a point mutation in its motor domain. This point mutation allows tight binding to microtubules, and the construct was previously used to anchor kinesin cargo to the microtubule track (Straube *et al.*, 2006). In a first step, we fused the entire Kin3 tail to the kinesin-1 motor region (Fig. 3A, K1r-K3t) and expressed this construct under the inducible *crg* promoter in cells that contained mCherry-Rab5a labelled EEs. In arabinose-containing medium, the EEs showed the characteristic Kin3-driven motility (Fig. 3B, Control; two kymographs are given to show variation between cells). We quantified the degree of motility inhibition by counting stationary EEs in a 1 second time interval and by measuring the pausing time of individual EEs in kymographs. We found that under these conditions one third of the EEs showed pausing, which typically lasted for less than a second (Fig. 3C, 3D, Control; 29.12±1.40% immobile EEs, n=1055 EEs in 50 cells; average pausing time of 1.04±0.61 s (mean±SEM), n=197 EEs). Expression of K1r-K3t strongly inhibited EE motility (Fig. 3B, 3C, 3D, K1r-K3t; 58.15±1.91% immobile EEs, n=931 EEs in 58 cells; average pausing time of 3.69±0.58 s (mean±SEM), n=54 EEs) and in some cells EE motions were almost completely blocked (Fig. 3B, K1r-K3t, right panel). We confirmed that this blockage is due to specific binding of the Kin3 tail to EEs

and not a consequence of a general "roadblock" of all transport along microtubules by deleting the putative cargo binding region in this construct (Fig. 3A, K1r-ΔDLP). In arabinose-containing medium this protein was strongly expressed (data not shown), but no effect on EE motility was found (Fig. 3C, 3D, K1r-ΔDLP; 30.71±1.57% immobile EEs, n=875 EEs in 50 cells; average pausing time of 1.197±0.11s; mean±SEM, n=99 EEs; not significantly different from the motility in arabinose-containing medium at P=0.6993, Mann-Whitney test). This confirmed that the K1r-K3t mediated inhibition of EE motility was due to the cargo-binding of the synthetic motor construct.

We next fused the kinesin-1 motor construct to the DUF3694 domain (Fig. 3A, K1r-D; amino acids 1198-1348), the most conserved part of the "linker" region (Fig. 3A, K1r-D2; amino acids 1345-1468) and the PH domain (Fig. 3A, K1-PH; amino acids 1566-1676). All proteins were strongly expressed when cells were grown in arabinose-containing medium (data not shown), but only K1r-D and K1r-D2 were able to inhibit EE motility (Fig. 3B, 3C, 3D; K1r-D; 48.05±1.52% immobile EEs, n=783 EEs in 43 cells; average pausing time was 1.58±0.07 s, mean±SEM, n=465 EEs; K1r-D2: 47.23±1.63% immobile EEs, n=881 EEs in 41 cells; average pausing time was 2.26±0.16 s, n=301 EEs; both are significantly different from the motility in arabinose-containing medium, P<0.0001, Mann-Whitney test). In contrast, no significant inhibition was found in the presence of the PH domain containing protein (Fig. 3B, 3C, 3D; K1r-PH; 33.29±1.75%, immobile EEs, n=763 EEs in 41 cells; average pausing time was 1.36±0.08 s, n=468 EEs; both are not significantly different from the motility in arabinose-containing medium, P=0.1235 and P=0.1058, respectively, Mann-Whitney test). These results are consistent with a role of the DUF3694 and the conserved "linker" region in cargo interaction of Kin3. In contrast, our results suggest that the PH domain is of minor importance for binding to the organelles.

The PH domain interacts with the Kin3 motor domain.

The results presented here suggested that the PH domain is of minor importance for cargo binding. Nevertheless, the PH domains of Kin3 and KIF1a share ~40% identical amino acids (Fig. S6). To investigate the spatial organization of these conserved amino acids, we constructed a homology

model based on a set of six previously determined PH domain structures from diverse sources. In addition, we predicted the orientation of the PH domain relative to the membrane using the Orientation of Proteins in Membranes server (for further details see Material and Methods). Our modelling predicted that the PH domains of KIF1A and Kin3 adopt a similar fold to canonical PH domains such as that of protein kinase B (Fig. S7). Surprisingly, many of the amino acids conserved between KIF1A and Kin3 were not found in other PH domains (Fig. 4A, green; Movie S2; for group of compared PH domains see Material and Methods). These identical amino acids lie mainly in two pairs of anti-parallel β-strands. These form a discrete surface, which is predicted to face away from the membrane (Fig. 4A; 4B, light blue). The clustering of a conserved surface patch, specific to the kinesin PH domains, is highly suggestive of a kinesin-3 specific protein-protein interaction.

Ultrastructural studies have demonstrated that unbound KIF1A adopts a globular shape (Okada *et al.*, 1995; Hirokawa, 1998), which suggested that the tail folds back towards the motor domain to inhibit motor activity of soluble KIF1A (Hammond *et al.*, 2009). However, we considered it possible that the globular confirmation is also found in active and organelle-bound motors. To test this, we fused the two halves of the yellow fluorescent protein (YFP) to the N- and the C-terminus of Kin3 (Fig. 4C). We expected to see YFP fluorescence only if the tail and the motor domain get in close proximity. When this motor construct was expressed in *kin3* null mutant, mCherry-Rab5a labelled EEs became mobile again, suggesting that the motor was functional. Indeed, we found fluorescent signals derived from interaction of both halves of YFP, but surprisingly these YFP signals were rapidly moving (Fig. 4C; Movie S3). This result strongly supports the idea that both ends of the Kin3-polypeptide are in close proximity while the motor moves its cargo along the microtubules. This finding raised the possibility that the PH domain interacts with the motor domain, which could serve as an explanation for the high sequence conservation in the motor and the PH domain of Kin3 and KIF1A. To test this, we expressed the Hisx6-PH domain (6xHis-tag fused to the amino acids 1566-1676 of the Kin3 tail) in bacteria and immobilized the recombinant protein on Ni-NTA agarose resin. We next expressed the motor domain of Kin3 (amino acid 1-367) in *U. maydis* and incubated the membrane-free cell extract with the

resin. In control experiment, most motor domain did not bind to the column and appeared in the "wash" fraction (Fig. 4D, Control). However, the motor domain was bound to the resin when the column was loaded with recombinant PH domain protein, and was released when the resin was eluted with 250 mM imidazole, suggesting that both indeed interact (Fig. 4D, +PH). To gain further support for this conclusion, we performed a yeast two-hybrid experiment in which the PH domain served as the "bait" and the motor domain represented the "prey". We fused the PH domain of Kin3 (amino acid 1566-1676) to the Gal4 DNA binding domain and the Kin3 motor domain (amino acid 1-367) to the Gal4 DNA activation domain. Interaction of both constructs was expected to induce nutrition marker genes and to support growth on tryptophan/leucine/histidine/adenine-deficient plates (see Fig. 4E; Positive control; see Material and Methods for details). Indeed, when both constructs were expressed in yeast cells that lack Trp, Leu, His, and Ade, both constructs restored growth on nutrient-deficient plates (Fig. 4E; right panel), whereas the negative control cell did not form colonies (Fig. 4E, middle panel; Negative control; see Material and Methods for details). Taken together these results strongly suggest that the PH domain interacts with the motor domain while Kin3 moves its cargo along microtubules.

The PH domain controls motor motility in the living cell.

The results described above suggested an interaction between the PH domain and the motor domain, which might explain the high sequence conservation in the PH domains of human KIF1A and fungal Kin3. Surprisingly, we found that this interaction occurs when motors were bound to their cargo. We therefore speculated that the PH domain might influence the motility properties of the motor. To investigate this, we measured the frequency and velocity of EE runs in *kin3* null mutants that expressed entire Kin3 and Kin3ΔPH. We found that 0.55±0.02 (mean±SEM, n=72 cells) EEs per seconds moved to the cell pole in yeast-like cells of *U. maydis*. This number was almost abolished in *kin3* null mutants, confirming that Kin3 is responsible for plus-end directed motility of EEs (Fig. 5A, ΔKin3). In the presence of Kin3ΔPH, which lacked the PH domain, significantly less EEs moved (Fig. 5A; 0.1±0.01 EE movements/s, n=90 cells; $P<0.0001$, Mann-Whitney test) and their velocity was significantly reduced (Fig.

5B; 1.41±0.04 µm/s, n=315 EEs; P<0.0001, Mann-Whitney test). These results demonstrate that the PH domain of Kin3 is required for full motor activity.

Our previous measurements (see above) implied a role of the PH domain in cargo binding, and we next determined the number of Kin3-GFP on mCherry-Ra5a labelled EEs by comparing the fluorescent intensity to that of an internal calibration standard (Schuster *et al.*, 2011a). In the control cell, we found at average 4 motors on a single EE (Fig. 5C), which is in agreement with our previous findings (Schuster *et al.*, 2011b). Deletion of the PH domain reduced this number to ~1.6 motors, which supported the notion that the PH domain is involved in cargo interaction. To test if this reduced number of motors is responsible for the reduced EE motility and velocity, we over-expressed Kin3ΔPH under the *crg* promoter. This led to an increase of soluble Kin3ΔPH (Fig. 5D), and also raised the number of Kin3ΔPH on EEs to ~6.3, which was significantly more than in control cells (Fig. 5C, P<0.0001, Mann Whitney test). Indeed, this increased the frequency of EE motility (Fig. 5A; 0.33±0.03 movements/s, n=60 cells) and their velocity (Fig. 5B; 1.87±0.03 µm/s, n=466 EEs), but both values were still significantly lower than that found in the presence of Kin3 in control cells (Mann Whitney test, P<0.0001). This demonstrated that high numbers of Kin3ΔPH on EEs are not able to compensate for the loss of the PH domain.

Finally, we set out to investigate the run-length of Kin3 and Kin3ΔPH in hyphal cells. We photo-bleached the apical 15 µm of the elongated cells and investigated the EE run-length from the bleaching front towards the point where the organelles turn for retrograde motility. When Kin3 was expressed in *kin3* null mutants, numerous EE signals moved towards the hyphal tip (Fig. 6A), with a median run-length of 5.8 µm (n=100 EE signals) before they change direction (Fig. 6B, Kin3). When Kin3ΔPH was expressed, less EEs moved (Fig. 6A, Kin3ΔPH), again arguing that the PH domain participates in cargo interaction. Surprisingly, high numbers of EE-bound motors after overexpression of Kin3ΔPH did not increase the number of motile EEs (Fig. 6A, Kin3ΔPH↑), indicating that the lack of motility in the absence of the PH domain is not due to reduced motor numbers. Furthermore, we found that the median run-length was significantly reduced to 2.4 µm (Fig. 6B, Kin3ΔPH) and 3.4 µm (Fig. 6B,

Kin3ΔPH↑), respectively. Taken together, these data indicate that the PH domain of Kin3 controls EE-associated motor numbers, but more importantly enables high EE transport frequency, EE velocity and EE run-length. This effect of the C-terminal PH domain might be linked to an interaction of the Kin tail with the N-terminal motor domain.

Discussion

Cargo binding of Kin3 involves the DUF3694 and a conserved "linker" domain.

In this study we focussed on the interaction of fungal KIF1A-like kinesin-3 and its cargo organelles. It is assumed that binding of kinesin to membranes involves the motor tail (Seiler *et al.*, 2000; Hirokawa *et al.*, 2009; Akhmanova and Hammer, 2010). We confirm this for Kin3 by showing that the tail (aa 423-1676) alone colocalizes with EEs in living cells. The binding is tight, as a fusion protein of a rigorously bound kinesin-1 motor head and the Kin3 tail (aa 370-1676) immobilizes EEs along their MT tracks. We next asked which part of the Kin3 tail is involved in cargo binding. It is well established that the N-terminal half of the kinesin-3 tail is involved in auto-inhibition of the motor activity (Lee *et al.*, 2004; Hammond *et al.*, 2009; Huo *et al.*, 2012), which suggests that the cargo interface is located in the C-terminal part of the Kin3 tail. This part of the motor contains a DUF3694 region (aa 1198-1348), a highly conserved "linker" region (aa 1349-1565) and the C-terminal PH domain (aa 1569-1669). We systematically deleted these domains and found that both DUF3694 and the "linker" are essential for the localization of Kin3-proteins to EEs, whereas the PH domain was of relatively minor importance for binding. The "linker" contains a highly conserved stretch of ~50 amino acids (42.3% identity to KIF1A) and when this domain of unknown function (D2) was fused to the Kinesin-1 rigor motor, it immobilised EE motility. A similar result was found for the DUF3694 domain, which suggests that both regions are mediating physical interaction with the cargo membrane. This result is reminiscent of results in mammalian cells, which showed that the stalk region of KIF1A and KIF1Bβ, which includes DUF3694 and the D2 region, interact with the Rab3-effector DENN/MADD

(Niwa *et al.*, 2008) that links the motor to vesicle-bound Rab3-GTP. The high sequence similarity between KIF1A and Kin3 in the DUF3694/"linker" region suggests that this part of the Kin3 tail interacts with conserved proteins, such as DENN/MADD homologues. However, the genome of *U. maydis* does only contain a very distantly related DENN domain containing protein (um3035; accession number: XP_759182.1) that lacks the death domain, shown to be necessary for the interaction with kinesin-3 motors (Niwa *et al.*, 2008). In addition, this DENN/MADD links neuronal KIF1A and KIF1Bβ to Rab3, a small GTPase that is specific for secretory synaptic vesicles (Fischer von Mollard *et al.*, 1990), whereas *U. maydis* kinesin-3 binds to EEs (Wedlich-Söldner *et al.*, 2002). Thus, we consider it most likely that the DUF3694 and the D2-containing "linker" region mediate interaction with the cargo via unknown adapter proteins. The molecular nature of these proteins is currently not known, but increasing evidence suggests an involvement of Rab-GTPases in binding motors to their cargo membrane (overview in Jordens *et al.*, 2005). This makes the endosomal GTPases Rab5a, Rab5b and Rab4 (Fuchs and Steinberg, 2005b) promising candidates for anchoring factors of kinesin-3 in *U. maydis.* Indeed, Rab5-like proteins are involved in EE motility in the fungus *Aspergillus nidulans* (Abenza *et al.*, 2010), and the kinesin-3 member Khc-73 from *Drosophila melanogaster* probably binds to Rab5-positive EEs via two DUF3694 domains (Huckaba *et al.*, 2011). Future studies have to show if Rab-effectors link Kin3 to EE membranes.

The PH domain of Kin3 is of minor importance for cargo binding.

PH domains are protein modules that can bind phosphatidylinositol lipids within membranes (Saraste and Hyvonen, 1995; Lemmon, 1999). It was shown that motors, such as myosin-X, dynein and kinesin-3, use PH domains to bind to their membranous cargo (Muresan *et al.*, 2001; Klopfenstein *et al.*, 2002; Yu *et al.*, 2012). Indeed, the PH domain of KIF1A is required for axonal transport of synaptic vesicles (Klopfenstein and Vale, 2004) and delivery of post-Golgi vesicles to the plasma membrane in non-polarized MDCK cells (Xue *et al.*, 2010). Therefore, it was tempting to speculate that the PH domain of Kin3 is mediating the association with the EEs. We deleted the PH domain in Kin3 and found that the number of Kin3ΔPH motors that were associated with EEs dropped from ~4 to ~1.6. This result suggested that the PH domain supports

association of Kin3 with the EE membrane. However, Kin3ΔPH was still able to restore EE motility in a *kin3* null mutant. Furthermore, a fusion protein of a rigorously binding Kin1 motor and the PH domain was not able to inhibit EE motility in wildtype cells, whereas other parts of the Kin3 tail inhibited EE motility. These results suggest that the PH domain of Kin3 is supporting the association of Kin3 to EEs, but the binding is weak and not of major importance for EE motility.

A genome-wide analysis of PH domains in the budding yeast revealed that only 7 of the 27 PH domains tested bind strongly to phosphoinositides in lipid overlay assays, whereas the majority shows weak or no binding (Yu *et al.*, 2004). Moreover, when expressed in living cells, 16 of 24 PH domains showed an unspecific cytoplasmic localization (Yu *et al.*, 2004), which confirmed localization studies on entire proteins (Huh *et al.*, 2003). These studies suggest that lipid binding might be a minor role for PH domains in the living cell. In fact, the recombinant Kin3 PH domain did not bind to phosphoinositides in lipid overlay assays. In addition, lipid binding of PH domains is correlated with a lysine close to the end of the β1 strand (Yu *et al.*, 2004). This residue is not found in the Kin3 PH domain, which might weaken the putative binding of the Kin3 PH domain to lipids. On the other hand, the PH domain from fungal Kin3 shares ~40% identity with the PH domain of human KIF1A. In general, PH domains have little sequence identity, ranging from 7 to 24% (Lemmon, 1999), and many of the conserved amino acids in KIF1A and Kin3 are not found in non-motor PH domains. Our modelling approach revealed that the conserved amino acids cluster in a discrete surface area, which is predicted to face away from the membrane. Thus it is likely that the kinesin-3 PH domain is involved in a protein-protein interaction, suggesting that the PH domain of Kin3 and KIF1A is involved in a kinesin-3 specific and evolutionary conserved function.

The PH domain controls the velocity and run length of Kin3.

We demonstrate here that the PH domain interacts with the Kin3 motor domain in yeast two-hybrid assays and that recombinant PH domain protein binds to motor heads in protein-affinity assays. This suggests that the tail of Kin3 can fold back towards the motor head. Ultrastructural studies have demonstrated

that KIF1A can adapt such a globular conformation (Okada *et al.*, 1995; Hirokawa, 1998). This is thought to represent the inactive state, in which the tail folds back to the motor head to allow an interaction between FHA and second coiled-coil (Lee *et al.*, 2004; Hammond *et al.*, 2009; reviewed in Verhey and Hammond, 2009). We confirmed the globular fold of Kin3 in living cells by fusing half of a yellow fluorescent protein to the motor domain and the other half to the C-terminal end of the PH domain. Under these conditions, a fluorescent signal was only expected when the YFP-halves at both ends of the Kin3 are in close proximity. Indeed, we observed strong YFP-fluorescence signals, suggesting that Kin3 adopts a globular conformation *in vivo*, which might involve an interaction of the PH domain and the motor head. Surprisingly, however, these YFP-signals were rapidly moving towards microtubule plus-ends. Furthermore, the YFP^{C}-Kin3-YFP^{N} protein rescued the phenotype of *kin3* null mutants, indicating that it is fully functional. These results suggest that folding of kinesin-3 is not necessarily correlated with motor inactivation.

A major finding of this study is that the deletion of the PH domain reduced the frequency, velocity and run-length of anterograde Kin3-driven organelle motility. One might argue that this is due to a reduced number of Kin3 motors on the organelles, as only ~1.6 Kin3ΔPH motors bound to the moving signals, whereas in control cells ~4 motors bind to the EEs. To compensate for the loss of motors due to deletion of the PH domain, we overexpressed Kin3ΔPH, which increased the number of motors on EEs to ~6.3. Indeed, the higher number of Kin3ΔPH slightly increased velocity, frequency and run-length of the organelles. However, despite the 50% excess of Kin3ΔPH motors, neither of these motility parameters was fully restored, and in particular transport frequency and EE run-length only reached ~60% of the control value, whereas overexpression of wildtype Kin3 motors increased the run-length of EEs to ~170% (Wedlich-Söldner *et al.*, 2002). Taken together, these results suggest that the PH domain of Kin3 interacts with and controls the motor domain during active transport of cargo. This novel function of the PH domain might be conserved amongst kinesin-3 motors, as a point mutation in a highly conserved amino acid within the PH domain of Unc-104 from *Caenorhabditis elegans* reduced the transport velocity, but did not alter lipid binding *in vitro* (Klopfenstein and Vale, 2004).

Conclusion

KIF1A-like kinesin-3 motors are major membrane transporters in eukaryotic cells. Increasing evidence demonstrates that they are involved in the motility of post-Golgi vesicles (Klopfenstein *et al.*, 2002; Klopfenstein and Vale, 2004; Xue *et al.*, 2010) and they interact with the vesicle lipid PI(4,5)P2 via a C-terminal PH domain. In the fungus *U. maydis*, the KIF1A-like motor Kin3 binds to EEs, which are enriched in PI(3)P, and our studies show that the PH domain is involved in this interaction. However, this binding is weak and not essential for Kin3-based motility. Instead, we report that the region upstream of the PH domain, which includes a conserved DUF3694 domain, is crucial for EE binding and motility. The adapters to which this part of the tail bind are not yet known, but Rab5 or Rab4-effectors are good candidates. The PH domain of Kin3 appears to interact directly with the motor domain, and this occurs while the motor actively transports organelles. The interaction seems to control the frequency, velocity and run-length of EE motility. This unexpected function could explain the high sequence conservation between the PH domains of fungal Kin3 and human KIF1A. The fact, that a point mutation in the PH domain of worm Unc-104 also decreases the transport velocity (Klopfenstein and Vale, 2004), indicates that the role of the kinesin-3 PH domains in supporting motor activity is a conserved feature.

Methods

Sequence analysis

Protein domains were predicted by SMART (http://smart.embl-heidelberg.de) and Pfam (http://pfam.sanger.ac.uk/) softwares. Coiled-coil domains were predicted by Coils Server software (http://www.ch.embnet.org/software/COILS_form.html (Lupas *et al.*, 1991). Windows of 14, 21 or 28 amino acids were used. Sequence comparison was done using ClustalW (http://www.ebi.ac.uk/Tools/msa/clustalw2/) and sequence identity and similarity was determined using EMBOSS Needle - Pairwise

Sequence Alignment (http://www.ebi.ac.uk/Tools/psa/emboss_needle/). All schemes were made in CorelDraw Graphics Suite X5.

Strains and plasmids

All *U. maydis* strains used in this study have the genetic background of AB33 (*a2 PnarbW2 PnarbE1, ble*^{R}; Brachmann *et al.*, 2001); see Supplementary Methods). All strains and plasmids used in this study are summarized in Supplementary Table 1. For introducing recombinant DNA sequences into *U. maydis*, the homologous recombination technique was used (Brachmann *et al.*, 2004). In conditional strains, the respective genes were expressed under the conditional *crg* promoter (Bottin *et al.*, 1996). All plasmids (see Supplementary Methods) were generated using standard techniques, *in vivo* recombination in *Saccharomyces cerevisiae* (Raymond *et al.*, 1999), LIC cloning strategy (Ligation Independent Cloning, (Haun *et al.*, 1992) or In-Fusion cloning (Clontech, USA) following published protocols.

Growth conditions

All cultures of *U. maydis* were grown overnight at 28°C in complete medium (CM; Holliday, 1974) containing 1% (w/v) glucose, shaken at 200 rpm. Hyphal growth was induced by shifting to NM liquid medium supplemented with 1% (w/v) glucose (Brachmann *et al.*, 2001). To induce expression of proteins under *crg* promoter strains AB33ΔKin3_GRab5a_rK3t$_{m}$Ch, AB33ΔKin3_GRab5a_rK3t$^{\Delta PH}{}_{m}$Ch, AB33_mChRab5a_rK1rG-K3^{tail}, AB33_mChRab5a_rK1rG-K3^{N,tail}, AB33_mChRab5a_rK1rG-D, AB33_mChRab5a_rK1rG-PX, AB33_mChRab5a_rK1rG-PH, AB33ΔKin3_mChRab5a_rKin3$^{\Delta PH}$G, AB33_mChRab5a_rMotorG were grown overnight in CM containing 1% (w/v) arabinose. Hyphal growth in the AB33ΔKin3_mChRab5a_rKin3$^{\Delta PH}$G strain was induced by shifting to NM liquid medium supplemented with 1% arabinose for 15 h (Brachmann *et al.*, 2001).

Protein extraction and immunodetection by Western blotting

Protein extracts were derived from 200 ml overnight cultures and were obtained by disruption of N2-frozen Ustilago cells grown to OD600>1.0 in a mixer mill MM 200 (Retsch, Germany) at frequency 30/s for 2 x 2.5 min. Depending on the pellet, thawed cell extracts were resuspended in 0.1-0.5 ml of 50 mM Hepes, 50 mM KCl, 1 mM EGTA, 1 mM $MgCl_2$ pH 7.0 complemented with protease inhibitor (Roche Complete Mini #11836153001) and centrifuged at 50,000 g for 30 minutes at 4°C. Concentrations of soluble fractions were analysed according to Bradford (Bradford, 1976). 30 ug of each sample were loaded on 8% SDS-polyacrylamide gels and transferred onto nitrocellulose membrane (GE Healthcare, United Kingdom) for 55 min at 190 mA in a semi-dry blot chamber (Fastblot, Analytik Jena, Germany). Each blot was blocked for an hour with 5% non-fat milk in TBS-1% Tween-20 and incubated with anti-GFP mouse IgG monoclonal antibodies in a 1:5000 dilution (Roche, #11814460001) overnight at 4°C followed by incubation with HRP-conjugated anti-mouse IgG in a 1:4000 dilution (Promega #W402B). Confirmation of the equivalent protein loading was done by stripping the membranes and re-probing them with mouse anti-α tubulin antibodies in a 1:5000 dilution (Oncogene Science, Cambridge, MA) followed by HRP-conjugated anti-mouse IgG in a 1:4000 dilution. All blots were developed using ECL Plus Western Blotting Detection system, following the manufacturer's instructions (GE Healthcare #RPN2132). Quantitative western analysis was performed using digital images and MetaMorph (Molecular Devices).

Protein affinity assays

For expression of the PH domain in *E. coli*, pNic28-PH domain plasmid was transformed into Rosetta™ 2(DE3) competent cells (Merck Chemicals, United Kingdom). Expression from the T7/LacO promoter was induced by the addition of 0.2 mM IPTG for 3 h at 37°C. Cell extract was obtained by sonication (6 x 10 s on ice with 20 s intervals) followed by centrifugation in the bench ultracentrifuge (13300 rpm, 30 min, 4°C). To avoid unspecific resin binding His6-tagged protein was bound to 1 ml Ni-NTA agarose (Novagen) in the presence of 10 mM imidazole (buffer-A: 20 mM Tris, 500 mM NaCl, 10 mM imidazole pH 7.6) for 2 h at 4°C. Immobilized PH domain was subsequently

mixed with 3 ml of fresh flow through fraction obtained after mixing (2 hours, 4°C) of the total cell extract from AB33_mChRab5a_rMotorG strain (see below) with 1 ml of pure Ni-NTA agarose. By using the flow through fraction the risk of unspecific binding of the motor domain to the Ni-NTA resin was reduced. After 2 hours of the incubation at 4°C flow through fraction was collected and the resin was extensively washed with 12 ml of wash buffer (20 mM Tris, 500 mM NaCl, 25 mM imidazole pH 7.6); fractions bound to the resin were eluted with 200 µl volumes of elution buffer (20 mM Tris, 500 mM NaCl, 250 mM imidazole pH 7.6). 20 µl samples of each fraction were loaded onto 10% SDS-polyacrylamide gel and transferred onto nitrocellulose membrane (GE Healthcare, United Kingdom) for 55 min at 190 mA in a semi-dry blot chamber (Fastblot, Analytik Jena, Germany).

Soluble cell extract of the AB33_mChRab5a_rMotorG strain was derived from 200 ml overnight culture. LN_2-frozen cell pellet was disrupted in a mixer mill MM400 (Retsch) at frequency 30/s for 2 x 2.5 min. Thawed cell extract was resuspended in 2 ml of buffer-A complemented with protease inhibitor (Roche Complete Mini #11836153001) and centrifuged at 50,000 g for 30 minutes at 4°C. 3 ml of a soluble cell extract obtained by the centrifugation was incubated at 4°C with 1 ml Ni-NTA agarose (Novagen) and after 2 hours flow fraction was collected for the affinity test. Resin was extensively washed with 12 ml of wash buffer. Fractions bound to the resin were eluted with 200 µl volumes of elution buffer. 20 µl samples of each fraction were loaded onto 10% SDS-polyacrylamide gel and transferred onto nitrocellulose membrane (GE Healthcare, United Kingdom) for 1.5 h at 190 mA in a semi-dry blot chamber (Fastblot, Analytik Jena, Germany). Quantitative western analysis was performed using digital images and MetaMorph.

Directed Y2H analysis

Interaction between motor domain ($kin3^{1-367}$) and PH domain ($kin3^{1566-1676}$) was analysed by directed Yeast Two Hybrid system (Matchmaker™ Gold Yeast-Two-Hybrid, Clontech). Bait plasmid pGBKT7-PH which contains the GAL4 DNA-BD and TRP1 marker was initially transformed into the *S. cerevisiae* strain Y2HGold (Yeastmaker Yeast Transformation System 2) and positives were

selected on SD-Trp plates (resulting in the Y2HGold[pGBKT7-PH] strain). As a next step the Y2HGold[pGBKT7-PH] strain was tested for autoactivation of reporter genes in Y2HGold in the absence of prey protein by spreading the transformation mixture onto SDO/X (SD/-Trp/X-α-Gal) and SDO/X/A (SD/-Trp/X-α-Gal/Aba) plate. After confirmation that the bait does not activate reporter genes (no colonies on SDO/X/A plate), mating with the prey plasmid (which contains the GAL4 DNA-AD and the LEU2 marker) transformed independently into *S. cerevisiae* strain Y2HGold (Y2HGold[pGADT7-motor]; Yeastmaker Yeast Transformation System 2) was performed as follows: a single colony of the Y2HGold[pGBKT7-PH] (from the SD/-Trp plate) and a single colony of the Y2HGold[pGADT7-motor] (from the SD/-Leu plate) were mated at 30°C in 500 µl 2xYPDA media containing glucose (4% final concentration). After 15 hours 100 µl of the mixture was plated onto SD/-DDO (SD/-Trp/-Leu) agar. After 4 days single colonies were transferred onto SD/-DDO (low stringency), SD/-TDO (SD/-Trp/-Leu/-His; medium stringency) and SD/-QDO (SD/-Trp/-Leu/-His/-Ade; high stringency) plates and analysed for protein-protein interactions within next 5 days. As a positive control in the mating experiment, mixtures of *S. cerevisiae* strains Y2HGold[pGBKT7-53] (encoding fusions between the GAL4 DNA-BD and murine p53) + Y187[pGADT7-T] (encoding fusions between the GAL4 DNA-AD and SV40 large T-antigen) were used. As a negative control in the mating experiment, mixtures of *S. cerevisiae* strains Y2HGold[pGBKT7-Lam] (encoding a fusion of the DNA-BD with human lamin C) + Y187[pGADT7-T] (as above) were used.

Laser-based epifluorescence microscopy, image processing and quantitative analysis

Microscopy was done essentially as previously described (Schuster *et al.*, 2011a; Schuster *et al.*, 2011b). In brief, cells from logarithmically growing cultures (28°C, 200rpm, overnight) were placed on a thin 2% agarose-layer and immediately observed using an IX81 microscope (Olympus) and a VS-LMS4 Laser-Merge-System (Visitron). The photobleaching experiment was performed using a 405 nm/60 mW diode laser. A Dual-View Microimager (Photometrics) and appropriate filters were used for colocalization studies. Images were captured using a Photometrics CoolSNAP HQ2 camera (Roper Scientific). All

parts of the system were controlled by MetaMorph (Molecular Devices). Image processing was performed using MetaMorph (Molecular Devices). Statistical analyses of data were performed using GraphPad Prism 5.03. Unless stated otherwise, all values are given as mean±SEM.

The degree of colocalization between EEs and Kin3 or Kin3 truncated versions, the entire yeast-like cells were observed using the Dual-View Microimager (Photometrics). All EEs signals were considered and their average signal intensities were measured (in the first frame) by drawing a region around the signal, copying the region next to the signal that was not influenced by other fluorescent signals and by subtracting the adjacent cellular background intensity from the measured signal intensity. Next two drawn regions (signal and background) were transferred to the second filter to measure Kin3-GFP and Kin3 truncated versions intensities. Positive values obtained after subtracting background signal from the Kin3-GFP signal (or Kin3 truncated versions) were counted as colocalized signals, while negative results as not colocalized signals. More details can be found in Supplementary Methods.

To obtain the ratio Kin3 to Rab5a the average intensities of Kin3 signals (colocalized with Rab5a) were measured in the first frame of dual movies and corrected for the adjacent cytoplasmic background and next divided by the average intensities derived from Rab5a also corrected for the adjacent cytoplasmic background.

Anterograde velocity of EEs in the AB33ΔKin3_mChRab5a_Kin3G, AB33ΔKin3_mChRab5a_Kin3$^{\Delta PH}$G, AB33ΔKin3_mChRab5a_rKin3$^{\Delta PH}$G and AB33ΔKin3_mChRab5a strains was measured in 50 frames taken within mother region of middle sized budded yeast-like cells using an exposure time of 150 ms, 561 nm laser at 100% and binning 1.

Anterograde frequency of EEs was measured 5 µm behind the distal mother region in middle sized budded yeast-like cell at conditions used for velocity measurements.

Measurement of the stationery EEs in the AB33_mChRab5a_rK1rG-K3t, AB33 mChRab5a_rK1rG-ΔDLP, AB33_mChRab5a_rK1rG-D, AB33_mChRab5a_rK1rG-D2 and AB33_mChRab5a_rK1rG-PH strains was

done within the entire middle sized budded yeast-like cells. 20 frame-movies were acquired using exposure time of 150 ms, 561 nm laser at 100% and binning 1. Analysis of stationery signals were done in first 7 frames (=1 s). Percentage of stationery signals was obtained by dividing of a number of nonmotile EE signals (for 1 s) by the number of total EE signals.

EEs pausing was analysed within the region of the highest expression of the chimera proteins (daughter cell, neck region and half of mother cell) in middle sized budded yeast-like cells. More details can be found in Supplementary Methods.

Measurements of anterograde run length of EEs were performed in the first 15 µm of the hyphal tips. More details can be found in Supplementary Methods.

Analysis of the Kin3 motor numbers colocalized with EEs was based on quantitative analysis of fluorescent intensities as described previously (Schuster *et al.*, 2011a). More details can be found in Supplementary Methods.

Split-YFP assay

To observe the interaction between the motor and PH domains *in vivo*, bimolecular fluorescence complementation (BIFC) technique was used. Signal derived from the split yellow fluorescent proteins of YFP^{C}-Kin3-YFP^{N} expressed in the hyphal cells was visualized using a USH-1030L Mercury Burner and a filter set for YFP (HC 500/24 and HC 542/27 AHF, Tuebingen, Germany). After acquiring movies composed of 100 frames at 150 ms exposure time and binning 2, kymographs were generated using MetaMorph (Molecular Devices).

Preparation of comparative models

Comparative models of the PH domains of *H. sapiens* KIF1A and *U. maydis* Kin3 were prepared using a selection of extant structures, identified as having strong structural similarity by the PHYRE2 (Kelley and Sternberg, 2009), FUGUE (Shi *et al.*, 2001) and LOMETS (Wu and Zhang, 2007) servers, preferring structures with bound ligands. A structure-based sequence alignment from the sequences from the structures of the PH domains from human TAPP1

(PDB id. 1EAZ), human protein kinase B (1H10), mouse SKAP-Hom (1U5E), human PDK1 (1W1D), human APPL1 (2ELB) and *Salmonella enterica* SifA (3CXB) was prepared using the MAMMOTH-mult (Lupyan *et al.*, 2005) and SUPERPOSE (Maiti *et al.*, 2004) servers, with careful hand-editing. Comparative models were prepared using MODELLER version 9.10 (Sali and Blundell, 1993), using the options for very thorough VTFM optimization and thorough MD optimization: 10 models were prepared, and the best selected on the basis of the MODELLER energy function, Ramachandran plot quality, and conservation of secondary structure. Models were prepared in complex with inositol-1,4,5-triphosphate. Prediction of membrane orientation was performed using the Orientations of Proteins in Membranes server (Lomize *et al.*, 2012). Images were prepared using PyMOL (The PyMOL Molecular Graphics System, Version 1.5.0.4 Schrödinger, LLC).

Lipid overlay assay

The assay was done according to Dowler *et al.*, 2002. PIP strips (Echelon, #P-6001, USA) were blocked with 1% fatty acid-free milk in PBS buffer (50 mM Tris, pH 8.0, 150 mM NaCl) at room temperature for 1 h. Recombinant protein was obtained as described above (see Protein affinity assays) and concentrated in PBS using a VivaSpin column (Vivascience, Germany) at a cut off of 5 kDa. The strips were then incubated with 0.45 µg/ml of Hisx6-PH^{Kin3} at 4^{o}C and overnight, followed by three washes in PBS-T buffer (PBS containing 0.1% Tween-20) for 10 minutes each, and subsequently incubated for 1 h with the anti-His antibody (in a 1:2000 dilution; His-Tag Mouse mAb; Cell Signaling, USA) at room temperature in blocking solution. After following three times washes in PBS-T buffer for 10 minutes each, membrane was incubated for 1 h at room temperature with the anti-Mouse IgG, HRP conjugated antibody (in a 1:2000 dilution; Promega, USA) at room temperature in 1% fatty acid-free milk in PBS buffer. After additional washing, the chemiluminescence was detected using the ECL Plus Western Blotting Detection system (GE Healthcare, United Kingdom).

Acknowledgement

We are grateful for receiving plasmids and strains from Dr. Sreedhar Kilaru (strain AB33ΔKin3_po^{C}GRab5a), Dr. Uta Fuchs (plasmid pSl-Yup-RFP-Hyg), Dr. Isabel Schuchardt, Göttingen, Germany (plasmid po^{C}GRab5a), Prof. Reinhard Fischer, Karlsruhe, Germany (plasmids pDV8 and pDV7) and Dr. Opher Gileadi, SGC Oxford, UK (plasmid pNic28-Bsa4). Dr. Catherine Collins is acknowledged for help with cloning pGBKT7-PH and the yeast-two-hybrid analysis. This work was supported by a grant from the Biotechnology and Biological Sciences Research Council (BB/F022956/1).

References

Abenza, J.F., Galindo, A., Pantazopoulou, A., Gil, C., de los Rios, V., and Penalva, M.A. (2010). *Aspergillus* RabB Rab5 integrates acquisition of degradative identity with the long distance movement of early endosomes. Mol Biol Cell *21*, 2756-2769.

Akhmanova, A., and Hammer, J.A., 3rd. (2010). Linking molecular motors to membrane cargo. Curr Opin Cell Biol *22*, 479-487.

Barkus, R.V., Klyachko, O., Horiuchi, D., Dickson, B.J., and Saxton, W.M. (2008). Identification of an axonal kinesin-3 motor for fast anterograde vesicle transport that facilitates retrograde transport of neuropeptides. Mol Biol Cell *19*, 274-283.

Baumann, S., Pohlmann, T., Jungbluth, M., Brachmann, A., and Feldbrügge, M. (2012). Kinesin-3 and dynein mediate microtubule-dependent co-transport of mRNPs and endosomes. J Cell Sci *125*, 2740-2752.

Bottin, A., Kamper, J., and Kahmann, R. (1996). Isolation of a carbon source-regulated gene from *Ustilago maydis*. Mol Gen Genet *253*, 342-352.

Brachmann, A., König, J., Julius, C., and Feldbrügge, M. (2004). A reverse genetic approach for generating gene replacement mutants in *Ustilago maydis*. Mol Genet Genomics *272*, 216-226.

Brachmann, A., Weinzierl, G., Kämper, J., and Kahmann, R. (2001). Identification of genes in the *bW/bE* regulatory cascade in *Ustilago maydis*. Mol Microbiol *42*, 1047-1063.

Bradford, M.M. (1976). A rapid and sensitive method for the quantitation of microgram quantities of protein utilizing the principle of protein-dye binding. Anal Biochem *72*, 248-254.

Dowler, S., Kular, G., and Alessi, D.R. (2002). Protein lipid overlay assay. Sci STKE *2002*, pl6.

Egan, M.J., McClintock, M.A., and Reck-Peterson, S.L. (2012b). Microtubule-based transport in filamentous fungi. Curr Opin Microbiol.

Fischer von Mollard, G., Mignery, G.A., Baumert, M., Perin, M.S., Hanson, T.J., Burger, P.M., Jahn, R., and Südhof, T.C. (1990). rab3 is a small GTP-binding protein exclusively localized to synaptic vesicles. Proc Natl Acad Sci U S A *87*, 1988-1992.

Fuchs, U., and Steinberg, G. (2005b). Endocytosis in the plant-pathogenic fungus *Ustilago maydis*. Protoplasma *226*, 75-80.

Hall, D.H., and Hedgecock, E.M. (1991). Kinesin-related gene unc-104 is required for axonal transport of synaptic vesicles in *C. elegans*. Cell *65*, 837-847.

Hammond, J.W., Cai, D., Blasius, T.L., Li, Z., Jiang, Y., Jih, G.T., Meyhofer, E., and Verhey, K.J. (2009). Mammalian Kinesin-3 motors are dimeric *in vivo* and move by processive motility upon release of autoinhibition. PLoS Biol *7*, e72.

Haun, R.S., Serventi, I.M., and Moss, J. (1992). Rapid, reliable ligation-independent cloning of PCR products using modified plasmid vectors. Biotechniques *13*, 515-518.

Hirokawa, N. (1998). Kinesin and dynein superfamily proteins and the mechanism of organelle transport. Science *279*, 519-526.

Hirokawa, N., Noda, Y., Tanaka, Y., and Niwa, S. (2009). Kinesin superfamily motor proteins and intracellular transport. Nat Rev Mol Cell Biol *10*, 682-696.

Hoepfner, S., Severin, F., Cabezas, A., Habermann, B., Runge, A., Gillooly, D., Stenmark, H., and Zerial, M. (2005). Modulation of receptor recycling and degradation by the endosomal kinesin KIF16B. Cell *121*, 437-450.

Holliday, R. (1974). *Ustilago maydis.* In Handbook of Genetics, ed. RC King, New York. Plenum Press, 575-595.

Huckaba, T.M., Gennerich, A., Wilhelm, J.E., Chishti, A.H., and Vale, R.D. (2011). Kinesin-73 is a processive motor that localizes to Rab5-containing organelles. J Biol Chem *286*, 7457-7467.

Huh, W.K., Falvo, J.V., Gerke, L.C., Carroll, A.S., Howson, R.W., Weissman, J.S., and O'Shea, E.K. (2003). Global analysis of protein localization in budding yeast. Nature *425*, 686-691.

Huo, L., Yue, Y., Ren, J., Yu, J., Liu, J., Yu, Y., Ye, F., Xu, T., Zhang, M., and Feng, W. (2012). The CC1-FHA tandem as a central hub for controlling the dimerization and activation of kinesin-3 KIF1A. Structure *20*, 1550-1561.

Jordens, I., Marsman, M., Kuijl, C., and Neefjes, J. (2005). Rab proteins, connecting transport and vesicle fusion. Traffic *6*, 1070-1077.

Kelley, L.A., and Sternberg, M.J. (2009). Protein structure prediction on the Web: a case study using the Phyre server. Nat Protoc *4*, 363-371.

Klopfenstein, D.R., Tomishige, M., Stuurman, N., and Vale, R.D. (2002). Role of phosphatidylinositol(4,5)bisphosphate organization in membrane transport by the Unc104 kinesin motor. Cell *109*, 347-358.

Klopfenstein, D.R., and Vale, R.D. (2004). The lipid binding pleckstrin homology domain in UNC-104 kinesin is necessary for synaptic vesicle transport in *Caenorhabditis elegans*. Mol Biol Cell *15*, 3729-3739.

Lawrence, C.J., Dawe, R.K., Christie, K.R., Cleveland, D.W., Dawson, S.C., Endow, S.A., Goldstein, L.S., Goodson, H.V., Hirokawa, N., Howard, J., Malmberg, R.L., McIntosh, J.R., Miki, H., Mitchison, T.J., Okada, Y., Reddy, A.S., Saxton, W.M., Schliwa, M., Scholey, J.M., Vale, R.D., Walczak, C.E., and Wordeman, L. (2004). A standardized kinesin nomenclature. J Cell Biol *167*, 19-22.

Lee, J.R., Shin, H., Choi, J., Ko, J., Kim, S., Lee, H.W., Kim, K., Rho, S.H., Lee, J.H., Song, H.E., Eom, S.H., and Kim, E. (2004). An intramolecular interaction between the FHA domain and a coiled coil negatively regulates the kinesin motor KIF1A. EMBO J *23*, 1506-1515.

Lemmon, M.A. (1999). Structural basis for high-affinity phosphoinositide binding by pleckstrin homology domains. Biochem Soc Trans *27*, 617-624.

Lenz, J.H., Schuchardt, I., Straube, A., and Steinberg, G. (2006). A dynein loading zone for retrograde endosome motility at microtubule plus-ends. EMBO J *25*, 2275-2286.

Liu, J.S., Schubert, C.R., Fu, X., Fourniol, F.J., Jaiswal, J.K., Houdusse, A., Stultz, C.M., Moores, C.A., and Walsh, C.A. (2012). Molecular basis for specific regulation of neuronal kinesin-3 motors by doublecortin family proteins. Mol Cell *47*, 707-721.

Lo, K.Y., Kuzmin, A., Unger, S.M., Petersen, J.D., and Silverman, M.A. (2011). KIF1A is the primary anterograde motor protein required for the axonal transport of dense-core vesicles in cultured hippocampal neurons. Neurosci Lett *491*, 168-173.

Lomize, M.A., Pogozheva, I.D., Joo, H., Mosberg, H.I., and Lomize, A.L. (2012). OPM database and PPM web server: resources for positioning of proteins in membranes. Nucleic Acids Res *40*, D370-376.

Lupas, A., Van Dyke, M., and Stock, J. (1991). Predicting coiled coils from protein sequences. Science *252*, 1162-1164.

Lupyan, D., Leo-Macias, A., and Ortiz, A.R. (2005). A new progressive-iterative algorithm for multiple structure alignment. Bioinformatics *21*, 3255-3263.

Maiti, R., Van Domselaar, G.H., Zhang, H., and Wishart, D.S. (2004). SuperPose: a simple server for sophisticated structural superposition. Nucleic Acids Res *32*, W590-594.

Mayinger, P. (2012). Phosphoinositides and vesicular membrane traffic. Biochim Biophys Acta *1821*, 1104-1113.

Miki, H., Okada, Y., and Hirokawa, N. (2005). Analysis of the kinesin superfamily: insights into structure and function. Trends Cell Biol *15*, 467-476.

Miki, H., Setou, M., Kaneshiro, K., and Hirokawa, N. (2001). All kinesin superfamily protein, KIF, genes in mouse and human. Proc Natl Acad Sci U S A *98*, 7004-7011.

Miller, K.E., DeProto, J., Kaufmann, N., Patel, B.N., Duckworth, A., and Van Vactor, D. (2005). Direct observation demonstrates that Liprin-alpha is required for trafficking of synaptic vesicles. Curr Biol *15*, 684-689.

Muresan, V., Stankewich, M.C., Steffen, W., Morrow, J.S., Holzbaur, E.L., and Schnapp, B.J. (2001). Dynactin-dependent, dynein-driven vesicle transport in the absence of membrane proteins: a role for spectrin and acidic phospholipids. Mol Cell *7*, 173-183.

Nangaku, M., Sato-Yoshitake, R., Okada, Y., Noda, Y., Takemura, R., Yamazaki, H., and Hirokawa, N. (1994). KIF1B, a novel microtubule plus end-directed monomeric motor protein for transport of mitochondria. Cell *79*, 1209-1220.

Niwa, S., Tanaka, Y., and Hirokawa, N. (2008). KIF1Bbeta- and KIF1A-mediated axonal transport of presynaptic regulator Rab3 occurs in a GTP-dependent manner through DENN/MADD. Nat Cell Biol *10*, 1269-1279.

Nonet, M.L., Saifee, O., Zhao, H., Rand, J.B., and Wei, L. (1998). Synaptic transmission deficits in *Caenorhabditis elegans* synaptobrevin mutants. J Neurosci *18*, 70-80.

Okada, Y., Yamazaki, H., Sekine-Aizawa, Y., and Hirokawa, N. (1995). The neuron-specific kinesin superfamily protein KIF1A is a unique monomeric motor for anterograde axonal transport of synaptic vesicle precursors. Cell *81*, 769-780.

Raymond, C.K., Pownder, T.A., and Sexson, S.L. (1999). General method for plasmid construction using homologous recombination. Biotechniques *26*, 134-138, 140-131.

Sali, A., and Blundell, T.L. (1993). Comparative protein modelling by satisfaction of spatial restraints. J Mol Biol *234*, 779-815.

Saraste, M., and Hyvonen, M. (1995). Pleckstrin homology domains: a fact file. Curr Opin Struct Biol *5*, 403-408.

Schuster, M., Kilaru, S., Ashwin, P., Lin, C., Severs, N.J., and Steinberg, G. (2011a). Controlled and stochastic retention concentrates dynein at microtubule ends to keep endosomes on track. EMBO J *30*, 652-664.

Schuster, M., Kilaru, S., Fink, G., Collemare, J., Roger, Y., and Steinberg, G. (2011c). Kinesin-3 and dynein cooperate in long-range retrograde endosome motility along a nonuniform microtubule array. Mol Biol Cell *22*, 3645-3657.

Schuster, M., Lipowsky, R., Assmann, M.A., Lenz, P., and Steinberg, G. (2011b). Transient binding of dynein controls bidirectional long-range motility of early endosomes. Proc Natl Acad Sci U S A *108*, 3618-3623.

Seiler, S., Kirchner, J., Horn, C., Kallipolitou, A., Woehlke, G., and Schliwa, M. (2000). Cargo binding and regulatory sites in the tail of fungal conventional kinesin. Nat Cell Biol *2*, 333-338.

Shi, J., Blundell, T.L., and Mizuguchi, K. (2001). FUGUE: sequence-structure homology recognition using environment-specific substitution tables and structure-dependent gap penalties. J Mol Biol *310*, 243-257.

Shin, H., Wyszynski, M., Huh, K.H., Valtschanoff, J.G., Lee, J.R., Ko, J., Streuli, M., Weinberg, R.J., Sheng, M., and Kim, E. (2003). Association of the kinesin motor KIF1A with the multimodular protein liprin-alpha. J Biol Chem *278*, 11393-11401.

Steinberg, G. (2007c). On the move: endosomes in fungal growth and pathogenicity. Nat Rev Microbiol *5*, 309-316.

Steinberg, G., and Perez-Martin, J. (2008). *Ustilago maydis*, a new fungal model system for cell biology. Trends Cell Biol *18*, 61-67.

Straube, A., Hause, G., Fink, G., and Steinberg, G. (2006). Conventional kinesin mediates microtubule-microtubule interactions *in vivo*. Mol Biol Cell *17*, 907-916.

Vale, R.D. (2003). The molecular motor toolbox for intracellular transport. Cell *112*, 467-480.

Verhey, K.J., and Hammond, J.W. (2009). Traffic control: regulation of kinesin motors. Nat Rev Mol Cell Biol *10*, 765-777.

Vicinanza, M., D'Angelo, G., Di Campli, A., and De Matteis, M.A. (2008). Phosphoinositides as regulators of membrane trafficking in health and disease. Cell Mol Life Sci *65*, 2833-2841.

Watt, S.A., Kular, G., Fleming, I.N., Downes, C.P., and Lucocq, J.M. (2002). Subcellular localization of phosphatidylinositol 4,5-bisphosphate using the pleckstrin homology domain of phospholipase C delta1. Biochem J *363*, 657-666.

Wedlich-Söldner, R., Bölker, M., Kahmann, R., and Steinberg, G. (2000). A putative endosomal t-SNARE links exo- and endocytosis in the phytopathogenic fungus *Ustilago maydis*. EMBO J *19*, 1974-1986.

Wedlich-Söldner, R., Straube, A., Friedrich, M.W., and Steinberg, G. (2002). A balance of KIF1A-like kinesin and dynein organizes early endosomes in the fungus *Ustilago maydis*. EMBO J *21*, 2946-2957.

Westerholm-Parvinen, A., Vernos, I., and Serrano, L. (2000). Kinesin subfamily UNC104 contains a FHA domain: boundaries and physicochemical characterization. FEBS Lett *486*, 285-290.

Wu, S., and Zhang, Y. (2007). LOMETS: a local meta-threading-server for protein structure prediction. Nucleic Acids Res *35*, 3375-3382.

Xue, X., Jaulin, F., Espenel, C., and Kreitzer, G. (2010). PH-domain-dependent selective transport of p75 by kinesin-3 family motors in non-polarized MDCK cells. J Cell Sci *123*, 1732-1741.

Yonekawa, Y., Harada, A., Okada, Y., Funakoshi, T., Kanai, Y., Takei, Y., Terada, S., Noda, T., and Hirokawa, N. (1998). Defect in synaptic vesicle precursor transport and neuronal cell death in KIF1A motor protein-deficient mice. J Cell Biol *141*, 431-441.

Yu, H., Wang, N., Ju, X., Yang, Y., Sun, D., Lai, M., Cui, L., Sheikh, M.A., Zhang, J., Wang, X., and Zhu, X. (2012). PtdIns (3,4,5) P3 recruitment of Myo10 is essential for axon development. PLoS One *7*, e36988.

Yu, J.W., Mendrola, J.M., Audhya, A., Singh, S., Keleti, D., DeWald, D.B., Murray, D., Emr, S.D., and Lemmon, M.A. (2004). Genome-wide analysis of membrane targeting by *S. cerevisiae* pleckstrin homology domains. Mol Cell *13*, 677-688.

Zhao, C., Takita, J., Tanaka, Y., Setou, M., Nakagawa, T., Takeda, S., Yang, H.W., Terada, S., Nakata, T., Takei, Y., Saito, M., Tsuji, S., Hayashi, Y., and Hirokawa, N. (2001). Charcot-Marie-Tooth disease type 2A caused by mutation in a microtubule motor KIF1Bbeta. Cell *105*, 587-597.

Figures and figure legends

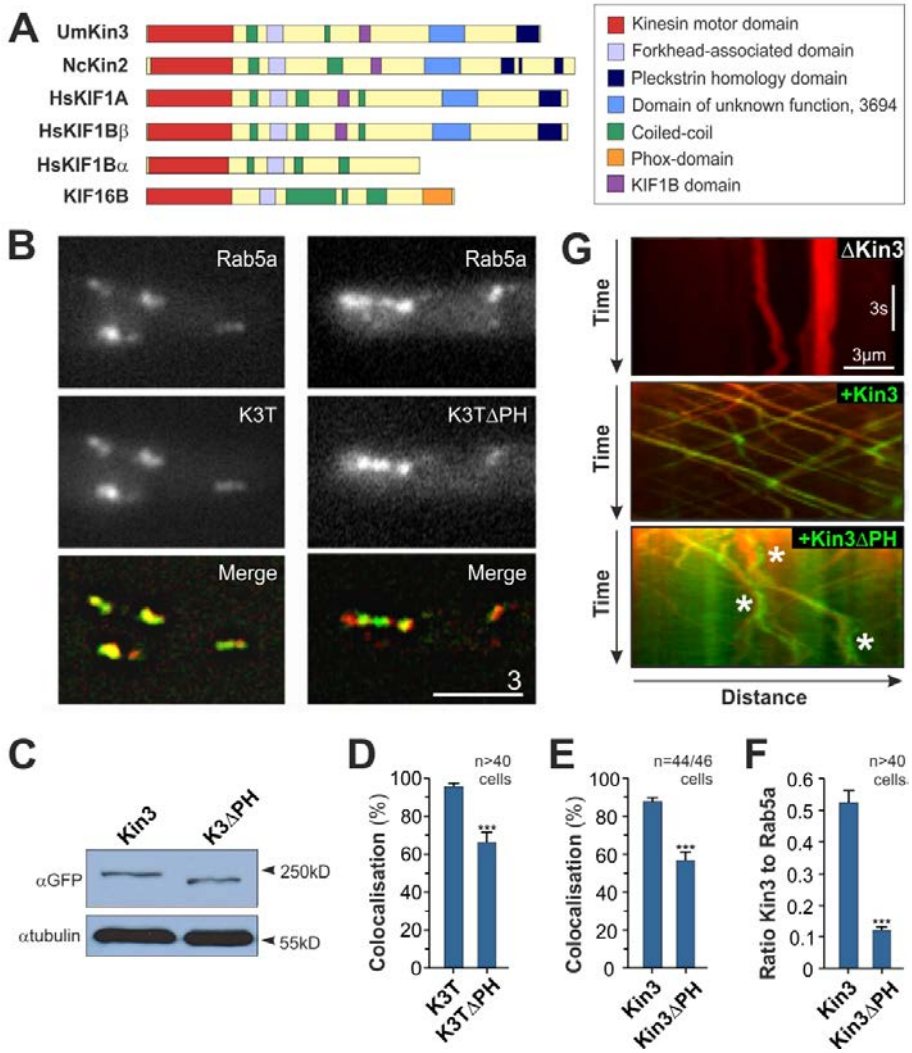

Figure 1. The role of the PH domain in motor-to-cargo association.
(**A**) Diagram depicting the domain organization of kinesin-3 motors. KIF16B uses the PX domain (orange) to transport EEs. UmKin3, kinesin-3 from *U. maydis* (accession number: XP_762398); NcKin2, kinesin-3 from *Neurospora crassa* (accession number: XP_960661); HsKIF1A, neuronal kinesin-3 from humans (accession number: NP_001230937); HsKIF1Bβ, neuronal kinesin-3 from humans, isoform beta (accession number: NP_055889); HsKIF1Bα, neuronal kinesin-3 from humans, isoform alpha (accession number: NP_904325); KIF16B, kinesin-3 from humans (accession number: NP_078980). For all accession numbers see http://www.ncbi.nlm.nih.gov/gene/. UmKin3 contains all domains typical for KIF1A/Unc-104 family. Note that HsKIF1A and HsKIF1Bβ bind synaptic vesicle precursors, whereas UmKin3 and KIF16B bind to early endosomes, and NcKin2 and HsKIF1Bα bind to mitochondria. (**B**) Colocalization of EEs labelled with GFP-Rab5a (Rab5a, green in merged image) and a Kin3-tail fused to mCherry (amino acids 423-1676; left panel, K3T; red in merged image), as well as a Kin3-tail that is lacking the PH domain fused to mCherry (amino acids 423-1676$^{\Delta 1566-1666}$; right panel; K3TΔPH; red in the merged image). The PH domain is not of essential importance for the association of Kin3 and EEs. Bar represents micrometers. (**C**) Immunoblot showing the expression of Kin3 and Kin3$^{\Delta PH}$ fused to GFP (Kin3; Kin3ΔPH). The truncated protein is stably expressed. αTubulin was detected as an internal loading control. (**D**) Bar chart showing the degree of colocalization between

GFP-Rab5a labelled EEs and Kin3-tail protein fused to mCherry (K3T) and Kin3-tail$^{\Delta PH}$ protein fused to mCherry (K3T∆PH). Note that the Kin3-fragments were expressed in a ∆kin3 background. All bars are given as mean±SEM, sample size *n* is indicated as total number of cells (158-161 EEs) from two independent experiments. Triple asterisk indicates statistical significance at P<0.0001, Mann Whitney test). (**E**) Bar chart showing the degree of colocalization between mCherry-Rab5a labelled EEs and entire Kin3 protein fused to GFP (Kin3) and Kin3 deleted in the PH domain (Kin3∆PH). Note that both GFP-*kin3* fusion constructs were integrated into the succinate-dehydrogenase locus in a *kin3* null mutant background. All bars are given as mean±SEM, sample size *n* is indicated as total number of cells (175-412 EEs) from two independent experiments. Triple asterisk indicates statistical significance at *P*<0.0001 (Mann-Whitney test). (**F**) Bar chart showing the ratio of the average intensities of EE-bound Kin3-GFP and Kin3$^{\Delta PH}$-GFP fluorescent signals and mCherry-Rab5a. Deletion of the PH domain drastically reduces the amount of the motor on the organelles. All bars are given as mean±SEM, sample size *n* is indicated as total number of cells (98-360 EEs) from two independent experiments. Triple asterisk indicates statistical significance at *P*<0.0001 (Mann-Whitney test). (**G**) Kymographs showing motility of mCherry-Rab5a labelled EEs (shown in red) in a *kin3* null mutant (∆Kin3; shown as vertical lines), a *kin3* null mutant rescued with the entire *kin3* gene fused to GFP (+Kin3; shown as green signals) and a *kin3* null mutant rescued with a *kin3* gene truncated in the PH domain gene fused to GFP (+Kin3∆PH; shown as green signals). The Kin3$^{\Delta PH}$ protein is still able to rescue EE motility. Note that motility was not fully restored and EEs cluster in the presence of Kin3$^{\Delta PH}$ (asterisks). Time is given in seconds, distance is given in micrometers. The image was contrast inverted. See also Movie S1.

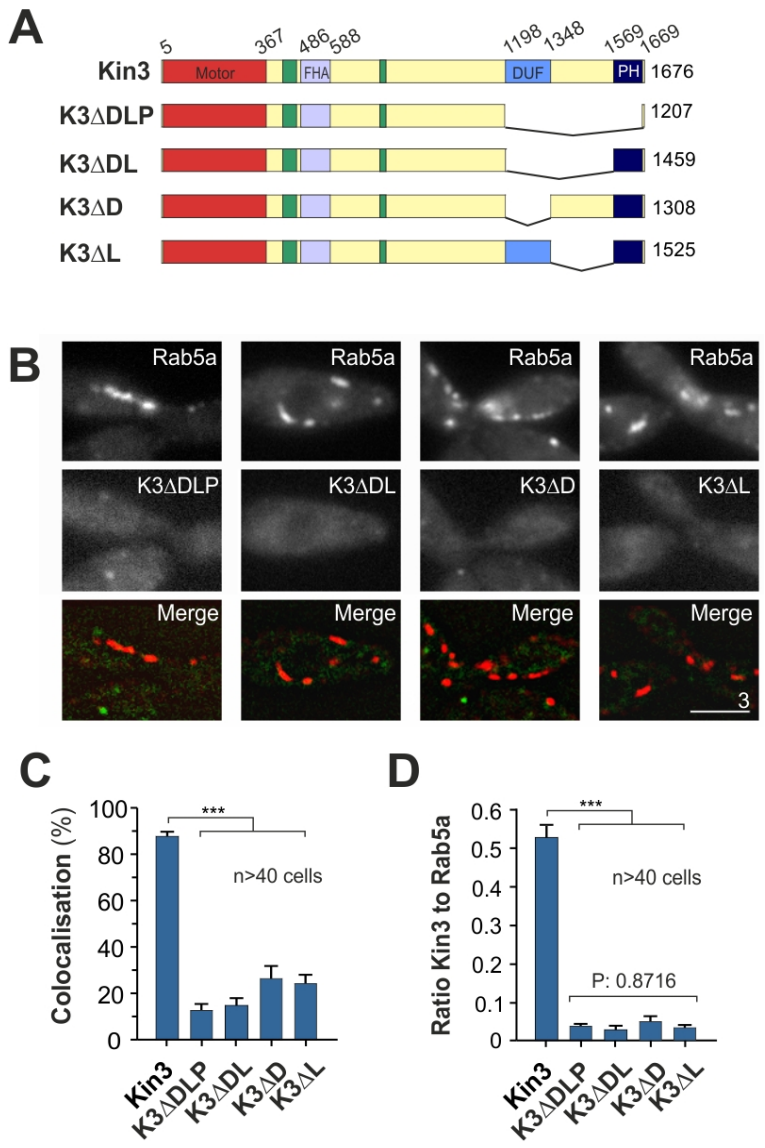

Figure 2. The role of the conserved regions in the Kin3 tail in cargo binding.
(**A**) Diagram depicting the domain organization of Kin3 and truncated Kin3 proteins lacking parts of the tail. Kin3ΔDLP: deletion of the DUF3694 domain, the conserved "linker" region and the PH domain (deleted in amino acids 1198-1666); Kin3ΔDL: deletion of the DUF3694 domain and the conserved “linker” region (deleted in amino acids 1198-1565); Kin3ΔD: deletion of the DUF3694 domain (deleted in amino acids 1198-1348); Kin3ΔL: deletion in the conserved "linker" region (deleted in amino acids 1349-1565). Numbers indicate amino acid positions. (**B**) Colocalization of EEs labelled with mCherry-Rab5a (Rab5a; red in merged image) and the truncated Kin3-GFP proteins lacking the DUF3694 domain, the conserved "linker" region and the PH domain (Kin3ΔDLP), the DUF3694 domain and the conserved "linker" region (Kin3ΔDL), the DUF3694 domain (Kin3ΔD) or the conserved "linker" region (Kin3ΔL; all green in merged images). Neither of the truncated proteins is able to bind to EEs. Note high cytoplasmic background derived from unbound motors. Bar represents micrometers. (**C**) Bar chart showing the degree of colocalization between mCherry-Rab5a labelled EEs, Kin3-G (Kin3) and truncated Kin3-GFP proteins lacking the DUF3694 domain, the conserved "linker" region and the PH domain (K3ΔDLP), the

DUF3694 domain and the conserved "linker" region (K3ΔDL), the DUF3694 domain (K3ΔD) or the conserved "linker" region (K3ΔL). All bars are given as mean±SEM, sample size *n* is indicated as total number of cells (114-239 EEs) from two independent experiments. Triple asterisk indicates statistical significance to control at P<0.0001 (Mann-Whitney test). No statistical significance is found between K3ΔD and K3ΔL (P=0.7661, Mann-Whitney test). (**D**) Bar chart showing the ratio of the average intensities of EE-bound Kin3-GFP and truncated Kin3-GFP proteins and mCherry-Rab5a. All bars are given as mean±SEM, sample size *n* is indicated as total number of cells (20-55 EEs) from two independent experiments. Triple asterisk indicates statistical significance to control at *P*<0.0001 (Mann-Whitney test). No difference was found between the truncated proteins (P=0.8716; one-way ANOVA test - Kruskal-Willis test result).

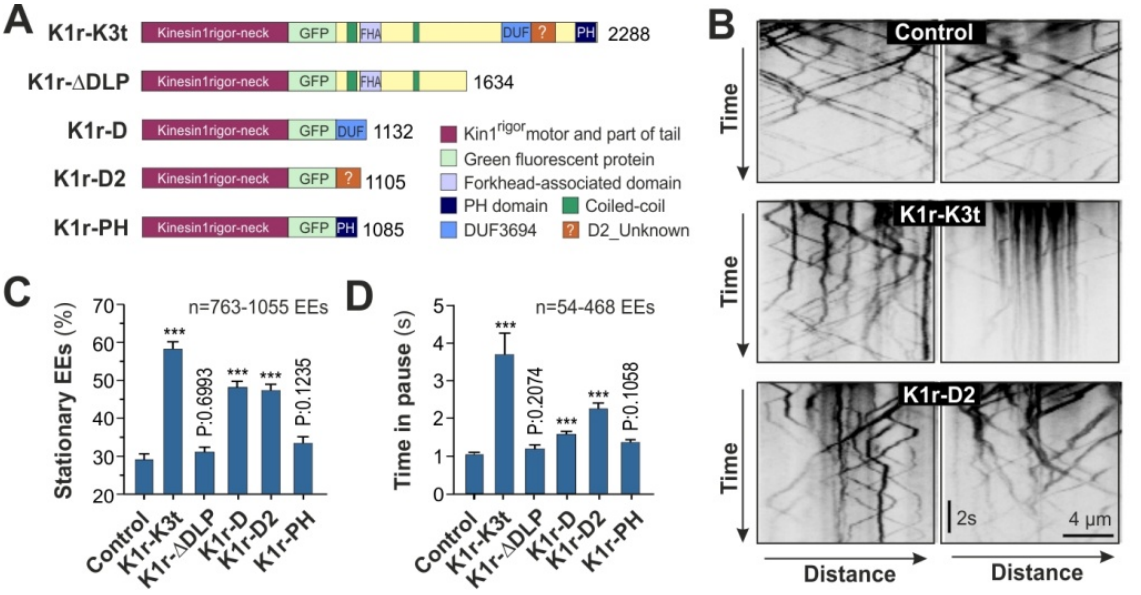

Figure 3. Anchorage of EEs by synthetic immobile motor proteins.
(**A**) Diagram depicting the domain organization of the synthetic motors used in this study. Each chimerical protein consists of a Kin1^{rigor} head-neck region (aa 1-739) that tightly binds to microtubules (Straube *et al.*, 2006), an internal GFP and several parts of the Kin3 tail (K1r-K3t: The Kin1^{rigor} head-neck region fused to the entire Kin3 tail (aa 370-1676); K1r-ΔDLP, The Kin1^{rigor} head-neck region fused to the N-terminal half of the Kin3 tail (aa 370-1022); K1r-D: The Kin1^{rigor} head-neck region fused to the DUF3694 domain (aa 1198-1348); K1r-D2: The Kin1^{rigor} head-neck region fused to the highly conserved amino acids stretch within "linker" region (aa 1345-1468); K1r-PH: The Kin1^{rigor} head-neck region fused to the PH domain (aa 1566-1676). Numbers indicate amino acids. Note that the chimerical proteins are stably expressed (data not shown). (**B**) Kymographs showing motility of mCherry-Rab5a labelled EEs in control cell that do not express the synthetic motor (Control) and after expression of K1r-K3t and K1r-D2. Note that all proteins were expressed under the inducible *crg* promoter and in the wildtype background. The expression levels varied between cells, resulting in variation in the phenotype, therefore two examples are provided. Time is given in seconds; distance is given in micrometers. The images were contrast inverted. Note that the conserved D2 region is able to bind EEs to microtubules, thereby inhibiting EE motility. (**C**) Bar chart showing the relative number of stationery EEs after expression of the nonmotile synthetic motors. Control: no expression of a synthetic motor; K1r-K3t: The Kin1^{rigor} head-neck region fused to the entire Kin3 tail; K1r-ΔDLP: The Kin1^{rigor} head-neck region fused to the N-terminal half of the Kin3 tail; K1r-D: The Kin1^{rigor} head-neck region fused to the DUF3694 domain (aa 1198-1348); K1r-D2: The Kin1^{rigor} head-neck region fused to the highly conserved amino acids stretch within "linker" region (aa 1345-1468); K1r-PH: The Kin1^{rigor} head-neck region fused to the PH domain (aa 1566-1676). All bars are given as mean±SEM, sample size *n* is indicated from two independent experiments (more than 40 cells).Triple asterisk indicates statistical significance to control at $P<0.0001$ (Mann Whitney test). P-values of non-significant differences are indicated above bars. (**D**) Bar chart showing pausing times of EEs that were anchored by chimerical synthetic motor proteins. Note that the pausing time of EE was not increased by K1r-PH, suggesting that the PH domain is not able to anchor the

organelles. Control: no expression of a synthetic motor; K1r-K3t: The Kin1^{rigor} head-neck region fused to the entire Kin3 tail; K1r-ΔDLP: The Kin1^{rigor} head-neck region fused to the N-terminal half of the Kin3 tail; K1r-D: The Kin1^{rigor} head-neck region fused to the DUF3694 domain (aa 1198-1348); K1r-D2: The Kin1^{rigor} head-neck region fused to the highly conserved amino acids stretch within "linker" region (aa 1345-1468); K1r-PH: The Kin1^{rigor} head-neck region fused to the PH domain (aa 1566-1676). All bars are given as mean±SEM, the sample size *n* is indicated. Triple asterisk indicates statistical significance to control at $P<0.0001$ (Mann-Whitney test). P-values of non-significant differences are indicated above bars.

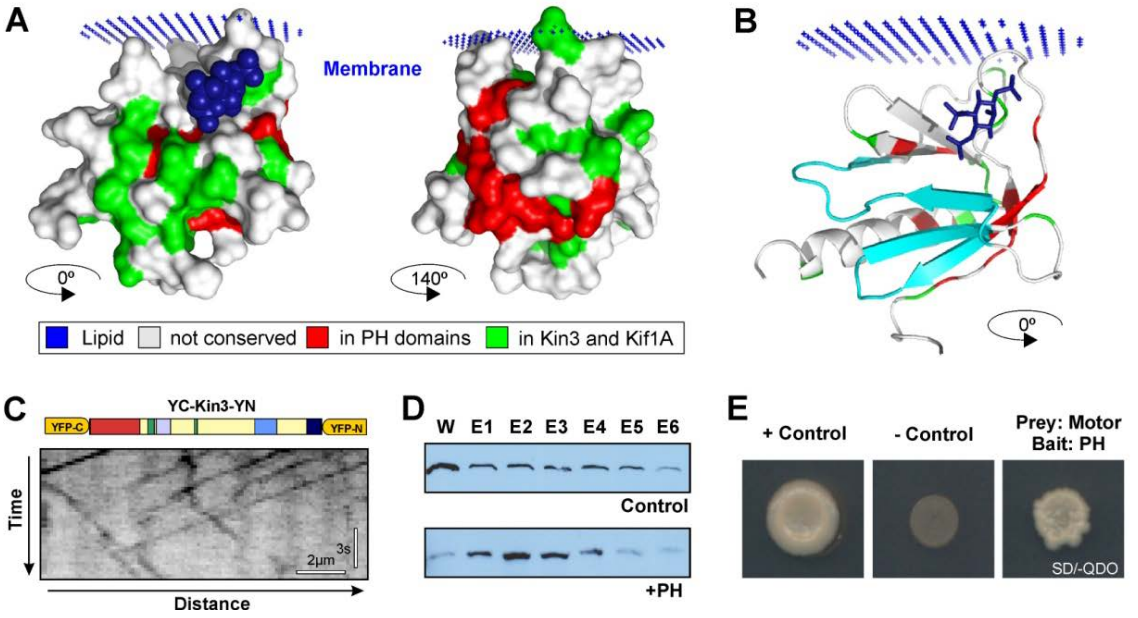

Figure 4. The PH domain interacts with motor domain *in vitro*.
(**A**) Structural model of the PH domain of Kin3 shown from two angles (0° and 140°). The pocket made at the apex of the β sandwich structure, cradled by the β1-β2 loops provides a suitable space to bind a lipid moiety (blue), confirming a potential membrane binding role of the PH domain. Amino acids that are found in PH domains of the kinesins Kin3, KIF1A, and the six parent structures are coloured (for accession numbers and further details see Material and Methods); amino acids that are only conserved between human KIF1A and fungal Kin3 are coloured green. Note the presence of patches of highly conserved amino acids (green region at 0°) that are facing away from the membrane (indicated by blue grid), suggestive of kinesin-specific functional interactions of kinesin-3 PH domains with other proteins or parts of the kinesin-3 motor. See also Movie S2. The model was based on published structures of PH domains. For proteins and PDB accession numbers see Material and Methods. (**B**) Cartoon model showing the structural organisation of the PH domain from Kin3. The model represents the model shown in Fig. 4A at 0º. Note the majority of the kinesin-specific amino acid conservations (see green patches in Fig. 4A) are located in two pairs of β-strands on one side of the domain structure. (**C**) Kymograph and diagram showing the organization and motility of Kin3 fused N- and C-terminally to split-YFP (YFP-C, YFP-N). Note that fluorescence can only be detected when the tail folds back to the motor domain thereby allowing interaction between YFP-C and YFP-N. This interaction does not impair motility, suggesting that it reflects the native conformation. Time is given in seconds; distance is given in micrometers. The image was contrast inverted. See also Movie S3. (**D**) Elution profile of the Kin3 motor domain, fused to GFP (amino acid 1-367) incubated with pure Ni-NTA resin (upper immunoblot) and after loading the resin with recombinant PH domain (lower immunoblot). The PH domain retains the motor domain, suggesting that both interact physically. W: Wash; E1-E6: Elution fractions, each 20 µl. (**E**) Plates showing the outcome of a yeast two-hybrid experiment using the Gal4 DNA binding domain (BD; able to bind to Gal4 promoter) fused to the PH domain of Kin3 (amino acid 1566-1676) as “bait” containing *TRP1* nutritional marker and the Gal4 DNA activation domain (AD; activates transcription of

the reporter genes) fused to the Kin3 motor domain (amino acid 1-367) as “prey” containing *LEU2* nutritional marker. Growth on tryptophan/leucine/histidine/adenine-deficient plates (Quadruple dropout; QDO; SD/–Ade/–His/–Leu/–Trp) occurs, suggesting the motor domain and the PH domain interact leading to activation of the reporter genes and expression of four deficient amino acids. The positive control (+Control), consisting of pGBKT7-53 and pGADT7-T encode fusions between the GAL4 DNA-BD and AD and murine p53 and SV40 large T-antigen, respectively, and the negative control (-Control), consisting of pGBKT7-Lam encoding a fusion of the DNA-BD with human lamin C and pGADT7-T, are given.

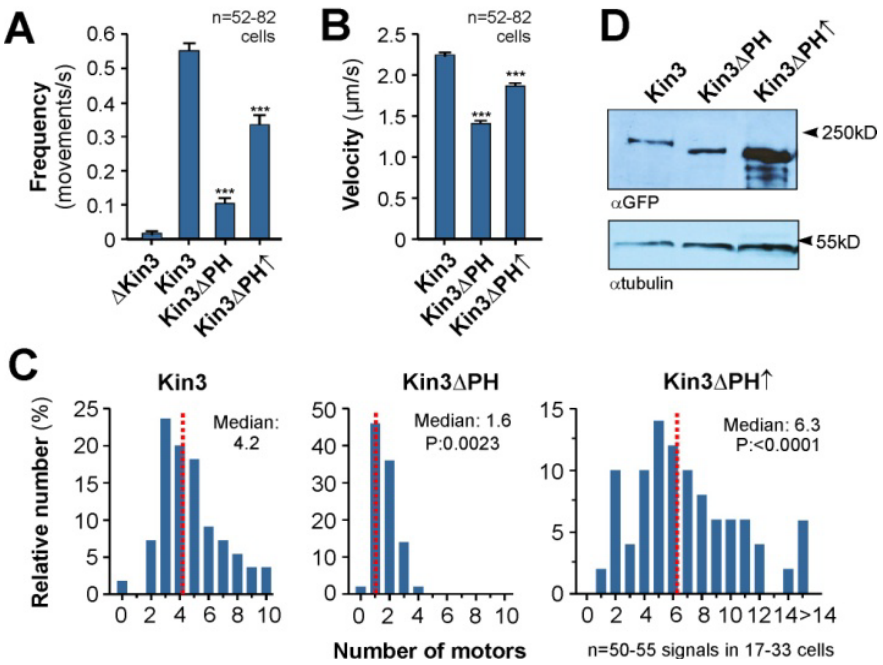

Figure 5. The PH domain is required for EE motility.
(**A**) Bar chart showing the frequency of plus-end directed EE transport. Deletion of Kin3 almost completely abolishes anterograde motility of EEs (ΔKin3). The deletion of the PH domain reduces the transport by ~80% (Kin3ΔPH). High expression of Kin3ΔPH is not able to fully restore the motility of the organelles (Kin3ΔPH↑). Note that data were obtained from *kin3* null strains that were complemented with intact or truncated Kin3 proteins. All bars are given as mean±SEM, sample size *n* is indicated as total number of cells (10-296 EEs) from five independent experiments. Triple asterisk indicates statistical significance at *P*<0.0001 (Mann-Whitney test). (**B**) Anterograde of plus-end directed EE motility. Deletion of Kin3 significantly reduces anterograde motility of EEs (ΔKin3). High expression of Kin3ΔPH is not able to fully restore this phenotype (Kin3ΔPH↑). Note that data were obtained from *kin3* null strains that were complemented with intact or truncated Kin3 proteins. Bars are given as mean±SEM, sample size *n* is indicated as total number of cells (315-534 EEs) from five independent experiments. Triple asterisk indicates statistical significance at *P*<0.0001 (Mann-Whitney test). (**C**) Bar charts showing the number of kinesin-3 motors bound to EEs. The numbers were estimated using fluorescent nuclear pore proteins as calibration standards (Schuster *et al.*, 2011a). The median and statistical significance at P=0.0023 and P<0.0001 is indicated (Mann-Whitney test). (**D**) Immunoblot showing expression of Kin3-GFP and Kin3-GFP that is lacking the PH domain (Kin3ΔPH) proteins, both expressed under the endogenous *kin3* promoter. Much more Kin3ΔPH protein is detected when the protein is expressed under the strong inducible *crg* promoter.

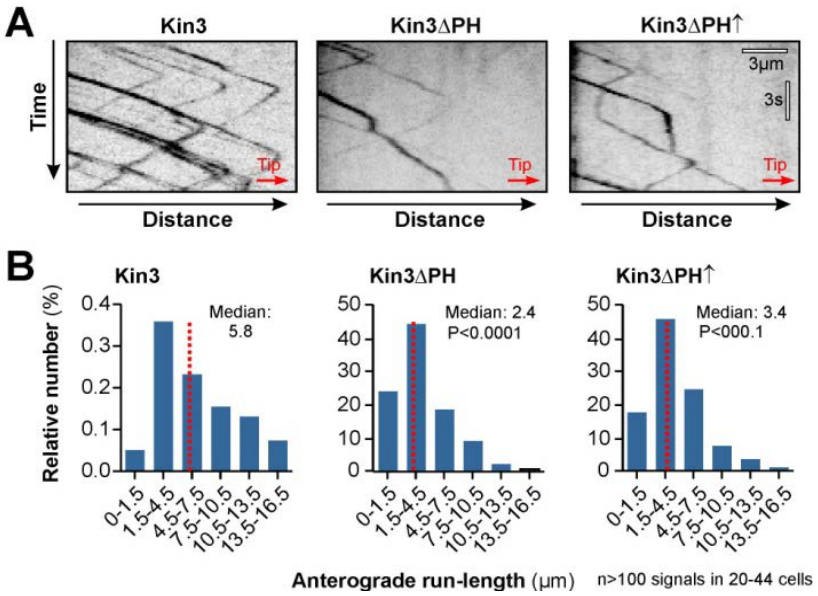

Figure 6. The PH domain is required for extended anterograde EE runs.
(**A**) Kymographs showing motility of mCherry-Rab5a labelled EEs in first 15 µm of hyphal cells that were photo-bleached to reduce interfering background. Deletion of the PH domain reduces frequency and velocity (see above Fig. 5), but also affects the length of individual runs (Kin3ΔPH). High expression the truncated Kin3ΔPH protein only partially restores organelle motility (Kin3ΔPH↑). Note that data were obtained from *kin3* null strains that were complemented with intact or truncated Kin3 proteins. The bars represent seconds and micrometers. (**B**) Bar charts showing anterograde run length of mCherry-Rab5a labelled EEs in control cells (Kin3) and in mutants expressing a Kin3ΔPH protein expressed under the *kin3* promoter (Kin3ΔPH), or the strong *crg* promoter (Kin3ΔPH↑). Note that data were obtained from *kin3* null strains that were complemented with intact or truncated Kin3 proteins. Statistical significance was tested using a non-parametric Mann-Whitney t-test and P-values for comparison with control data set are given. Sample size for moving EEs (n) and total number of analysed cells are given.

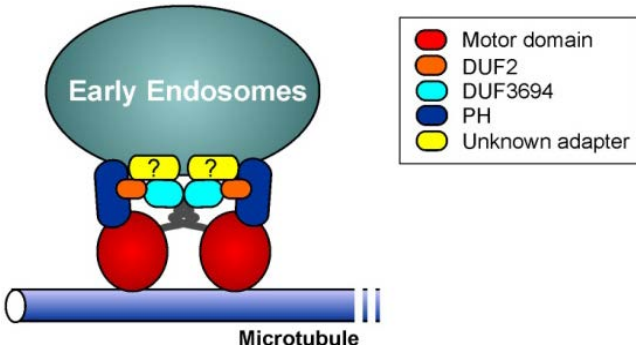

Figure 7. Model of the organization of EE-bound Kin3.
The cargo-bound motor adopts a compact conformation and the motor domain interacts with the PH domain. In addition, the PH domain has a minor role in membrane anchorage, which is mainly mediated by two domains (DUF364 and D2) within the Kin3 tail that are conserved probably due to interaction with unknown adapters on the organelle membrane.

Supplementary online material

Supplementary Figures

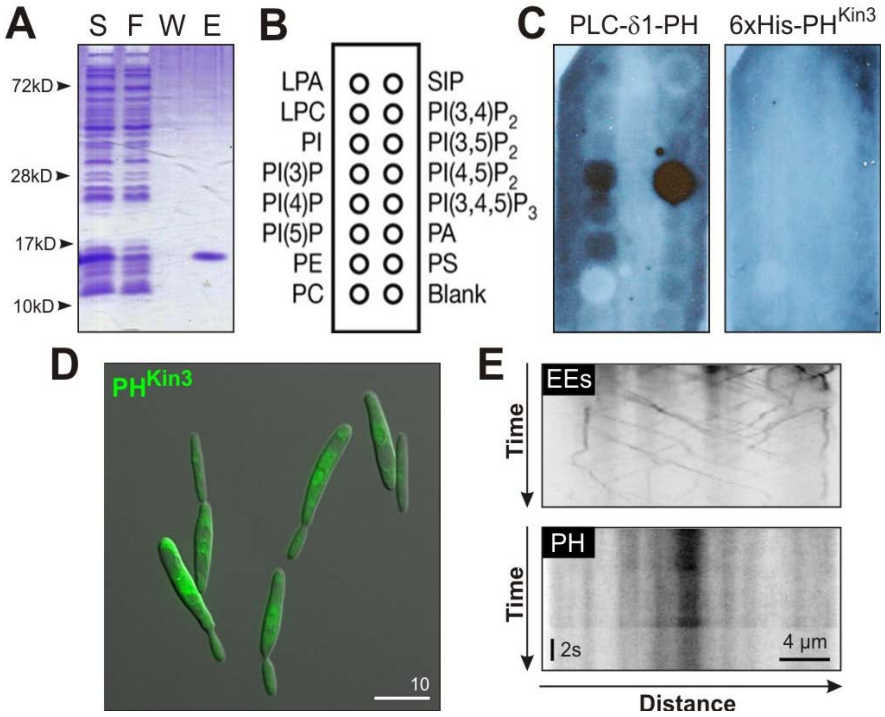

Figure S1. *In vitro* and *in vivo* binding capacity of the Kin3 PH domain.
(**A**) 15% SDS-PAGE purification steps of the PH^{Kin3} domain tagged N-terminally to 6xHis. Abbreviations for the purification fractions: S, soluble fraction after ultracentrifugation; F, flow through the Ni-NTA column; W, wash fraction; E, eluted fraction. Purified protein band corresponds to 15.8 kDa. (**B**) Diagram of the phospholipids spotted on a cellulose MicroStrip membrane. The amount of lipid per spot was 100 pmol. Abbreviations for the lipids: LPA, lysophosphatidic acid; LPC, lysophosphocholine; PI, phosphatidylinositol; PE, phosphatidylethanolamine; PC, phosphatidylcholine; SIP, sphingosine-1-phosphate; PA, phosphatidic acid; PS, phosphatidylserine; PI(3)P, phosphatidylinositol 3-phosphate; PI(4)P, phosphatidylinositol 4-phosphate; PI(5)P, phosphatidylinositol 5-phosphate; PI(3,4)P2, phosphatidylinositol 3,4-bisphosphate; PI(3,5)P2, phosphatidylinositol 3,5-bisphosphate; PI(4,5)P2, phosphatidylinositol 4,5-bisphosphate; PI(3,4,5)P3, phosphatidylinositol (3,4,5) trisphosphate. (**C**) Lipid overlay assay results. The positive control, the PH domain of phospholipase C-δ1 (PLC-δ1-PH) fused N-terminally to GST specifically binds to PI(4,5)P2. Purified 6xHis-PH^{Kin3} domain does not bind to any lipids spotted on the MicroStrip membrane. (**D**) No specific localization of the PH domain was detected after expression of the PH^{Kin3}-GFP domain in living cells of *U. maydis*. Bar is given in micrometers. (**E**) The PH^{Kin3}-GFP protein (PH) did not colocalize with motile EEs labelled with mCherry-Rab5a which is shown by kymographs. Time is given in seconds, distance is given in micrometers. The images were contrast inverted.

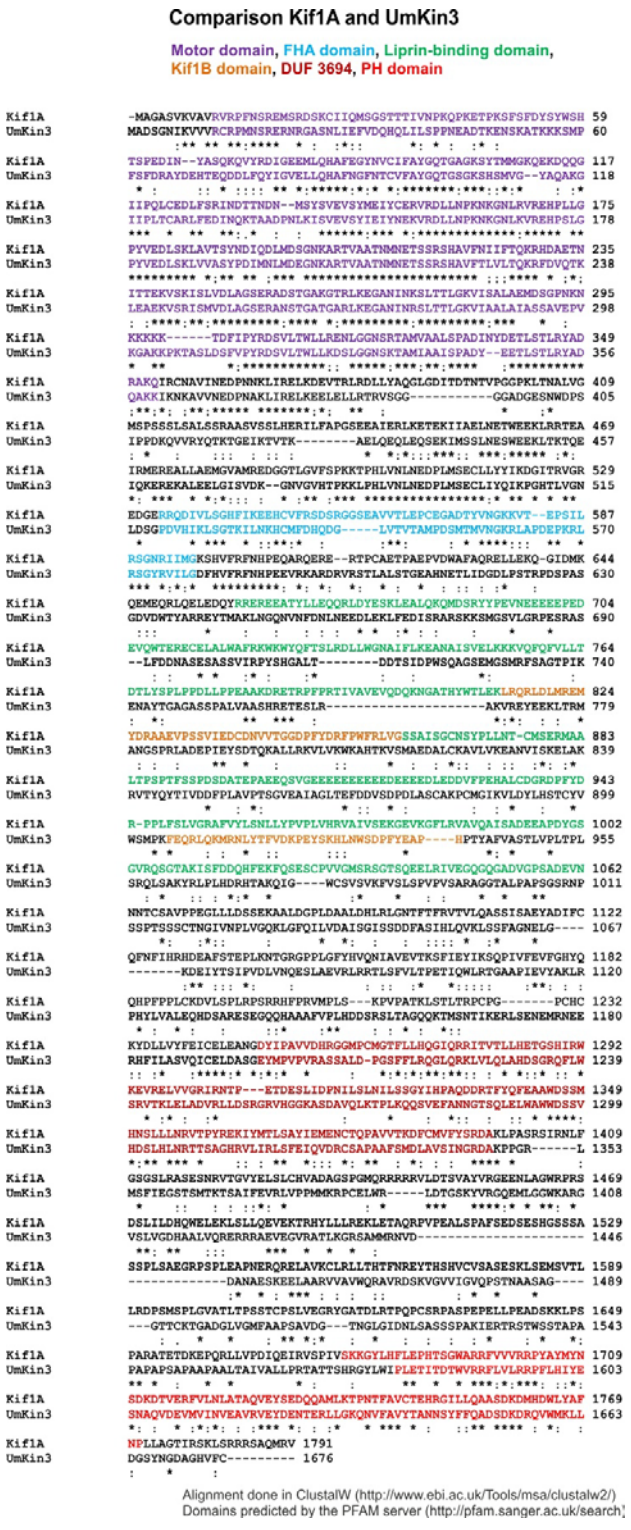

Figure S2. Primary sequence comparison of *U. maydis* Kin3 (accession number: XP_762398) **and KIF1A from human** (accession number: NP_001230)**.**
Predicted protein domains are given in colours (see figure for legend); identical amino acids are indicated by asterisks, similar amino acids are indicated by double points.

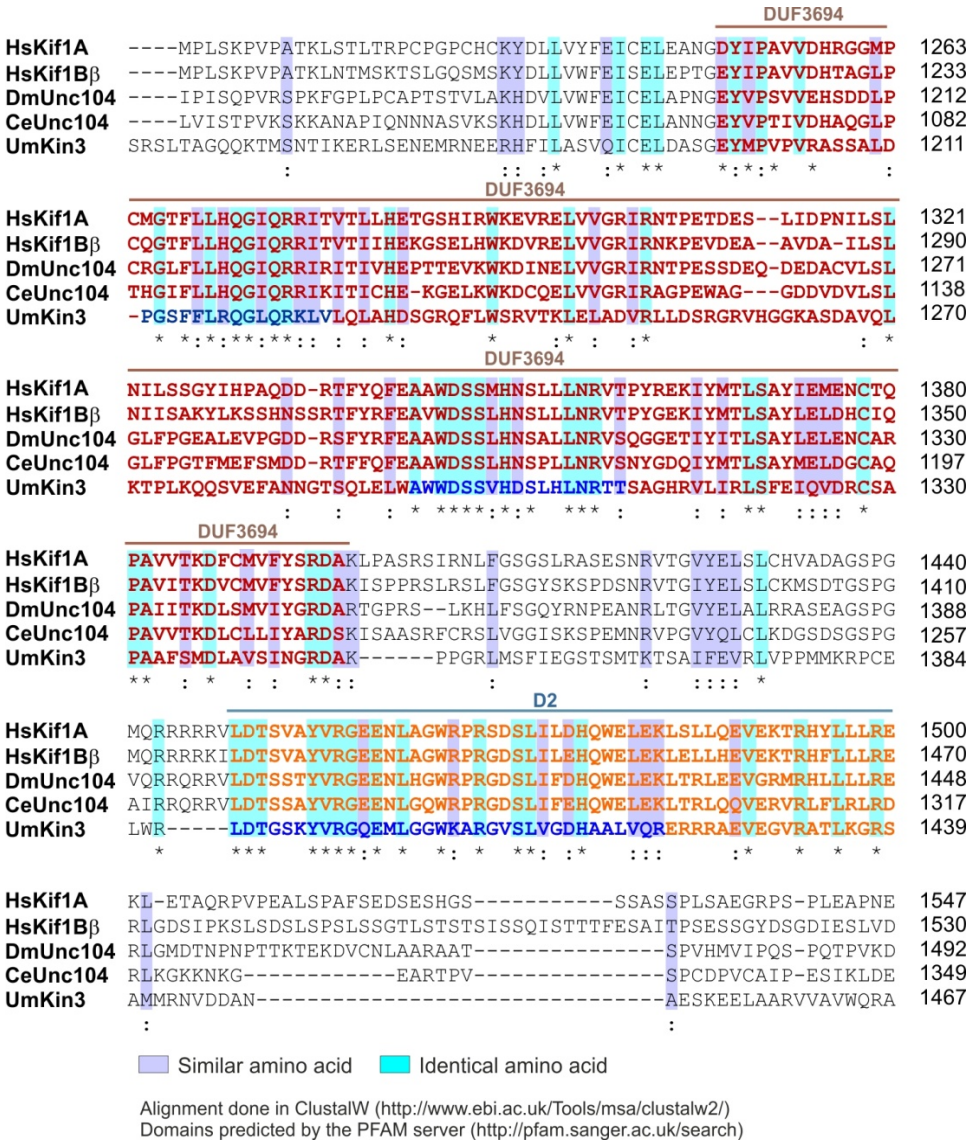

Figure S3. Primary sequence comparison of the conserved tail (excluding the PH domain) of Kin3 from *U. maydis* (UmKin3; accession number: XP_762398), KIF1A from human (HsKIF1A; accession number: NP_001230), KIF1Bβ from human (HsKIF1Bβ; accession number: NP_055889), Unc104 from fruit flies (DmUnc104; accession number: NP_725610) and Unc104 from the worm *Caenorhabditis elegans* (CeUnc104; accession number: NP_741019). Highly conserved amino acid stretches within DUF3694 (red) and the region D2 (orange) are indicated in blue.

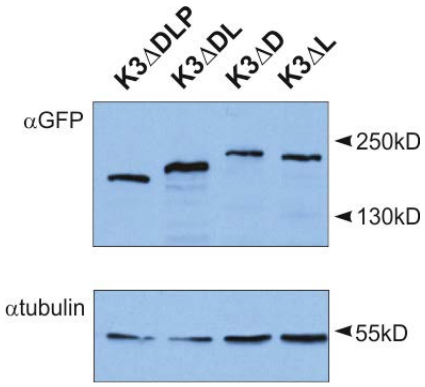

Figure S4. Immunoblot showing the expression of truncated Kin3-GFP proteins.
K3ΔDLP: Kin3-GFP lacking the DUF3694 domain, the conserved "linker" region and the PH domain; K3ΔDL: Kin3-GFP lacking the DUF3694 domain and the conserved "linker" region; K3ΔD: Kin3-GFP lacking the DUF3694 domain; K3ΔL: Kin3-GFP lacking the conserved "linker" region.

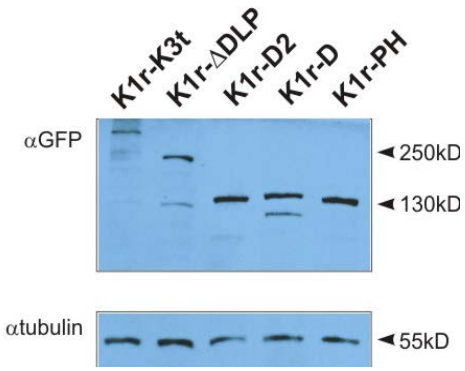

Figure S5. Immunoblot showing the expression of chimerical synthetic motor proteins.
K1r-K3t: the Kin1^{rigor} head-neck region fused to the entire Kin3 tail; K1r-ΔDLP: the Kin1^{rigor} head-neck region fused to the N-terminal half of the Kin3 tail; K1r-D2: the Kin1^{rigor} head-neck region fused to the highly conserved amino acids stretch within the "linker" region; K1r-D: the Kin1^{rigor} head-neck region fused to the DUF3694 domain; K1r-PH: The Kin1^{rigor} head-neck region fused to the PH domain.

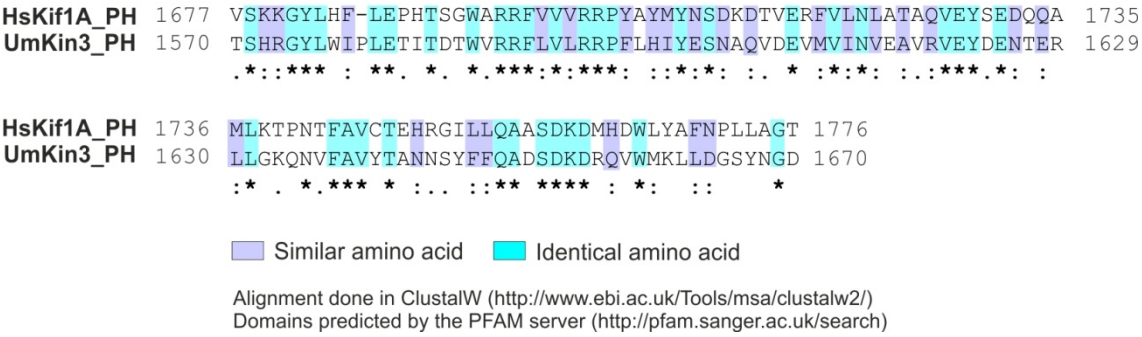

Figure S6. Primary sequence comparison of the PH domain of Kin3 from *U. maydis* (UmKin3_PH) and KIF1A from human (HsKIF1A_PH).
The alignment was done in ClustalW. Note that both domains share 38.1% identity and 53.3% similarity in their amino acid sequences (Emboss pairwise alignment http://www.ebi.ac.uk/Tools/psa/emboss_needle/).

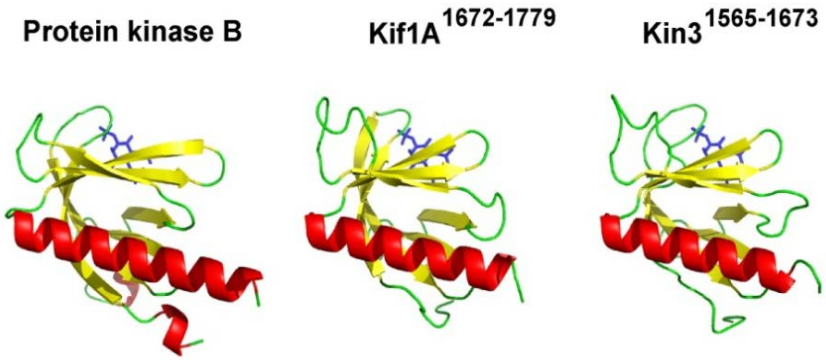

Figure S7. Structural models of the PH domains from protein kinase B (PDB accession number: 1H10), KIF1A from human and Kin3 from *U. maydis*.
The interacting lipid is shown in blue. The modelling was done using MODELLER version 9.10.

Supplementary Methods

Strains

To test the role of domains in the tail of Kin3, various *kin3* constructs were expressed in a *kin3* null mutant (AB33ΔKin3) that was generated by homologous integration of the linearized with *PvuI* plasmid pΔKin3 (Schuster *et al.*, 2011b) into *kin3* locus of the *U. maydis* AB33 (Brachmann *et al.*, 2001). Subsequently, the plasmids po^{C}GRab5a and po$^{H}{}_{m}$ChRab5a (Schuster *et al.*, 2011d) were linearized and integrated ectopically into the AB33ΔKin3 strain resulting in the AB33ΔKin3_GRab5a and AB33ΔKin3_mChRab5a strains, respectively. To obtain control strain AB33_mChRab5a, plasmid po$_{m}$ChRab5a (Schuster *et al.*, 2011b) was linearized and integrated ectopically into the AB33 strain.

To test for a role of the PH domain, plasmid pcrgPHG was linearized by *AgeI* and integrated into the *succinate dehydrogenase* locus of the AB33_mChRab5a strain, resulting in the AB33_mChRab5a_rPHG strain.

To test for a role of the Kin3 tail in EE binding, plasmids pcrgKin3$^{tail}{}_{m}$Ch and pcrgKin3$^{tail\Delta PH}{}_{m}$Ch were linearized by *SspI* and ectopically integrated into AB33ΔKin3_GRab5a, resulting in the AB33ΔKin3_GRab5a_rK3t$_{m}$Ch and AB33ΔKin3_GRab5a_rK3t$^{\Delta PH}{}_{m}$Ch strains, respectively.

In order to analyse protein expression level and Kin3 behaviour, Kin3 protein was fused to eGFP at its C-terminus resulting in the plasmid pKin3G (Wedlich-Söldner *et al.*, 2002), which was linearized within the carboxin resistance cassette, using the enzyme *SspI,* and integrated into the *succinate dehydrogenase* locus of the AB33ΔKin3_mChRab5a strain, resulting in the AB33ΔKin3_mChRab5a_Kin3G strain.

To obtain truncated versions of Kinesin-3-eGFP under control of *kin3* promoter, plasmids pKin3$^{\Delta DLP}$G, pKin3$^{\Delta L}$G, pKin3$^{\Delta DL}$G, pKin3$^{\Delta D}$G and pKin3$^{\Delta PH}$G were linearized by *SspI* within the carboxin resistance cassette and integrated into the *succinate dehydrogenase* locus of the AB33ΔKin3_mChRab5a, resulting in the AB33ΔKin3_mChRab5a_Kin3$^{\Delta DLP}$G, AB33ΔKin3_mChRab5a_Kin3$^{\Delta L}$G, AB33ΔKin3_mChRab5a_Kin3$^{\Delta DL}$G and AB33ΔKin3_mChRab5a_Kin3$^{\Delta D}$G and AB33ΔKin3_mChRab5a_Kin3$^{\Delta PH}$G strains, respectively.

To analyse EEs motility behaviour in the presence of the synthetic anchors, plasmids pcrgK1rG-K3t, pcrgK1rG-ΔDLP, pcrgK1rG-D, pcrgK1rG-D2 and pcrgK1rG-PH were linearized by *ScaI* and ectopically integrated into the AB33_mChRab5a strain resulting in the AB33_mChRab5a_rK1rG-K3t, AB33_mChRab5a_rK1rG-ΔDLP, AB33_mChRab5a_rK1rG-D, AB33_mChRab5a_rK1rG-D2 and AB33_mChRab5a_rK1rG-PH strains, respectively.

To increase the motor number bound to EEs, plasmid pcrgKin3$^{\Delta PH}$G was linearized by *ScaI* and ectopically integrated into the AB33ΔKin3_mChRab5a strain resulting in the AB33ΔKin3_mChRab5a_rKin3$^{\Delta PH}$G strain.

In order to express Kin3 motor domain for the pull down experiment, plasmid pcrgMotorG was linearized by digestion with *ScaI* and ectopically integrated into the AB33_mChRab5a strain, resulting in AB33_mChRab5a_rMotorG.

To observe the interaction between the motor and the PH domains *in vivo*, bimolecular fluorescence complementation (BIFC) technique was used. C-terminal half of yellow fluorescent protein (YFP^{C}) was fused in front of the motor domain and N-terminal half of YFP (YFP^{N}) was added behind the PH domain. Plasmid YFP^{C}-Kin3-YFP^{N} was linearized by *SspI* within the carboxin resistance cassette and integrated into the *succinate dehydrogenase* locus of the AB33ΔKin3 strain, resulting in the AB33ΔKin3_YFP^{C}-Kin3-YFP^{N} strain.

Plasmids

pcrgPHG: This plasmid contains the Kin3 PH domain (aa 1566-1676) which is fused C-terminally to GFP. The construct is fused behind the *crg* promoter and contains the carboxin resistance cassette. The plasmid was generated through *in vivo* recombination in the yeast *S. cerevisiae.* A fragment encoding the PH domain and eGFP was amplified from the plasmid pKin3G (Wedlich-Söldner *et al.*, 2002) using sets of primers $_{f}$EB46-$_{r}$TU180 (primers sequences are summarized in Supplementary Table 3). The fragment, purified from an agarose gel, was cloned into a linearized (by *EcoNI*) yeast vector pcrgPeb1$^{211–268}$ (Schuster *et al.*, 2011a) using *in vivo* recombination in the yeast *S. cerevisiae*.

pcrgKin3$^{tail}{}_{m}$Ch: This plasmid contains a Kin3 tail encoding region (aa 423-1676), truncated in the motor domain, and fused C-terminally to mCherry. The construct is fused behind the *crg* promoter and contains hygromycin resistance cassette. The plasmid was generated through *in vivo* recombination in the yeast *S. cerevisiae* in two steps. First, fragments encoding Kin3 tail (aa 423-1676), eGFP, short Tnos terminator and 30-bp overhangs were amplified from the plasmid pKin3G (Wedlich-Söldner *et al.*, 2002) using sets of primers $_{f}$EB91-$_{r}$EB12 and $_{f}$EB13-$_{r}$SK120 (primers sequences are summarized in Supplementary Table 3). Fragments were purified from the agarose gel and cloned into the vector pcrgPeb1$^{211–268}$ (Schuster *et al.*, 2011a) resulting in the plasmid pcrgKin3^{tail}G. Next, a 6144-bp fragment encoding part of *crg* promoter (- 2731-bp) and part of Kin3 tail (3413-bp encoding Met and 1136 amino acids of Kin3 tail$^{423\text{-}1558}$) was cut out from the plasmid pcrgKin3^{tail}G using restriction enzymes *HpaI* and *MunI*. Fragments encoding remaining 777-bp of *crg* promoter and 352-bp of Kin3 tail were amplified from the plasmid pcrgKin3^{tail}G with 30-bp overhangs (using primers $_{f}$EB352-$_{r}$EB351 and $_{f}$SK213-$_{r}$EB353, respectively) and were cloned into the yeast vector containing flanks composed of mCherry (downstream flank) and hygromycin resistance cassette (upstream flank) resulting in the plasmid pcrgKin3$^{tail}{}_{m}$Ch.

pcrgKin3$^{tail\Delta PH}{}_{m}$Ch: This plasmid contains a Kin3 tail depleted of the motor and PH domains encoding regions (aa 423-1676$^{\Delta 1566\text{-}1666}$) and fused C-terminally to mCherry. The construct is fused behind the *crg* promoter and contains hygromycin resistance cassette. To generate the plasmid, a 6144-bp fragment encoding part of *crg* promoter and part of Kin3 tail was cut out from the plasmid pcrgKin3^{tail}G using restriction enzymes *HpaI* and *MunI*, Fragment encoding remaining 777-bp of *crg* promoter (plus 30-bp overhangs) was amplified from the plasmid pcrgKin3^{tail}G using primers $_{f}$EB352 and $_{r}$EB351. Fragment encoding remaining Kin3 tail depleted of PH domain (Δ1566-1666) was amplified with 30-bp overhangs from the plasmid pKin3$^{\Delta PH}$G using $_{f}$EB356 and $_{r}$EB353 primers (Supplementary Table 3). All three fragments were cloned into the yeast vector containing flanks composed of mCherry (downstream flank) and hygromycin cassette (upstream flank) resulting in the plasmid pcrgKin3$^{tail\Delta PH}{}_{m}$Ch.

pKin3$^{\Delta PH}$G: This plasmid contains a *kin3* gene, truncated in the PH domain, and fused C-terminally to eGFP. The construct is fused behind the *kin3* promoter

and the plasmid is designed for integration into the succinate-dehydrogenase locus. The plasmid was generated through *in vivo* recombination in the yeast *S. cerevisiae.* Fragments encoding *kin3* promoter (1790-bp, primers $_f$EB9-$_r$EB15), *kin3* gene depleted of the sequence encoding PH domain (Δ1566-1666) and eGFP were amplified from the plasmid pKin3G (Wedlich-Söldner *et al.*, 2002) using sets of primers $_f$EB16-$_r$EB23, $_f$EB24-$_r$EB25 and $_f$EB26-$_r$EB14 (Supplementary Table 3). Fragments purified from agarose gels were cloned into the yeast vector pNEBcbx-yeast resulting in the plasmid pKin3$^{\Delta PH}$G-3xSspI. To remove two *SspI* sites, plasmid pKin3$^{\Delta PH}$G-3xSspI was digested by *AscI* and *HpaI* and ligated with a 2111-bp region encoding oriC and AmpR cut (by *AscI* and *SspI*) from the plasmid pNEB-Hyg(-) (Brachmann *et al.*, 2001).

pKin3$^{\Delta DLP}$G: This plasmid contains a *kin3* gene truncated in the DUF3694-"linker"-PH domain, and fused C-terminally to eGFP. The construct is fused behind the *kin3* promoter and the plasmid is designed for integration into the succinate-dehydrogenase locus. The plasmid was generated by amplification of three fragments from the plasmid pKin3G (Wedlich-Söldner *et al.*, 2002) encoding *kin3* promoter, *kin3* gene depleted of the sequence encoding DUF3694-PH domain region (aa 1198-1666) and eGFP sequence using sets of primers $_f$EB9-$_r$EB27, $_f$EB24-$_r$EB54, $_f$EB85-$_r$EB14 (Supplementary Table 3). The fragments were purified from agarose gel and cloned into the yeast vector pNEBcbx-yeast-1xSspI (Chapter 3) digested by *EcoRI* and *SacI*.

pKin3$^{\Delta L}$G: This plasmid contains a kin3 gene truncated in the "linker" region and fused C-terminally to eGFP. The construct is fused behind the *kin3* promoter and the plasmid is designed for integration into the succinate-dehydrogenase locus. The plasmid was derived by amplification of three fragments from the plasmid pKin3G (Wedlich-Söldner *et al.*, 2002) encoding *kin3* promoter, *kin3* gene depleted of the sequence encoding region between DUF3694 and PH domain (aa 1349-1565) and eGFP sequence using sets of primers $_f$EB9-$_r$EB27, $_f$EB24-$_r$EB62 and $_f$EB63-$_r$EB14 (Supplementary Table 3). The fragments were purified from agarose gel and cloned into the yeast vector pNEBcbx-yeast-1xSspI (Chapter 3) digested by *EcoRI* and *SacI*.

pKin3$^{\Delta DL}$G: This plasmid contains a kin3 gene truncated in the DUF3694-"linker" region and fused C-terminally to eGFP. The construct is fused behind

the *kin3* promoter and the plasmid is designed for integration into the succinate-dehydrogenase locus. The plasmid was obtained by amplification of a 537-bp fragment upstream of the region encoding DUF3694 (using primers $_{f}$EB276-$_{r}$EB371; Supplementary Table 3) and 1063-bp fragment encoding PH domain fused to eGFP (using primers $_{f}$EB206-$_{r}$SK238; Supplementary Table 3) from the plasmid pKin3G (Wedlich-Söldner *et al.*, 2002) using and cloning them into the plasmid pKin3$^{\Delta L}$G digested by *PflMI* and *PmlI*.

pKin3$^{\Delta D}$G: This plasmid contains a kin3 gene truncated in the DUF3694 domain and fused C-terminally to eGFP. The construct is fused behind the *kin3* promoter and the plasmid is designed for integration into the succinate-dehydrogenase locus. The plasmid was derived by amplification of four fragments from the plasmid pKin3G (Wedlich-Söldner *et al.*, 2002), encoding *kin3* promoter (using primers $_{f}$EB9-$_{r}$EB15; Supplementary Table 3), *kin3* gene upstream of DUF3694 region (using primers $_{f}$EB16-$_{r}$EB27; Supplementary Table 3), *kin3* gene downstream of DUF3694 region (using primers $_{f}$EB24-$_{r}$EB54; Supplementary Table 3) and eGFP sequence (using primers $_{f}$EB53-$_{r}$EB14; Supplementary Table 3). The fragments were purified from agarose gel and cloned into the yeast vector pNEBcbx-yeast-1xSspI (Chapter 3) digested by *EcoRI* and *SacI*.

In order to obtain chimera constructs composed of Kin1^{G96E} (aa 1-739) and Kin3 tail or truncated versions of Kin3 tail, the plasmid pcrg^{C}K1rG-PX (presented in Chapter 3) was used to allow further cloning:

pcrgK1rG-K3t: This plasmid contains a kin1 rigor (G96E) gene truncated in the third coiled-coil and the globular tail domain (Straube *et al.*, 2006), internal eGFP and is C-terminally fused to the Kin3 truncated in the motor domain (aa 370-1676). The construct is fused behind the *crg* promoter and the plasmid contains the carboxin resistance cassette. The plasmid was derived from the plasmid pcrg^{C}K1rG-PX (Chapter 3; linearized by *BamHI and AflII*) into which were cloned three fragments encoding following regions of kinesin-3 tail (aa 370-1676): a 1288-bp (primers $_{f}$EB231-$_{r}$EB23; Supplementary Table 3), a 1555-bp (primers $_{f}$EB24-$_{r}$EB12; Supplementary Table 3) and a 1691-bp (primers $_{f}$EB13-$_{r}$SK120; Supplementary Table 3) fragments amplified from the plasmid pKin3G (Wedlich-Söldner *et al.*, 2002).

pcrgK1rG-ΔDLP: This plasmid contains a kin1 rigor (G96E) gene truncated in the third coiled-coil and the globular tail domain (Straube *et al.*, 2006), internal eGFP and is C-terminally fused to the Kin3 truncated in the motor domain and the second half of the Kin3 tail (aa 370-1022). The construct is fused behind the *crg* promoter and the plasmid contains the carboxin resistance cassette. The plasmid was derived from the plasmid pcrg^{C}K1rG-PX (Chapter 3; linearized by *BamHI*) into which was cloned a 2032-bp fragments encoding N'-terminal part of *kin3* tail (aa 370-1022) amplified from the plasmid pKin3G (Wedlich-Söldner *et al.*, 2002) using primers $_{f}$EB231-$_{r}$EB241 (Supplementary Table 3).

pcrgK1rG-D: This plasmid contains a kin1 rigor (G96E) gene truncated in the third coiled-coil and the globular tail domain (Straube *et al.*, 2006), internal eGFP and is C-terminally fused to the DUF3694 domain from Kin3 (aa 1198-1348). The construct is fused behind the *crg* promoter and the plasmid contains carboxin resistance cassette. The plasmid was obtained by amplifying of a 526-bp fragment encoding DUF3694 region (aa 1198-1348) and 30-bp overhangs (using primers $_{f}$EB233-$_{r}$EB137; Supplementary Table 3) from the plasmid pKin3G (Wedlich-Söldner *et al.*, 2002) and by cloning it into linearized (by *BamHI*) plasmid pcrg^{C}K1rG-PX (Chapter 3).

pcrgK1rG-D2: This plasmid contains a kin1 rigor (G96E) gene truncated in the third coiled-coil and the globular tail domain (Straube *et al.*, 2006), internal eGFP and is C-terminally fused to the D2 region (aa 1345-1468) localized in the "linker" region from Kin3. The construct is fused behind the *crg* promoter and the plasmid contains carboxin resistance cassette. The plasmid was obtained by amplifying of a 445-bp fragment encoding overhangs and highly conserved region localized within the "linker" region (aa 1345-1468) from the plasmid pKin3G (Wedlich-Söldner *et al.*, 2002) using primers $_{f}$EB265-$_{r}$EB266 (Supplementary Table 3) and by cloning it into linearized (by *BamHI*) plasmid pcrg^{C}K1rG-PX (Chapter 3).

pcrgK1rG-PH: This plasmid contains a kin1 rigor (G96E) gene truncated in the third coiled-coil and the globular tail domain (Straube *et al.*, 2006), internal eGFP and is C-terminally fused to the PH domain (aa 1566-1676) from Kin3. The construct is fused behind the *crg* promoter and the plasmid contains carboxin resistance cassette. The plasmid was obtained by amplification of a 406-bp fragment encoding overhangs and PH domain region (aa 1566-1676)

from the plasmid pKin3G (Wedlich-Söldner *et al.*, 2002) using primers $_{f}$EB336-$_{r}$EB67 (Supplementary Table 3) and by cloning it into linearized (by *BamHI*) plasmid pcrg^{C}K1rG-PX (Chapter 3).

pcrgKin3$^{\Delta PH}$G: This plasmid contains a *kin3* gene, truncated in the PH domain, and fused C-terminally to eGFP. The construct is fused behind the *crg* promoter and the plasmid contains carboxin resistance cassette. The plasmid was generated through *in vivo* recombination in the yeast *S. cerevisiae* in two steps. First, plasmid pcrgKin3$^{tail\Delta PH}$G was derived by amplification of a 1776-bp region of Kin3 tail depleted of PH domain (Δ1566-1666) from the plasmid pKin3$^{\Delta PH}$G using primers $_{f}$CC54 and $_{r}$EB277 and cloning into digested by *HindIII* and *AflII* plasmid pcrgKin3^{tail}G. Second, the plasmid pcrgKin3$^{tail\Delta PH}$G was linearized by *BamHI* and ligated with a region encoding a 333-bp fragment of *crg* promoter followed by a 1806-bp N-terminal fragment of *kin3* gene from the plasmid pcrgKin3 (Wedlich-Söldner *et al.*, 2002) using primers $_{f}$EB175 and $_{r}$CC52 (Supplementary Table 3).

pcrgMotorG: This plasmid contains the Kin3 motor domain (aa 1-367) fused C-terminally to the eGFP. The construct is fused behind the *crg* promoter and the plasmid contains carboxin resistance cassette. The plasmid was generated by amplification of a 1248-bp fragment encoding motor domain (aa 1-367) from the plasmid pcrgKin3 (Wedlich-Söldner *et al.*, 2002) using primers $_{f}$SM59 and $_{r}$EB131 (Supplementary Table 3) into the plasmid pcrgPeb1$^{211–268}$ (Schuster *et al.*, 2011a) digested by *BamHI*.

pNic28-His$_{6x}$-PH: This plasmid contains the Kin3 PH domain (aa 1566-1676) which is fused behind the sequence encoding His$_{x6}$ tag followed by sequence recognized by TEV-protease. The plasmid contains kanamycin resistance cassette. The plasmid was obtained using LIC cloning strategy (Ligation Independent Cloning, Haun *et al.*, 1992). A 369-bp PCR product encoding Kin3 PH domain (aa 1566-1676) and 15-bp overhangs was amplified from the plasmid pKin3G (Wedlich-Söldner *et al.*, 2002) using primers $_{f}$EB70 and $_{r}$EB71 (Supplementary Table 3). pNic28-Bsa4 vector (gift of Opher Gileadi, SGC Oxford; Savitsky *et al.*, 2010) was digested by *BsaI*. Both, a PCR product and digested plasmid were treated with T4 DNA polymerase and were annealed

resulting in $_{UmKin3}$PH domain fused N-terminally to His_{x6} tag followed by sequence recognized by TEV-protease.

pGBKT7-PH: This bait plasmid contains the Kin3 PH domain (aa 1566-1666) fused behind the *GAL4* DNA binding domain of the bait plasmid pGBKT7 (Clontech, United States) and contains *TRP1* nutritional marker and kanamycin resistance cassette. The plasmid was obtained by In-Fusion ligation (Clontech; protocol In-Fusion® Advantage PCR Cloning Kit User Manual; PT4065-2) of a 365-bp PCR product encoding Kin3 PH domain (aa 1566-1666; using primers $_f$EB160-$_r$EB161; Supplementary Table 3) with vector encoding the Gal4 DNA-binding domain (pGBKT7 DNA-BD, Matchmaker™ Gold Yeast Two-Hybrid System, Clontech; United States) digested by *BamHI* and *EcoRI*. The PCR product was derived from the plasmid pKin3G (Wedlich-Söldner *et al.*, 2002).

pGADT7-motor: This prey plasmid contains the Kin3 motor domain (aa 1-367) fused behind the *GAL4* DNA activation domain of the bait plasmid pGADT7 (Clontech, United States) and contains *LEU2* nutritional marker and kanamycin resistance cassette. The plasmid was delivered by cloning of a 1161-bp region encoding Kin3 motor domain (aa 1-367) and 15-bp overhangs (using primers $_f$EB158-$_r$EB159; Supplementary Table 3) into the digested plasmid pGADT7-Rec (by *SmaI*) in In-Fusion ligation (Clontech; protocol In-Fusion® Advantage PCR Cloning Kit User Manual; PT4065-2).

pYFP^C-Kin3-YFP^N: This plasmid contains the *kin3* gene which is fused N-terminally to split YFP^C and C-terminally to split YFP^N. The construct is fused behind the *kin3* promoter and the plasmid is designed for integration into the succinate-dehydrogenase locus. The construct was obtained by *in vivo* recombination in the yeast *S. cerevisiae* by cloning of seven fragments into the plasmid pKin3$^{\Delta DLP}$G linearized by *RsIII* and *AflII*. Five fragments were derived from the plasmid pKin3G (Wedlich-Söldner *et al.*, 2002): a 469-bp region of *kin3* promoter (amplified by primers $_f$EB363-$_r$EB119; Supplementary Table 3) upstream of *kin3* gene, a 560-bp fragment encoding part of a motor domain (amplified by primers $_f$EB366-$_r$CC43; Supplementary Table 3), a 554-bp C-terminal fragment of *kin3* gene (amplified by primers $_f$EB3-$_r$EB367; Supplementary Table 3), a 295-bp region encoding Tnos terminator region (amplified by primers $_f$EB370-$_r$EB60; Supplementary Table 3) and a 3998-bp region encoding Kin3$^{177\text{-}1508}$ [obtained by digestion of pKin3G (Wedlich-Söldner

et al., 2002) with *AvrII* and *SacII*]. Plasmids pDV8 and pDV7 (kindly provided by Prof. R. Fisher, Takeshita *et al.*, 2008) served as templates for an amplification of a 309-bp region of split YFP^C with additional 30-bp overhangs for *kin3* promoter and *kin3* gene (using primers $_f$EB364-$_r$EB365; Supplementary Table 3) and a 541-bp region of split YFP^N with additional 30-bp overhangs for *kin3* gene and Tnos terminator (using primers $_f$EB368-$_r$EB369; Supplementary Table 3), respectively.

Light microscopy and quantitative analysis

To analyse the degree of colocalization between K3T$_m$Ch or K3t$^{\Delta PH}{}_m$Ch and GRab5a in the AB33ΔKin3_GRab5a_rK3t$_m$Ch and AB33ΔKin3_GRab5a_rK3t$^{\Delta PH}{}_m$Ch strains the entire yeast-like cells were observed using the Dual-View Microimager (Photometrics) and the 488 nm observation laser at 10% output power and the 561 nm observation laser at 100% output power at an exposure time of 150 ms and image binning 1. To analyse the degree of colocalization between K3G, truncated kinesin-3 protein tagged with GFP and mChRab5a in the AB33ΔKin3_mChRab5a_Kin3G, AB33ΔKin3_mChRab5a_Kin3$^{\Delta PH}$G, AB33ΔKin3_mChRab5a_Kin3$^{\Delta DLP}$G, AB33ΔKin3_mChRab5a_Kin3$^{\Delta DL}$G, AB33ΔKin3_mChRab5a_Kin3$^{\Delta D}$G, AB33ΔKin3_mChRab5a_Kin3$^{\Delta L}$G strains the entire yeast-like cells were observed using the Dual-View Microimager (Photometrics) and the 488 nm observation laser at 100% output power and the 561 nm observation laser at 100% output power at an exposure time of 150 ms and image binning 1.

EEs pausing was analysed within the region of the highest expression of the chimera proteins (daughter cell, neck region and half of mother cell) in middle sized budded yeast-like cells. After acquiring movies composed of 100 frames at 150 ms exposure time and binning 2 using 100% 561 nm laser, kymographs were generated using MetaMorph (Molecular Devices). 100 um^2 region within obtained kymographs served for measuring of the pausing of stationery EE signals.

Measurements of anterograde run length of EEs were performed in the first 15 µm of the hyphal tips of shifted overnight strains AB33ΔKin3_mChRab5a_Kin3G, AB33ΔKin3_mChRab5a_Kin3$^{\Delta PH}$G,

AB33ΔKin3_mChRab5a_rKin3$^{\Delta PH}$G. The first 15 µm of the hyphae were photobleached using a 2D-VisiFRAP system (Visitron Systems) consisting of a 405 nm/60 mW diode laser, which was dimmed by a neutral density 0.6 filter, resulting in 15 mW output power. Followed by immediate observation with the 561 nm observation laser at 50% output power, an exposure time of 150 ms an image series of 100 frames were taken. The run length was analysed in kymographs that were generated from these image series using MetaMorph.

Analysis of the Kin3 motor numbers colocalized with EEs in the AB33ΔKin3_mChRab5a_Kin3G, AB33ΔKin3_mChRab5a_Kin3$^{\Delta PH}$G and AB33ΔKin3_mChRab5a_rKin3$^{\Delta PH}$G strains was based on quantitative analysis of fluorescent intensities as described previously (Schuster *et al.*, 2011a). In brief, strains expressing mCherry labelled Rab5a and Kin3-GFP or truncated versions of Kin3-GFP were imaged using a Dual-View Microimager (Photometrics) and appropriate filters with an exposure time of 150 ms and the 75 mW, 488 nm laser at 100% output power and the 75 mW, 561 nm laser at 25% output power. Only those Kin3-GFP signals were considered which were colocalized with EEs and were moving in an anterograde direction. Only from those signals the integrated signal intensities were measured in the first plain and corrected for the adjacent cellular background by copying the region of interest next to the signal that was not influenced by other fluorescent signals. The intensity of this region was subtracted from the measured signal intensity. Obtained fluorescent intensities were compared with the internal calibration standard, nucleoporin Nup107-GFP. A strain that expresses a fusion protein of the endogenous nucleoporin Nup107 and GFP was imaged using the same settings and the integrated intensity of single pores was measured and background corrected as described above. Nup107-GFP is found in a single pore 16 times, which allowed estimating of the intensity of a single GFP in the living cell. This value was used to calculate the number of Kinesin-3 motors, given that each Kinesin-3 dimer contains two GFPs.

Supplementary Tables

Supplementary Table 1. Strains and plasmids used in this study.

Strain name	Genotype	Source
AB33ΔKin3	*a2 Pnar-bW2 Pnar-bE1, ble^R Δkin3::nat^R*	Chapter 3
AB33ΔKin3_GRab5a	*a2 Pnar-bW2 Pnar-bE1, ble^R Δkin3:: nat^R/ Potef-egfp-rab5a, cbx^R*	Chapter 3
AB33ΔKin3_mChRab5a	*a2 Pnar-bW2 Pnar-bE1, ble^R Δkin3::nat^R/ Potef-mcherry-rab5a, hyg^R*	Chapter 3
AB33_mChRab5a	*a2 Pnar-bW2 Pnar-bE1, ble^R/ Potef-mcherry-rab5a, nat^R*	Chapter 3
AB33ΔKin3_mChRab5a_Kin3G	*a2 Pnar-bW2 Pnar-bE1, ble^R Δkin3::nat^R/ Potef-mcherry-rab5a, hyg^R/ Pkin3-kin3-egfp, cbx^R*	Chapter 3
AB33_mChRab5a_rPHG	*a2 Pnar-bW2 Pnar-bE1, ble^R / Potef-mcherry-Rab5a, nat^R/ Pcrg-ph-egfp, cbx^R*	This study
AB33ΔKin3_mChRab5a_Kin3^{ΔPH}G	*a2 Pnar-bW2 Pnar-bE1, ble^R Δkin3::nat^R/ Potef-mcherry-rab5a, hyg^R/ Pkin3-kin3$^{Δ1566-1666}$-egfp, cbx^R*	This study
AB33ΔKin3_GRab5a_rK3t$_m$Ch	*a2 Pnar-bW2 Pnar-bE1, ble^R Δkin3::nat^R/ Potef-gfp-rab5a, cbx^R/ Pcrg-kin3$^{423-1676}$-mcherry, hyg^R*	This study
AB33ΔKin3_GRab5a_rK3t$^{ΔPH}{}_m$Ch	*a2 Pnar-bW2 Pnar-bE1, ble^R Δkin3::nat^R/ Potef-gfp-rab5a, cbx^R/ Pcrg-kin3$^{tail(Δ1566-1666)}$-mcherry, hyg^R*	This study
AB33ΔKin3_mChRab5a_Kin3^{ΔDLP}G	*a2 Pnar-bW2 Pnar-bE1, ble^R Δkin3::nat^R/ Potef-mcherry-rab5a, hyg^R/ Pkin3-kin3$^{Δ1198-1666}$-egfp, cbx^R*	This study
AB33ΔKin3_mChRab5a_Kin3^{ΔDL}G	*a2 Pnar-bW2 Pnar-bE1, ble^R Δkin3::nat^R/ Potef-mcherry-rab5a, hyg^R/ Pkin3-kin3$^{Δ1198-1565}$-egfp, cbx^R*	This study
AB33ΔKin3_mChRab5a_Kin3^{ΔD}G	*a2 Pnar-bW2 Pnar-bE1, ble^R Δkin3::nat^R/ Potef-mcherry-rab5a, hyg^R/ Pkin3-kin3$^{Δ1198-1348}$-egfp, cbx^R*	This study
AB33ΔKin3_mChRab5a_Kin3^{ΔL}G	*a2 Pnar-bW2 Pnar-bE1, ble^R Δkin3::nat^R/ Potef-mcherry-rab5a, hyg^R/ Pkin3-kin3$^{Δ1349-1565}$-egfp, cbx^R*	This study
AB33_mChRab5a_rK1rG-K3t	*a2 Pnar-bW2 Pnar-bE1, ble^R/ Potef-mcherry-rab5a, nat^R/ Pcrg-kin1$^{G96E,(1-739)}$-egfp-kin3$^{370-1676}$-egfp, cbx^R*	This study
AB33_mChRab5a_rK1rG-ΔDLP	*a2 Pnar-bW2 Pnar-bE1, ble^R/ Potef-mcherry-rab5a, nat^R/ Pcrg-kin1$^{G96E,(1-739)}$-egfp- kin3$^{370-1022}$, cbx^R*	This study
AB33_mChRab5a_rK1rG-D	*a2 Pnar-bW2 Pnar-bE1, ble^R/ Potef-mcherry-rab5a, nat^R/ Pcrg-kin1$^{G96E,(1-739)}$-egfp-kin3$^{1197-1348}$, cbx^R*	This study

AB33_mChRab5a_rK1rG-D2	*a2 Pnar-bW2 Pnar-bE1, ble^{R}/ Potef-mcherry-rab5a, nat^{R}/ Pcrg-kin1$^{G96E,(1-739)}$-egfp-kin3$^{1345-1468}$, cbx^{R}*	This study
AB33_mChRab5a_rK1rG-PH	*a2 Pnar-bW2 Pnar-bE1, ble^{R}/ Potef-mcherry-rab5a, nat^{R}/ Pcrg-kin1$^{G96E,(1-739)}$-egfp-kin3$^{1566-1676}$, cbx^{R}*	This study
AB33ΔKin3_mChRab5a_rKin3$^{\Delta PH}$G	*a2 Pnar-bW2 Pnar-bE1, ble^{R} Δkin3::nat^{R}/ Potef-mcherry-rab5a, hyg^{R}/ Pcrg-kin3$^{\Delta 1566-1666}$-egfp, cbx^{R}*	This study
AB33_mChRab5a_rMotorG	*a2 Pnar-bW2 Pnar-bE1, ble^{R}/ Potef-mcherry-rab5a, nat^{R}/ Pcrg-kin3$^{1-367}$-egfp, cbx^{R}*	This study
AB33ΔKin3_YFP^{C}-Kin3-YFP^{N}	*a2 Pnar-bW2 Pnar-bE1, ble^{R} Δkin3::nat^{R}/ Pkin3-yfp^{C}-kin3-yfp^{N}, cbx^{R}*	This study
ΔKin3	*Δkin3, nat^{R}*	(Schuster *et al.*, 2011b)
po^{C}GRab5a	*Potef-egfp-rab5a, cbx^{R}*	Chapter 3
po$^{H}{}_{m}$ChRab5a	*Potef-mcherry-rab5a, hyg^{R}*	(Schuster *et al.*, 2011d)
po$_{m}$ChRab5a	*Potef-mcherry-rab5a, nat^{R}*	(Schuster *et al.*, 2011b)
pKin3G	*Pkin3-kin3-egfp, cbx^{R}*	(Wedlich-Söldner *et al.*, 2002)
pNEBcbx-yeast-1xSspI	*pNEBcbx-yeast-1xSspI, cbx^{R}*	Chapter 3
pcrgPHG	*Pcrg-kin3$^{1566-1676}$-egfp, cbx^{R}*	This study
pKin3$^{\Delta PH}$G	*Pkin3-kin3$^{\Delta 1566-1666}$-egfp, cbx^{R}*	This study
pcrgKin3^{tail}G	*Pcrg-kin3$^{423-1676}$-egfp, cbx^{R}*	This study
pcrgKin3$^{tail\Delta PH}$G	*Pcrg-kin3$^{tail\Delta 1566-1666}$-egfp, cbx^{R}*	This study
pcrgKin3$^{tail}{}_{m}$Ch	*Pcrg-kin3$^{423-1676}$-mcherry, hyg^{R}*	This study
pcrgKin3$^{tail\Delta PH}{}_{m}$Ch	*Pcrg-kin3$^{tail\Delta 1566-1666}$-mcherry, hyg^{R}*	This study
pKin3$^{\Delta DLP}$G	*Pkin3-kin3$^{\Delta 1198-1666}$-egfp, cbx^{R}*	This study
pKin3$^{\Delta L}$G	*Pkin3-kin3$^{\Delta 1349-1565}$-egfp, cbx^{R}*	This study
pKin3$^{\Delta DL}$G	*Pkin3-kin3$^{\Delta 1198-1565}$-egfp, cbx^{R}*	This study
pKin3$^{\Delta D}$G	*Pkin3-kin3$^{\Delta 1198-1348}$-egfp, cbx^{R}*	This study
pcrg^{C}K1r-PX	*Pcrg-kin1$^{G96E,(1-739)}$-yup1$^{4-148}$, cbx^{R}*	Chapter 3
pcrg^{C}K1rG-PX	*Pcrg-kin1$^{G96E,(1-739)}$-egfp-^{BamHI}-yup1$^{4-148}$, cbx^{R}*	Chapter 3

pcrgK1rG-K3t	*Pcrg-kin1*$^{G96E,(1-739)}$*-egfp-kin3*$^{370-1676}$*-egfp, cbx*^{R}	This study
pcrgK1rG-K3ΔDLP	*Pcrg-kin1*$^{G96E,(1-739)}$*-egfp-kin3*$^{370-1022}$*, cbx*^{R}	This study
pcrgK1rG-D	*Pcrg-kin1*$^{G96E,(1-739)}$*-egfp-kin3*$^{1198-1348}$*, cbx*^{R}	This study
pcrgK1rG-D2	*Pcrg-kin1*$^{G96E,(1-739)}$*-egfp-kin3*$^{1345-1468}$*, cbx*^{R}	This study
pcrgK1rG-PH	*Pcrg-kin1*$^{G96E,(1-739)}$*-egfp-kin3*$^{1566-1676}$*, cbx*^{R}	This study
pcrgKin3$^{\Delta PH}$G	*Pcrg-kin3*$^{\Delta 1566-1666}$*-egfp, cbx*^{R}	This study
pcrgMotorG	*Pcrg-kin3*$^{1-367}$*-egfp, cbx*^{R}	This study
pGBKT7-PH	*pGBKT7-kin3*$^{1566-1666}$	This study
pGADT7-motor	*pGADT7-Rec-kin3*$^{1-367}$	This study
pNic28-His$_{6x}$-PH	*pNic28-His*$_{6x}$*-kin3*$^{1566-1676}$	This study
YFP^{C}-Kin3-YFP^{N}	*Pkin3-yfp*^{C}*-kin3-yfp*^{N}*, cbx*^{R}	This study

a, *b*, mating type loci; *P*, promoter; -, fusion; *Δ*, deletion; */*, ectopically integrated; *hyg*^{R}, hygromycin resistance; *ble*^{R}, phleomycin resistance; *nat*^{R}, nourseothricin resistance; *cbx*^{R}, carboxin resistance; *crg*, conditional arabinose-induced promoter; *otef*, constitutive promoter; *nar*, conditional nitrate reductase promoter; *E1*, *W2*, genes of the *b* mating-type locus; *egfp*, enhanced green fluorescent protein; *mCherry*, monomeric Cherry; *yfp*, yellow fluorescent protein; *kin1*, kinesin-1; *kin3*, kinesin-3; *PX*, Phox domain from Yup1; *PH*, pleckstrin homology domain, *DUF3694*, domain of unknown function 3694; *rab5a*, small endosomal Rab5-like GTPase; *His*$_{6x}$, hexahistidine

Supplementary Table 2. Experimental usage of strains.

Strain name	Assay	Figure
AB33_mChRab5a_rPHG	Localization of the PH domain from Kin3 in the cell	Fig. S1
AB33ΔKin3_GRab5a_rK3t$_m$Ch	Colocalization of EE and Kin3 tail	Fig. 1B, 1D
AB33ΔKin3_GRab5a_rK3t$^{\Delta PH}{}_m$Ch	Colocalization of EE and Kin3 tailΔPH	Fig. 1B, 1D
AB33ΔKin3_mChRab5a_Kin3G	Colocalization/motility of EE and Kin3	Fig. 1C, 1E, 1F, 1G, 2D, 2E, 5A, 5B, 5C, 5D, 6A, 6B; Movie S1
AB33ΔKin3_mChRab5a_Kin3$^{\Delta PH}$G	Colocalization/motility of EE and Kin3ΔPH	Fig. 1C, 1E, 1F, 1G, 2D, 2E, 5A, 5B, 5C, 5D, 6A, 6B; Movie S1
AB33ΔKin3_mChRab5a	Motility of EEs	Fig. 1G, 5A; Movie S1
AB33ΔKin3_mChRab5a_Kin3$^{\Delta DLP}$G	Colocalization/motility of EE and Kin3ΔDLP	Fig. 2C, 2D, 2E, S4
AB33ΔKin3_mChRab5a_Kin3$^{\Delta DL}$G	Colocalization/motility of EE and Kin3ΔDL	Fig. 2C, 2D, 2E, S4
AB33ΔKin3_mChRab5a_Kin3$^{\Delta D}$G	Colocalization/motility of EE and Kin3ΔD	Fig. 2C, 2D, 2E, S4
AB33ΔKin3_mChRab5a_Kin3$^{\Delta L}$G	Colocalization/motility of EE and Kin3ΔL	Fig. 2C, 2D, 2E, S4
AB33_mChRab5a	Molecular synthetic anchor assay	Fig. 3B, 3C, 3D
AB33_mChRab5a_rK1rG-K3t	Molecular synthetic anchor assay	Fig. 3B, 3C, 3D
AB33_mChRab5a_rK1rG-D2	Molecular synthetic anchor assay	Fig. 3B, 3C, 3D
AB33_mChRab5a_rK1rG-ΔDLP	Molecular synthetic anchor assay	Fig. 3C, 3D
AB33_mChRab5a_rK1rG-D	Molecular synthetic anchor assay	Fig. 3C, 3D
AB33_mChRab5a_rK1rG-PH	Molecular synthetic anchor assay	Fig. 3C, 3D
AB33ΔKin3_YFP^C-Kin3-YFP^N	BIFC assay – split YFP	Fig. 4C; Movie S3
Y2HGold[pGBKT7-kin3$^{1566-1666}$] + Y2HGold [pGADT7-Rec-kin3$^{1-367}$]	Y2H assay	Fig. 4D
AB33_mChRab5a_rMotorG	Affinity assay	Fig. 4E
AB33ΔKin3_mChRab5a_rKin3$^{\Delta PH}$G	Motility of EEs	Fig. 5A, 5B, 5C, 5D, 6A, 6B

Supplementary Table 3. Primers used in this study.

Name	Sequence (5' to 3')
EB3	CGTGTAAGACTGGTGCGGAT
EB9	AACTGTTGGGAAGGGCGATCGGTGCGGGCC GCAGCTGAAGCTTGCATGCC
EB12	CAGTTGGACGGCGTCGGAAG
EB13	GTTGCAGTTGGCGCACGATTC
EB14	GTACGAAAGCGAGACGAGTTGAGCGAAGAT CTCATGTTTGACAGCTTATCATCG
EB15	GAGTGCAGTGCGGATGACGAAC
EB16	CTGCAGCTTACGCACCAACC
EB23	CTTCTGTGTGTCGCTGTATTCG
EB24	GGCGCTTGTTGCTGCAAGCC
EB25	TGGGAGCAGTGCGACAATTGC
EB26	GCGCTGACGGCAATTGTCGCACTGCTCCCA TACAACGGCGATGCGGGCCA
EB27	AGGCTCATCGGCTAGGCGG
EB39	AATGTTGAATACTCATACTCTTCCTTTTTC GATGCCGGGAGCAGACAAGC
EB40	AAGCCCCAAAAACAGGAAGATTGTATAAGC AGTGTCACCTAAATCGTATG
EB46	GGTGAAACTCGATGAGGCCAAAAAAGATAC ATGCGCACTGCCACCACATC
EB53	GTGCAGATTTGCGAGTTGGACGCATCTGGA CCACCGGGAAGGCTGATGAG
EB54	TCCAGATGCGTCCAACTC
EB60	CTCATGTTTGACAGCTTATC ATCGG
EB62	CTTTGCGTCCCTGCCATTGA
EB63	GCCGTGTCGATCAATGGCAGGGACGCAAAG CGCACTGCCACCACATCTCA
EB67	GTTTGAACGATCTGCAGCCGGGCGGCCGCT TCAGCAAAACACATGGCCCGCATC
EB70	TACTTCCAATCC ATG GCG CGCACTGCCACCACATCTC
EB71	TATCCACCTTTACTG TCA GCAAAACACATGGCCCGC
EB85	GTGCAGATTTGCGAGTTGGACGCATCTGGA TACAACGGCGATGCGGGCCATG
EB91	GAAACTCGATGAGGCCAAAAAAGATAC ATG AAAACCGTCACCAAGGCCGAG
EB119	GATGGCGGAGCTCTATGGAG
EB131	CTCGCCCTTGCTCACCATGGCTGCTGCTG CGACGACGGCCTTGTTCTTG
EB137	GTTTGAACGATCTGCAGCCGGGCGGCCGCTTTA CTTTGCGTCCCTGCCATTG
EB158	CACCCAAGCAGTGGTATCAACGCAGAGTGG ATGGCCGACTCGGGCAACATC
EB159	CACCCTCTAGAGGCCGAGGCGGCCGACATG GACGACGGCCTTGTTCTTG
EB160	CATGGAGGCCGAATTC CGCACTGCCACCACATCTCATCGG

EB161	GCAGGTCGACGGATCC GCAAAACACATGGCCCGCATCGCC
EB170	GGTGAAACTCGATGAGGCCAAAAAAGATAC ATGTCCAACAACATCAAGGTC
EB171	AGTGGTGACGGCAAACGCGCG
EB172	GAGCTCAAGCGCGCGTTTGCCGTCACCACT ACACAGCCACTCCAAGGAATC
EB173	GAACGATCTGCAGCCGGGCGGCCGCTTTA CGGCCATTCGATAAACTGCTTG
EB175	CGTGCACGAAGATCTCCGGTAC
EB195	GAGCTCAAGCGCGCGTTTGCCGTCACCACT ATGGTGAGCAAGGGCGAGGAG
EB197	GGATCC CTTGTACAGCTCGTCCATGCCG
EB206	GTGCAGATTTGCGAGTTGGACGCATCTGGA CGCACTGCCACCACATCTCATC
EB231	GATCACTCTCGGCATGGACGAGCTGTACAAG GGATCC ATG GACCCCAACGCAAAACTCATCCG
EB233	GATCACTCTCGGCATGGACGAGCTGTACAAG GGATCC ATG GAGTACATGCCTGTGCCCGTG
EB241	GTTTGAACGATCTGCAGCCGGGCGGCCGCT TCA ACCGTTCGTACAAGATGAAGACG
EB265	GATCACTCTCGGCATGGACGAGCTGTACAAG GGATCC ATG AGGGACGCAAAGCCACCGGG
EB266	GTTTGAACGATCTGCAGCCGGGCGGCCGCT TCA CACAGCGCGCTGCCACACCG
EB276	GTACGAACGGTATCGTGAATCC
EB277	GCAAGACCGGCAACAGGATTC
EB336	GATCACTCTCGGCATGGACGAGCTGTACAAG GGATCC ATG CGCACTGCCACCACATCTCATC
EB351	GCGAGGCGCTTTTGTCTGCG
EB352	GTTTTGTAGCACACGACTCACATCTGCCGCC GATCCCGCGATACGCACCTTG
EB353	CATGTTATCCTCCTCGCCCTTGCTCACCAT GGCTGCTGCTGCGCAAAACAC
EB356	GTGCAGCCCAGTACGAATGCC
EB363	GAAGAGCAACACACGCAGGAC
EB364	CACTTGCCACCTCCATAGAGCTCCGCCATC ATGGCCGACAAGCAGAAGAAC
EB365	GACGACCTTGATGTTGCCCGAGTCGGCCAT GTGGTTCATGACCTTCTGTTTC
EB366	CATGGCCGACTCGGGCAAC
EB367	GCAAAACACATGGCCCGCATC
EB368	GTACAACGGCGATGCGGGCCATGTGTTTTGC ATGGTGAGCAAGGGCGAGGAG
EB369	GTTTGAACGATCTGCAGCCGGGCGGCCGCT TTA CGTGGCGATGGAGCGCATG
EB370	AGCGGCCGCCCGGCTGCAGATC

EB371	G TCCAGATGCGTCCAACTCGC
CC43	GCTTGCTGAGATCCTCGACG
CC52	GGTGGACCGGACACGATCTC
CC54	GGACAGCCGAGGTAGAGTGC
SK120	CACACAGGAAACAGCTATGACCATGATTACCATCGATGAATTCTCATGTTTGAC
SK213	CACCGTCAGCACCGGCAGCA
SK238	CTTGTACAGCTCGTCCATGCCG
SM59	TCCAGAACGATGCAGTCTGG
TU180	CATCGAATTCTCATGTTTGACAGC

Supplementary Movie legends

Movie S1. Motility of mCherry-Rab5a labelled early endosomes in a *kin3* null mutant (ΔKin3), a *kin3* null mutant complemented with Kin3-GFP (+Kin3) and a *kin3* null mutant complemented with Kin3ΔPH-GFP (+Kin3ΔPH). Note Kin3ΔPH-GFP is able to mediate some motility, indicating that the truncated motor is still able to bind to the organelle. Time is given in seconds:milliseconds; the bar indicates micrometers.

Movie S2. Structural model of the PH domain of Kin3 from *Ustilago maydis*. Red: Amino acids that are identical between human KIF1A and *U. maydis* Kin3; green: Amino acids found in Kin3, KIF1A and in 6 additional PH domains from various non-motor proteins (see Material and Methods of main text). For details on methods and accession numbers see the Method section in the main text.

Movie S3. Motility of YFP^N-Kin3-YFP^C. Fluorescence is only detectable when the two halves of the yellow fluorescent protein interacting. This strongly indicates that the tail and the motor head are in close proximity while the motor moves its cargo along microtubules. Note that the cells show no growth defect indicating that the YFP^N-Kin3-YFP^C protein is biological functional. Time is given in seconds:milliseconds; the bar indicates micrometers.

References for Supplementary online material

Brachmann, A., Weinzierl, G., Kämper, J., and Kahmann, R. (2001). Identification of genes in the *bW/bE* regulatory cascade in *Ustilago maydis*. Mol Microbiol *42*, 1047-1063.

Haun, R.S., Serventi, I.M., and Moss, J. (1992). Rapid, reliable ligation-independent cloning of PCR products using modified plasmid vectors. Biotechniques *13*, 515-518.

Savitsky, P., Bray, J., Cooper, C.D., Marsden, B.D., Mahajan, P., Burgess-Brown, N.A., and Gileadi, O. (2010). High-throughput production of human proteins for crystallization: the SGC experience. J Struct Biol *172*, 3-13.

Schuster, M., Kilaru, S., Ashwin, P., Lin, C., Severs, N.J., and Steinberg, G. (2011a). Controlled and stochastic retention concentrates dynein at microtubule ends to keep endosomes on track. EMBO J *30*, 652-664.

Schuster, M., Lipowsky, R., Assmann, M.A., Lenz, P., and Steinberg, G. (2011b). Transient binding of dynein controls bidirectional long-range motility of early endosomes. Proc Natl Acad Sci U S A *108*, 3618-3623.

Schuster, M., Treitschke, S., Kilaru, S., Molloy, J., Harmer, N.J., and Steinberg, G. (2011d). Myosin-5, kinesin-1 and myosin-17 cooperate in secretion of fungal chitin synthase. EMBO J *31*, 214-227.

Straube, A., Hause, G., Fink, G., and Steinberg, G. (2006). Conventional kinesin mediates microtubule-microtubule interactions *in vivo*. Mol Biol Cell *17*, 907-916.

Takeshita, N., Higashitsuji, Y., Konzack, S., and Fischer, R. (2008). Apical sterol-rich membranes are essential for localizing cell end markers that determine growth directionality in the filamentous fungus *Aspergillus nidulans*. Mol Biol Cell *19*, 339-351.

Wedlich-Söldner, R., Straube, A., Friedrich, M.W., and Steinberg, G. (2002). A balance of KIF1A-like kinesin and dynein organizes early endosomes in the fungus *Ustilago maydis*. EMBO J *21*, 2946-2957.

Chapter 6

Conclusions

EE motility is essential during initial steps of pathogenic development of *Ustilago maydis*.

Active transport of organelles by molecular motors is one of the fundamental processes in eukaryotic cells (Welte, 2004). Bidirectional motility of EEs has become a hot scientific topic recently and a challenging subject with evidence to suggest that EE motility functions not only in endocytosis, degradation and recycling, but also in signalling and cell migration in eukaryotes (Le Roy and Wrana, 2005).

As shown in **Chapter 3**, the colonization process of *U. maydis* starts with the formation of long hyphal cells, which undergo shortening and branching after 2 dpi within the host plant cell. At all stages of the infection long-range bidirectional motility of EEs was observed indicating that this process serves an important purpose during the plant invasion. To test more specifically for the importance of EE motility, I used a molecular anchor for EEs, $K1^{r}PX$. Overexpression of $K1^{r}PX$ blocked motility of ~90% of EEs which were tightly bound to MTs and did not move during 10 sec observations. This in turn led to a release of some Kin3 motors from EEs as I found a threefold increase of independent Kin3 motility after expression of the $K1^{r}PX$, indicating that MT tracks were not blocked for MT-dependent transport. This also suggests that Kin3 can move without EEs although in the WT strain most of Kin3 (~96%) are found on EEs which is in agreement with a previous study (Schuster *et al.*, 2011c). The blockage of EE motility did not lead to high CSD observed after deletion of *kin3* or after overexpression of $Kin3^{rigor}$, which suggests an EE-independent role of Kin3 in cell separation rather than involvement of motile EEs in this process (compare to Schink and Bölker, 2009). In contrast, the blockage of EE motility in hyphal cells led to changes in hyphal morphology where the presence of bipolar filaments, similarly to null *kin3* mutants (Lenz *et al.*, 2006) was observed, indicating that blockage of EE motility might disturb cell polarity. The EE motility blockage led also to ~ twofold decrease in the growth rate of hyphal cells in comparison to the wildtype strain and was not significantly different to the growth rate obtained after deletion of Kin3, indicating that EE motility is crucial for the hyphal growth.

Why are EEs important during early infection stage? **Chapter 3** provides evidence that EEs are involved in the initial steps of pathogenic development in the corn smut *U. maydis* which in part confirms previous results (Fuchs *et al.*, 2006). A previous study on kinesin-1 and kinesin-3 revealed that these motor proteins cooperate in hyphal growth and that null *kin1* and *kin3* mutants exhibit bipolar morphology and a twofold reduction in hyphal growth rate (Schuchardt *et al.*, 2005). Both motors are involved in motility of EEs (Lenz *et al.*, 2006). The blockage of EE motility leads to hyphal growth reduction and the presence of short bipolar hyphae indicates disturbed cell polarity. It suggests that motile EEs are involved in elongation of the filaments and might be involved in the maintenance of the cell polarity most probably by delivery of apical proteins to the Spitzenkörper or to the cell wall. A previous study, where *yup1*^{ts} disrupted EE motility and a defect in secretion of cell wall components was observed (Wedlich-Söldner *et al.*, 2000) strongly confirms that possibility. In addition, it was suggested that EEs can serve as multifunctional platforms on which special sets of molecular machines are assembled (Gould and Lippincott-Schwartz, 2009) and research in *U. maydis* about EE-based transport of mRNA (Baumann *et al.*, 2012; Vollmeister *et al.*, 2012) strongly supports this feature of fungal EEs. Moreover, it was speculated that bidirectional motility of EEs might serve for communication purposes between cell ends allowing synchronization between septum formation and tip advancement (Schuster *et al.*, 2011c).

U. maydis hyphal growth is correlated with the early stages of infection (up to 3 dpi) when cells undergo morphological transition from non-pathogenic yeast-like cells to invasive elongated hyphae (Snetselaar and Mims, 1994; Doehlemann *et al.*, 2008b; Mendoza-Mendoza *et al.*, 2009) which allows intracellular growth within the plant. Three days after infection hyphae undergo shortening and start to grow intercelullarly (Snetselaar and Mims, 1994). A study on the chitin synthase V, Mcs1, suggests that properly formed hyphae are necessary in order to remain undetected by the plant defence system (Treitschke *et al.*, 2010). Mutants depleted of *mcs1* showed swollen hyphae which were no longer able to maintain hyphal polarization and were unable to avoid plant responses. A mutant strain with blocked motility of EEs during initial stages of the pathogenic development was also recognized by the plant defence system suggesting that the EE motility might have a role in secretion of virulence effectors. Surviving the host defence depends on secretion of special virulence

effectors and allows the pathogen to colonize the host organism (Kämper *et al.*, 2006; Müller *et al.*, 2008; Wahl *et al.*, 2009; de Jonge *et al.*, 2011; Djamei *et al.*, 2011; Doehlemann *et al.*, 2011; Hemetsberger *et al.*, 2012; Rafiqi *et al.*, 2012). Moreover, the transition from yeast to hypha, called a dimorphic switch, observed in many pathogenic fungi, is correlated with virulence and successful host colonization by the pathogen (Madhani and Fink, 1998; Nadal *et al.*, 2008; Brand, 2012; Talbot, 2012; Wang and Lin, 2012). How the pathogen communicates with its host is not well understood nor is how the secretion machinery localized at fast growing hyphal tip communicates with the nucleus. One hypothesis is that bidirectional motility of EEs might serve this purpose in *U. maydis* (Steinberg, 2007c). As upregulation of the gene clusters encoding putative effectors, including virulence factors, occurs during plant colonization (Kämper *et al.*, 2006), it is tempting to speculate that EEs might be involved in signal transduction similar to EEs in higher eukaryotes (Murphy *et al.*, 2009; Platta and Stenmark, 2011). The importance of EE motility in early steps of pathogenic development raises a few interesting questions for future study (see below).

1. Do fungal EEs have a role in signalling?
2. How important is hyphal elongation-based movement in pathogenic development?
3. Does EE motility have a role in determining growth direction of fast growing hyphae?
4. Are EEs involved in secretion? Based on previous reports in *U. maydis* that Kin3 is involved in secretion of acid phosphatase (Schuchardt *et al.*, 2005) and that Kin3 is almost always associated with EEs (Chapter 3, Fig. 2G and (Schuster *et al.*, 2011b; Schuster *et al.*, 2011c) it is tempting to speculate that EEs are indeed involved in secretion. On the other hand, study on secretion vesicles, chitosomes, showed that their movement is Kin3 independent (Schuster *et al.*, 2011d).

The PH domain of kinesin-3 controls motor motility *in vivo*.

Ustilago maydis kinesin-3 (Kin3), a homologue of KIF1A and Unc-104 and member of the Kinesin-3 family, transports early endosomes (EEs) in a bidirectional manner (Wedlich-Söldner *et al.*, 2002). As Kin3 is almost always associated with EEs (Schuster *et al.*, 2011c) and its motility drives the movement of EEs and all other proteins attached to EEs, it is crucial to understand how Kin3 binds to EEs. Other kinesin-3 homologues involved in EE transport, in order to bind EEs, use domains that are not found in Kin3 e.g. PX domain. The domain organization of kinesin-3 homologues differs much more between those proteins which were shown as being involved in transport of EEs (e.g. UmKin3 and HsKIF16B) to those with different cargo binding ability (e.g. UmKin3 and HsKIF1A or HsKIF1Bβ or CeUnc-104), therefore the project presented in **Chapter 5** became the most challenging one amongst others discussed in this thesis.

To start with I showed that the tail of Kin3 is able to bind to the EEs. It was not a surprise, as most of the kinesins use their non-motor regions for cargo binding purposes (Hirokawa *et al.*, 2009). Surprisingly, the PH domain, localized at the C-terminus of the tail, can have a role in controlling motor motility of Kin3, whereas it was shown in higher organisms as a lipid binding domain necessary for organelle binding by *in vitro* studies (Klopfenstein *et al.*, 2002; Klopfenstein and Vale, 2004). Deletion of the PH domain from Kin3 reduced EE binding capacity of Kin3 by ~36% indicating that the truncated version of Kin3 lacking the PH domain is sufficient to bind organelles *in vivo* but decreases the motility parameters. This is in agreement with the results obtained for CeUnc-104 in *C. elegans* (Klopfenstein and Vale, 2004), although the data presented there were explained in a different way. The authors showed that some point mutations within the PH domain that interfered with PI(4,5)P2 binding *in vitro* also interfered with Unc-104 function *in vivo* leading to reduced movement velocity and processivity of individual motor proteins in neurites.

By using of a synthetic molecular trap composed of the kinesin-1 rigor motor-neck (aa 1-739; K1r), intramolecular GFP followed by selected domains found in the Kin3 tail region (Fig. 3A in Chapter 5) I identified Kin3 tail domains

involved in EE binding. The Kin1 motor-neck region composed of the first globular and two coiled-coils domains but lacking the last coiled-coil and last globular domains did not show MT bundling activity typical for the full length Kin1 (Straube *et al.*, 2006) and a point mutation at G96E in the ATP binding site within the motor domain allowed the rigorous binding of the Kin1 motor head to MTs. This approach identified the DUF3694 and D2 domains as being involved in the binding of EEs. Surprisingly, after overexpression of the K1^{r}PH, the PH domain did not show the ability to immobilise the EEs on the MTs.

In order to obtain additional positive evidence for the role of the selected domains in EE binding several experiments were carried out. Unfortunately overexpression of each domain *in vivo* was unsuccessful, due to weak expression of truncated versions of proteins or protein subcellular mislocalization. I also tried the expression of the domains *in vitro* that would serve in lipid overlay assay, but recombinant proteins expressed in *E. coli* remained insoluble except for the PH domain which did not show any binding to the lipids. Moreover in collaboration with Dr. Michael Schrader's group I attempted to colocalize each selected domain with an endosomal fraction using organelle fractionation but due to the 'stickiness' of the negative control we were unable to distinguish between true and false results.

How does the PH domain bind simultaneously to the organelles and the motor domain? There are few possibilities:

1) Probably the interaction between the PH domain and the motor domain enhances or leads to proper protein folding (Fig. 1B; model 1). The interaction between motor and the tail would serve to expose DUF3694 and D2 regions for cargo binding. In other words, the presence of the PH domain is necessary for EE binding in respect to the folding back to the motor domain and to expose cargo binding domains (DUF3694 and D2). This can explain increased cytosolic background after deletion of the PH domain as a result of higher amount of unbound truncated Kin3. This hypothesis is supported by a previous study (Klopfenstein and Vale, 2004), where substitutions of the PH domain in CeUnc-104 by another lipid binding module (specific for PI(4,5)P2) did not rescue or only weakly rescued the *unc-104* phenotype. This also suggests that the interaction between PH domain and the motor domain could be very specific. I performed a similar

experiment (data not shown) where I substituted the PH domain in Kin3 with the PX domain from *U. maydis* Yup1. The PX domain from Yup1 is specific for EEs and colocalization between EEs labelled with mCherry-Rab5a and PX^{Yup1}-GFP revealed 93.4±1.6% of colocalization events (n=40 cells; Fig. 2C in Chapter 3). Although the substitution recovered colocalization between EEs and the chimera protein to the WT level, neither EE velocities, nor EE run length were restored and were similar to the values obtained for the $Kin3^{\Delta PH}$ (data not shown).

2) Another possibility that could explain the dual role of the PH domain, in binding to the organelles and the motor domain is its activating role in relieving Kin3 from the autoinhibited state resulting in fast processive movement (Fig. 1B; model 2). In this scenario the PH domain would initially participate in organelle binding and then would bind to the motor domain allowing the tail domain to fold back thereby relieving the autoinhibition which, according to the literature, is based on the interaction between the domains localized in the N-terminal part of the tail. The regions involved in the autoinhibition of the KIF1A/Unc-104 (Lee *et al.*, 2004; Hammond *et al.*, 2009) are also responsible for dimerization (Al-Bassam *et al.*, 2003; Rashid *et al.*, 2005; Hammond *et al.*, 2009; Huo *et al.*, 2012). This hypothesis is supported by a previous study (Wedlich-Söldner *et al.*, 2002) where a truncated Kin3 protein containing the first 674 amino acids was not able to bind MTs and did not show any ATPase activity *in vitro*, suggesting autoinhibition of the protein. The same results, but *in vivo* were presented in Hammond *et al.*, 2009, where a region containing FHA and CC2 (aa 1–726) was not able to bind to MTs and remained cytosolic. In the case of mammalian and fungal kinesin-3, KIF1A and Kin3 respectively, shorter constructs containing only motor domains followed by a coiled-coil, was strongly bound to MTs (Wedlich-Söldner *et al.*, 2002; Hammond *et al.*, 2009). These results imply the autoinhibition mechanism could be relieved upon binding to the cargo. After deletion of the PH domain, observed cytosolic background could be a pool of autoinhibited Kin3 dimers where lack of the PH domain did not allow the abrogation of some potential autoinhibition.

3) The PH domain bound to the motor domain could also prevent binding to MT-associated proteins which in turn would allow unrestricted movement

along MTs (Fig. 1B; model 3). This idea is based on the study by Tien *et al.*, 2011, where the PH domain has been identified as a regulator of tau-binding to CeUnc-104. In worms expressing Unc-104$^{\Delta PH}$ the amount of association between Ptl-1 (tau homologue) and truncated version of kinesin-3 increased which was confirmed by co-immunoprecipitation studies. *U. maydis* genome does not encode any tau protein homologue, but I cannot exclude the participation of other MT-associated proteins as binding partners of Kin3. If this is true, it could be used towards explaining observed reduction in motility parameters after deletion of the PH domain. A recent study on Vamp2 trafficking revealed that KIF1A run length depends also on the interaction with another group of MAPs – doublecortin family proteins and that KIF1A requires them for proper localization in neurons (Liu *et al.*, 2012).

4) Another possibility which can be taken into consideration is that the interaction between motor and PH domains happens between different Kin3 molecules (Fig. 1B; model 4). That would result in triggering more motors to the cargo, thereby enhancing the dimerization between Kin3 proteins and promoting processivity.

By using *in vitro* and *in vivo* assays, I showed that Kin3 is a compact, globular protein and its PH domain directly interacts with the motor domain promoting run length of the EEs. Why the presence of highly conserved PH domain is so important and evolutionary conserved in *U. maydis* instead of a domain that would serve as a simple lipid binding domain to bind PI(3)P abundant in EE membranes (Gillooly *et al.*, 2000) is unclear. Despite the fact that Kin3 and KIF1A/KIF1Bβ are involved in the transport of different organelles, they both share some important characteristics: 1) both motors are fast with an average velocity greater than 1 µm/sec (Okada *et al.*, 1995; Zhou *et al.*, 2001; Klopfenstein *et al.*, 2002; Wedlich-Söldner *et al.*, 2002; Lee *et al.*, 2003; Barkus *et al.*, 2008; Zekert and Fischer, 2009); 2) both are selective for their cargo; 3) they are highly processive and take their cargo over long distances. Lack of the PH domain in human KIF16B, which contains the PX domain, may result in lower motility parameters observed in EEs transport in HeLa cells (velocity ~0.35 µm/s *in vivo*, distances ~3 µm *in vitro*; Hoepfner *et al.*, 2005; Blatner *et al.*, 2007). Thus, the PH domain of KIF1A-like kinesin-3 motors could foster

cargo transport over long distances within polarized cells, such as axons or fungal hyphae.

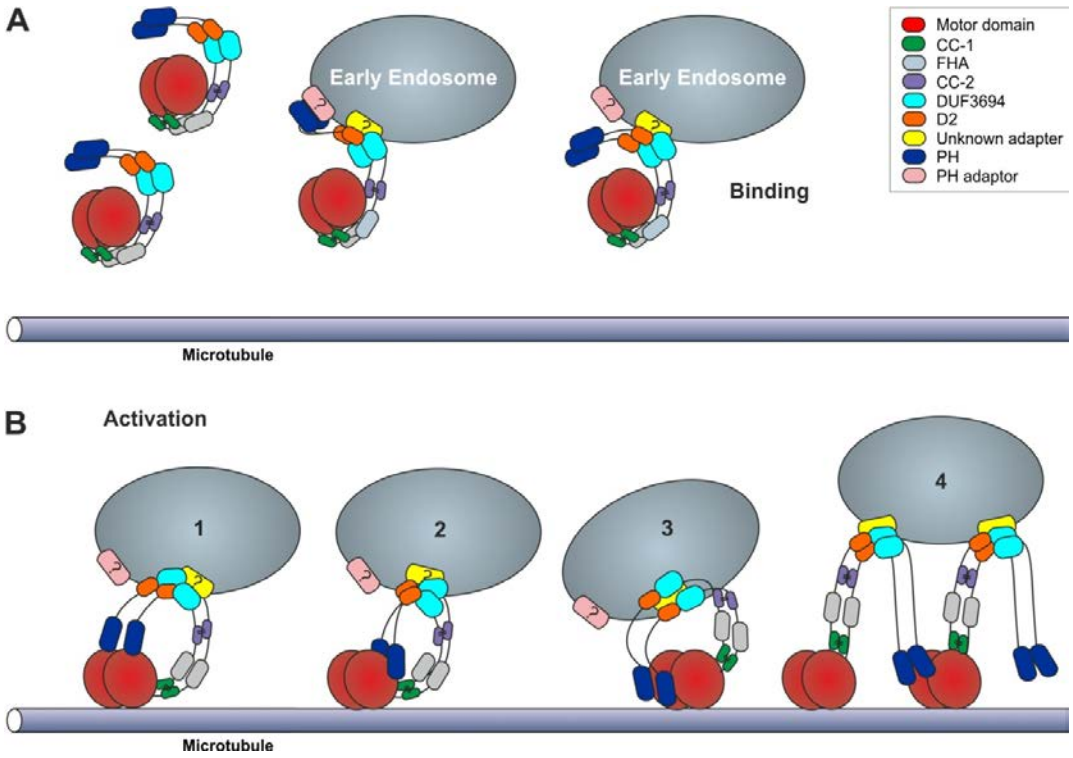

Figure 1. Proposed model of the regulation of the Kin3 by the PH domain.
Kin3 must be relieved from the autoinhibition state after binding to the cargo in order to activate the motility. (A) Cytosolic fraction of autoinhibited pool of Kin3 might bind to the EEs initially via the PH domain (unknown PH adaptor is shown in pink) and later via DUF3694 and D2 domains (unknown adapter is shown in yellow). (B) Binding of the PH domain might relieve the intramolecular inhibition of Kin3 by binding to its motor domain which allows processive movement (activation). **Model 1**: After binding to the cargo, Kin3 changes its conformation by interaction between motor and the PH domain. Changed conformation relieves autoinhibition. **Model 2**: After binding to the cargo, Kin3 changes its conformation, the PH domain competes with the autoinhibition region for binding to the same site within motor domain. After winning, the autoinhibition is relieved. **Model 3**: After binding to the cargo, Kin3 changes its conformation and interaction between motor and the PH domain occurs. This interaction prevents binding of potential MT-associated proteins and allows movement. **Model 4**: After binding to the cargo, interaction motor - PH domain could occur between different dimers which in turn would allow attaching of more motors to the cargo.

The other parts of the Kin3 tail, conserved DUF3694 and D2 domains which were able to immobilise EEs on MTs, might interact with the cargo via an adaptor protein localized on EEs. Likely candidates could be Rab proteins, as their role in targeting of the motor proteins recruitment to the cargo membrane

was already documented (reviewed in Jordens *et al.*, 2005). There is evidence that four kinesin-3 homologues also use the Rab proteins:

1. Membrane localization of human KIF16B most likely depends on Rab5-mediated PI(3)P production (Hoepfner *et al.*, 2005);
2. Mouse KIF16B associates directly with the Rab14-GTP adaptor on FGFR-containing vesicles (Ueno *et al.*, 2011), but not with the Rab5;
3. Mouse KIF1A and KIF1Bβ stalk domains interact via DENN/MADD protein with GTP–Rab3 located on synaptic vesicle precursors carrying Rab3 (Niwa *et al.*, 2008).

The role of the small GTPase Rab5a, other than EE marker is not well understood in *U. maydis*, although deletion of Rab5a, which leads to impairment of EE motility (Gulay Dagdas, unpublished), suggests that it can have functions described in other eukaryotes.

The main questions which have arisen during my studies that still need further investigation are:

1) Kin3 proteins, at least those detectable by fluorescence microscopy, are almost always associated with EEs (Schuster *et al.*, 2011b; Schuster *et al.*, 2011c) and Kin3 activity must be properly repressed during retrograde transport when dynein takes over and is switched on after releasing of dynein when Kin3 takes the lead. What does make Kin3 inactive during retrograde transport while being still attached to the cargo?
2) How the PH domain binding to the organelles/motor domain is controlled?
3) If my hypothesis (Fig.1, Model 1 and 2) is true, how binding to the cargo relieves the Kin3 autoinhibition?

Although further studies are needed, it is clear that Kin3-based motility of EEs is of essential importance for the morphogenesis and pathogenicity of the fungus *U. maydis.*

Ustilago maydis kinesin-3 is a nonselective motor protein for microtubule tracks.

Similarly to neurons, *U. maydis* hyphal cells are highly polarized and elongated cells that do not undergo mitosis (Garcia-Muse *et al.*, 2003). Moreover they contain unipolar plus-ends of MT bundles near the cell poles, whereas antipolar bundles are found in the middle region of the cell (Lenz *et al.*, 2006; Schuster *et al.*, 2011c). This complicated MT array is used by dynein and kinesin-3, which move EEs in a bidirectional fashion (Wedlich-Söldner *et al.*, 2002; Lenz *et al.*, 2006; Schuster *et al.*, 2011c). Bidirectional motility of EEs is crucial during initial stages of pathogenic development as shown in Chapter 3.

The results shown in **Chapter 4** indicate that Kin3 uses all MT tracks present in *U. maydis* hypha. This is in contrast to the *A. nidulans*, where UncA, Kin3 homologue, uses only a subset of MTs, which are detyrosinated (Zekert and Fischer, 2009). An interesting aspect is that these kinesin-3 proteins, responsible for transport of EEs in filamentous fungi, developed different strategies to maintain cargo delivery. As *U. maydis* hyphal cells are arrested in a postreplicative G2 phase (Garcia-Muse *et al.*, 2003), Kin3 uses almost all the MT tracks, while UncA in *A. nidulans* uses tracks that are stable during mitosis.

It is known that MTs can undergo post-translational modifications (PTMs) named as ‘tubulin code’ (Verdier-Pinard *et al.*, 2009). PTMs are especially important in neurons which allow some motor protein e.g. kinesin-1 to differentiate between axons and dendrites (Nakata and Hirokawa, 2003). In case of kinesin-3 homologues, their preference for subsets of MTs is quite difficult to estimate and most probably it depends on kinesin-3 cargoes and tissue (or cell) construction. In animals, a truncated version of KIF1A (aa 1-393) does not select subsets of MTs in COS cells (Cai *et al.*, 2009), but lack of polyglutamylated α-tubulins in mouse neurites results in accumulation of KIF1A in the soma (Ikegami *et al.*, 2007). Recent studies on destination selection among neuronal kinesins revealed that truncated KIF1A (aa 1-393) and KIF1B (aa 1-386) are not selective motors and are found in both axons and dendrites (Huang and Banker, 2012; Jenkins *et al.*, 2012) although different PTMs are found in both neurites (Fukushima *et al.*, 2009; Hammond *et al.*, 2010; Janke

and Kneussel, 2010). Recognition of different subpopulations of MTs by kinesin-3 motors was shown in the filamentous fungus *A. nidulans*, where a subpopulation of less dynamic, detyrosinated MTs is preferred by UncA in vesicle delivery (Zekert and Fischer, 2009). Most of the above results were based on truncated versions of motors, however the kinesin-3 tail may be necessary to recognize modified MTs as was shown for UncA (Seidel *et al.*, 2012). The tail region of UncA responsible for the MT recognition (aa 1316-1402) is overlapping with the D2 region involved in cargo binding found in Kin3 (Chapter 5), however Clustal alignment (see Fig. 1C in Chapter 4) suggests that the tail of *U. maydis* Kin3 is more closely related to that of human KIF1A. In addition UncA contains a BAR domain (reviewed in Frost *et al.*, 2009), which could permit EE binding. ClustalX alignment (Fig. 2, below) and pairwise alignment between sequence encoding UncA BAR domain and UmKin3 tail did not reveal high homology between them (18.5% identity and 29.8% similarity; Emboss pairwise sequence alignment http://www.ebi.ac.uk/Tools/psa/emboss_needle/; matrix EBLOSUM62) suggesting that both proteins not only developed different cargo binding domains but also different selectivity for MTs. This might be due to a different organization of the MT array (see Fig. 3 in Chapter 4).

Figure 2. ClustalX sequence alignment of fungal kinesins-3 between BAR domain AnUncA and UmKin3 tail region.
Note that BAR domain region (area shaded in light yellow) is less conserved between both proteins than a following region. Identical amino acids are indicated by asterisks, similar amino acids are indicated by double points. Accession numbers: *U. maydis* UmKin3 (XP_762398) and *A. nidulans* AnUncA (XP_680816).

The presence of PTMs of MTs in *U. maydis* is currently unknown, although there is the possibility that PTMs of MTs in *U. maydis* occur. The *U. maydis* genome encodes a number of genes which are homologous to known enzymes involved in PTMs of MTs (reviewed in Wloga and Gaertig, 2011), like

acetyltransferases (um01576) and deacetylases which are involved in PTMs of tubulin Lysine residues (um02102, um11308, um11828, um02065, um04234, um05892, um05758, um12006, um05239, um00963). It also encodes TTL and CCP1 homologues (um03366 and um05109, respectively), enzymes responsible for tyrosination/polyglutamylation and detyrosination of the terminal Tyrosine residue. Although, to answer the question if *U. maydis* MTs undergo PTMs further research is necessary.

Appendix

During my PhD I was also involved in the project: Identification of septin interacting proteins in *Magnaporthe oryzae*. By developing a co-immunoprecipitation assay using GFP-Trap (Chromotek) I helped Yasin Dagdas to identify interactors of Sep5-GFP (homolog of Cdc11 from *S. cerevisiae*). Although my contribution to the project was minor, it helped to prove direct interaction between sets of septins and the results were presented in Table S1 in the publication:

Dagdas, Y.F., Yoshino, K., Dagdas, G., Ryder, L.S., Bielska, E., Steinberg, G., and Talbot, N.J. (2012). Septin-mediated plant cell invasion by the rice blast fungus, *Magnaporthe oryzae*. Science *336*, 1590-1595.

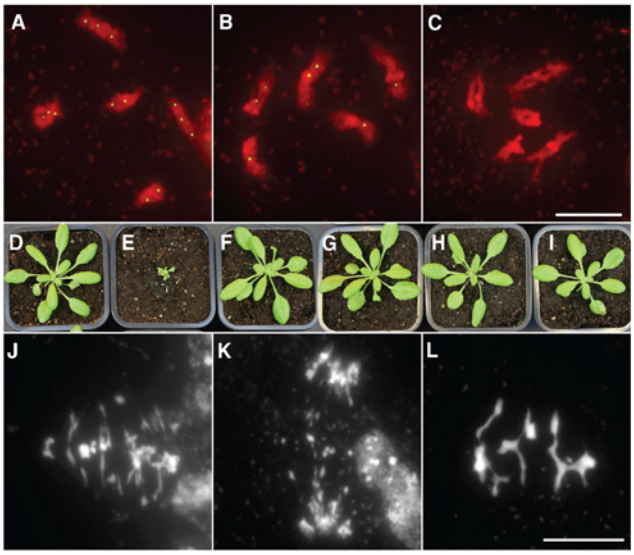

Fig. 4. *fancm* extra COs are MUS81 dependent. (**A** to **C**) MLH1 immunolocalization at diakinesis. (A) Wild type. (B) *fancm-1*. (C) *fancm-1 zip4*. (**D** to **I**) Analysis of the *fancm mus81* synthetic growth defect. (D) Wild type. (E) *fancm mus81*. (F) *fancm mus81 rad51*. (G) *fancm*. (H) *mus81*. (I) *rad51*. (**J** to **L**) Meiotic chromosome spreads. (J) *fancm-1 zip4 mus81* with chromosome fragmentation at the metaphase I to anaphase I transition. (K and L) *fancm-1 mus81* showing chromosome fragmentation at anaphase I and five bivalent-like structures at metaphase I, respectively. Scale bars: 10 μm.

of ZMM-dependent COs is indifferent to the defective MUS81 FANCM pathways.

In mitotic cells, budding and fission yeast orthologs of the FANCM helicase—Mph1 and Fml1, respectively—have been shown to unwind displacement loops (D loops) in NCO pathways and to be somatic CO suppressors (*13*, *14*). The biochemical properties of FANCM helicases are likely similar at mitosis and meiosis. We suggest that FANCM processes meiotic DSB repair intermediates, possibly D loops, driving them toward NCO resolution (or sister chromatid events) (fig. S1). In the absence of FANCM, MUS81 repairs these intermediates as interference-insensitive COs, whereas ZMMs cannot process these intermediates as COs. This implies that recombination intermediates on which FANCM can act are distinct from the intermediates that ZMMs converts to COs, supporting an early irreversible channeling of intermediates toward the ZMM or MUS81 pathways (*9*). To date, only two other meiotic anti-CO factors have been described (*1*): R-TEL in *Caenorhabditis elegans* (*15*) and Sgs1 in budding yeast (*16*, *17*). Thus, anti-CO factors identified so far are helicases, raising the possibility that different helicases are used in various organisms to prevent excessive COs. Additionally, our findings show that, although most eukaryotes have only one to three COs per chromosome on average, CO number can be largely increased without obvious negative phenotypic effects, suggesting that COs are naturally constrained below their possible maximum. This finding supports the idea that crossover frequency is maintained by natural selection at a specific equilibrium between the long-term advantages and costs of recombination (*18*). Finally, the hyperrecombination provoked by *fancm* mutation could be of great interest for crop improvement, which relies on the production of new allele combinations through meiotic recombination whose frequency is a limiting factor (*19*).

References and Notes

1. J. L. Youds, S. J. Boulton, *J. Cell Sci.* **124**, 501 (2011).
2. L. E. Berchowitz, G. P. Copenhaver, *Curr. Genomics* **11**, 91 (2010).
3. L. Chelysheva *et al.*, *PLoS Genet.* **3**, e83 (2007).
4. M. C. Whitby, *DNA Repair (Amst.)* **9**, 224 (2010).
5. A. R. Meetei *et al.*, *Nat. Genet.* **37**, 958 (2005).
6. L. E. Berchowitz, G. P. Copenhaver, *Nat. Protoc.* **3**, 41 (2008).
7. A. Malkova *et al.*, *Genetics* **168**, 49 (2004).
8. L. Chelysheva *et al.*, *Cytogenet. Genome Res.* **129**, 143 (2010).
9. G. V. Börner, N. Kleckner, N. Hunter, *Cell* **117**, 29 (2004).
10. F. W. Stahl, *Genetics* **179**, 701 (2008).
11. J. D. Higgins, E. F. Buckling, F. C. H. Franklin, G. H. Jones, *Plant J.* **54**, 152 (2008).
12. L. E. Berchowitz, K. E. Francis, A. L. Bey, G. P. Copenhaver, *PLoS Genet.* **3**, e132 (2007).
13. W. Sun *et al.*, *Mol. Cell* **32**, 118 (2008).
14. R. Prakash *et al.*, *Genes Dev.* **23**, 67 (2009).
15. J. L. Youds *et al.*, *Science* **327**, 1254 (2010).
16. S. D. Oh *et al.*, *Cell* **130**, 259 (2007).
17. A. De Muyt *et al.*, *Mol. Cell* **46**, 43 (2012).
18. L. Hadany, J. M. Comeron, *Ann. N.Y. Acad. Sci.* **1133**, 26 (2008).
19. E. Wijnker, H. de Jong, *Trends Plant Sci.* **13**, 640 (2008).
20. D. D. Perkins, *Genetics* **34**, 607 (1949).

Acknowledgments: R.M. and J.L.S. thank the EU-FP7 program (Meiosys-KBBE-2009-222883), and G.P.C. thanks the NSF (MCB-1121563) for financial support. We thank V. Borde, M. Grelon, C. Mézard, F. Nogué, A. Demuyt, and O. Loudet for critical reading of the manuscript and helpful discussions. A provisional patent application based on the work has been filed by INRA.

Supplementary Materials

www.sciencemag.org/cgi/content/full/336/6088/1588/DC1
Materials and Methods
Figs. S1 to S8
Tables S1 to S5
References (*21*–*30*)

10 February 2012; accepted 17 April 2012
10.1126/science.1220381

Septin-Mediated Plant Cell Invasion by the Rice Blast Fungus, *Magnaporthe oryzae*

Yasin F. Dagdas,[1] Kae Yoshino,[1,2] Gulay Dagdas,[1] Lauren S. Ryder,[1] Ewa Bielska,[1] Gero Steinberg,[1] Nicholas J. Talbot[1]*

To cause rice blast disease, the fungus *Magnaporthe oryzae* develops a pressurized dome-shaped cell called an appressorium, which physically ruptures the leaf cuticle to gain entry to plant tissue. Here, we report that a toroidal F-actin network assembles in the appressorium by means of four septin guanosine triphosphatases, which polymerize into a dynamic, hetero-oligomeric ring. Septins scaffold F-actin, via the ezrin-radixin-moesin protein Tea1, and phosphatidylinositide interactions at the appressorium plasma membrane. The septin ring assembles in a Cdc42- and Chm1-dependent manner and forms a diffusion barrier to localize the inverse-bin-amphiphysin-RVS–domain protein Rvs167 and the Wiskott-Aldrich syndrome protein Las17 at the point of penetration. Septins thereby provide the cortical rigidity and membrane curvature necessary for protrusion of a rigid penetration peg to breach the leaf surface.

Rice blast is the most devastating disease of cultivated rice and a constant threat to global food security. Each year up to 30% of the rice harvest is lost to blast disease—enough grain to feed 60 million people—and finding an effective way to control rice blast is therefore a

priority. To infect rice leaves, *Magnaporthe oryzae* develops a special infection structure called an appressorium (Fig. 1), which generates turgor of up to 8.0 MPa (equivalent to 40 times that of a car tire) and translates this extreme pressure into physical force to break the leaf surface. Appressorium turgor is generated by rapid influx of water into the cell against a concentration gradient of glycerol, maintained in the appressorium by a specialized, melanin-rich cell wall (*1*). Turgor is translated into physical force and applied to the leaf surface by a narrow penetration peg that mechanically ruptures the tough leaf cuticle (*2*, *3*). The cellular mechanism by which an appressorium breaches the cuticle is not known.

We set out to investigate how the appressorium causes plant infection. We first carried out live-cell imaging of the actin cytoskeleton during appressorium maturation by expressing the actin-binding protein gene fusion, LifeAct-RFP (where RFP is red fluorescent protein) (*4*), in *M. oryzae*.

[1]School of Biosciences, University of Exeter, Geoffrey Pope Building, Exeter EX4 4QG, UK. [2]Division of Applied Biosciences, Graduate School of Agriculture, Kyoto University, Sakyo-ku, Kyoto 606-8502, Japan.

*To whom correspondence should be addressed. E-mail: n.j.talbot@exeter.ac.uk

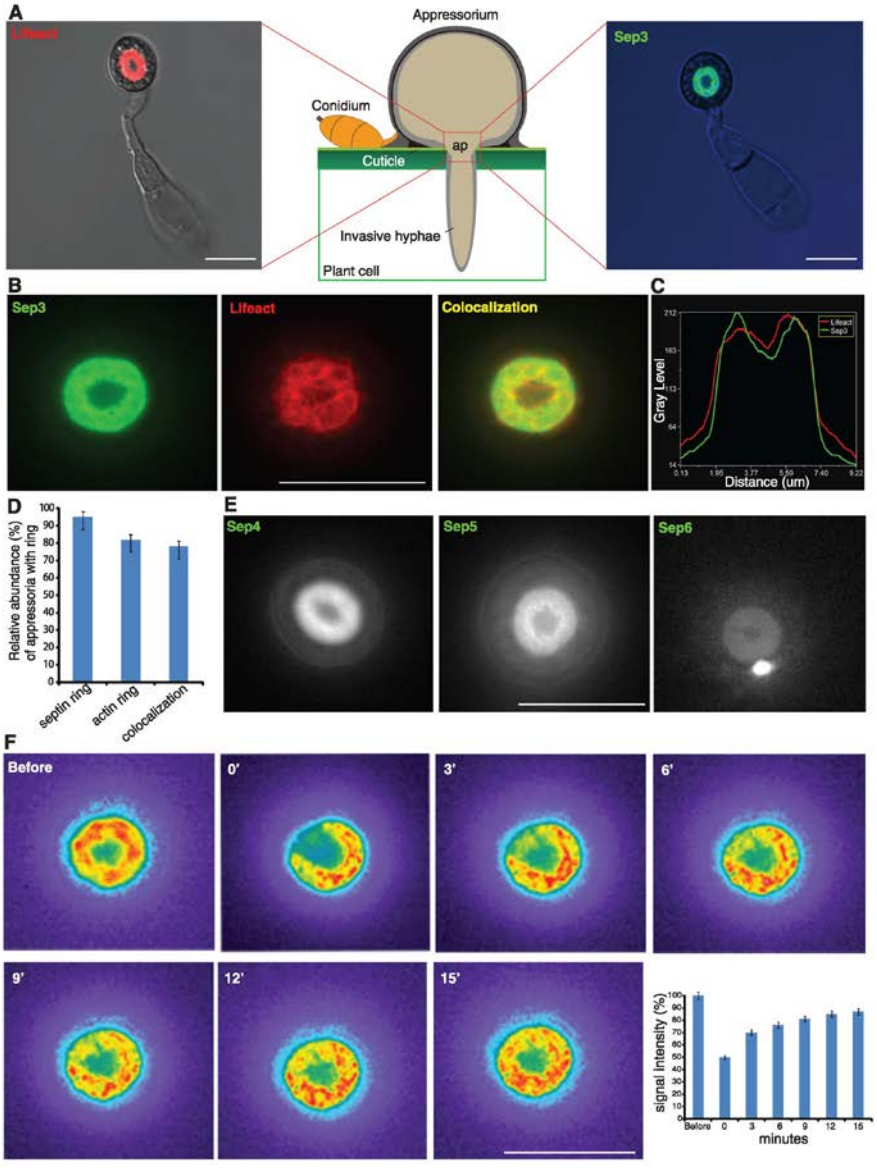

Fig. 1. A toroidal-shaped F-actin network and septin ring assemble at the appressorium pore in *M. oryzae*. **(A)** Cellular localization of LifeAct-RFP and Sep3-GFP visualized by laser confocal and laser excitation epifluorescence microscopy, respectively. ap indicates appressorium pore. **(B)** Sep3-GFP and LifeAct-RFP colocalization in the appressorium. **(C)** Linescan graph consistent with colocalization of the septin ring and F-actin network. **(D)** Bar charts showing septin ring and F-actin colocalization (mean ± SD, three experiments, n = 300). **(E)** Sep3-GFP, Sep4-GFP, Sep5-GFP, and Sep6-GFP form a ring at the appressorium pore. Sep6 also forms a distinct punctum. **(F)** Recovery of Sep3-GFP ring after partial photobleaching, with 87% recovery in fluorescence after 15 min (mean ± SD, three experiments). Scale bars indicate 10 μm.

This revealed an extensive toroidal F-actin network at the base of the infection cell surrounding the appressorium pore (Fig. 1A), a circular region that marks the point at which the penetration peg emerges to rupture the leaf cuticle (*2*). The appressorium pore initially lacks a cell wall, and the fungal plasma membrane makes direct contact with the rice leaf surface (*2*). Then, as the appressorium inflates to full turgor (with a mean diameter of 8.0 μm), a pore wall overlay develops, and a narrow (780-nm mean diameter) penetration peg emerges. Assembly of an F-actin network during appressorium turgor generation, just before plant infection, suggests that specific reorientation of the F-actin cytoskeleton takes place at the base of the appressorium to facilitate plant infection (*2*). To investigate how actin is organized at this location, we decided to investigate the septin gene family in *M. oryzae*. Septins are small morphogenetic guanosine triphosphatases (GTPases); conserved from yeast to humans (*5*, *6*); and involved in cytokinesis, polarity determination, and secretion (*7*, *8*). Importantly, septins are thought to reorient and reorganize the cytoskeleton to determine cell shape (*9*–*12*) and act as partitioning diffusion barriers to recruit and maintain specific proteins at discrete subcellular locations (*9*, *10*). We identified a family of five septin genes in *M. oryzae*, four of which showed similarity to core septins identified in the budding yeast *Saccharomyces cerevisiae* (Cdc3, Cdc10, Cd11, and Cdc12) (*9*). Sep3 showed 47% amino acid identity to Cdc3, Sep4 showed 55% identity to Cdc10, Sep5 showed 45% identity to Cdc11, and Sep6 showed 57% identity to Cdc12. We expressed the *M. oryzae* genes in temperature-sensitive *S. cerevisiae* septin mutants that show defects in cell division and in all cases observed complementation of the cell separation defect consistent with the *M. oryzae* proteins acting as functional septins (fig. S1). Next, we expressed Sep3-GFP, Sep4-GFP, Sep5-GFP, and Sep6-GFP (where GFP is green fluorescent protein) gene fusions in *M. oryzae*, and each septin formed a 5.9-μm ring that colocalized with the F-actin network at the appressorium pore (Fig. 1, A and D, and movie S1). In the case of Sep6-GFP, we also observed an additional bright punctate structure consistently associated with the appressorium septin ring (Fig. 1D). *M. oryzae* septins formed a wider range of structures in hyphae and during invasive growth, including bars, gauzes, collars, and rings (figs. S2 and S3). As expected, they also formed rings at sites of septation (*10*), such as the neck of nascent appressoria (fig. S2). To understand the nature of the septin ring, we investigated fluorescence recovery after partial photobleaching. We found 87% recovery of fluorescence after 15 min, consistent with the appressorium septin ring being a dynamic structure (Fig. 1F). We then carried out targeted gene deletions to produce isogenic mutants lacking *SEP3*, *SEP4*, *SEP5*, or *SEP6* (fig. S4). Septin null mutants showed mislocalization of the remaining septin-GFPs (fig. S5). Core *M. oryzae* septins therefore act cooperatively to form hetero-oligomers, which assemble into the large ring surrounding the appressorium pore. Consistent with this idea, coimmunoprecipitation experi-

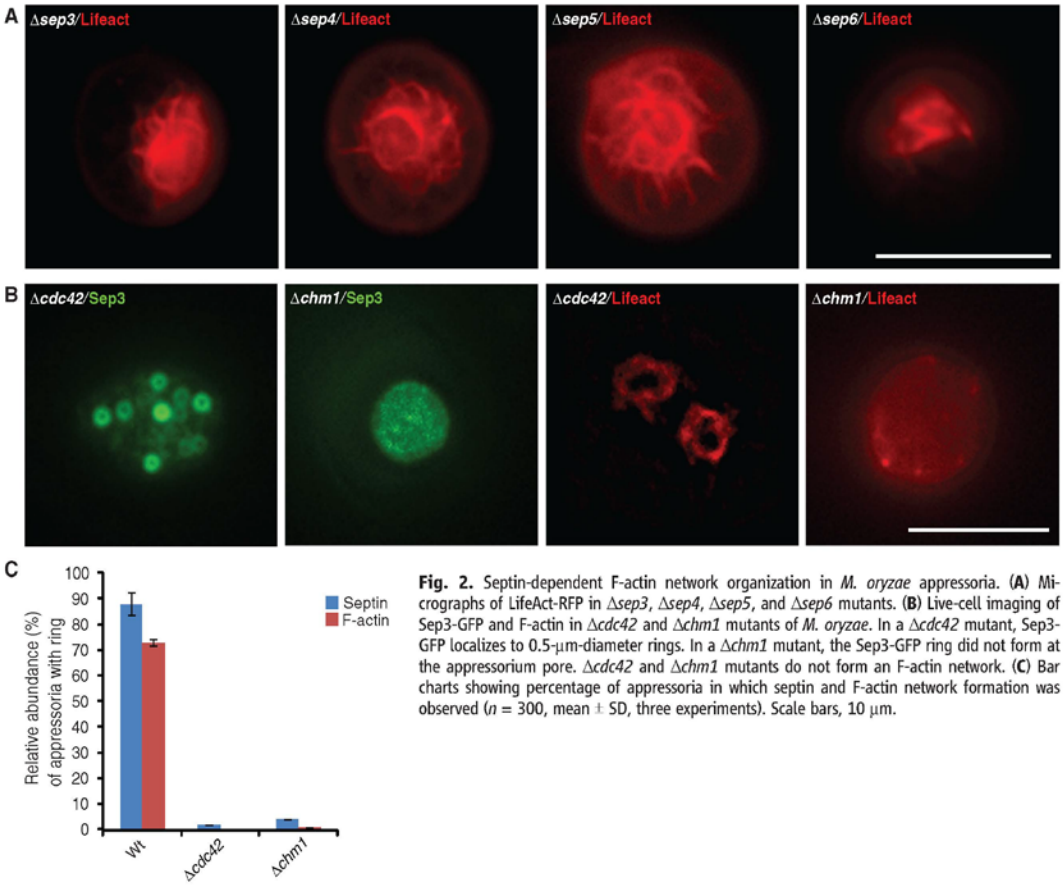

Fig. 2. Septin-dependent F-actin network organization in *M. oryzae* appressoria. (**A**) Micrographs of LifeAct-RFP in Δ*sep3*, Δ*sep4*, Δ*sep5*, and Δ*sep6* mutants. (**B**) Live-cell imaging of Sep3-GFP and F-actin in Δ*cdc42* and Δ*chm1* mutants of *M. oryzae*. In a Δ*cdc42* mutant, Sep3-GFP localizes to 0.5-μm-diameter rings. In a Δ*chm1* mutant, the Sep3-GFP ring did not form at the appressorium pore. Δ*cdc42* and Δ*chm1* mutants do not form an F-actin network. (**C**) Bar charts showing percentage of appressoria in which septin and F-actin network formation was observed (n = 300, mean ± SD, three experiments). Scale bars, 10 μm.

ments using Sep5-GFP identified Sep3, Sep4, and Sep6 interactions as well as physical interaction with actin, tubulins, and the Lte1 cell cycle control protein (*11*) (table S1). *M. oryzae* septin mutants showed a number of developmental phenotypes (fig. S6). Multiple rounds of nuclear division, for instance, took place during appressorium development in septin mutants (fig. S7, A and B) compared with a single round of mitosis and autophagy-associated cell death, which normally occurs in *M. oryzae* (*12*, *13*). Septins took part in cytokinesis within hyphae (*7*–*10*), and localization of myosin II and myosin light chain to the septum, which separates the germ tube and appressorium (*10*), required septins (fig. S7, C and D).

We next decided to investigate the effect of deleting *M. oryzae* septin genes on actin organization and found that the appressorium F-actin network was disorganized in Δ*sep3*, Δ*sep4*, Δ*sep5*, and Δ*sep6* mutants (Fig. 2A). We reasoned that F-actin, scaffolded by septins, might therefore provide cortical rigidity before peg emergence in a manner analogous to a yeast bud, where assembly of F-actin cables requires Cdc42 and the formins Bni1 and Bnr1 (*14*–*16*). To test this idea, we investigated F-actin and septin localization in a *M. oryzae* Δ*cdc42* mutant (Fig. 2). We observed many aberrant, ~0.5-μm-diameter Sep3-GFP rings in a Δ*cdc42* mutant but no central septin ring in the appressorium (Fig. 2, B and C).

Similarly, targeted deletion of *M. oryzae CHM1* (*17*, *18*) prevented formation of either the septin or F-actin networks (Fig. 2, B and C). In yeast, Chm1 encodes a kinase that phosphorylates septins (*17*). Septin ring formation also required the cell integrity mitogen-activated protein kinase Mps1 (*19*) and the Mst12 transcription factor (*20*), which are necessary for appressorium function (fig. S8). Furthermore, we discovered that septin ring formation depends on cell cycle progression, which regulates appressorium development in *M. oryzae* (*12*) (fig. S9). Taken together, we conclude that septin ring assembly is necessary to scaffold F-actin as a toroidal network at the base of the appressorium before plant infection.

To test whether septin-dependent assembly of the F-actin network is essential for rice blast disease, we inoculated a susceptible rice cultivar with each septin null mutant and scored disease symptoms. Septin mutants were nonpathogenic, causing either no symptoms at all (Δ*sep3*) or small necrotic flecks associated with abortive infection attempts that stimulate a rice defense response (Fig. 3, A and B). Transmission electron microscopy and live-cell imaging of rice leaf sheath infections by Δ*sep3* mutants confirmed the inability of appressoria from septin mutants to rupture plant cuticles efficiently (Fig. 3, C and D). All septin mutant phenotypes were complemented by reintroduction of either a wild-type allele or the corresponding septin-GFP fusion (fig. S10).

To understand the nature of the cortical F-actin network in appressoria, we decided to investigate plasma membrane linkages at the appressorium base. It has been suggested that some F-actin–plasma membrane linkages may occur via ezrin, radixin, moesin (ERM) proteins, which contain a C-terminal actin-binding domain and an N-terminal ERM domain that binds transmembrane proteins, such as integrins (*21*). We identified a putative ERM protein-encoding gene in *M. oryzae*, *TEA1* (which showed 61% identity to *S. pombe* Tea1), and found that Tea1-GFP localized as a punctate ring in the appressorium, colocated with the F-actin and septin networks (Fig. 4A and fig. S11B). By contrast, in a Δ*sep5* mutant, Tea1-GFP was mislocalized (Fig. 4A and fig. S11E). Phosphorylation of ERM proteins is potentiated by phosphatidylinositol (PtdIns)–4,5-bisphosphate binding (*22*). Yeast septins, for example, associate with PtdIns-4-phosphate and PtdIns-4,5-bisphosphate via an N-terminal polybasic domain (*23*, *24*). We identified the *M. oryzae* PtdIns-4-kinase–encoding gene, *STT4* (showing 53% identity to *S. cerevisiae STT4*), and the PtdIns-4-phosphate-5-kinase–encoding gene, *MSS4* (64% identity), and found that Stt4-GFP and Mss4-GFP localized to the appressorium pore, bounded by F-actin and the septin ring (Fig. 4B). To test

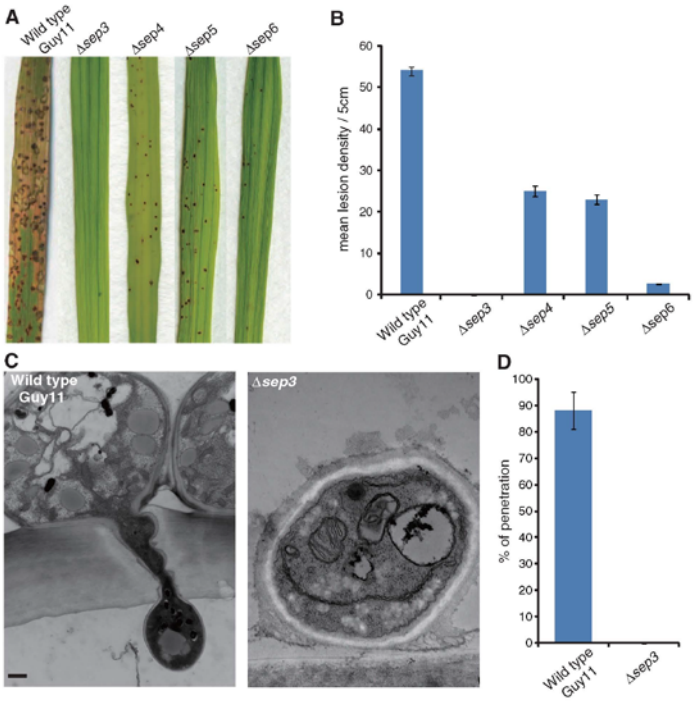

Fig. 3. *M. oryzae* septin mutants are unable to cause rice blast disease. (**A**) Targeted deletion of septin genes resulted in loss of pathogenicity on susceptible rice cultivar CO-39. The Δ*sep3* mutant caused no disease symptoms; Δ*sep4*, Δ*sep5*, and Δ*sep6* mutants elicited necrotic flecks because of abortive infection attempts. Septin mutants did not produce spreading disease lesions observed in the isogenic wild-type Guy11. (**B**) Bar chart shows frequency of disease lesions or necrotic flecks per 5 cm^2 of leaf surface (n = 30 plants) (mean ± SD, three experiments), reflecting frequency of penetration attempts. (**C**) Transmission electron micrographs of transverse section of wild-type (24 hours) and Δ*sep3* mutant appressoria (36 hours) during leaf infection. No penetration pegs were observed in Δ*sep3* mutants. Scale bar, 2 μm. (**D**) Bar chart showing frequency of rice epidermal cell rupture at 400 infection sites, 36 hours after conidial germination in wild type (Guy11) and Δ*sep3* mutants (mean ± SD, three experiments).

whether *M. oryzae* septins associated with membrane domains enriched in phosphoinositides, we deleted the N-terminal polybasic domain of *M. oryzae* Sep5 and expressed the resulting Sep5Δpb-GFP fusion protein in a Δ*sep5* mutant. The Sep5Δpb-GFP formed normal septin rings at hyphal septa or the neck of the nascent appressorium, demonstrating that stability of the septin was unaffected by deletion of the polybasic domain (Fig. 4C). However, the septin ring at the base of the appressorium did not form (Fig. 4C). We conclude that septin-PtdIns interactions and ERM protein-actin linkages occur at the appressorium pore. *M. oryzae* Chm1-GFP also localized to the appressorium pore (Fig. 4D and fig. S11, A and F), consistent with a role in septin phosphorylation (*25*).

We reasoned that, as well as scaffolding F-actin, the septin ring might also act as a diffusion barrier to constrain lateral diffusion of membrane-associated proteins involved in plant infection. Septin rings are known, for example, to act as diffusion barriers at the mother bud neck in *S. cerevisiae* (*26*, *27*). We decided to test whether *M. oryzae* septins affect distribution of proteins potentially involved in penetration peg development. Bin-amphiphysin-Rvs (BAR) domain proteins have been shown to form oligomeric scaffolds involved in membrane curvature (*28*). Whereas F-BAR proteins are well known to play roles in membrane invagination during endocytosis, the inverse BAR (I-BAR) proteins are involved in negative membrane curvature leading to cellular protrusions (*28*). Because emergence of a penetration hypha from the appressorium requires extreme negative membrane curvature (*2*, *29*), we decided to ask whether septins play a role in I-BAR protein localization. *M. oryzae* Rvs167 contains an I-BAR domain, showing 75% identity to *S. cerevisiae* Rvs167p. We found that Rvs167-GFP localized to the center of the appressorium pore, before penetration peg emergence. However, distribution of Rvs167-GFP was disrupted in a Δ*sep5* mutant (Fig. 4E and fig. S11, C and G). I-BAR proteins are proposed to link curved membrane structures to polymerization of cortical F-actin via nonspecific electrostatic interactions (*30*) mediated by Src homology 3 (SH3) domains of I-BAR proteins and components of the Wiskott-Aldrich syndrome protein (WASP)/WASP-family verprolin-homologous protein (WAVE) complex (*31*). We isolated a WASP/Arp2/3 complex component, Las17 (*32*), homologous to Las17p of *S. cerevisiae*. *M. oryzae* Las17-GFP localized to the base of the appressorium, bounded by the septin ring (Fig. 4F), whereas in a Δ*sep5* mutant Las17-GFP localization was disrupted, with the protein distributed diffusely in the cytoplasm and plasma membrane (Fig. 4F and fig. S11, D and H).

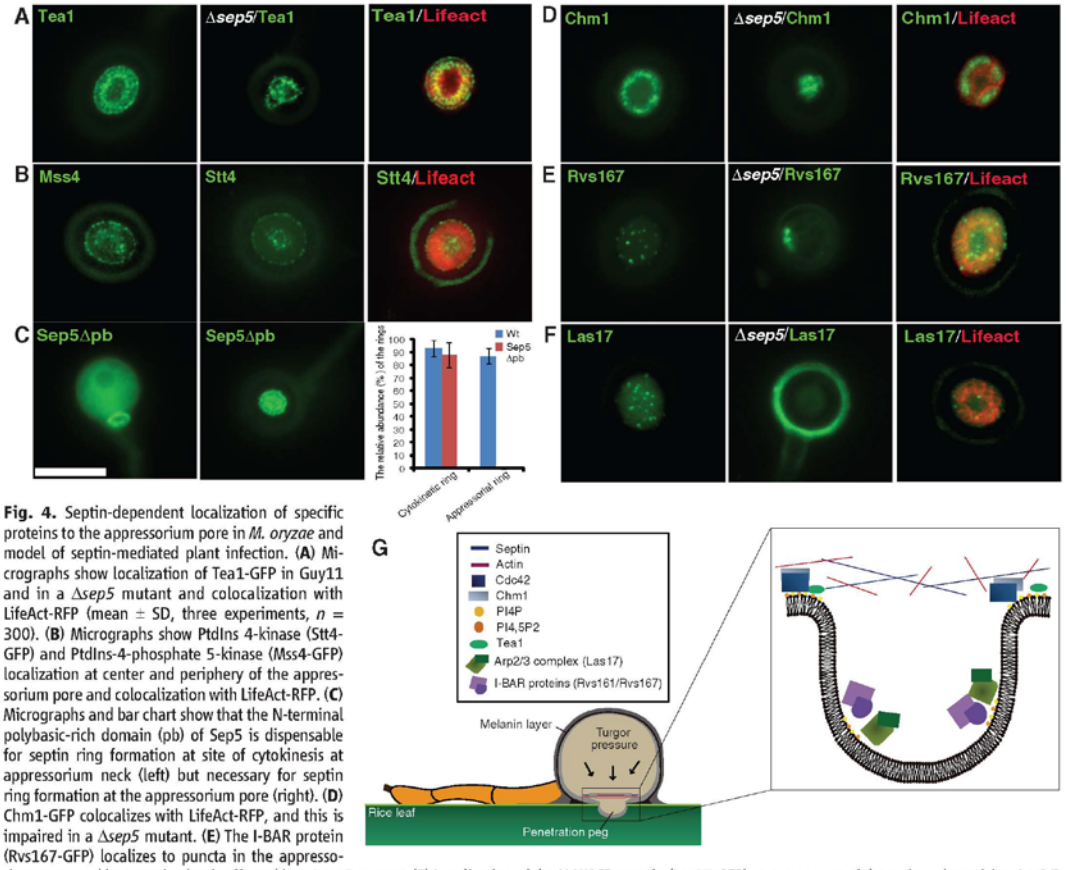

Fig. 4. Septin-dependent localization of specific proteins to the appressorium pore in *M. oryzae* and model of septin-mediated plant infection. **(A)** Micrographs show localization of Tea1-GFP in Guy11 and in a Δ*sep5* mutant and colocalization with LifeAct-RFP (mean ± SD, three experiments, n = 300). **(B)** Micrographs show PtdIns 4-kinase (Stt4-GFP) and PtdIns-4-phosphate 5-kinase (Mss4-GFP) localization at center and periphery of the appressorium pore and colocalization with LifeAct-RFP. **(C)** Micrographs and bar chart show that the N-terminal polybasic-rich domain (pb) of Sep5 is dispensable for septin ring formation at site of cytokinesis at appressorium neck (left) but necessary for septin ring formation at the appressorium pore (right). **(D)** Chm1-GFP colocalizes with LifeAct-RFP, and this is impaired in a Δ*sep5* mutant. **(E)** The I-BAR protein (Rvs167-GFP) localizes to puncta in the appressorium pore, and its organization is affected in a Δ*sep5* mutant. **(F)** Localization of the N-WASP protein (Las17-GFP), a component of the actin-polymerizing Arp2/3 complex, to the center of the appressorium pore septin ring and impairment of its localization in a Δ*sep5* mutant. Scale bar, 10 μm. **(G)** Model to show septin-mediated rice leaf infection by *M. oryzae*.

On the basis of the evidence presented in this report, we propose that appressoria of the rice blast fungus infect plants by using a septin-dependent mechanism summarized in Fig. 4G. In this model, isotropic expansion of the pressurized appressorium is directed into mechanical force at the base of the infection cell. This is dependent on assembly of an extensive toroidal F-actin network at the appressorium pore to provide cortical rigidity at the initially wall-less region of the appressorium. Septins organize the actin network, making direct phosphoinositide linkages to the plasma membrane and facilitating the action of ERM proteins, such as Tea1, which link cortical F-actin to the membrane. The septin ring also acts as a diffusion barrier to ensure localization of proteins, such as the Rvs167 I-BAR protein, and the WASP/WAVE complex involved in membrane curvature at the tip of the emerging penetration peg and F-actin polymerization (Fig. 4G). In this way, the rice blast fungus extends a rigid penetration peg that ruptures the leaf cuticle and invades the host plant tissue.

References and Notes

1. J. C. de Jong, B. J. McCormack, N. Smirnoff, N. J. Talbot, *Nature* **389**, 244 (1997).
2. T. M. Bourett, R. J. Howard, *Can. J. Bot.* **68**, 329 (1990).
3. C. Bechinger *et al.*, *Science* **285**, 1896 (1999).
4. A. Berepiki, A. Lichius, J. Y. Shoji, J. Tilsner, N. D. Read, *Eukaryot. Cell* **9**, 547 (2010).
5. A. S. Gladfelter, L. Kozubowski, T. R. Zyla, D. J. Lew, *J. Cell Sci.* **118**, 1617 (2005).
6. R. Lindsey, M. Momany, *Curr. Opin. Microbiol.* **9**, 559 (2006).
7. L. M. Douglas, F. J. Alvarez, C. McCreary, J. B. Konopka, *Eukaryot. Cell* **4**, 1503 (2005).
8. E. T. Spiliotis, W. J. Nelson, *J. Cell Sci.* **119**, 4 (2006).
9. L. H. Hartwell, *Exp. Cell Res.* **69**, 265 (1971).
10. D. G. Saunders, Y. F. Dagdas, N. J. Talbot, *Plant Cell* **22**, 2417 (2010).
11. G. A. Castillon *et al.*, *Curr. Biol.* **13**, 654 (2003).
12. D. G. Saunders, S. J. Aves, N. J. Talbot, *Plant Cell* **22**, 497 (2010).
13. C. Veneault-Fourrey, M. Barooah, M. Egan, G. Wakley, N. J. Talbot, *Science* **312**, 580 (2006).
14. E. Bi *et al.*, *J. Cell Biol.* **142**, 1301 (1998).
15. A. E. Adams, D. I. Johnson, R. M. Longnecker, B. F. Sloat, J. R. Pringle, *J. Cell Biol.* **111**, 131 (1990).
16. I. Sagot, S. K. Klee, D. Pellman, *Nat. Cell Biol.* **4**, 42 (2002).
17. M. Versele, J. Thorner, *J. Cell Biol.* **164**, 701 (2004).
18. L. Li, C. Xue, K. Bruno, M. Nishimura, J. R. Xu, *Mol. Plant Microbe Interact.* **17**, 547 (2004).
19. J. R. Xu, C. J. Staiger, J. E. Hamer, *Proc. Natl. Acad. Sci. U.S.A.* **95**, 12713 (1998).
20. G. Park, C. Xue, L. Zheng, S. Lam, J. R. Xu, *Mol. Plant Microbe Interact.* **15**, 183 (2002).
21. J. Gilden, M. F. Krummel, *Cytoskeleton* **67**, 477 (2010).
22. B. T. Fievet *et al.*, *J. Cell Biol.* **164**, 653 (2004).
23. A. Casamayor, M. Snyder, *Mol. Cell. Biol.* **23**, 2762 (2003).
24. M. Onishi *et al.*, *Mol. Cell. Biol.* **30**, 2057 (2010).
25. M. Iwase *et al.*, *Mol. Biol. Cell* **17**, 1110 (2006).
26. Y. Barral, V. Mermall, M. S. Mooseker, M. Snyder, *Mol. Cell* **5**, 841 (2000).
27. P. A. Takizawa, J. L. DeRisi, J. E. Wilhelm, R. D. Vale, *Science* **290**, 341 (2000).
28. H. Zhao, A. Pykäläinen, P. Lappalainen, *Curr. Opin. Cell Biol.* **23**, 14 (2011).
29. M. J. Egan, Z. Y. Wang, M. A. Jones, N. Smirnoff, N. J. Talbot, *Proc. Natl. Acad. Sci. U.S.A.* **104**, 11772 (2007).
30. P. K. Mattila *et al.*, *J. Cell Biol.* **176**, 953 (2007).
31. T. Takenawa, S. Suetsugu, *Nat. Rev. Mol. Cell Biol.* **8**, 37 (2007).
32. A. Madania *et al.*, *Mol. Biol. Cell* **10**, 3521 (1999).

Acknowledgments: We thank J. Thorner (UC Berkeley) for providing yeast septin mutants, M. Momany for critical reading of the manuscript and valuable discussions, H. Florence from Exeter Mass Spectrometry facility, and M. Schuster from the Exeter Bio-imaging Centre. This work was funded by a Halpin Scholarship for rice blast research to Y.F.D. and grants to N.J.T. from the Biotechnology and Biological Sciences Research Council and the European Research Council. K.Y. is funded by the Kyoto University Foundation. Accession numbers are provided in supplementary materials.

Supplementary Materials

www.sciencemag.org/cgi/content/full/336/6088/1590/DC1
Materials and Methods
Figs. S1 to S12
Tables S1 and S2
References (*33*–*40*)
Movie S1

4 April 2012; accepted 15 May 2012
10.1126/science.1222934

The *lac* Repressor Displays Facilitated Diffusion in Living Cells

Petter Hammar, Prune Leroy, Anel Mahmutovic, Erik G. Marklund, Otto G. Berg, Johan Elf*

Transcription factors (TFs) are proteins that regulate the expression of genes by binding sequence-specific sites on the chromosome. It has been proposed that to find these sites fast and accurately, TFs combine one-dimensional (1D) sliding on DNA with 3D diffusion in the cytoplasm. This facilitated diffusion mechanism has been demonstrated in vitro, but it has not been shown experimentally to be exploited in living cells. We have developed a single-molecule assay that allows us to investigate the sliding process in living bacteria. Here we show that the *lac* repressor slides 45 ± 10 base pairs on chromosomal DNA and that sliding can be obstructed by other DNA-bound proteins near the operator. Furthermore, the repressor frequently (>90%) slides over its natural $lacO_1$ operator several times before binding. This suggests a trade-off between rapid search on nonspecific sequences and fast binding at the specific sequence.

Transcription factors (TFs) have evolved to rapidly find their specific binding sites among millions of nonspecific sites on chromosomal DNA (*1*). In 1970, Riggs *et al.* showed that in vitro the *lac* repressor (LacI) finds its operator apparently faster than the rate limit for three-dimensional (3D) diffusion (*2*). These experiments were explained by the facilitated diffusion theory (*3*, *4*), which posits that TFs search for their binding sites through a combination of 3D diffusion in the cytoplasm and 1D diffusion (sliding) along the DNA. The sliding effectively extends the target region to the sliding distance, which facilitates the search process. Since then, sliding on DNA has been studied in various in vitro assays (*5*–*8*), including direct observations in single-molecule experiments (*9*, *10*). However, the physiological relevance of the long sliding distances observed at low salt concentrations in vitro has been questioned (*11*, *12*). This is because the high intracellular concentrations of salt and nucleoid proteins are expected to reduce sliding distances (*13*). Therefore, whether facilitated diffusion is used in living cells, and if so, how far a TF slides on chromosomal DNA, remain unanswered questions.

Single-molecule imaging provides the time resolution necessary to study TF binding kinetics in living cells. Using a yellow fluorescent protein labeled LacI in *Escherichia coli* cells, we developed an assay for measuring the search time based on the distinction between localized and diffuse fluorescence signals (*14*). On a 4-s time scale, individual operator-bound LacI-Venus molecules appear as diffraction-limited spots over the background of freely diffusing molecules (Fig. 1A). By measuring the average number of fluorescent spots per cell as a function of time after removing the inducer isopropyl-β-D-1-thiogalactopyranoside (IPTG) (fig. S7), the kinetics of TF binding to an individual operator site in the *E. coli* chromosome can be monitored at a time resolution of seconds (Fig. 1B) (*15*). The fusion to Venus prevents LacI from forming tetramers, thus removing the possibility that the protein will loop DNA. The accuracy of the assay depends on limiting the total number of repressors to three to five molecules per cell (*14*, *16*). This can be achieved (fig. S6) by increasing the autorepression through a single artificial $lacO_{sym}$ operator site partially overlapping the repressor coding region (Fig. 1B, inset).

When we measured the association rate in the strain with a single $lacO_{sym}$ (JE101), we found that it took an average time of 56 ± 2 s (SEM) for any of the three to five fully active (supplementary text) LacI-Venus dimers to bind the operator site (Fig. 1B). This implies that the time required

Department of Cell and Molecular Biology, Science for Life Laboratory, Uppsala University, Sweden.

*To whom correspondence should be addressed. E-mail: johan.elf@icm.uu.se

Acknowledgements

First, I would like to thank Prof. Gero Steinberg and the University of Exeter for providing me the opportunity to study and work towards the PhD and I am very grateful to the University of Exeter and RKT for providing financial support during my studies.

Again, I would like to thank all co-authors who were involved in my projects.

I thank Ms Tina Schrader, Dr. Markus Islinger and Dr. Michael Schrader for their time and effort in performing the organelle fractionation experiment.

I thank all lab members for their intellectual and technical support.

I thank Marta Staff, Anna Shiel, Dr. Adokiye Berepiki and Prof. Gero Steinberg for their time spent in correcting my dissertation.

I also thank Dr. Helen Dawe for her help, suggestions and mental support.

In a special way I would like to thank my lab friends, Ania and Marta for their support, understanding and all the great laughs we shared together.

...

In a very special way I would like to thank my parents and my parents-in-law for their faith in me, encouragements and endless love.

...

Finally, I would like to thank my Partner for all love, care, support, patience, great ideas and laughter. I have done this PhD thanks to You…

Bibliography

Abenza, J.F., Galindo, A., Pantazopoulou, A., Gil, C., de los Rios, V., and Penalva, M.A. (2010). *Aspergillus* RabB Rab5 integrates acquisition of degradative identity with the long distance movement of early endosomes. Mol Biol Cell *21*, 2756-2769.

Abenza, J.F., Pantazopoulou, A., Rodriguez, J.M., Galindo, A., and Penalva, M.A. (2009). Long-distance movement of *Aspergillus nidulans* early endosomes on microtubule tracks. Traffic *10*, 57-75.

Aizawa, H., Sekine, Y., Takemura, R., Zhang, Z., Nangaku, M., and Hirokawa, N. (1992). Kinesin family in murine central nervous system. J Cell Biol *119*, 1287-1296.

Akhmanova, A., and Hammer, J.A., 3rd. (2010). Linking molecular motors to membrane cargo. Curr Opin Cell Biol *22*, 479-487.

Al-Bassam, J., Cui, Y., Klopfenstein, D., Carragher, B.O., Vale, R.D., and Milligan, R.A. (2003). Distinct conformations of the kinesin Unc104 neck regulate a monomer to dimer motor transition. J Cell Biol *163*, 743-753.

Allen, R.D., Metuzals, J., Tasaki, I., Brady, S.T., and Gilbert, S.P. (1982). Fast axonal transport in squid giant axon. Science *218*, 1127-1129.

Andrews, D.L., Egan, J.D., Mayorga, M.E., and Gold, S.E. (2000). The *Ustilago maydis* ubc4 and ubc5 genes encode members of a MAP kinase cascade required for filamentous growth. Mol Plant Microbe Interact *13*, 781-786.

Apostol, I., Heinstein, P.F., and Low, P.S. (1989). Rapid Stimulation of an Oxidative Burst during Elicitation of Cultured Plant Cells: Role in Defense and Signal Transduction. Plant Physiol *90*, 109-116.

Baas, P.W., Deitch, J.S., Black, M.M., and Banker, G.A. (1988). Polarity orientation of microtubules in hippocampal neurons: uniformity in the axon and nonuniformity in the dendrite. Proc Natl Acad Sci U S A *85*, 8335-8339.

Bahn, Y.S., Xue, C., Idnurm, A., Rutherford, J.C., Heitman, J., and Cardenas, M.E. (2007). Sensing the environment: lessons from fungi. Nat Rev Microbiol *5*, 57-69.

Bananis, E., Murray, J.W., Stockert, R.J., Satir, P., and Wolkoff, A.W. (2000). Microtubule and motor-dependent endocytic vesicle sorting *in vitro*. J Cell Biol *151*, 179-186.

Bananis, E., Murray, J.W., Stockert, R.J., Satir, P., and Wolkoff, A.W. (2003). Regulation of early endocytic vesicle motility and fission in a reconstituted system. J Cell Sci *116*, 2749-2761.

Banuett, F. (1995). Genetics of *Ustilago maydis*, a fungal pathogen that induces tumors in maize. Annu Rev Genet *29*, 179-208.

Banuett, F., and Herskowitz, I. (1989). Different *a* alleles of *Ustilago maydis* are necessary for maintenance of filamentous growth but not for meiosis. Proc Natl Acad Sci U S A *86*, 5878-5882.

Banuett, F., and Herskowitz, I. (1994). Identification of fuz7, a *Ustilago maydis* MEK/MAPKK homolog required for a-locus-dependent and -independent steps in the fungal life cycle. Genes Dev *8*, 1367-1378.

Banuett, F., and Herskowitz, I. (1996). Discrete developmental stages during teliospore formation in the corn smut fungus, *Ustilago maydis*. Development *122*, 2965-2976.

Banuett, F., and Herskowitz, I. (2002). Bud morphogenesis and the actin and microtubule cytoskeletons during budding in the corn smut fungus, *Ustilago maydis*. Fungal Genet Biol *37*, 149-170.

Banuett, F., Quintanilla, R.H., Jr., and Reynaga-Pena, C.G. (2008). The machinery for cell polarity, cell morphogenesis, and the cytoskeleton in the Basidiomycete fungus *Ustilago maydis*-a survey of the genome sequence. Fungal Genet Biol *45 Suppl 1*, S3-S14.

Barkus, R.V., Klyachko, O., Horiuchi, D., Dickson, B.J., and Saxton, W.M. (2008). Identification of an axonal kinesin-3 motor for fast anterograde vesicle transport that facilitates retrograde transport of neuropeptides. Mol Biol Cell *19*, 274-283.

Bartnicki-Garcia, S. (1968). Cell wall chemistry, morphogenesis, and taxonomy of fungi. Annu Rev Microbiol *22*, 87-108.

Basse, C.W., and Steinberg, G. (2004). *Ustilago maydis*, model system for analysis of the molecular basis of fungal pathogenicity. Mol Plant Pathol *5*, 83-92.

Basse, C.W., Stumpferl, S., and Kahmann, R. (2000). Characterization of a *Ustilago maydis* gene specifically induced during the biotrophic phase: evidence for negative as well as positive regulation. Mol Cell Biol *20*, 329-339.

Baumann, S., Pohlmann, T., Jungbluth, M., Brachmann, A., and Feldbrügge, M. (2012). Kinesin-3 and dynein mediate microtubule-dependent co-transport of mRNPs and endosomes. J Cell Sci *125*, 2740-2752.

Becht, P., Konig, J., and Feldbrügge, M. (2006). The RNA-binding protein Rrm4 is essential for polarity in *Ustilago maydis* and shuttles along microtubules. J Cell Sci *119*, 4964-4973.

Becht, P., Vollmeister, E., and Feldbrügge, M. (2005). Role for RNA-binding proteins implicated in pathogenic development of *Ustilago maydis*. Eukaryot Cell *4*, 121-133.

Berepiki, A., Lichius, A., and Read, N.D. (2011). Actin organization and dynamics in filamentous fungi. Nat Rev Microbiol *9*, 876-887.

Bindschedler, L.V., Dewdney, J., Blee, K.A., Stone, J.M., Asai, T., Plotnikov, J., Denoux, C., Hayes, T., Gerrish, C., Davies, D.R., Ausubel, F.M., and Bolwell, G.P. (2006). Peroxidase-dependent apoplastic oxidative burst in *Arabidopsis* required for pathogen resistance. Plant J *47*, 851-863.

Birnboim, H.C. (1983). A rapid alkaline extraction method for the isolation of plasmid DNA. Methods Enzymol *100*, 243-255.

Birnboim, H.C., and Doly, J. (1979). A rapid alkaline extraction procedure for screening recombinant plasmid DNA. Nucleic Acids Res *7*, 1513-1523.

Blatner, N.R., Wilson, M.I., Lei, C., Hong, W., Murray, D., Williams, R.L., and Cho, W. (2007). The structural basis of novel endosome anchoring activity of KIF16B kinesin. EMBO J *26*, 3709-3719.

Bölker, M., Genin, S., Lehmler, C., and Kahmann, R. (1995). Genetic regulation of mating and dimorphism in *Ustilago maydis*. Canadian Journal of Botany *73*, 320-325.

Bölker, M., Urban, M., and Kahmann, R. (1992). The *a* mating type locus of *U. maydis* specifies cell signaling components. Cell *68*, 441-450.

Bottin, A., Kamper, J., and Kahmann, R. (1996). Isolation of a carbon source-regulated gene from *Ustilago maydis*. Mol Gen Genet *253*, 342-352.

Boyce, K.J., Chang, H., D'Souza, C.A., and Kronstad, J.W. (2005). An *Ustilago maydis* septin is required for filamentous growth in culture and for full symptom development on maize. Eukaryot Cell *4*, 2044-2056.

Boyle, J.S., and Lew, A.M. (1995). An inexpensive alternative to glassmilk for DNA purification. Trends Genet *11*, 8.

Brachmann, A., König, J., Julius, C., and Feldbrügge, M. (2004). A reverse genetic approach for generating gene replacement mutants in *Ustilago maydis*. Mol Genet Genomics *272*, 216-226.

Brachmann, A., Schirawski, J., Muller, P., and Kahmann, R. (2003). An unusual MAP kinase is required for efficient penetration of the plant surface by *Ustilago maydis*. EMBO J *22*, 2199-2210.

Brachmann, A., Weinzierl, G., Kämper, J., and Kahmann, R. (2001). Identification of genes in the *bW/bE* regulatory cascade in *Ustilago maydis*. Mol Microbiol *42*, 1047-1063.

Bradford, M.M. (1976). A rapid and sensitive method for the quantitation of microgram quantities of protein utilizing the principle of protein-dye binding. Anal Biochem *72*, 248-254.

Brand, A. (2012). Hyphal growth in human fungal pathogens and its role in virulence. Int J Microbiol *2012*, 517529.

Bravo, J., Karathanassis, D., Pacold, C.M., Pacold, M.E., Ellson, C.D., Anderson, K.E., Butler, P.J., Lavenir, I., Perisic, O., Hawkins, P.T., Stephens, L., and Williams, R.L. (2001). The crystal structure of the PX domain from p40(phox) bound to phosphatidylinositol 3-phosphate. Mol Cell *8*, 829-839.

Brefort, T., Doehlemann, G., Mendoza-Mendoza, A., Reissmann, S., Djamei, A., and Kahmann, R. (2009). *Ustilago maydis* as a Pathogen. Annu Rev Phytopathol *47*, 423-445.

Bucci, C., Parton, R.G., Mather, I.H., Stunnenberg, H., Simons, K., Hoflack, B., and Zerial, M. (1992). The small GTPase rab5 functions as a regulatory factor in the early endocytic pathway. Cell *70*, 715-728.

Cai, D., McEwen, D.P., Martens, J.R., Meyhofer, E., and Verhey, K.J. (2009). Single molecule imaging reveals differences in microtubule track selection between Kinesin motors. PLoS Biol *7*, e1000216.

Campanoni, P., and Blatt, M.R. (2007). Membrane trafficking and polar growth in root hairs and pollen tubes. J Exp Bot *58*, 65-74.

Caviston, J.P., and Holzbaur, E.L. (2006). Microtubule motors at the intersection of trafficking and transport. Trends Cell Biol *16*, 530-537.

Christensen, J.J. (1963). Corn smut caused by *Ustilago maydis.* In *American Phytopathology Society Monograph No. 2*, 1-41.

Christoforidis, S., McBride, H.M., Burgoyne, R.D., and Zerial, M. (1999). The Rab5 effector EEA1 is a core component of endosome docking. Nature *397*, 621-625.

Clarke, M., Kohler, J., Heuser, J., and Gerisch, G. (2002). Endosome fusion and microtubule-based dynamics in the early endocytic pathway of *Dictyostelium*. Traffic *3*, 791-800.

Cosker, K.E., Courchesne, S.L., and Segal, R.A. (2008). Action in the axon: generation and transport of signaling endosomes. Curr Opin Neurobiol *18*, 270-275.

Couturier, M., Navarro, D., Olive, C., Chevret, D., Haon, M., Favel, A., Lesage-Meessen, L., Henrissat, B., Coutinho, P.M., and Berrin, J.G. (2012). Post-genomic analyses of fungal lignocellulosic biomass degradation reveal the unexpected potential of the plant pathogen *Ustilago maydis*. BMC Genomics *13*, 57.

Dai, Y., Taru, H., Deken, S.L., Grill, B., Ackley, B., Nonet, M.L., and Jin, Y. (2006). SYD-2 Liprin-alpha organizes presynaptic active zone formation through ELKS. Nat Neurosci *9*, 1479-1487.

Daudi, A., Cheng, Z., O'Brien, J.A., Mammarella, N., Khan, S., Ausubel, F.M., and Bolwell, G.P. (2012). The apoplastic oxidative burst peroxidase in *Arabidopsis* is a major component of pattern-triggered immunity. Plant Cell *24*, 275-287.

Day, P.R., Anagnostakis, S.L., and Puhalla, J.E. (1971). Pathogenicity resulting from mutation at the *b* locus of *Ustilago maydis*. Proc Natl Acad Sci U S A *68*, 533-535.

de Hoop, M.J., Huber, L.A., Stenmark, H., Williamson, E., Zerial, M., Parton, R.G., and Dotti, C.G. (1994). The involvement of the small GTP-binding protein Rab5a in neuronal endocytosis. Neuron *13*, 11-22.

de Jonge, R., Bolton, M.D., and Thomma, B.P. (2011). How filamentous pathogens co-opt plants: the ins and outs of fungal effectors. Curr Opin Plant Biol *14*, 400-406.

Dean, R., Van Kan, J.A., Pretorius, Z.A., Hammond-Kosack, K.E., Di Pietro, A., Spanu, P.D., Rudd, J.J., Dickman, M., Kahmann, R., Ellis, J., and Foster, G.D. (2012). The Top 10 fungal pathogens in molecular plant pathology. Mol Plant Pathol *13*, 414-430.

Desai, A., and Mitchison, T.J. (1997). Microtubule polymerization dynamics. Annu Rev Cell Dev Biol *13*, 83-117.

Djamei, A., Schipper, K., Rabe, F., Ghosh, A., Vincon, V., Kahnt, J., Osorio, S., Tohge, T., Fernie, A.R., Feussner, I., Feussner, K., Meinicke, P., Stierhof, Y.D., Schwarz, H., Macek, B., Mann, M., and Kahmann, R. (2011). Metabolic priming by a secreted fungal effector. Nature *478*, 395-398.

Doehlemann, G., Reissmann, S., Assmann, D., Fleckenstein, M., and Kahmann, R. (2011). Two linked genes encoding a secreted effector and a membrane protein are essential for *Ustilago maydis*-induced tumour formation. Mol Microbiol *81*, 751-766.

Doehlemann, G., van der Linde, K., Assmann, D., Schwammbach, D., Hof, A., Mohanty, A., Jackson, D., and Kahmann, R. (2009). Pep1, a secreted effector protein of *Ustilago maydis*, is required for successful invasion of plant cells. PLoS Pathog *5*, e1000290.

Doehlemann, G., Wahl, R., Horst, R.J., Voll, L.M., Usadel, B., Poree, F., Stitt, M., Pons-Kuhnemann, J., Sonnewald, U., Kahmann, R., and Kämper, J. (2008b). Reprogramming a maize plant: transcriptional and metabolic changes induced by the fungal biotroph *Ustilago maydis*. Plant J *56*, 181-195.

Doehlemann, G., Wahl, R., Vranes, M., de Vries, R.P., Kämper, J., and Kahmann, R. (2008a). Establishment of compatibility in the *Ustilago maydis*/maize pathosystem. J Plant Physiol *165*, 29-40.

Dowler, S., Kular, G., and Alessi, D.R. (2002). Protein lipid overlay assay. Sci STKE *2002*, pl6.
Driscoll, P.C. (2001). Solving the FYVE domain--PtdIns(3)P puzzle. Nat Struct Biol *8*, 287-290.

Driskell, O.J., Mironov, A., Allan, V.J., and Woodman, P.G. (2007). Dynein is required for receptor sorting and the morphogenesis of early endosomes. Nat Cell Biol *9*, 113-120.

Du, C., and Chong, K. (2011). ARF-GTPase activating protein mediates auxin influx carrier AUX1 early endosome trafficking to regulate auxin dependent plant development. Plant Signal Behav *6*, 1644-1646.

Durrenberger, F., Wong, K., and Kronstad, J.W. (1998). Identification of a cAMP-dependent protein kinase catalytic subunit required for virulence and morphogenesis in *Ustilago maydis*. Proc Natl Acad Sci U S A *95*, 5684-5689.

Egan, M.J., McClintock, M.A., and Reck-Peterson, S.L. (2012b). Microtubule-based transport in filamentous fungi. Curr Opin Microbiol *15*, 637-645.

Egan, M.J., Tan, K., and Reck-Peterson, S.L. (2012a). Lis1 is an initiation factor for dynein-driven organelle transport. J Cell Biol *197*, 971-982.

Feldbrügge, M., Kämper, J., Steinberg, G., and Kahmann, R. (2004). Regulation of mating and pathogenic development in *Ustilago maydis*. Curr Opin Microbiol *7*, 666-672.

Feldbrügge, M., Zarnack, K., Vollmeister, E., Baumann, S., Koepke, J., Konig, J., Munsterkotter, M., and Mannhaupt, G. (2008). The posttranscriptional machinery of *Ustilago maydis*. Fungal Genet Biol *45 Suppl 1*, S40-46.

Fischer-Parton, S., Parton, R.M., Hickey, P.C., Dijksterhuis, J., Atkinson, H.A., and Read, N.D. (2000). Confocal microscopy of FM4-64 as a tool for analysing endocytosis and vesicle trafficking in living fungal hyphae. J Microsc *198*, 246-259.

Fischer von Mollard, G., Mignery, G.A., Baumert, M., Perin, M.S., Hanson, T.J., Burger, P.M., Jahn, R., and Südhof, T.C. (1990). rab3 is a small GTP-binding protein exclusively localized to synaptic vesicles. Proc Natl Acad Sci U S A *87*, 1988-1992.

Fisher, M.C., Henk, D.A., Briggs, C.J., Brownstein, J.S., Madoff, L.C., McCraw, S.L., and Gurr, S.J. (2012). Emerging fungal threats to animal, plant and ecosystem health. Nature *484*, 186-194.

Freitag, J., Lanver, D., Bohmer, C., Schink, K.O., Bölker, M., and Sandrock, B. (2011). Septation of infectious hyphae is critical for appressoria formation and virulence in the smut fungus *Ustilago maydis*. PLoS Pathog *7*, e1002044.

Froeliger, E.H., and Leong, S.A. (1991). The a mating-type alleles of *Ustilago maydis* are idiomorphs. Gene *100*, 113-122.

Frost, A., Unger, V.M., and De Camilli, P. (2009). The BAR domain superfamily: membrane-molding macromolecules. Cell *137*, 191-196.

Fuchs, F., and Westermann, B. (2005). Role of Unc104/KIF1-related motor proteins in mitochondrial transport in *Neurospora crassa*. Mol Biol Cell *16*, 153-161.

Fuchs, U., Hause, G., Schuchardt, I., and Steinberg, G. (2006). Endocytosis is essential for pathogenic development in the corn smut fungus *Ustilago maydis*. Plant Cell *18*, 2066-2081.

Fuchs, U., Manns, I., and Steinberg, G. (2005a). Microtubules are dispensable for the initial pathogenic development but required for long-distance hyphal growth in the corn smut fungus *Ustilago maydis*. Mol Biol Cell *16*, 2746-2758.

Fuchs, U., and Steinberg, G. (2005b). Endocytosis in the plant-pathogenic fungus *Ustilago maydis*. Protoplasma *226*, 75-80.

Fukushima, N., Furuta, D., Hidaka, Y., Moriyama, R., and Tsujiuchi, T. (2009). Post-translational modifications of tubulin in the nervous system, vol. 109: Blackwell Publishing Ltd, 683-693.

Garcia-Muse, T., Steinberg, G., and Perez-Martin, J. (2003). Pheromone-induced G2 arrest in the phytopathogenic fungus *Ustilago maydis*. Eukaryot Cell *2*, 494-500.

Garrido, E., and Perez-Martin, J. (2003). The crk1 gene encodes an Ime2-related protein that is required for morphogenesis in the plant pathogen *Ustilago maydis*. Mol Microbiol *47*, 729-743.

Geldner, N., Hyman, D.L., Wang, X., Schumacher, K., and Chory, J. (2007). Endosomal signaling of plant steroid receptor kinase BRI1. Genes Dev *21*, 1598-1602.

Geli, M.I., and Riezman, H. (1998). Endocytic internalization in yeast and animal cells: similar and different. J Cell Sci *111 (Pt 8)*, 1031-1037.

Gillissen, B., Bergemann, J., Sandmann, C., Schroeer, B., Bölker, M., and Kahmann, R. (1992). A two-component regulatory system for self/non-self recognition in *Ustilago maydis*. Cell *68*, 647-657.

Gillooly, D.J., Morrow, I.C., Lindsay, M., Gould, R., Bryant, N.J., Gaullier, J.M., Parton, R.G., and Stenmark, H. (2000). Localization of phosphatidylinositol 3-phosphate in yeast and mammalian cells. EMBO J *19*, 4577-4588.

Gillooly, D.J., Simonsen, A., and Stenmark, H. (2001). Cellular functions of phosphatidylinositol 3-phosphate and FYVE domain proteins. Biochem J *355*, 249-258.

Gold, S., Duncan, G., Barrett, K., and Kronstad, J. (1994). cAMP regulates morphogenesis in the fungal pathogen *Ustilago maydis*. Genes Dev *8*, 2805-2816.

Gold, S.E., Brogdon, S.M., Mayorga, M.E., and Kronstad, J.W. (1997). The *Ustilago maydis* regulatory subunit of a cAMP-dependent protein kinase is required for gall formation in maize. Plant Cell *9*, 1585-1594.

Goldstein, L.S., and Yang, Z. (2000). Microtubule-based transport systems in neurons: the roles of kinesins and dyneins. Annu Rev Neurosci *23*, 39-71.

Gorvel, J.P., Chavrier, P., Zerial, M., and Gruenberg, J. (1991). rab5 controls early endosome fusion *in vitro*. Cell *64*, 915-925.

Gould, G.W., and Lippincott-Schwartz, J. (2009). New roles for endosomes: from vesicular carriers to multi-purpose platforms. Nat Rev Mol Cell Biol *10*, 287-292.

Gow, N.A., Brown, A.J., and Odds, F.C. (2002). Fungal morphogenesis and host invasion. Curr Opin Microbiol *5*, 366-371.

Hall, D.H., and Hedgecock, E.M. (1991). Kinesin-related gene unc-104 is required for axonal transport of synaptic vesicles in *C. elegans*. Cell *65*, 837-847.

Hammond, J.W., Cai, D., Blasius, T.L., Li, Z., Jiang, Y., Jih, G.T., Meyhofer, E., and Verhey, K.J. (2009). Mammalian Kinesin-3 motors are dimeric *in vivo* and move by processive motility upon release of autoinhibition. PLoS Biol *7*, e72.

Hammond, J.W., Huang, C.F., Kaech, S., Jacobson, C., Banker, G., and Verhey, K.J. (2010). Posttranslational modifications of tubulin and the polarized transport of kinesin-1 in neurons. Mol Biol Cell *21*, 572-583.

Han, G., Liu, B., Zhang, J., Zuo, W., Morris, N.R., and Xiang, X. (2001). The *Aspergillus* cytoplasmic dynein heavy chain and NUDF localize to microtubule ends and affect microtubule dynamics. Curr Biol *11*, 719-724.

Hanahan, D. (1985). Techniques for transformation of *E. coli*. In DNA cloning: A Practical Approach. (Ed. D. M. Glover) Oxford: IRL Press *1*, 49–78.

Harris, S.D. (2006). Cell polarity in filamentous fungi: shaping the mold. Int Rev Cytol *251*, 41-77.

Harris, S.D. (2009b). The Spitzenkorper: a signalling hub for the control of fungal development? Mol Microbiol *73*, 733-736.

Harris, S.D. (2011). Hyphal morphogenesis: an evolutionary perspective. Fungal Biol *115*, 475-484.

Harris, S.D., Read, N.D., Roberson, R.W., Shaw, B., Seiler, S., Plamann, M., and Momany, M. (2005). Polarisome meets spitzenkorper: microscopy, genetics, and genomics converge. Eukaryot Cell *4*, 225-229.

Harris, S.D., Turner, G., Meyer, V., Espeso, E.A., Specht, T., Takeshita, N., and Helmstedt, K. (2009a). Morphology and development in *Aspergillus nidulans*: a complex puzzle. Fungal Genet Biol *46 Suppl 1*, S82-S92.

Hartmann, H.A., Kahmann, R., and Bölker, M. (1996). The pheromone response factor coordinates filamentous growth and pathogenicity in *Ustilago maydis*. EMBO J *15*, 1632-1641.
Hartmann, H.A., Krüger, J., Lottspeich, F., and Kahmann, R. (1999). Environmental signals controlling sexual development of the corn Smut fungus *Ustilago maydis* through the transcriptional regulator Prf1. Plant Cell *11*, 1293-1306.

Haun, R.S., Serventi, I.M., and Moss, J. (1992). Rapid, reliable ligation-independent cloning of PCR products using modified plasmid vectors. Biotechniques *13*, 515-518.

Hayes, S., Chawla, A., and Corvera, S. (2002). TGF beta receptor internalization into EEA1-enriched early endosomes: role in signaling to Smad2. J Cell Biol *158*, 1239-1249.

Heath, I.B., Gupta, G., and Bai, S. (2000). Plasma membrane-adjacent actin filaments, but not microtubules, are essential for both polarization and hyphal tip morphogenesis in Saprolegnia ferax and *Neurospora crassa*. Fungal Genet Biol *30*, 45-62.

Heath, I.B., and Steinberg, G. (1999). Mechanisms of hyphal tip growth: tube dwelling amebae revisited. Fungal Genet Biol *28*, 79-93.

Heidemann, S.R., Landers, J.M., and Hamborg, M.A. (1981). Polarity orientation of axonal microtubules. J Cell Biol *91*, 661-665.

Heimel, K., Scherer, M., Schuler, D., and Kämper, J. (2010b). The *Ustilago maydis* Clp1 protein orchestrates pheromone and b-dependent signaling pathways to coordinate the cell cycle and pathogenic development. Plant Cell *22*, 2908-2922.

Heimel, K., Scherer, M., Vranes, M., Wahl, R., Pothiratana, C., Schuler, D., Vincon, V., Finkernagel, F., Flor-Parra, I., and Kämper, J. (2010a). The transcription factor Rbf1 is the master regulator for b-mating type controlled pathogenic development in *Ustilago maydis*. PLoS Pathog *6*, e1001035.

Hemetsberger, C., Herrberger, C., Zechmann, B., Hillmer, M., and Doehlemann, G. (2012). The *Ustilago maydis* effector Pep1 suppresses plant immunity by inhibition of host peroxidase activity. PLoS Pathog *8*, e1002684.

Hibbett, D.S., Binder, M., Bischoff, J.F., Blackwell, M., Cannon, P.F., Eriksson, O.E., Huhndorf, S., James, T., Kirk, P.M., Lucking, R., Thorsten Lumbsch, H., Lutzoni, F., Matheny, P.B., McLaughlin, D.J., Powell, M.J., Redhead, S., Schoch, C.L., Spatafora, J.W., Stalpers, J.A., Vilgalys, R., Aime, M.C., Aptroot, A., Bauer, R., Begerow, D., Benny, G.L., Castlebury, L.A., Crous, P.W., Dai, Y.C., Gams, W., Geiser, D.M., Griffith, G.W., Gueidan, C., Hawksworth, D.L., Hestmark, G., Hosaka, K., Humber, R.A., Hyde, K.D., Ironside, J.E., Koljalg, U., Kurtzman, C.P., Larsson, K.H., Lichtwardt, R., Longcore, J., Miadlikowska, J., Miller, A., Moncalvo, J.M., Mozley-Standridge, S., Oberwinkler, F., Parmasto, E., Reeb, V., Rogers, J.D., Roux, C., Ryvarden, L., Sampaio, J.P., Schussler, A., Sugiyama, J., Thorn, R.G., Tibell, L., Untereiner, W.A., Walker, C., Wang, Z., Weir, A., Weiss, M., White, M.M., Winka, K., Yao, Y.J., and Zhang, N. (2007). A higher-level phylogenetic classification of the Fungi. Mycol Res *111*, 509-547.

Higuchi, Y., Nakahama, T., Shoji, J.Y., Arioka, M., and Kitamoto, K. (2006). Visualization of the endocytic pathway in the filamentous fungus *Aspergillus oryzae* using an EGFP-fused plasma membrane protein. Biochem Biophys Res Commun *340*, 784-791.

Hirokawa, N. (1982). Cross-linker system between neurofilaments, microtubules, and membranous organelles in frog axons revealed by the quick-freeze, deep-etching method. J Cell Biol *94*, 129-142.

Hirokawa, N. (1998). Kinesin and dynein superfamily proteins and the mechanism of organelle transport. Science *279*, 519-526.

Hirokawa, N., Niwa, S., and Tanaka, Y. (2010). Molecular motors in neurons: transport mechanisms and roles in brain function, development, and disease. Neuron *68*, 610-638.

Hirokawa, N., Noda, Y., Tanaka, Y., and Niwa, S. (2009). Kinesin superfamily motor proteins and intracellular transport. Nat Rev Mol Cell Biol *10*, 682-696.

Hlubek, A., Schink, K.O., Mahlert, M., Sandrock, B., and Bölker, M. (2008). Selective activation by the guanine nucleotide exchange factor Don1 is a main determinant of Cdc42 signalling specificity in *Ustilago maydis*. Mol Microbiol *68*, 615-623.

Hoepfner, S., Severin, F., Cabezas, A., Habermann, B., Runge, A., Gillooly, D., Stenmark, H., and Zerial, M. (2005). Modulation of receptor recycling and degradation by the endosomal kinesin KIF16B. Cell *121*, 437-450.

Hoffmann, J., and Mendgen, K. (1998). Endocytosis and membrane turnover in the germ tube of *Uromyces fabae*. Fungal Genet Biol *24*, 77-85.

Holliday, R. (1961). Induced mitotic crossing-over in *Ustilago maydis*. Genetical Research, 231-248.

Holliday, R. (1974). *Ustilago maydis.* In Handbook of Genetics, ed. RC King, New York. Plenum Press, 575-595.

Holliday, R. (2004). Early studies on recombination and DNA repair in *Ustilago maydis*. DNA Repair (Amst) *3*, 671-682.

Horio, T. (2007). Role of microtubules in tip growth of fungi. J Plant Res *120*, 53-60.

Horio, T., and Oakley, B.R. (2005). The role of microtubules in rapid hyphal tip growth of *Aspergillus nidulans*. Mol Biol Cell *16*, 918-926.

Howard, R.J. (1981). Ultrastructural analysis of hyphal tip cell growth in fungi: Spitzenkorper, cytoskeleton and endomembranes after freeze-substitution. J Cell Sci *48*, 89-103.

Hsu, C.C., Moncaleano, J.D., and Wagner, O.I. (2011). Sub-cellular distribution of UNC-104(KIF1A) upon binding to adaptors as UNC-16(JIP3), DNC-1(DCTN1/Glued) and SYD-2(Liprin-alpha) in *C. elegans* neurons. Neuroscience *176*, 39-52.

Huang, C.F., and Banker, G. (2012). The Translocation Selectivity of the Kinesins that Mediate Neuronal Organelle Transport. Traffic.

Huckaba, T.M., Gennerich, A., Wilhelm, J.E., Chishti, A.H., and Vale, R.D. (2011). Kinesin-73 is a processive motor that localizes to Rab5-containing organelles. J Biol Chem *286*, 7457-7467.

Huh, W.K., Falvo, J.V., Gerke, L.C., Carroll, A.S., Howson, R.W., Weissman, J.S., and O'Shea, E.K. (2003). Global analysis of protein localization in budding yeast. Nature *425*, 686-691.

Huo, L., Yue, Y., Ren, J., Yu, J., Liu, J., Yu, Y., Ye, F., Xu, T., Zhang, M., and Feng, W. (2012). The CC1-FHA tandem as a central hub for controlling the dimerization and activation of kinesin-3 KIF1A. Structure *20*, 1550-1561.

Ikegami, K., Heier, R.L., Taruishi, M., Takagi, H., Mukai, M., Shimma, S., Taira, S., Hatanaka, K., Morone, N., Yao, I., Campbell, P.K., Yuasa, S., Janke, C., Macgregor, G.R., and Setou, M. (2007). Loss of alpha-tubulin polyglutamylation in ROSA22 mice is associated with abnormal targeting of KIF1A and modulated synaptic function. Proc Natl Acad Sci U S A *104*, 3213-3218.

Janke, C., and Kneussel, M. (2010). Tubulin post-translational modifications: encoding functions on the neuronal microtubule cytoskeleton. Trends Neurosci *33*, 362-372.

Jenkins, B., Decker, H., Bentley, M., Luisi, J., and Banker, G. (2012). A novel split kinesin assay identifies motor proteins that interact with distinct vesicle populations. J Cell Biol *198*, 749-761.

Jermy, A. (2010). Evolution: Bacterial endocytosis uncovered. Nat Rev Microbiol *8*, 534.

Jordens, I., Marsman, M., Kuijl, C., and Neefjes, J. (2005). Rab proteins, connecting transport and vesicle fusion. Traffic *6*, 1070-1077.

Juarez-Montiel, M., Ruiloba de Leon, S., Chavez-Camarillo, G., Hernandez-Rodriguez, C., and Villa-Tanaca, L. (2011). Huitlacoche (corn smut), caused by the phytopathogenic fungus *Ustilago maydis*, as a functional food. Rev Iberoam Micol *28*, 69-73.

Jung, H., Yoon, B.C., and Holt, C.E. (2012). Axonal mRNA localization and local protein synthesis in nervous system assembly, maintenance and repair. Nat Rev Neurosci *13*, 308-324.

Kaffarnik, F., Muller, P., Leibundgut, M., Kahmann, R., and Feldbrügge, M. (2003). PKA and MAPK phosphorylation of Prf1 allows promoter discrimination in *Ustilago maydis*. EMBO J *22*, 5817-5826.

Kämper, J., Kahmann, R., Bölker, M., Ma, L.J., Brefort, T., Saville, B.J., Banuett, F., Kronstad, J.W., Gold, S.E., Muller, O., Perlin, M.H., Wosten, H.A., de Vries, R., Ruiz-Herrera, J., Reynaga-Pena, C.G., Snetselaar, K., McCann, M., Perez-Martin, J., Feldbrügge, M., Basse, C.W., Steinberg, G., Ibeas, J.I., Holloman, W., Guzman, P., Farman, M., Stajich, J.E., Sentandreu, R., Gonzalez-Prieto, J.M., Kennell, J.C., Molina, L., Schirawski, J., Mendoza-Mendoza, A., Greilinger, D., Munch, K., Rossel, N., Scherer, M., Vranes, M., Ladendorf, O., Vincon, V., Fuchs, U., Sandrock, B., Meng, S., Ho, E.C., Cahill, M.J., Boyce, K.J., Klose, J., Klosterman, S.J., Deelstra, H.J., Ortiz-Castellanos, L., Li, W., Sanchez-Alonso, P., Schreier, P.H., Hauser-Hahn, I., Vaupel, M., Koopmann, E., Friedrich, G., Voss, H., Schluter, T., Margolis, J., Platt, D., Swimmer, C., Gnirke, A., Chen, F., Vysotskaia, V., Mannhaupt, G., Guldener, U., Munsterkotter, M., Haase, D., Oesterheld, M., Mewes, H.W., Mauceli, E.W., DeCaprio, D., Wade, C.M., Butler, J., Young, S., Jaffe, D.B., Calvo, S., Nusbaum, C., Galagan, J., and Birren, B.W. (2006). Insights from the genome of the biotrophic fungal plant pathogen *Ustilago maydis*. Nature *444*, 97-101.

Kämper, J., Reichmann, M., Romeis, T., Bölker, M., and Kahmann, R. (1995). Multiallelic recognition: nonself-dependent dimerization of the *bE* and *bW* homeodomain proteins in *Ustilago maydis*. Cell *81*, 73-83.

Kelley, L.A., and Sternberg, M.J. (2009). Protein structure prediction on the Web: a case study using the Phyre server. Nat Protoc *4*, 363-371.

Kim, J.H., Kim, H.W., Heo, D.H., Chang, M., Baek, I.J., and Yun, C.W. (2009). FgEnd1 is a putative component of the endocytic machinery and mediates ferrichrome uptake in *F. graminearum*. Curr Genet *55*, 593-600.

Klopfenstein, D.R., Tomishige, M., Stuurman, N., and Vale, R.D. (2002). Role of phosphatidylinositol(4,5)bisphosphate organization in membrane transport by the Unc104 kinesin motor. Cell *109*, 347-358.

Klopfenstein, D.R., and Vale, R.D. (2004). The lipid binding pleckstrin homology domain in UNC-104 kinesin is necessary for synaptic vesicle transport in *Caenorhabditis elegans*. Mol Biol Cell *15*, 3729-3739.

Klose, J., de Sa, M.M., and Kronstad, J.W. (2004). Lipid-induced filamentous growth in *Ustilago maydis*. Mol Microbiol *52*, 823-835.

Koepke, J., Kaffarnik, F., Haag, C., Zarnack, K., Luscombe, N.M., Konig, J., Ule, J., Kellner, R., Begerow, D., and Feldbrügge, M. (2011). The RNA-binding protein Rrm4 is essential for efficient secretion of endochitinase Cts1. Mol Cell Proteomics *10*, M111 011213.

König, J., Baumann, S., Koepke, J., Pohlmann, T., Zarnack, K., and Feldbrügge, M. (2009). The fungal RNA-binding protein Rrm4 mediates long-distance transport of ubi1 and rho3 mRNAs. EMBO J *28*, 1855-1866.

Konzack, S., Rischitor, P.E., Enke, C., and Fischer, R. (2005). The role of the kinesin motor KipA in microtubule organization and polarized growth of *Aspergillus nidulans*. Mol Biol Cell *16*, 497-506.

Kronstad, J.W., and Leong, S.A. (1989). Isolation of two alleles of the *b* locus of *Ustilago maydis*. Proc Natl Acad Sci U S A *86*, 978-982.

Kronstad, J.W., and Leong, S.A. (1990). The *b* mating-type locus of *Ustilago maydis* contains variable and constant regions. Genes Dev *4*, 1384-1395.

Krüger, J., Loubradou, G., Regenfelder, E., Hartmann, A., and Kahmann, R. (1998). Crosstalk between cAMP and pheromone signalling pathways in *Ustilago maydis*. Mol Gen Genet *260*, 193-198.

Kumar, J., Choudhary, B.C., Metpally, R., Zheng, Q., Nonet, M.L., Ramanathan, S., Klopfenstein, D.R., and Koushika, S.P. (2010). The *Caenorhabditis elegans* Kinesin-3 motor UNC-104/KIF1A is degraded upon loss of specific binding to cargo. PLoS Genet *6*, e1001200.

Kutateladze, T.G., Ogburn, K.D., Watson, W.T., de Beer, T., Emr, S.D., Burd, C.G., and Overduin, M. (1999). Phosphatidylinositol 3-phosphate recognition by the FYVE domain. Mol Cell *3*, 805-811.

Laity, C., Giasson, L., Campbell, R., and Kronstad, J. (1995). Heterozygosity at the *b* mating-type locus attenuates fusion in *Ustilago maydis*. Curr Genet *27*, 451-459.

Langford, G.M. (1995). Actin- and microtubule-dependent organelle motors: interrelationships between the two motility systems. Curr Opin Cell Biol *7*, 82-88.

Lanzetti, L. (2012). A novel function of Rab5 in mitosis. Small GTPases *3*, 168-172.

Lasiecka, Z.M., Yap, C.C., Caplan, S., and Winckler, B. (2010). Neuronal early endosomes require EHD1 for L1/NgCAM trafficking. J Neurosci *30*, 16485-16497.

Lawe, D.C., Patki, V., Heller-Harrison, R., Lambright, D., and Corvera, S. (2000). The FYVE domain of early endosome antigen 1 is required for both phosphatidylinositol 3-phosphate and Rab5 binding. Critical role of this dual interaction for endosomal localization. J Biol Chem *275*, 3699-3705.

Lawrence, C.J., Dawe, R.K., Christie, K.R., Cleveland, D.W., Dawson, S.C., Endow, S.A., Goldstein, L.S., Goodson, H.V., Hirokawa, N., Howard, J., Malmberg, R.L., McIntosh, J.R., Miki, H., Mitchison, T.J., Okada, Y., Reddy, A.S., Saxton, W.M., Schliwa, M., Scholey, J.M., Vale, R.D., Walczak, C.E., and Wordeman, L. (2004). A standardized kinesin nomenclature. J Cell Biol *167*, 19-22.

Le Roy, C., and Wrana, J.L. (2005). Signaling and endocytosis: a team effort for cell migration. Dev Cell *9*, 167-168.

Lee, J.R., Shin, H., Choi, J., Ko, J., Kim, S., Lee, H.W., Kim, K., Rho, S.H., Lee, J.H., Song, H.E., Eom, S.H., and Kim, E. (2004). An intramolecular interaction between the FHA domain and a coiled coil negatively regulates the kinesin motor KIF1A. EMBO J *23*, 1506-1515.

Lee, J.R., Shin, H., Ko, J., Choi, J., Lee, H., and Kim, E. (2003). Characterization of the movement of the kinesin motor KIF1A in living cultured neurons. J Biol Chem *278*, 2624-2629.

Lee, N., and Kronstad, J.W. (2002). ras2 Controls morphogenesis, pheromone response, and pathogenicity in the fungal pathogen *Ustilago maydis*. Eukaryot Cell *1*, 954-966.

Lehmler, C., Steinberg, G., Snetselaar, K.M., Schliwa, M., Kahmann, R., and Bölker, M. (1997). Identification of a motor protein required for filamentous growth in *Ustilago maydis*. EMBO J *16*, 3464-3473.

Lemmon, M.A. (1999). Structural basis for high-affinity phosphoinositide binding by pleckstrin homology domains. Biochem Soc Trans *27*, 617-624.

Lemmon, M.A. (2003). Phosphoinositide recognition domains. Traffic *4*, 201-213.

Lemmon, M.A. (2004). Pleckstrin homology domains: not just for phosphoinositides. Biochem Soc Trans *32*, 707-711.

Lemmon, M.A. (2008). Membrane recognition by phospholipid-binding domains. Nat Rev Mol Cell Biol *9*, 99-111.

Lenz, J.H., Schuchardt, I., Straube, A., and Steinberg, G. (2006). A dynein loading zone for retrograde endosome motility at microtubule plus-ends. EMBO J *25*, 2275-2286.

Li, H.P., Liu, Z.M., and Nirenberg, M. (1997). Kinesin-73 in the nervous system of *Drosophila* embryos. Proc Natl Acad Sci U S A *94*, 1086-1091.

Lichius, A., Berepiki, A., and Read, N.D. (2011). Form follows function -- the versatile fungal cytoskeleton. Fungal Biol *115*, 518-540.

Liu, G., Greenshields, D.L., Sammynaiken, R., Hirji, R.N., Selvaraj, G., and Wei, Y. (2007). Targeted alterations in iron homeostasis underlie plant defense responses. J Cell Sci *120*, 596-605.

Liu, J.S., Schubert, C.R., Fu, X., Fourniol, F.J., Jaiswal, J.K., Houdusse, A., Stultz, C.M., Moores, C.A., and Walsh, C.A. (2012). Molecular basis for specific regulation of neuronal kinesin-3 motors by doublecortin family proteins. Mol Cell *47*, 707-721.

Lloyd, T.E., Machamer, J., O'Hara, K., Kim, J.H., Collins, S.E., Wong, M.Y., Sahin, B., Imlach, W., Yang, Y., Levitan, E.S., McCabe, B.D., and Kolodkin, A.L. (2012). The p150(Glued) CAP-Gly domain regulates initiation of retrograde transport at synaptic termini. Neuron *74*, 344-360.

Lo, H.J., Kohler, J.R., DiDomenico, B., Loebenberg, D., Cacciapuoti, A., and Fink, G.R. (1997). Nonfilamentous *C. albicans* mutants are avirulent. Cell *90*, 939-949.

Lo, K.Y., Kuzmin, A., Unger, S.M., Petersen, J.D., and Silverman, M.A. (2011). KIF1A is the primary anterograde motor protein required for the axonal transport of dense-core vesicles in cultured hippocampal neurons. Neurosci Lett *491*, 168-173.

Lomize, M.A., Pogozheva, I.D., Joo, H., Mosberg, H.I., and Lomize, A.L. (2012). OPM database and PPM web server: resources for positioning of proteins in membranes. Nucleic Acids Res *40*, D370-376.

Lonhienne, T.G., Sagulenko, E., Webb, R.I., Lee, K.C., Franke, J., Devos, D.P., Nouwens, A., Carroll, B.J., and Fuerst, J.A. (2010). Endocytosis-like protein uptake in the bacterium *Gemmata obscuriglobus*. Proc Natl Acad Sci U S A *107*, 12883-12888.

Loubery, S., Wilhelm, C., Hurbain, I., Neveu, S., Louvard, D., and Coudrier, E. (2008). Different microtubule motors move early and late endocytic compartments. Traffic *9*, 492-509.

Lupas, A., Van Dyke, M., and Stock, J. (1991). Predicting coiled coils from protein sequences. Science *252*, 1162-1164.

Lupyan, D., Leo-Macias, A., and Ortiz, A.R. (2005). A new progressive-iterative algorithm for multiple structure alignment. Bioinformatics *21*, 3255-3263.

Madhani, H.D., and Fink, G.R. (1998). The control of filamentous differentiation and virulence in fungi. Trends Cell Biol *8*, 348-353.

Mahlert, M., Leveleki, L., Hlubek, A., Sandrock, B., and Bölker, M. (2006). Rac1 and Cdc42 regulate hyphal growth and cytokinesis in the dimorphic fungus *Ustilago maydis*. Mol Microbiol *59*, 567-578.

Maiti, R., Van Domselaar, G.H., Zhang, H., and Wishart, D.S. (2004). SuperPose: a simple server for sophisticated structural superposition. Nucleic Acids Res *32*, W590-594.

Makarow, M. (1985). Endocytosis in *Saccharomyces cerevisiae*: internalization of enveloped viruses into spheroplasts. EMBO J *4*, 1855-1860.

Martinez-Espinoza, A.D., Garcia-Pedrajas, M.D., and Gold, S.E. (2002). The Ustilaginales as plant pests and model systems. Fungal Genet Biol *35*, 1-20.
Matsushita, M., Yamamoto, R., Mitsui, K., and Kanazawa, H. (2009). Altered motor activity of alternative splice variants of the mammalian kinesin-3 protein KIF1B. Traffic *10*, 1647-1654.

Mayinger, P. (2012). Phosphoinositides and vesicular membrane traffic. Biochim Biophys Acta *1821*, 1104-1113.

Mayorga, M.E., and Gold, S.E. (1999). A MAP kinase encoded by the ubc3 gene of *Ustilago maydis* is required for filamentous growth and full virulence. Mol Microbiol *34*, 485-497.

Mayorga, M.E., and Gold, S.E. (2001). The ubc2 gene of *Ustilago maydis* encodes a putative novel adaptor protein required for filamentous growth, pheromone response and virulence. Mol Microbiol *41*, 1365-1379.

McGoldrick, C.A., Gruver, C., and May, G.S. (1995). myoA of *Aspergillus nidulans* encodes an essential myosin I required for secretion and polarized growth. J Cell Biol *128*, 577-587.

Mendoza-Mendoza, A., Berndt, P., Djamei, A., Weise, C., Linne, U., Marahiel, M., Vranes, M., Kämper, J., and Kahmann, R. (2009). Physical-chemical plant-derived signals induce differentiation in *Ustilago maydis*. Mol Microbiol *71*, 895-911.

Miaczynska, M., Christoforidis, S., Giner, A., Shevchenko, A., Uttenweiler-Joseph, S., Habermann, B., Wilm, M., Parton, R.G., and Zerial, M. (2004). APPL proteins link Rab5 to nuclear signal transduction via an endosomal compartment. Cell *116*, 445-456.

Mielnichuk, N., Sgarlata, C., and Perez-Martin, J. (2009). A role for the DNA-damage checkpoint kinase Chk1 in the virulence program of the fungus *Ustilago maydis*. J Cell Sci *122*, 4130-4140.

Miki, H., Okada, Y., and Hirokawa, N. (2005). Analysis of the kinesin superfamily: insights into structure and function. Trends Cell Biol *15*, 467-476.

Miki, H., Setou, M., Kaneshiro, K., and Hirokawa, N. (2001). All kinesin superfamily protein, KIF, genes in mouse and human. Proc Natl Acad Sci U S A *98*, 7004-7011.

Miller, K.E., DeProto, J., Kaufmann, N., Patel, B.N., Duckworth, A., and Van Vactor, D. (2005). Direct observation demonstrates that Liprin-alpha is required for trafficking of synaptic vesicles. Curr Biol *15*, 684-689.

Miller, R.H., and Lasek, R.J. (1985). Cross-bridges mediate anterograde and retrograde vesicle transport along microtubules in squid axoplasm. J Cell Biol *101*, 2181-2193.

Mills, L.J., and Kotzé, J.M. (1981). Scanning Electron Microscopy of the Germination, Growth and Infection of *Ustilago maydis* on Maize. Journal of Phytopathology *102*, 21-27.

Misra, S., and Hurley, J.H. (1999). Crystal structure of a phosphatidylinositol 3-phosphate-specific membrane-targeting motif, the FYVE domain of Vps27p. Cell *97*, 657-666.

Molina, L., and Kahmann, R. (2007). An *Ustilago maydis* gene involved in H2O2 detoxification is required for virulence. Plant Cell *19*, 2293-2309.

Mu, F.T., Callaghan, J.M., Steele-Mortimer, O., Stenmark, H., Parton, R.G., Campbell, P.L., McCluskey, J., Yeo, J.P., Tock, E.P., and Toh, B.H. (1995). EEA1, an early endosome-associated protein. EEA1 is a conserved alpha-helical peripheral membrane protein flanked by cysteine "fingers" and contains a calmodulin-binding IQ motif. J Biol Chem *270*, 13503-13511.

Mueller, O., Kahmann, R., Aguilar, G., Trejo-Aguilar, B., Wu, A., and de Vries, R.P. (2008). The secretome of the maize pathogen *Ustilago maydis*. Fungal Genet Biol *45 Suppl 1*, S63-70.

Müller, O., Schreier, P.H., and Uhrig, J.F. (2008). Identification and characterization of secreted and pathogenesis-related proteins in *Ustilago maydis*. Mol Genet Genomics *279*, 27-39.

Müller, P., Aichinger, C., Feldbrügge, M., and Kahmann, R. (1999). The MAP kinase kpp2 regulates mating and pathogenic development in *Ustilago maydis*. Mol Microbiol *34*, 1007-1017.

Müller, P., Weinzierl, G., Brachmann, A., Feldbrügge, M., and Kahmann, R. (2003). Mating and pathogenic development of the Smut fungus *Ustilago maydis* are regulated by one mitogen-activated protein kinase cascade. Eukaryot Cell *2*, 1187-1199.

Münsterkötter, M., and Steinberg, G. (2007). The fungus *Ustilago maydis* and humans share disease-related proteins that are not found in *Saccharomyces cerevisiae*. BMC Genomics *8*, 473.

Muresan, V., Stankewich, M.C., Steffen, W., Morrow, J.S., Holzbaur, E.L., and Schnapp, B.J. (2001). Dynactin-dependent, dynein-driven vesicle transport in the absence of membrane proteins: a role for spectrin and acidic phospholipids. Mol Cell *7*, 173-183.

Murphy, J.E., Padilla, B.E., Hasdemir, B., Cottrell, G.S., and Bunnett, N.W. (2009). Endosomes: a legitimate platform for the signaling train. Proc Natl Acad Sci U S A *106*, 17615-17622.

Murray, J.W., Bananis, E., and Wolkoff, A.W. (2000). Reconstitution of ATP-dependent movement of endocytic vesicles along microtubules *in vitro*: an oscillatory bidirectional process. Mol Biol Cell *11*, 419-433.

Nadal, M., Garcia-Pedrajas, M.D., and Gold, S.E. (2008). Dimorphism in fungal plant pathogens. FEMS Microbiol Lett *284*, 127-134.

Nakata, T., and Hirokawa, N. (2003). Microtubules provide directional cues for polarized axonal transport through interaction with kinesin motor head. The Journal of Cell Biology *162*, 1045-1055.

Nangaku, M., Sato-Yoshitake, R., Okada, Y., Noda, Y., Takemura, R., Yamazaki, H., and Hirokawa, N. (1994). KIF1B, a novel microtubule plus end-directed monomeric motor protein for transport of mitochondria. Cell *79*, 1209-1220.

Nath, S., Bananis, E., Sarkar, S., Stockert, R.J., Sperry, A.O., Murray, J.W., and Wolkoff, A.W. (2007). KIF5B and KIFc1 interact and are required for motility and fission of early endocytic vesicles in mouse liver. Mol Biol Cell *18*, 1839-1849.

Nielsen, E., Severin, F., Backer, J.M., Hyman, A.A., and Zerial, M. (1999). Rab5 regulates motility of early endosomes on microtubules. Nat Cell Biol *1*, 376-382.

Niwa, S., Tanaka, Y., and Hirokawa, N. (2008). KIF1Bbeta- and KIF1A-mediated axonal transport of presynaptic regulator Rab3 occurs in a GTP-dependent manner through DENN/MADD. Nat Cell Biol *10*, 1269-1279.

Nonet, M.L. (1999). Visualization of synaptic specializations in live *C. elegans* with synaptic vesicle protein-GFP fusions. J Neurosci Methods *89*, 33-40.

Nonet, M.L., Saifee, O., Zhao, H., Rand, J.B., and Wei, L. (1998). Synaptic transmission deficits in *Caenorhabditis elegans* synaptobrevin mutants. J Neurosci *18*, 70-80.

Oberholzer, U., Marcil, A., Leberer, E., Thomas, D.Y., and Whiteway, M. (2002). Myosin I is required for hypha formation in *Candida albicans*. Eukaryot Cell *1*, 213-228.

Okada, Y., Yamazaki, H., Sekine-Aizawa, Y., and Hirokawa, N. (1995). The neuron-specific kinesin superfamily protein KIF1A is a unique monomeric motor for anterograde axonal transport of synaptic vesicle precursors. Cell *81*, 769-780.

Osherov, N., Yamashita, R.A., Chung, Y.S., and May, G.S. (1998). Structural requirements for *in vivo* myosin I function in *Aspergillus nidulans*. J Biol Chem *273*, 27017-27025.

Otsuka, A.J., Jeyaprakash, A., Garcia-Anoveros, J., Tang, L.Z., Fisk, G., Hartshorne, T., Franco, R., and Born, T. (1991). The *C. elegans* unc-104 gene encodes a putative kinesin heavy chain-like protein. Neuron *6*, 113-122.

Parton, R.G., Simons, K., and Dotti, C.G. (1992). Axonal and dendritic endocytic pathways in cultured neurons. J Cell Biol *119*, 123-137.
Penalva, M.A. (2005). Tracing the endocytic pathway of *Aspergillus nidulans* with FM4-64. Fungal Genet Biol *42*, 963-975.

Penalva, M.A. (2010). Endocytosis in filamentous fungi: Cinderella gets her reward. Curr Opin Microbiol *13*, 684-692.

Plamann, M. (2009). Cytoplasmic streaming in neurospora: disperse the plug to increase the flow? PLoS Genet *5*, e1000526.

Plamann, M., Minke, P.F., Tinsley, J.H., and Bruno, K.S. (1994). Cytoplasmic dynein and actin-related protein Arp1 are required for normal nuclear distribution in filamentous fungi. J Cell Biol *127*, 139-149.

Platta, H.W., and Stenmark, H. (2011). Endocytosis and signaling. Curr Opin Cell Biol *23*, 393-403.

Pollock, N., de Hostos, E.L., Turck, C.W., and Vale, R.D. (1999). Reconstitution of membrane transport powered by a novel dimeric kinesin motor of the Unc104/KIF1A family purified from *Dictyostelium*. J Cell Biol *147*, 493-506.

Pollock, N., Koonce, M.P., de Hostos, E.L., and Vale, R.D. (1998). *In vitro* microtubule-based organelle transport in wild-type *Dictyostelium* and cells overexpressing a truncated dynein heavy chain. Cell Motil Cytoskeleton *40*, 304-314.

Puhalla, J.E. (1968). Compatibility reactions on solid medium and interstrain inhibition in *Ustilago maydis*. Genetics *60*, 461-474.

Rafiqi, M., Ellis, J.G., Ludowici, V.A., Hardham, A.R., and Dodds, P.N. (2012). Challenges and progress towards understanding the role of effectors in plant-fungal interactions. Curr Opin Plant Biol *15*, 477-482.

Raikhel, N., and Hicks, G. (2007). Signaling from plant endosomes: compartments with something to say! Genes Dev *21*, 1578-1580.

Rashid, D.J., Bononi, J., Tripet, B.P., Hodges, R.S., and Pierce, D.W. (2005). Monomeric and dimeric states exhibited by the kinesin-related motor protein KIF1A. J Pept Res *65*, 538-549.

Raymond, C.K., Pownder, T.A., and Sexson, S.L. (1999). General method for plasmid construction using homologous recombination. Biotechniques *26*, 134-138, 140-131.

Read, N.D., and Kalkman, E.R. (2003). Does endocytosis occur in fungal hyphae? Fungal Genet Biol *39*, 199-203.

Regenfelder, E., Spellig, T., Hartmann, A., Lauenstein, S., Bölker, M., and Kahmann, R. (1997). G proteins in *Ustilago maydis*: transmission of multiple signals? EMBO J *16*, 1934-1942.

Ren, J., Wen, L., Gao, X., Jin, C., Xue, Y., and Yao, X. (2009). DOG 1.0: illustrator of protein domain structures. Cell Res *19*, 271-273.

Requena, N., Alberti-Segui, C., Winzenburg, E., Horn, C., Schliwa, M., Philippsen, P., Liese, R., and Fischer, R. (2001). Genetic evidence for a microtubule-destabilizing effect of conventional kinesin and analysis of its consequences for the control of nuclear distribution in *Aspergillus nidulans*. Mol Microbiol *42*, 121-132.

Richter, S., Muller, L.M., Stierhof, Y.D., Mayer, U., Takada, N., Kost, B., Vieten, A., Geldner, N., Koncz, C., and Jurgens, G. (2011). Polarized cell growth in *Arabidopsis* requires endosomal recycling mediated by GBF1-related ARF exchange factors. Nat Cell Biol *14*, 80-86.

Riquelme, M., Fischer, R., and Bartnicki-Garcia, S. (2003). Apical growth and mitosis are independent processes in *Aspergillus nidulans*. Protoplasma *222*, 211-215.

Riquelme, M., Gierz, G., and Bartnicki-Garcia, S. (2000). Dynein and dynactin deficiencies affect the formation and function of the Spitzenkorper and distort hyphal morphogenesis of *Neurospora crassa*. Microbiology *146 (Pt 7)*, 1743-1752.

Robledo-Briones, M., and Ruiz-Herrera, J. (2012). Regulation of genes involved in cell wall synthesis and structure during *Ustilago maydis* dimorphism. FEMS Yeast Res.

Rodriguez-Kessler, M., Baeza-Montanez, L., Garcia-Pedrajas, M.D., Tapia-Moreno, A., Gold, S., Jimenez-Bremont, J.F., and Ruiz-Herrera, J. (2012). Isolation of UmRrm75, a gene involved in dimorphism and virulence of *Ustilago maydis*. Microbiol Res *167*, 270-282.

Rojas, A.M., Fuentes, G., Rausell, A., and Valencia, A. (2012). The Ras protein superfamily: Evolutionary tree and role of conserved amino acids. J. Cell Biol. *196*, 189-201.

Romeis, T., Kämper, J., and Kahmann, R. (1997). Single-chain fusions of two unrelated homeodomain proteins trigger pathogenicity in *Ustilago maydis*. Proc Natl Acad Sci U S A *94*, 1230-1234.

Roth, M.G. (2004). Phosphoinositides in constitutive membrane traffic. Physiol Rev *84*, 699-730.

Rowell, J.B. (1955). Segregation of Sex Factors in a Diploid Line of *Ustilago zeae* Induced by Alpha Radiation. Science *121*, 304-306.

Ruiz-Herrera, J., Leon, C.G., Carabez-Trejo, A., and Reyes-Salinas, E. (1996). Structure and chemical composition of the cell walls from the haploid yeast and mycelial forms of *Ustilago maydis*. Fungal Genet Biol *20*, 133-142.

Ruiz-Herrera, J., Ortiz-Castellanos, L., Martinez, A.I., Leon-Ramirez, C., and Sentandreu, R. (2008). Analysis of the proteins involved in the structure and synthesis of the cell wall of *Ustilago maydis*. Fungal Genet Biol *45 Suppl 1*, S71-76.

Sali, A., and Blundell, T.L. (1993). Comparative protein modelling by satisfaction of spatial restraints. J Mol Biol *234*, 779-815.

Sambrook, J., Fritsch, E.F., and Maniatis, T. (1989). Molecular Cloning: a laboratory manual. 2-nd Edition. New York. Cold Spring Harbor laboratory. Cold Spring Harbor Press.

Sampson, K., and Heath, I.B. (2005). The dynamic behaviour of microtubules and their contributions to hyphal tip growth in *Aspergillus nidulans*. Microbiology *151*, 1543-1555.

Sanchez-Martinez, C., and Perez-Martin, J. (2001). Dimorphism in fungal pathogens: *Candida albicans* and *Ustilago maydis*--similar inputs, different outputs. Curr Opin Microbiol *4*, 214-221.

Saraste, M., and Hyvonen, M. (1995). Pleckstrin homology domains: a fact file. Curr Opin Struct Biol *5*, 403-408.

Satoh, D., Sato, D., Tsuyama, T., Saito, M., Ohkura, H., Rolls, M.M., Ishikawa, F., and Uemura, T. (2008). Spatial control of branching within dendritic arbors by dynein-dependent transport of Rab5-endosomes. Nat Cell Biol *10*, 1164-1171.

Savitsky, P., Bray, J., Cooper, C.D., Marsden, B.D., Mahajan, P., Burgess-Brown, N.A., and Gileadi, O. (2010). High-throughput production of human proteins for crystallization: the SGC experience. J Struct Biol *172*, 3-13.

Schink, K.O., and Bölker, M. (2009). Coordination of cytokinesis and cell separation by endosomal targeting of a Cdc42-specific guanine nucleotide exchange factor in *Ustilago maydis*. Mol Biol Cell *20*, 1081-1088.

Schlesinger, R., Kahmann, R., and Kämper, J. (1997). The homeodomains of the heterodimeric *bE* and *bW* proteins of *Ustilago maydis* are both critical for function. Mol Gen Genet *254*, 514-519.

Schoch, C.L., Aist, J.R., Yoder, O.C., and Gillian Turgeon, B. (2003). A complete inventory of fungal kinesins in representative filamentous ascomycetes. Fungal Genet Biol *39*, 1-15.

Schuchardt, I., Assmann, D., Thines, E., Schuberth, C., and Steinberg, G. (2005). Myosin-V, Kinesin-1, and Kinesin-3 cooperate in hyphal growth of the fungus *Ustilago maydis*. Mol Biol Cell *16*, 5191-5201.

Schulz, B., Banuett, F., Dahl, M., Schlesinger, R., Schafer, W., Martin, T., Herskowitz, I., and Kahmann, R. (1990). The *b* alleles of *U. maydis*, whose combinations program pathogenic development, code for polypeptides containing a homeodomain-related motif. Cell *60*, 295-306.

Schuster, M., Kilaru, S., Ashwin, P., Lin, C., Severs, N.J., and Steinberg, G. (2011a). Controlled and stochastic retention concentrates dynein at microtubule ends to keep endosomes on track. EMBO J *30*, 652-664.

Schuster, M., Kilaru, S., Fink, G., Collemare, J., Roger, Y., and Steinberg, G. (2011c). Kinesin-3 and dynein cooperate in long-range retrograde endosome motility along a nonuniform microtubule array. Mol Biol Cell *22*, 3645-3657.

Schuster, M., Lipowsky, R., Assmann, M.A., Lenz, P., and Steinberg, G. (2011b). Transient binding of dynein controls bidirectional long-range motility of early endosomes. Proc Natl Acad Sci U S A *108*, 3618-3623.

Schuster, M., Treitschke, S., Kilaru, S., Molloy, J., Harmer, N.J., and Steinberg, G. (2011d). Myosin-5, kinesin-1 and myosin-17 cooperate in secretion of fungal chitin synthase. EMBO J *31*, 214-227.

Seet, L.F., and Hong, W. (2006). The Phox (PX) domain proteins and membrane traffic. Biochim Biophys Acta *1761*, 878-896.

Seidel, C., Zekert, N., and Fischer, R. (2012). The *Aspergillus nidulans* kinesin-3 tail is necessary and sufficient to recognize modified microtubules. PLoS One *7*, e30976.

Seiler, S., Kirchner, J., Horn, C., Kallipolitou, A., Woehlke, G., and Schliwa, M. (2000). Cargo binding and regulatory sites in the tail of fungal conventional kinesin. Nat Cell Biol *2*, 333-338.

Seiler, S., Nargang, F.E., Steinberg, G., and Schliwa, M. (1997). Kinesin is essential for cell morphogenesis and polarized secretion in *Neurospora crassa*. EMBO J *16*, 3025-3034.

Shaw, B.D., Chung, D.W., Wang, C.L., Quintanilla, L.A., and Upadhyay, S. (2011). A role for endocytic recycling in hyphal growth. Fungal Biol *115*, 541-546.

Shi, J., Blundell, T.L., and Mizuguchi, K. (2001). FUGUE: sequence-structure homology recognition using environment-specific substitution tables and structure-dependent gap penalties. J Mol Biol *310*, 243-257.

Shieh, J.C., Schaar, B.T., Srinivasan, K., Brodsky, F.M., and McConnell, S.K. (2011). Endocytosis regulates cell soma translocation and the distribution of adhesion proteins in migrating neurons. PLoS One *6*, e17802.

Shimizu, H., Kawamura, S., and Ozaki, K. (2003). An essential role of Rab5 in uniformity of synaptic vesicle size. J Cell Sci *116*, 3583-3590.

Shin, H., Wyszynski, M., Huh, K.H., Valtschanoff, J.G., Lee, J.R., Ko, J., Streuli, M., Weinberg, R.J., Sheng, M., and Kim, E. (2003). Association of the kinesin motor KIF1A with the multimodular protein liprin-alpha. J Biol Chem *278*, 11393-11401.

Skibbe, D.S., Doehlemann, G., Fernandes, J., and Walbot, V. (2010). Maize tumors caused by *Ustilago maydis* require organ-specific genes in host and pathogen. Science *328*, 89-92.

Smith, T.J. (2011). Engineering Fungal Resistance in Crop Plants using Antifungal Proteins from Viruses. ISB NEWS REPORT.

Snetselaar, K.M., Bölker, M., and Kahmann, R. (1996). *Ustilago maydis* Mating Hyphae Orient Their Growth toward Pheromone Sources. Fungal Genet Biol *20*, 299-312.

Snetselaar, K.M., and Mims, C.W. (1993). Infection of Maize Stigmas by *Ustilago maydis*: Light and Electron Microscopy. Phytopathology *83*, 843-850.

Snetselaar, K.M., and Mims, C.W. (1994). Light and electron microscopy of *Ustilago maydis* hyphae in maize. Mycological Research *98*, 347-355.

Soppina, V., Rai, A.K., Ramaiya, A.J., Barak, P., and Mallik, R. (2009). Tug-of-war between dissimilar teams of microtubule motors regulates transport and fission of endosomes. Proc Natl Acad Sci U S A *106*, 19381-19386.

Spellig, T., Bölker, M., Lottspeich, F., Frank, R.W., and Kahmann, R. (1994a). Pheromones trigger filamentous growth in *Ustilago maydis*. EMBO J *13*, 1620-1627.

Spellig, T., Regenfelder, E., Reichmann, M., Schauwecker, F., Bohlmann, R., Urban, M., Bölker, M., Kämper, J., and Kahmann, R. (1994b). Control of mating and development in *Ustilago maydis*. Antonie Van Leeuwenhoek *65*, 191-197.

Steinberg, G. (1998b). Organelle transport and molecular motors in fungi. Fungal Genet Biol *24*, 161-177.

Steinberg, G. (2000). The cellular roles of molecular motors in fungi. Trends Microbiol *8*, 162-168.

Steinberg, G. (2007a). Preparing the way: fungal motors in microtubule organization. Trends Microbiol *15*, 14-21.

Steinberg, G. (2007b). Hyphal growth: a tale of motors, lipids, and the Spitzenkorper. Eukaryot Cell *6*, 351-360.

Steinberg, G. (2007c). On the move: endosomes in fungal growth and pathogenicity. Nat Rev Microbiol *5*, 309-316.

Steinberg, G. (2007d). Tracks for traffic: microtubules in the plant pathogen *Ustilago maydis*. New Phytol *174*, 721-733.

Steinberg, G. (2012). The transport machinery for motility of fungal endosomes. Fungal Genet Biol *49*, 675-676.

Steinberg, G., and Perez-Martin, J. (2008). *Ustilago maydis*, a new fungal model system for cell biology. Trends Cell Biol *18*, 61-67.

Steinberg, G., Schliwa, M., Lehmler, C., Bolker, M., Kahmann, R., and McIntosh, J.R. (1998a). Kinesin from the plant pathogenic fungus *Ustilago maydis* is involved in vacuole formation and cytoplasmic migration. J Cell Sci *111 (Pt 15)*, 2235-2246.

Steinberg, G., Wedlich-Söldner, R., Brill, M., and Schulz, I. (2001). Microtubules in the fungal pathogen *Ustilago maydis* are highly dynamic and determine cell polarity. J Cell Sci *114*, 609-622.

Stenmark, H., Aasland, R., Toh, B.H., and D'Arrigo, A. (1996). Endosomal localization of the autoantigen EEA1 is mediated by a zinc-binding FYVE finger. J Biol Chem *271*, 24048-24054.

Straube, A., Brill, M., Oakley, B.R., Horio, T., and Steinberg, G. (2003). Microtubule organization requires cell cycle-dependent nucleation at dispersed cytoplasmic sites: polar and perinuclear microtubule organizing centers in the plant pathogen *Ustilago maydis*. Mol Biol Cell *14*, 642-657.

Straube, A., Enard, W., Berner, A., Wedlich-Soldner, R., Kahmann, R., and Steinberg, G. (2001). A split motor domain in a cytoplasmic dynein. EMBO J *20*, 5091-5100.

Straube, A., Hause, G., Fink, G., and Steinberg, G. (2006). Conventional kinesin mediates microtubule-microtubule interactions *in vivo*. Mol Biol Cell *17*, 907-916.

Taheri-Talesh, N., Horio, T., Araujo-Bazan, L., Dou, X., Espeso, E.A., Penalva, M.A., Osmani, S.A., and Oakley, B.R. (2008). The tip growth apparatus of *Aspergillus nidulans*. Mol Biol Cell *19*, 1439-1449.

Takemoto, D., Tanaka, A., and Scott, B. (2007). NADPH oxidases in fungi: diverse roles of reactive oxygen species in fungal cellular differentiation. Fungal Genet Biol *44*, 1065-1076.

Takeshita, N., Higashitsuji, Y., Konzack, S., and Fischer, R. (2008). Apical sterol-rich membranes are essential for localizing cell end markers that determine growth directionality in the filamentous fungus *Aspergillus nidulans*. Mol Biol Cell *19*, 339-351.

Talbot, N.J. (2012). Regulating morphogenetic transitions during development and pathogenesis of microbial eukaryotes. Curr Opin Microbiol *15*, 633-636.

Tang, B.L. (2008). Emerging aspects of membrane traffic in neuronal dendrite growth. Biochim Biophys Acta *1783*, 169-176.

Taru, H., and Jin, Y. (2011). The Liprin homology domain is essential for the homomeric interaction of SYD-2/Liprin-alpha protein in presynaptic assembly. J Neurosci *31*, 16261-16268.

Theisen, U., Straube, A., and Steinberg, G. (2008). Dynamic rearrangement of nucleoporins during fungal "open" mitosis. Mol Biol Cell *19*, 1230-1240.

Thordal-Christensen, H., Zhang, Z., Wei, Y., and Collinge, D.B. (1997). Subcellular localization of H_2O_2 in plants. H_2O_2 accumulation in papillae and hypersensitive response during the barley-powdery mildew interaction. The Plant Journal *11*, 1187-1194.

Tien, N.W., Wu, G.H., Hsu, C.C., Chang, C.Y., and Wagner, O.I. (2011). Tau/PTL-1 associates with kinesin-3 KIF1A/UNC-104 and affects the motor's motility characteristics in *C. elegans* neurons. Neurobiol Dis *43*, 495-506.

Treitschke, S., Doehlemann, G., Schuster, M., and Steinberg, G. (2010). The myosin motor domain of fungal chitin synthase V is dispensable for vesicle motility but required for virulence of the maize pathogen *Ustilago maydis*. Plant Cell *22*, 2476-2494.

Ueda, T., Uemura, T., Sato, M.H., and Nakano, A. (2004). Functional differentiation of endosomes in *Arabidopsis* cells. Plant J *40*, 783-789.

Ueno, H., Huang, X., Tanaka, Y., and Hirokawa, N. (2011). KIF16B/Rab14 molecular motor complex is critical for early embryonic development by transporting FGF receptor. Dev Cell *20*, 60-71.

Urban, M., Kahmann, R., and Bölker, M. (1996). Identification of the pheromone response element in *Ustilago maydis*. Mol Gen Genet *251*, 31-37.

Vale, R.D. (2003). The molecular motor toolbox for intracellular transport. Cell *112*, 467-480.

Vale, R.D., and Milligan, R.A. (2000). The way things move: looking under the hood of molecular motor proteins. Science *288*, 88-95.

Vale, R.D., Reese, T.S., and Sheetz, M.P. (1985). Identification of a novel force-generating protein, kinesin, involved in microtubule-based motility. Cell *42*, 39-50.

Valverde, M.E., Paredes-Lopez, O., Pataky, J.K., and Guevara-Lara, F. (1995). Huitlacoche (*Ustilago maydis*) as a food source--biology, composition, and production. Crit Rev Food Sci Nutr *35*, 191-229.

van der Sluijs, P., Hull, M., Zahraoui, A., Tavitian, A., Goud, B., and Mellman, I. (1991). The small GTP-binding protein rab4 is associated with early endosomes. Proc Natl Acad Sci U S A *88*, 6313-6317.

Veith, D., Scherr, N., Efimov, V.P., and Fischer, R. (2005). Role of the spindle-pole-body protein ApsB and the cortex protein ApsA in microtubule organization and nuclear migration in *Aspergillus nidulans*. J Cell Sci *118*, 3705-3716.

Verdier-Pinard, P., Pasquier, E., Xiao, H., Burd, B., Villard, C., Lafitte, D., Miller, L.M., Angeletti, R.H., Horwitz, S.B., and Braguer, D. (2009). Tubulin proteomics: towards breaking the code. Anal Biochem *384*, 197-206.

Verhey, K.J., and Hammond, J.W. (2009). Traffic control: regulation of kinesin motors. Nat Rev Mol Cell Biol *10*, 765-777.

Vicinanza, M., D'Angelo, G., Di Campli, A., and De Matteis, M.A. (2008). Phosphoinositides as regulators of membrane trafficking in health and disease. Cell Mol Life Sci *65*, 2833-2841.

Viotti, C., Bubeck, J., Stierhof, Y.D., Krebs, M., Langhans, M., van den Berg, W., van Dongen, W., Richter, S., Geldner, N., Takano, J., Jurgens, G., de Vries, S.C., Robinson, D.G., and Schumacher, K. (2010). Endocytic and secretory traffic in *Arabidopsis* merge in the trans-Golgi network/early endosome, an independent and highly dynamic organelle. Plant Cell *22*, 1344-1357.

Voigt, B., Timmers, A.C., Samaj, J., Hlavacka, A., Ueda, T., Preuss, M., Nielsen, E., Mathur, J., Emans, N., Stenmark, H., Nakano, A., Baluska, F., and Menzel, D. (2005). Actin-based motility of endosomes is linked to the polar tip growth of root hairs. Eur J Cell Biol *84*, 609-621.

Vollmeister, E., and Feldbrügge, M. (2010). Posttranscriptional control of growth and development in *Ustilago maydis*. Curr Opin Microbiol *13*, 693-699.

Vollmeister, E., Schipper, K., Baumann, S., Haag, C., Pohlmann, T., Stock, J., and Feldbrügge, M. (2011). Fungal development of the plant pathogen *Ustilago maydis*. FEMS Microbiol Rev *36*, 59-77.

Vollmeister, E., Schipper, K., and Feldbrügge, M. (2012). Microtubule-dependent mRNA transport in the model microorganism *Ustilago maydis*. RNA Biol *9*, 261-268.

Wahl, R., Zahiri, A., and Kämper, J. (2009). The *Ustilago maydis b* mating type locus controls hyphal proliferation and expression of secreted virulence factors in planta. Mol Microbiol *75*, 208-220.

Walbot, V., and Skibbe, D.S. (2010). Maize host requirements for *Ustilago maydis* tumor induction. Sex Plant Reprod *23*, 1-13.

Wang, L., and Lin, X. (2012). Morphogenesis in fungal pathogenicity: shape, size, and surface. PLoS Pathog *8*, e1003027.

Watt, S.A., Kular, G., Fleming, I.N., Downes, C.P., and Lucocq, J.M. (2002). Subcellular localization of phosphatidylinositol 4,5-bisphosphate using the pleckstrin homology domain of phospholipase C delta1. Biochem J *363*, 657-666.

Weber, I., Assmann, D., Thines, E., and Steinberg, G. (2006). Polar localizing class V myosin chitin synthases are essential during early plant infection in the plant pathogenic fungus *Ustilago maydis*. Plant Cell *18*, 225-242.

Weber, I., Gruber, C., and Steinberg, G. (2003). A class-V myosin required for mating, hyphal growth, and pathogenicity in the dimorphic plant pathogen *Ustilago maydis*. Plant Cell *15*, 2826-2842.

Wedlich-Söldner, R., Bölker, M., Kahmann, R., and Steinberg, G. (2000). A putative endosomal t-SNARE links exo- and endocytosis in the phytopathogenic fungus *Ustilago maydis*. EMBO J *19*, 1974-1986.

Wedlich-Söldner, R., Straube, A., Friedrich, M.W., and Steinberg, G. (2002). A balance of KIF1A-like kinesin and dynein organizes early endosomes in the fungus *Ustilago maydis*. EMBO J *21*, 2946-2957.

Weinzierl, G., Leveleki, L., Hassel, A., Kost, G., Wanner, G., and Bölker, M. (2002). Regulation of cell separation in the dimorphic fungus *Ustilago maydis*. Mol Microbiol *45*, 219-231.

Welte, M.A. (2004). Bidirectional transport along microtubules. Curr Biol *14*, R525-537.

Westerholm-Parvinen, A., Vernos, I., and Serrano, L. (2000). Kinesin subfamily UNC104 contains a FHA domain: boundaries and physicochemical characterization. FEBS Lett *486*, 285-290.

Wiese, C., and Zheng, Y. (2006). Microtubule nucleation: gamma-tubulin and beyond. J Cell Sci *119*, 4143-4153.

Wilson, J.M., de Hoop, M., Zorzi, N., Toh, B.H., Dotti, C.G., and Parton, R.G. (2000). EEA1, a tethering protein of the early sorting endosome, shows a polarized distribution in hippocampal neurons, epithelial cells, and fibroblasts. Mol Biol Cell *11*, 2657-2671.

Wloga, D., and Gaertig, J. (2011). Post-translational modifications of microtubules. J Cell Sci *123*, 3447-3455.

Wojtaszek, P. (1997). Oxidative burst: an early plant response to pathogen infection. Biochem J *322 (Pt 3)*, 681-692.

Woo, M., Lee, K., and Song, K. (2003). MYO2 is not essential for viability, but is required for polarized growth and dimorphic switches in *Candida albicans*. FEMS Microbiol Lett *218*, 195-202.

Wu, Q., Sandrock, T.M., Turgeon, B.G., Yoder, O.C., Wirsel, S.G., and Aist, J.R. (1998). A fungal kinesin required for organelle motility, hyphal growth, and morphogenesis. Mol Biol Cell *9*, 89-101.

Wu, S., and Zhang, Y. (2007). LOMETS: a local meta-threading-server for protein structure prediction. Nucleic Acids Res *35*, 3375-3382.

Wyszynski, M., Kim, E., Dunah, A.W., Passafaro, M., Valtschanoff, J.G., Serra-Pages, C., Streuli, M., Weinberg, R.J., and Sheng, M. (2002). Interaction between GRIP and liprin-alpha/SYD2 is required for AMPA receptor targeting. Neuron *34*, 39-52.

Xiang, X., Roghi, C., and Morris, N.R. (1995). Characterization and localization of the cytoplasmic dynein heavy chain in *Aspergillus nidulans*. Proc Natl Acad Sci U S A *92*, 9890-9894.

Xu, Y., Seet, L.F., Hanson, B., and Hong, W. (2001). The Phox homology (PX) domain, a new player in phosphoinositide signalling. Biochem J *360*, 513-530.

Xue, X., Jaulin, F., Espenel, C., and Kreitzer, G. (2010). PH-domain-dependent selective transport of p75 by kinesin-3 family motors in non-polarized MDCK cells. J Cell Sci *123*, 1732-1741.

Yamashita, R.A., and May, G.S. (1998a). Motoring along the hyphae: molecular motors and the fungal cytoskeleton. Curr Opin Cell Biol *10*, 74-79.

Yamashita, R.A., and May, G.S. (1998b). Constitutive activation of endocytosis by mutation of myoA, the myosin I gene of *Aspergillus nidulans*. J Biol Chem *273*, 14644-14648.

Yao, X., Zhang, J., Zhou, H., Wang, E., and Xiang, X. (2011). *In vivo* roles of the basic domain of dynactin p150 in microtubule plus-end tracking and dynein function. Traffic *13*, 375-387.

Yap, C.C., and Winckler, B. (2012). Harnessing the power of the endosome to regulate neural development. Neuron *74*, 440-451.

Yonekawa, Y., Harada, A., Okada, Y., Funakoshi, T., Kanai, Y., Takei, Y., Terada, S., Noda, T., and Hirokawa, N. (1998). Defect in synaptic vesicle precursor transport and neuronal cell death in KIF1A motor protein-deficient mice. J Cell Biol *141*, 431-441.

Yu, H., Wang, N., Ju, X., Yang, Y., Sun, D., Lai, M., Cui, L., Sheikh, M.A., Zhang, J., Wang, X., and Zhu, X. (2012). PtdIns (3,4,5) P3 recruitment of Myo10 is essential for axon development. PLoS One *7*, e36988.

Yu, J.W., Mendrola, J.M., Audhya, A., Singh, S., Keleti, D., DeWald, D.B., Murray, D., Emr, S.D., and Lemmon, M.A. (2004). Genome-wide analysis of membrane targeting by *S. cerevisiae* pleckstrin homology domains. Mol Cell *13*, 677-688.

Yutin, N., Wolf, M.Y., Wolf, Y.I., and Koonin, E.V. (2009). The origins of phagocytosis and eukaryogenesis. Biol Direct *4*, 9.

Zarnack, K., and Feldbrügge, M. (2010). Microtubule-dependent mRNA transport in fungi. Eukaryot Cell *9*, 982-990.

Zeigerer, A., Gilleron, J., Bogorad, R.L., Marsico, G., Nonaka, H., Seifert, S., Epstein-Barash, H., Kuchimanchi, S., Peng, C.G., Ruda, V.M., Del Conte-Zerial, P., Hengstler, J.G., Kalaidzidis, Y., Koteliansky, V., and Zerial, M. (2012). Rab5 is necessary for the biogenesis of the endolysosomal system *in vivo*. Nature *485*, 465-470.

Zekert, N., and Fischer, R. (2009). The *Aspergillus nidulans* kinesin-3 UncA motor moves vesicles along a subpopulation of microtubules. Mol Biol Cell *20*, 673-684.

Zhang, J., Li, S., Fischer, R., and Xiang, X. (2003). Accumulation of cytoplasmic dynein and dynactin at microtubule plus ends in *Aspergillus nidulans* is kinesin dependent. Mol Biol Cell *14*, 1479-1488.

Zhang, J., Tan, K., Wu, X., Chen, G., Sun, J., Reck-Peterson, S.L., Hammer, J.A., 3rd, and Xiang, X. (2011). *Aspergillus* myosin-V supports polarized growth in the absence of microtubule-based transport. PLoS One *6*, e28575.

Zhang, J., Zhuang, L., Lee, Y., Abenza, J.F., Penalva, M.A., and Xiang, X. (2010). The microtubule plus-end localization of *Aspergillus* dynein is important for dynein-early-endosome interaction but not for dynein ATPase activation. J Cell Sci *123*, 3596-3604.

Zhao, C., Takita, J., Tanaka, Y., Setou, M., Nakagawa, T., Takeda, S., Yang, H.W., Terada, S., Nakata, T., Takei, Y., Saito, M., Tsuji, S., Hayashi, Y., and Hirokawa, N. (2001). Charcot-Marie-Tooth disease type 2A caused by mutation in a microtubule motor KIF1Bbeta. Cell *105*, 587-597.

Zhou, H.M., Brust-Mascher, I., and Scholey, J.M. (2001). Direct visualization of the movement of the monomeric axonal transport motor UNC-104 along neuronal processes in living *Caenorhabditis elegans*. J Neurosci *21*, 3749-3755.